Collision Resistance of Fibre Reinforced Polymer Lock Gates

A study of the behaviour and damage during collision

Ben Edmondson

Technische Universiteit Delft

Iv-Infra

Delft University of Technology

Challenge the future

Collision Resistance of Fibre Reinforced Polymer Lock Gates

A study of the behaviour and damage during collision

by

Ben Edmondson

in partial fulfilment of the requirements for the degree of

Master of Science

in Civil Engineering

at the Delft University of Technology,

to be defended publicly on Wednesday August 16, 2017 at 10:30 AM.

Supervisor:	Prof. dr. ir. S. N. Jonkman	TU Delft
Thesis committee:	Dr. ir. J. G. de Gijt,	TU Delft
	Ir. W. F. Molenaar,	TU Delft
	Dr. ir. P. C. J. Hoogenboom,	TU Delft
	Dr. ir. F. P. van der Meer,	TU Delft
	Th. P. M. van der Tol,	IV-Infra

An electronic version of this thesis is available at http://repository.tudelft.nl/.

Preface

This report represents the finalisation of my Master of Science in Civil Engineering at Delft University of Technology. During my time at the faculty of Civil Engineering and Geosciences I have had the privilege of being taught my field by some of the leading professionals and I would like to whole heartily thank every one of my lecturers who has bought me to this point. Also to all my colleagues with whom I completed the project orientated side of studies I would like to extend a word of gratitude.

To all my colleagues at IV-Infra during my graduation process I would like to say thank you for your hospitality. At both the Amsterdam and Sliedrecht offices I was made to fell welcome which made my time much more enjoyable. A special thanks goes out to Dirk van der Tol whose expertise proved invaluable in completing this report. I sincerely hope that I'll get the chance to work with you on projects in the future.

I would also like to thank my graduation committee from Delft University of Technology consisting of Prof. dr. ir. S.N. Jonkman, Dr. ir. J.G. de Gijt, Ir. W.F. Molenaar, Dr. ir. P.C.J. Hoogenboom, Dr. ir. F.P. van der Meer, for their guidance and critique. Without it my final result would not be comparable to the document it is now. An extra thank you to Mr. Molenaar for helping with the organisational issues which come with such a large committee.

Finally I would like to thank all my friends and family who kept me going throughout the course of my studies. Without all of you the past years wouldn't have been nearly as enjoyable.

Ben Edmondson
Delft, June 2017

Abstract

Over the past years Fibre Reinforced Polymers, or FRP, have started making more of an appearance in civil engineering structures. They have the advantages that they are light-weight, do not corrode and theoretically require little maintenance during their lifespan. Originally they were used to construct reinforcement, cables and small bridges but more and more they are finding uses for larger scale structures. One of these newer applications is in lock gates.

Locks are structures which are responsible for enabling water based transport while also retaining high water where necessary and are critical links in the water defence system of a region. Their gates also have a relatively large risk of collision due to the amount of moving vessels passing through them. In order to safely construct these lock gates from FRP laminates it is important that their response to such collision loads is well understood. This is the focus of this study with the aim to construct a model to help better understand the collision scenario.

To make the theory concrete a case study is done on the lock gates of Sluis III which is situated in the Wilhelminakanaal in Tilburg. These gates are, at the time of writing, the largest FRP lock gates in the world. With the down stream gates being 13.9 by 6.3 meters. The event in which a Class III vessel collides with these gates will be examined in detail.

The collision is schematised as a one dimensional collision using a series of springs and dampers to obtain understanding of the general collision behaviour. From this model it is concluded that the application of a load from the ship's engine or taking elastic deformations of the ships bow into account has negligible influence of the results (in the order of 2%), simplifying the calculations considerably. This simple model is later advanced in three ways: Two numerical finite element models are used to determine the structural response of the gate elements on a global and local scale and a more advanced analytical model is made to account for non-elastic deformation in the ship's bow.

The gate's structure consists of multiple overlapping laminates which together form the skins of the gate. The numerical model is set up in two ways, one of which is used to determine the overall response of the gate element and the other to focus on the interlaminar resin layer in the skins. The results show that it is of importance to apply the load in a realistic manner as the results may vary widely depending on bow shape and point of impact. The approximation suggested in the Dutch codes in which the load is applied as a distributed load of a 0.5m^2 areas proved to be inaccurate. For this reason a dynamic LS-Dyna calculation is run using a rigid model of the ships bow to apply the load. The outcome of this analysis shows minor damage to the gate over a large area around to point of impact, but the stresses remain under the failure limit of the laminates except for the internal flanges directly under the impact. These flanges will fail, but this will not threaten the water retention of the gate. The stresses in the resin layer also remain under their critical limit. It can be concluded that the gate satisfies the requirements but significant repairs will be necessary to restore it to a fully operational state.

The expanded analytical model is based on the fact that the force between the bow and the gate is larger than the failure load of the bow itself. The failure which will then take place will dissipate large portions of energy (in the order of 50%) making the current approach, in which this does not take place, highly conservative. The model suggested here is a segmented failure model in which parts of the ship bow fail completely once their failure load in reached. The results of this model are dependant on a series of inputs based on the ships structure and the damping during collision, but for all input values within their expected regions it shows a significant reduction in the amount of the energy that must be retained by the gate as well as a decreased sensitivity to the, hard to predict, damping factor. This model shows potential to reduce material usage for lock gates in which collision are considered governing. With further refinement this model could be used during the design of future lock gates to come to a cheaper design. Experimental data would serve an important purpose during this refinement.

Contents

Preface iii

Abstract v

1 Introduction 1

1.1 Problem Statement 1
1.2 Objective 2
1.3 Report Structure 2

2 Case Description - Wilhelminakanaal Tilburg 5

2.1 Locking Structures 5
  2.1.1 Locking Process 6
  2.1.2 Mitre Gates 6
2.2 Fibre Reinforced Polymers 8
2.3 Project Description 9
2.4 Gate Design 10
  2.4.1 Laminate Properties 11
  2.4.2 Gate Properties 12
2.5 Collision Load Scenario's 14
  2.5.1 Upstream Collisions 14
  2.5.2 Downstream Collisions 15
  2.5.3 Governing Collision Cases 16
2.6 Safety Factors 16

3 Analytical Collision Analysis 19

3.1 Modelling Aspects 19
  3.1.1 Static System 20

3.1.2 Collision Orientation . . . 21
3.1.3 Hydrodynamic Added Mass . . . 22
3.1.4 Collision Velocity . . . 23
3.1.5 Model Stiffnesses . . . 24
3.1.6 Energy Dissipation Mechanisms . . . 25
3.1.7 Load . . . 25
3.1.8 Loading Capacity of the Gate . . . 28
3.2 Difference to Steel Designs . . . 29
3.3 Collision Model . . . 31
3.4 Performed Analyses . . . 31
3.4.1 Static Analysis . . . 31
3.4.2 Differential Equation . . . 34
3.4.3 Numerical Calculation . . . 39
3.5 Discussion . . . 41

4 Global Gate Behaviour - Numerical Analysis 43

4.1 Collision Model . . . 44
4.1.1 Element Data . . . 44
4.1.2 Geometry . . . 44
4.1.3 Constraints . . . 46
4.1.4 Load conditions . . . 48
4.2 Analysis Results . . . 50
4.2.1 Static . . . 50
4.2.2 Dynamic . . . 52
4.3 Comparison and Discussion . . . 52
4.3.1 Comparison of Analyses . . . 53
4.3.2 Results and Discussion . . . 54

5 Local Delamination Analysis **57**

5.1 Collision Model . . . 57

5.1.1 Geometry . . . 57

5.1.2 Constraints . . . 60

5.1.3 Load conditions . . . 60

5.2 Model Authentication . . . 61

5.2.1 Resin Layers . . . 61

5.2.2 Core Geometry . . . 63

5.3 Results and Discussion . . . 64

6 Non-Elastic Ship Behaviour **69**

6.1 Simplifications in the Current Model . . . 69

6.2 Non-Elastic Ship Behaviour Model . . . 70

6.2.1 Changing Cross-section . . . 70

6.2.2 Non-Elastic Behaviour and Failure . . . 71

6.2.3 Resulting Model . . . 72

6.2.4 Collision Force . . . 72

6.2.5 Example Calculation . . . 73

6.2.6 Discussion . . . 75

6.3 Effect of the Influencing Parameters . . . 76

6.3.1 Failure Load . . . 77

6.3.2 Segment Length . . . 78

6.3.3 Gate Stiffness . . . 81

6.3.4 Input Energy . . . 81

6.3.5 Damping Factor . . . 81

6.4 Conclusions and Discussion . . . 83

7 Conclusions **85**

8 Recommendations **87**

List of Figures 89

List of Tables 95

Bibliography 97

A Locks and Collisions 101

A.1 Lock Parts 101

A.2 Lock Gates 102

A.2.1 Gate Functions 102

A.2.2 Gate Types 102

A.3 Collisions in Locks 104

A.3.1 Causes of Lock Collision 104

A.3.2 Probability of Lock Collision 105

A.3.3 Velocity of Lock Collision 106

A.3.4 Ship Classes 107

B Shipping Categories 109

C Ship Bow Shapes 113

D Additional Information on Fibre Reinforced Polymers 117

D.1 Composition 117

D.1.1 Fibres 117

D.1.2 Resins 119

D.1.3 Gel Coats 121

D.1.4 Additives 122

D.1.5 Laminate build-up 122

D.2 Production of FRP elements 124

D.2.1 Open Mould Production 125

D.2.2 Closed Mould Production 126

D.2.3 Continuous Production 128

D.3 Current Applications . . . 128
D.3.1 Civil Engineering . . . 128
D.3.2 Aerospace . . . 132
D.3.3 Automotive . . . 132
D.3.4 Maritime . . . 133
D.3.5 Other . . . 133

E Classical Laminate Theory **135**

E.1 Introduction . . . 135
E.1.1 Definition of a Laminate . . . 135
E.1.2 Area of Validity . . . 135
E.2 Derivation of the Classical Laminate Theory . . . 136
E.2.1 Classical Laminate Theory on Ply Scale . . . 136
E.2.2 Expansion to Laminate Scale . . . 139

F CUR Recommendations **143**

F.1 Introduction in the CUR Recommendation 96 . . . 143
F.2 Safety Calculations . . . 143
F.2.1 Load Factors . . . 144
F.2.2 Material Factors . . . 144
F.2.3 Conversion Factors . . . 145
F.3 Laminate Properties . . . 146
F.3.1 Stiffness Properties . . . 146
F.3.2 Strength Properties . . . 148
F.3.3 Other Properties . . . 148
F.4 Calculations . . . 148
F.4.1 Stiffness Calculations . . . 148
F.4.2 Stability Calculations . . . 148
F.4.3 Strength Calculations . . . 149

G Reference Projects 151

G.1 Pedestrian bridge - Koegelwieck 151

G.2 Mitre Gates - Spieringssluis 152

G.2.1 Preliminary Design Concepts 153

G.2.2 Final Design 156

H InfraCore Inside 159

H.1 Sandwich Panels 159

H.2 Multi Beam Plates 159

I Analytical Results - Diagrams 163

I.1 Static Analysis 163

I.2 Differential Equation 166

I.2.1 Level of Damping 166

I.2.2 Engine Force 166

I.2.3 Ship Stiffness 167

I.3 Numerical Analysis 167

J Numerical Model Images 175

J.1 Images for the Global Analysis 175

J.1.1 Static geometry 175

J.1.2 Dynamic Geometry 175

J.1.3 Static Loads 175

J.1.4 Static Results 179

J.1.5 Dynamic Results 179

J.2 Images for the Local Analysis 185

K MatLab Code - Non Elastic Ship Model 187

K.1 MatLab Code 188

1

Introduction

Locks are important structures for both water retention and facilitating transport over water. They make it possible to traverse direct routes where the surrounding topography and water levels would normally not allow. As such the locks situated in our waterways are used daily by many vessels. Naturally having moving vessels pass through them on a regular basis brings with it the chance of collision, especially for the elements which are located in the waterway such as the gates. Understanding these collisions is important as they can take place at different locations and to different degrees and each collision has the potential to threaten the water tightness of the lock and hinder transport for a long period of time.

Simultaneously the design of lock gates is going through a shift in mindset. More commonly the traditionally steel lock gates are being constructed of Fibre Reinforced Polymers [FRP] due to their superior corrosion resistance and their theoretically high durability[1]. These FRP lock gates are relatively new to the industry and do not have the knowledge base behind them that more traditional materials can rely on. As FRP lock gates are being produced in an increasing scale whilst being closely monitored more trust is being gained in what may become the standard material for such structures.

In this thesis these two topics are combined and the response of such a FRP lock gate to ship collision is investigated. The combination of a high dynamic loading condition with a relatively new material such as FRP is topic on which little literature is available. The driving force behind what little research has been done are the companies which fabricate such structures who, to protect their business interests, do not make all their findings public. By subjecting a known FRP structure to a series of analytical and finite element calculations a better understanding of the behaviour of such a collision will be obtained, which will aid during future design processes and determine the relevance of FRP as a lock gate construction material.

1.1. Problem Statement

From the situation described above the general problem statement is formulated as:

Collisions are complex, dynamic load cases which are difficult and time consuming to model in detail. They consist of a large amount of variables and have the potential to cause large damage to structures. For this reason they are often simplified in a conservative manner to ensure a safe design. Doing so runs the risk of an over dimensioned structure which is undesirable. If a simple model were to be developed which could take the non-linearity's of these collision scenario's into account there is potential for large

savings due to the additional non-elastic deformations.

When this load case is combined with a relatively new and unproven material, such as Fibre Reinforced Polymer laminates, a situation comes to pass for which very little literature is available. Considering the growth in interest for FRP in the civil engineering sector and its use in collision sensitive structures such as lock gates it is of import to gather more information on this complex case.

1.2. Objective

The objectives of this study are threefold:

- Determine whether the FRP lock gate constructed in Tilburg is able to withstand the governing collision scenario and if the coinciding damage is reparable without replacing the entire gate.
- Analyse the stress concentrations within the given gate design to determine the extent of the local damage.
- Develop a model with which the non-linearity's of the ships behaviour during collision can be taken into account and discuss the value of such a model.

1.3. Report Structure

The structure of this report is schematically shown in Figure 1.1. To begin with the case in question, Sluis III in Tilburg, is discussed in Chapter 2 and general properties are determined which will be used in the analysis steps. Chapter 3 covers the analytical calculations which will serve as a base for the following chapters. From here the report splits into a numerical calculation and an analytical calculation.

The numerical branch consists of Chapter 4 in which the analytical results are verified numerically with both a static and dynamic calculation on a global scale and Chapter 5 in which a closer look is taken as to the local deformation of the gate around the point of impact. The analytical branch is Chapter 6 in which non-linear ship behaviour is taken into account and how it affects the solution is examined. Finally conclusions and recommendations are given in Chapters 7 and 8 respectively.

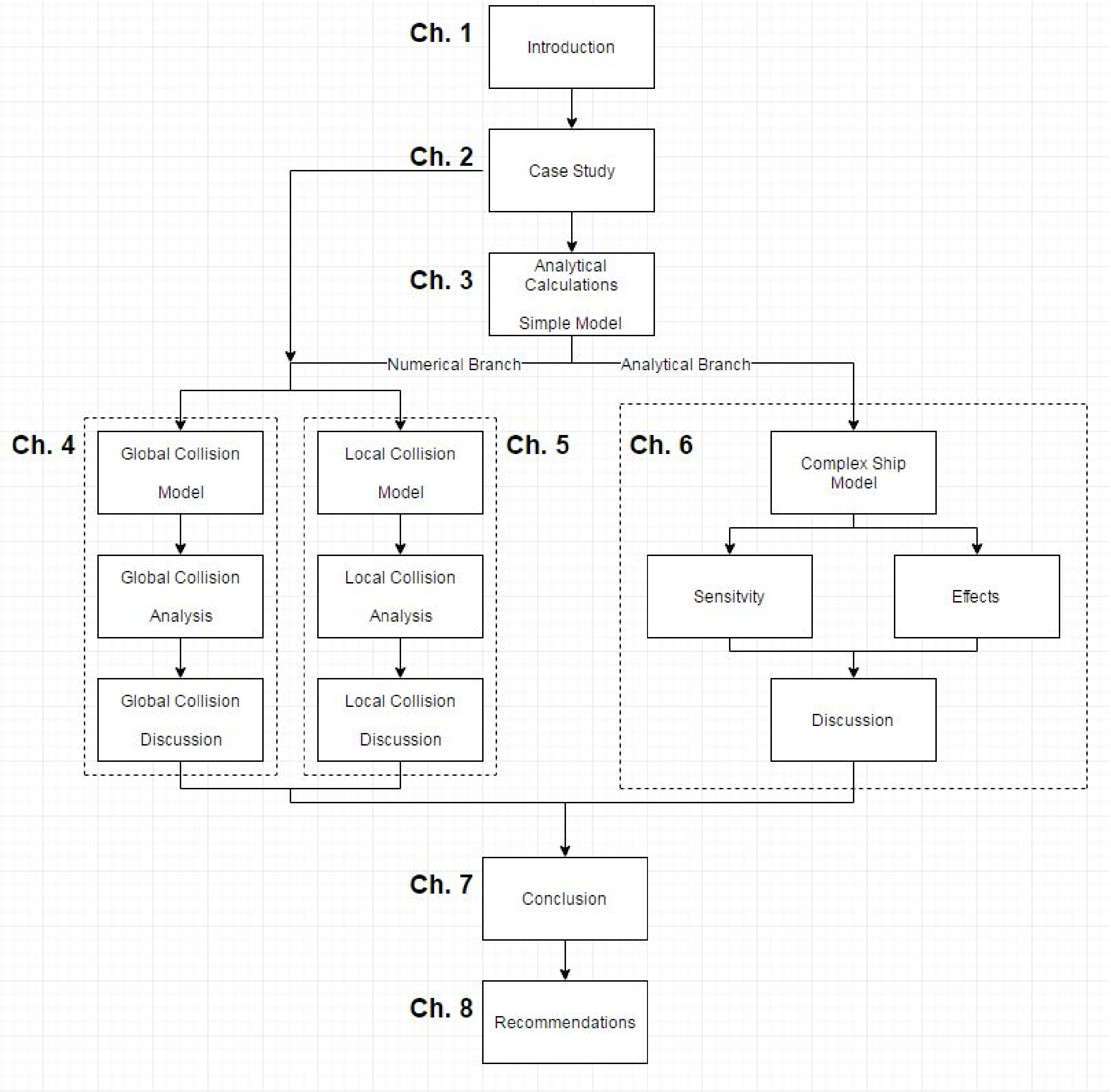
Ch. 1
Introduction
Ch. 2
Case Study
Ch. 3
Analytical Calculations
Simple Model
Numerical Branch
Analytical Branch
Ch. 4
Global Collision Model
Global Collision Analysis
Global Collision Discussion
Local Collision Model
Local Collision Analysis
Local Collision Discussion
Ch. 5
Ch. 6
Complex Ship Model
Sensitvity
Effects
Discussion
Ch. 7
Conclusion
Ch. 8
Recommendations

Figure 1.1: Flowchart of the report structure

2

Case Description - Wilhelminakanaal Tilburg

The case project discussed in this chapter will serve as a basis for all further calculations in this study. This will serve both to supply the calculations with physical quantities and to allow easy comparison between sets of results. As a case the lock gate in the Wilhelminakanaal in Tilburg is chosen because it is the largest FRP lock gate that has been constructed at the time of writing. For FRP to be a viable choice of construction material for large projects it is of import that inevitable ship collisions can be handled in a reliable manner without total failure of the gate.

In Chapter 2.1 some general information of locking structures will be given followed by an introduction to Fibre Reinforced Polymers in Chapter 2.2. The following chapters address the case project itself, beginning with Chapter 2.3 discussing the project specifics. The design of the gate is expanded on in Chapter 2.4. The manner in which loading will take place can be found in Chapter 2.5 and finally in Chapter 2.6 the required material safety factors are provided.

The section below is based on documents supplied by FibreCore who were responsible for the design of the FRP gate for this project.[2]

2.1. Locking Structures

This chapter gives a brief introduction to aspects of lock structures which are relevant to this case. Further information can be found in Appendix A.

In this thesis locks are treated synonymously with navigation locks, which in reality is a sub group. Other type of lock include dewatering gates, stop locks and guard locks, but these locks are not made to aid the passing of vessel which is the main issue for this report. Furthermore other structures which may serve a similar purpose, such as boat lifts, are not discussed.

A lock is a structure which serves to allow a water vessel to pass from one section of waterway to another with a different water level. When a waterway is made navigable the water level is often predetermined in order to be sure that there is enough depth for the governing vessel and that the embankment and other water defences are high enough. Another reason a lock may be applied is to prevent tidal effects in a stretch of river near the ocean. Although locks can vary greatly in both their dimensions and their retainment height they share a similar composition, namely a chamber in which the water level can be varied with gates at both sides. An example of this with two different filling systems is given in Figure 2.1.

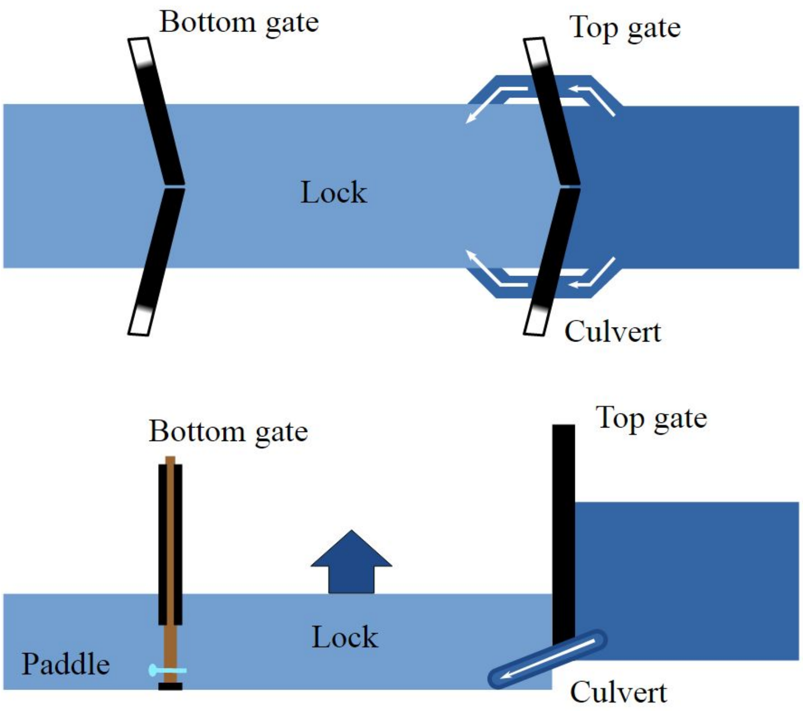

Figure 2.1: Schematic of a sample lock. Top- and side view[3]

2.1.1. Locking Process

The standard locking process can be seen as a series of steps: (Illustrated in Figure 2.2)

1. The vessel enters the lock through one of the sets of gates.
2. The gates are closed behind it to seal off the chamber.
3. The filling system in the opposite gate, be it culverts or simple paddles in the gates, are used to raise/lower the water level to that of the destination waterway
4. The opposite gates are opened when the water level difference is very small. A difference of 10-20cm is acceptable as the loads on the vessel will be within set boundaries. [4]
5. The vessel leaves the lock through the gates and can continue its journey.

If a vessel encounters a lock in which the water level is not equal to that of the waterway it is in the lock chamber must first be filled/emptied before the gates can be opened. Where possible this is avoided due to increase locking times and water loss.

2.1.2. Mitre Gates

Mitre gates are commonly used for locks in the Netherlands up to widths of roughly 24 meters. They consist of two gates which rotate around a vertical axis, each spanning half the lock width, which come together at an angle in the middle of the lock. This angle is often chosen as 1:3[4]. The gates point towards high water so that the excess water pressure from the locks lift pushes the gates closed. The loads are then carried through a combination of normal forces and bending in the gates to the chamber walls. Effectively each gate functions as a beam on two supports with potential extra support where the gate leans against the sill.

This design makes mitre gates only function as a unilateral retention systems, although with some extra

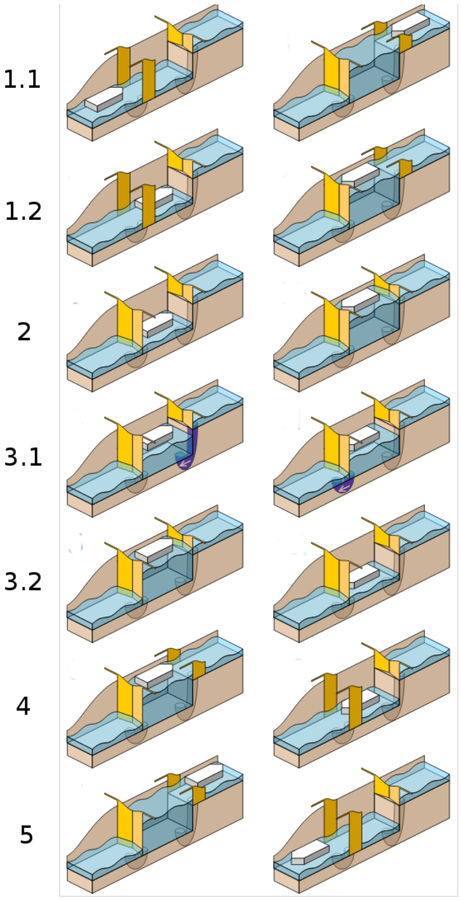

Figure 2.2: Visual representation of the locking process. Left: Locking upstream, Right: Locking downstream[3]

precautions small negative water pressures can also be retained allowing a certain amount of leakage. Where bilateral retention is necessary and mitre gates are desired two sets of gates are needed at each end of the lock. A schematic top view for both uni- and bilateral retention is shown in Figure 2.3. The lock in the Wilhelminakanaal considered here is an example of a uni-directional retention mitre gate.

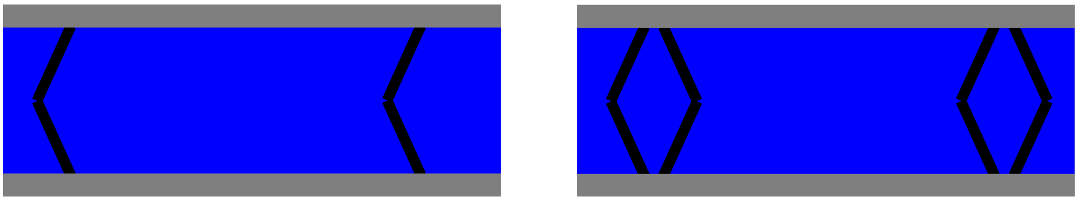

Figure 2.3: Top view of a lock with mitre gates. Left: Uni-lateral retention. Right: Bi-lateral retention

Briefly summarised the advantages and disadvantages are as follows:

Advantages:

- Due to the design which carries loads as normal forces, instead of pure bending, an economic use of materials is obtained.
- The opening mechanism is relatively simple when compared to other gate types.
- When open the gates can be stored in a shallow recess in the chambers side.

Disadvantages:

- Precise dimensions are required to ensure water tightness.
- The gates are susceptible to waste and ice formation.
- A vessel colliding with the gates form the low water side may push the gates open.
- Collision is possible even when the gates are open due to their being stored in the side of the lock chamber.

2.2. Fibre Reinforced Polymers

Fibre Reinforced Polymers, or as often abbreviated FRP, is a general name for a composite material which consists of a polymer resin and a fibrous material. This chapter gives an introduction to the material sub set and reference is made to Appendix D for further information.

Composites themselves can be defined as material structures which consist of at least two separate materials, that can be distinguished on a macroscopic level, working together to form a whole with significantly better properties.[5] This group of materials has found applications in many different industries over the past decades, especially the aerospace-, maritime- and automotive industries. This is, for a large part, due to the fact that FRP's are low weight and can be freely shaped with relative ease. In these industries the importance of weight outweighs the fact that FRP is often more expensive than the traditional materials it replaces. [1]

It is only relatively recently that FRP has found solid ground within the civil engineering sector. This is partially because the civil engineering sector in known for begin conservative and partially because the technical advancements needed to meet the requirements for the sector have only been made more recently[5]. Some example of civil engineering projects which have been excuted with the use of FRP are given in Appendix G.

Although the exact properties of a FRP are dependant on many factors (which will be discussed further on) the general pros and cons of FRP are shown in Table 2.1.

Table 2.1: Pros and Cons of FRP in the construction industry [5]

Pros	Cons
Light weight	High material costs
Easily shapable	Little practical design experience
Low maintenance costs	High investment costs
Customisable properties	Complex detailing
Resistant to chemicals	Susceptible to UV and fire
Long Fatigue Life	Low Stiffness

It is common for FRP elements to be executed as laminates. Such as laminate consists of multiple structural layers called plies, each with their own thickness, fibre ratio and fibre orientation consolidated together to function as a single element. This is very much comparable with multiplex wood panels. A schematic representation of a laminate is given in Figure 2.4, the fibre angle is clearly visible. The properties of the element as a whole is dependant on the properties and position of each ply and can be adjusted dependant on the load situation. To simplify matters it is often chosen to vary only the fibre orientation and to keep a laminate symmetrical around its middle plain (to avoid torsion), but this is by no means compulsory.

Calculations with laminates are more complex than for an element with uniform properties and for this reason classical laminate theory is used to determine how the element as a whole behaves. Traditional laminate theory is elaborated on in Appendix E.

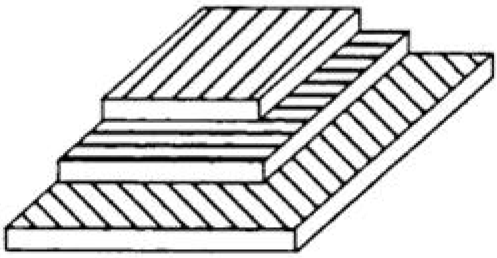

Figure 2.4: Schematic representation of a laminate structure[6]

2.3. Project Description

In 2015 a project was executed in the Wilhelminakanaal in Tilburg, it consisted of the widening and deepening of the canal over a length of 4 kilometres and the construction of a new lock. Through these measures the canal was up-scaled to meet the governments vision of increased accessibility for Brabant by facilitating class IV shipping.

The lock in question, also referred to as 'Sluis III', is situated within the city borders of Tilburg and can be seen in Figure 2.5. The exact location can be seen in Figure 2.6.

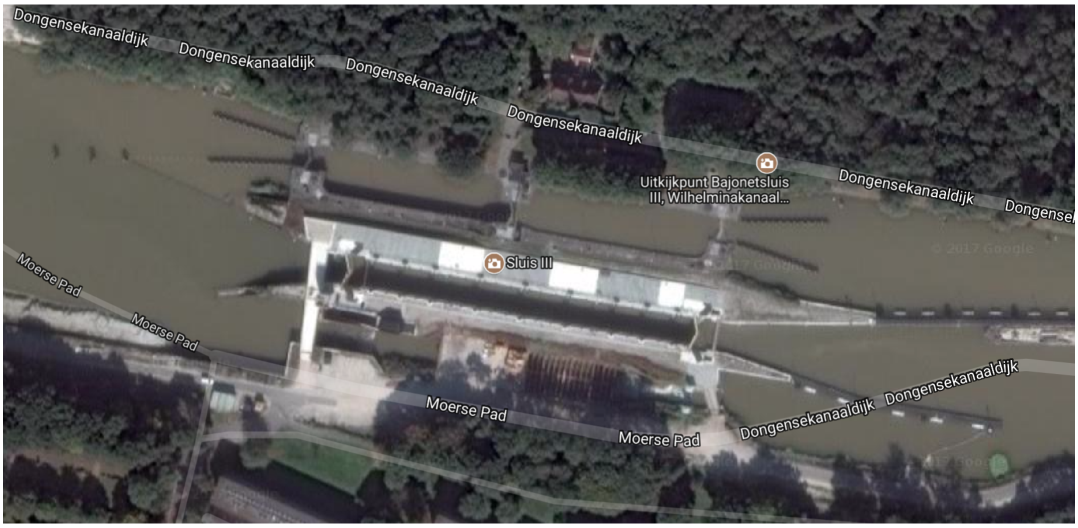
Dongensekanaaldijk
Dongensekanaaldijk
Dongensekanaaldijk
Dongensekanaaldijk
Uitkijkpunt Bajonetsluis III, Wilhelminakanaal...
Dongensekanaaldijk
Dongense
Sluis III
Moerse Pad
Moerse Pad
Moerse Pad
Moerse Pad
Dongensekanaaldijk
Dongensekanaaldijk
© 2017 Google

Figure 2.5: Aerial view of the Sluis III complex[7]

For the design of the new lock innovation was set as an important criteria and the choice was made for the construction of a FRP gate. Due to the size of the lock it has had the added advantage of being the largest FRP lock gate ever constructed and thus an achievement for the region and the companies involved. The design of this gate was completed by FibreCore, the operating mechanism by Witteveen & Bos and the connections between the gate and the chamber by IV-Infra.

Sluis III is constructed to facilitate shipping class IV (See Appendix B) and has a length of 115 metres, a width of 10.5 metres and a sill level of +1.35m NAP downstream and +8.75m NAP upstream. The lock is fitted with uni-directional retaining mitre gates at each end which are subjected to different water levels and are thus designed with different retention heights in mind. The difference is quite large with the upstream gate retaining 4.42 and the downstream 7.9 metres of water height difference (See Figure 2.7. As an effect of this the gate design also differs between the two gates. This mainly shows itself through different panel thicknesses. In Chapter 2.4 the design of the lock gate will be discussed in detail.

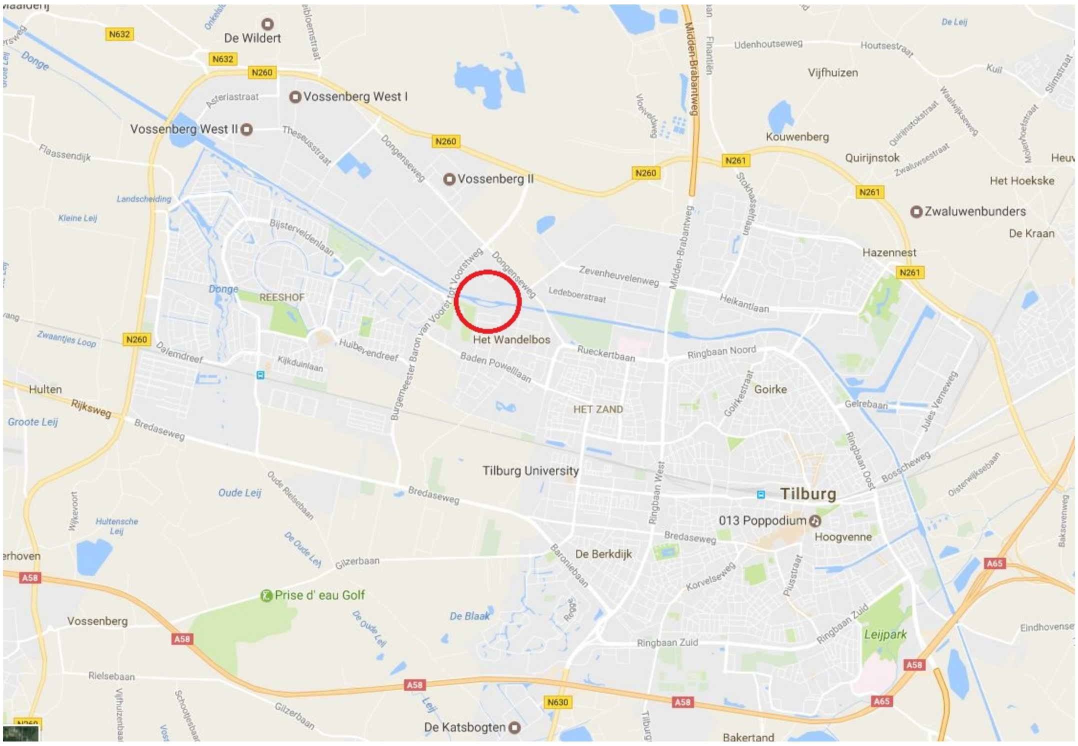

Figure 2.6: Location of Sluis III in the Wilhelminakanaal - Tilburg[8]

2.4. Gate Design

The locking complex Sluis III consists of two mitre gates allowing for unilateral retention. These gates have vastly different sill heights and water retention levels as mentioned above, because of this their designs also vary somewhat. The gate characteristics are summarised below in Table 2.2.

Table 2.2: Gate properties of the up- and downstream lock gates [2]

	Upstream Gate	Downstream Gate
Gate Length	6.2 m	6.3 m
Unsupported Length	5.96 m	6.0 m
Retention Height	4.8 m	12.3 m
Construction Height	5.6 m	13.9 m
Thickness	0.37 m	0.51 m
Sill Level	+8.75 NAP	+1.35 NAP
Water Retention	4.42 m	7.9 m
Gate Panel Mass	8,000 kg	21,225 kg
Total Mass	20,000 kg	35,000 kg
Skin Thickness	30 mm	30 mm
Internal Plate Thickness	5 mm	5 mm
H.t.h. internal plates	100 mm	100 mm

As can be seen in the Table 2.2 the main dimensions of the gates are different for the two gates. The FRP laminates, skins and internal plates, however are equally thick for both the upstream and downstream gates. Also the heart to heart distance of the internal plates remains unchanged. This is most likely for ease in production. More information on these internal plates is supplied in Appendix H.

The gates were designed as flat panels (i.e. with no curvature) and all non FRP parts must be removable for application on another gate. All contact areas between gates and between the gate and the chamber

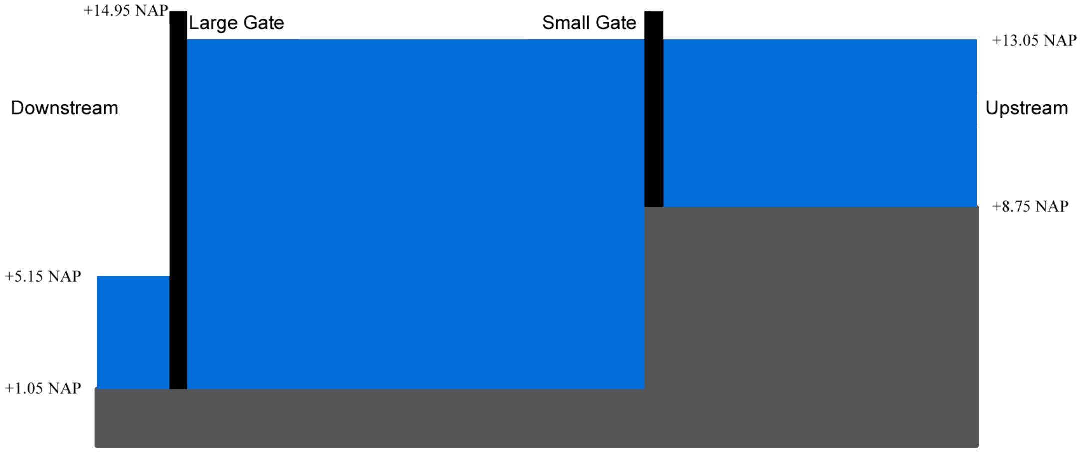

Figure 2.7: Schematic sideview of Sluis III in the Wilhelminakanaal - Tilburg, including sill and water levels[2]

were fitted with wooded bumpers. The soft wood not only protects the FRP but also improves the water-tightness. The locking process takes place through use of valves in the gate which are accommodated for by circular gaps in the gate structure. The choice was made to construct the gate as a sandwich panel reinforced with internal plates. In addition to the internal plates the weak core material is replaced with solid FRP sections in places where concentrated forces are applied to the structure (e.g. hinges).

The laminate lay-up was executed in a specific manner to which FibreCore owns a patent, naming it InfraCore Inside™. For more information on this particular manner of lamination see Appendix H. A photograph of the gate is shown in Figure 2.8 and an overview of the gate elements is shown in Figure 2.9.

2.4.1. Laminate Properties

The laminates were constructed from glass fibre reinforced polyester, which is the most commonly used type of FRP due to its low costs, with a top coat of ISO-npg polyester. This top coat is well tested and known for its water resistant properties[2]. Each laminate is layed up in manner that has the most fibres are in the direction of the dominant loading, with other direction fitted with some fibres to carry local and secondary loads. A more detailed overview of the laminates is given in Table 2.3. Noticeable is that the outer shell, consisting of the skins and edges have a much larger fibre percentage than the internal panels. This is because they contribute the most to the strength of the panel as a whole and investing in stronger, and thus more expensive, laminates here will have a largest effect.

The design took place using the CUR96 recommendation for FRP structures with loads as defined by the ROK 1.2.

Table 2.3: Laminate build-ups for 'Sluis III' in the Wilhelminakanaal, Tilburg [2]

Element	Ply Build-up	Fibre Fraction	Thickness
Skins	$0_{75}/90_{25}$	52%	30 mm
Edges	$0_{50}/90_{50}$	52%	60 mm
Internal Flanges	$0_{50}/90_{50}$	28%	5mm

With the known build-ups above laminate theory can be applied (See Appendix E) to determine the properties of the laminates. This was done the the Wilhelminakanaal project by FibreCore and resulted in the values shown in Table 2.4.

This information, together with a gates measurements will be used in following section to calculate the global properties of the gates.

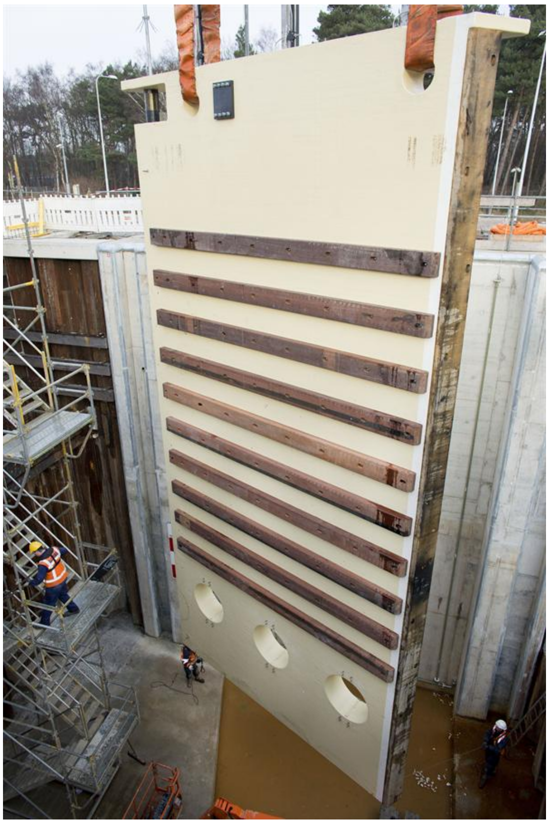

Figure 2.8: Image of the gate being lifted into place[9]

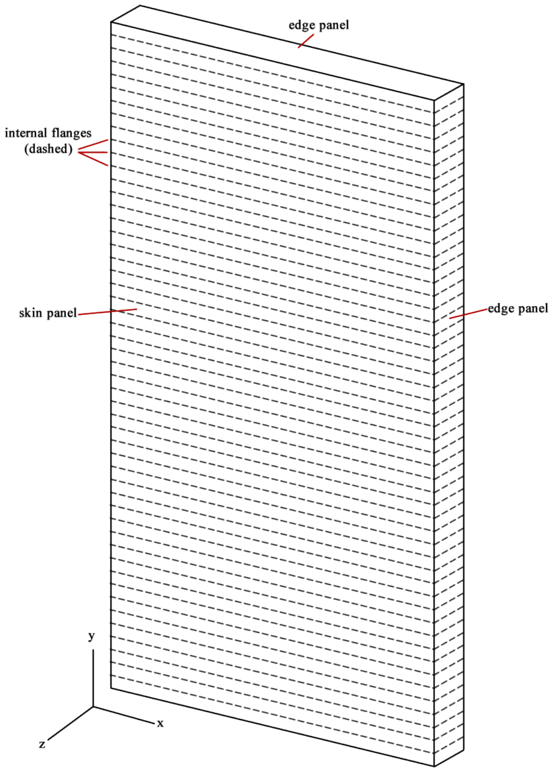

Figure 2.9: Overview of the gate elements

Table 2.4: Laminate properties for 'Sluis III' in the Wilhelminakanaal, Tilburg [2]

Property	Skins	Edges	Straight internal panels
E_x [MPa]	32300	25100	13820
E_y [MPa]	17850	25100	13820
G_{xy}=G_{xz} [MPa]	6050	6050	3050
ρ [kg/m^3]	1815	1815	1480

2.4.2. Gate Properties

To begin calculating the response of the structure to collisions (as will be done in Chapter 3) the behaviour of the gate must be summarised in some basic properties. The most likely loading conditions the gate will be subjected to will be axial loading and bending, which require the global EA and EI moduli respectively. These values are calculated in the following sections. For this the core material was assumed to have no significant strength of its own, this simplifies calculations but is somewhat conservative. This is realistic seen as the laminates are roughly a thousand times as stiff as the core making the cores contributed insignificant[2].

EA Modulus

The possible axial loads on the gate will be horizontally orientated from the end of the gates to the chamber wall. In this situation the values in x-direction from Table 2.4 are the relevant ones. It can be said that the EA modulus of the section as a whole is the sum of its parts as shown in Equation 2.1.

$$EA_{gate} = \sum E_x A_x \tag{2.1}$$

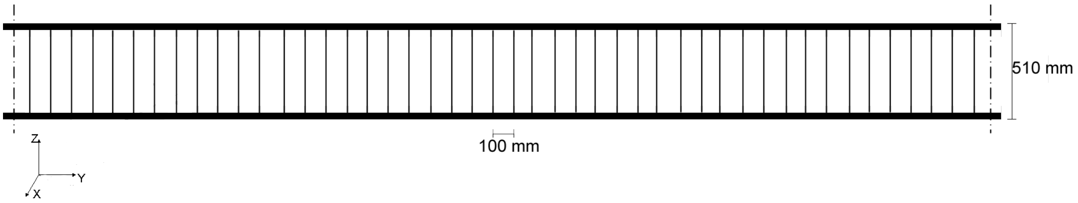

Figure 2.10: Cross section of the gate structure

In which:

E_x is the modulus of elasticity in the x-direction for that element.
A_x is the cross-sectional area of that element in the x-direction.

As the core has no strength of its own the parts which must be summed are the two skins, the 138 ($\frac{13.9}{0.1} - 1$) internal flanges and the plate edges. This method assumes the entire cross-section will carry the load evenly, which when considering a point loading such as a collision, is not completely accurate. It is however adequate for a first round of analytical calculations. Also the cross-section is quite stiff thanks to the inclusion of the perpendicular flanges making this approach more accurate.

$$EA_{gate} = 2 * (32300 * 0.03 * 13.9) + 138 * (13820 * 0.005 * 0.45) + 2 * (25100 * 0.06 * 0.45) \\ EA_{gate} = 3.26 * 10^4 MN \tag{2.2}$$

This value will be used in following section. Interestingly FibreCores own calculation for this project gave a EA for the gate of 3.41*10^7kN which is 4,6% higher. This is most likely due to the fact that they made use of a software packet to calculate the value which can take more detail into account.

EI Modulus

When the gate is subjected to bending as a first estimate it will respond as either a simply supported beam or a hinged beam (see Chapter 3.1.1). In both cases the rotation axis will be the same with rotation around the y-axis and displacements in the z-axi. The EI modulus which coincides with this bending can be determined through use of the parallel axis theorem, also known as Steiner's theorem, which can be be written as follows:

$$EI_{gate} = \sum E_x(I_x + A_x * e_x^2) \tag{2.3}$$

In which:

E_x is the modulus of elasticity in the x-direction for that element.
I_x is the moment of inertia of an element around its own centre of gravity.
A_x is the cross-sectional area of that element.
e_x is the eccentricity of the element from the centre of gravity of the cross-section as a whole.

As for the EA modulus the parts which must be summed are the skins, the 138 internal flanges and the edges of the plate. The plate as a whole is symmetrical so its centre of gravity will be in the middle of the cross-section. This is used to determine the eccentricities. The core material has an insignificant

Table 2.5: Values for the calculation of the gates EI modulus [2]

Element	#	E_x [MPa]	I_x [m^4]	A_x [m^2]	e_x [m]	Steiner
Skins	2	32300	$3.1*10^{-5}$	0.417	0.24	0.024
Internal Flanges	138	13820	$3.8*10^{-5}$	$2.25*10^{-3}$	0	0
Edges	2	25100	$4.56*10^{-4}$	0.027	0	0

contribution to this value. The values for E_x, I_x, A_x, and e_x are given below in Table 2.5 as well as the Steiner value ($A_x * e_x^2$).

Using Equation 2.3 and Table 2.5 the EI modulus for the gate can be determined as $1.65*10^{15}$ Nmm^2.

2.5. Collision Load Scenario's

Now that the gate structure has been defined the loading shall be examined. In a full structural calculation of a lock gate there are many different sources of loading. In all cases the governing load combination is said to be the collision load combined with the water level at high lock level with their representative load factors. In gates in question have been designed with the governing load combination in mind with the exception of potential collision loads. These loads have been calculated by FibreCore, but an intervention by Heijmans and Rijkswaterstaat set them to zero. The exact reason for this is unclear, but also of no importance to this thesis.

For the sake of this research the governing scenario which includes the collision load will be examined. Collision can take place from two directions:

1. From upstream, colliding with the front of the gates
2. From downstream, colliding with the back of the gates

There are also two gates with which the collision can take place:

1. The first gate while approaching the lock
2. The second gate at the end of the locking chamber.

Combining these leads to four possible collision scenario's for which the probability and consequences should be examined to determine whether or not they can be said to be the least favourable. Due to the large difference in sill height between the upstream and downstream of the lock (see Figure 2.7) the downstream collision with the second gate is impossible. Instead the gate will collision with the concrete sill. Any damages caused by this are outside of the scope of this study.

2.5.1. Upstream Collisions

In the case that a ship approaches the lock from upstream the first gate encountered will be the smaller gate and the second gate will be the larger gate, as can be seen in Figure 2.7. The two collision scenario's are compared below in Table 2.6 and briefly discussed in the following paragraph. Note that the criteria are judged relative to each other.

Table 2.6: Comparison of the collision scenario's for upstream collision

Criteria	First Gate (small)	Second Gate (large)
Chance of collision	Low	High
Consequence of collision	Low	High
Favourable load condition	Yes	No

Chance of Collision

The possible causes for collision are discussed in Appendix A.3.1 and the probability of these aspects are discussed in Appendix A.3.2. Herein is stated that collision with the second gate is more likely because a ship will generally not approach the lock if the first gate is closed.

Consequence of Collision

If the gate in question was to fail completely due to the collision it would lose all its water retention capabilities. If the first gate fails this leads to loss of the ability to lock ships and a constant high water level in the lock chamber. If the second gate fails the lock also becomes unable to function, but in addition the hinterland will become prone to flooding due to the formation of a unblocked water corridor. This is illustrated in Figure 2.11. How bad the flooding is depends on whether or not the first gate can be closed in the now flowing water. This is the worse scenario.

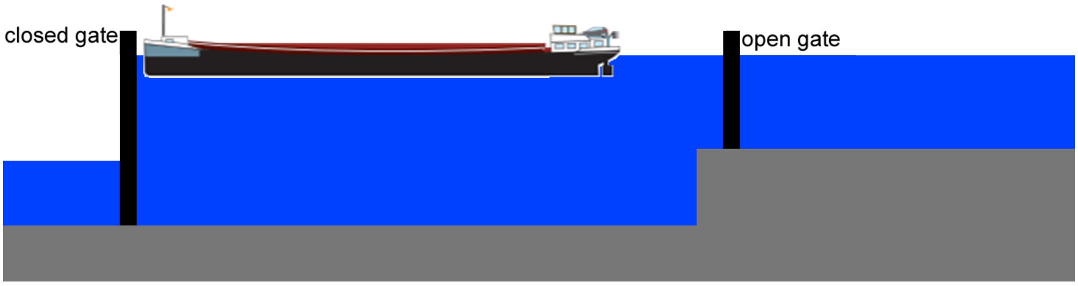

Figure 2.11: Overview of the collision between a vessel and the second gate from a upstream direction

Favourable Load Condition

In the of upstream collision the higher water level is on the side of the ship. Therefore the larger the gate the more water pressure in the direction of the collision load leading to an unfavourable situation.

Conclusion

All three criteria would dictate that the governing upstream collision scenario is a collision with the second gate after the ship enters the locking chamber in combination with the highest level of water retention during which locking still takes place.

2.5.2. Downstream Collisions

In the case that a ship approaches the lock from downstream the larger gate will be encountered first and the smaller gate will be at the end of the locking chamber, as can be seen in Figure 2.7. The two collision scenario's are compared below in Table 2.7 and briefly discussed in the following paragraph. Note that the criteria are judged relative to each other.

Table 2.7: Comparison of the collision scenario's for downstream collision

Criteria	First Gate (large)	Second Gate (small)
Chance of collision	Low	High
Consequence of collision	Low	Low or None
Favourable load condition	Yes	No

Chance of Collision

As with the upstream collision it is more likely that collision takes place with the second gate after entering the locking chamber. This is due to the fact that ships will not approach the lock unless the first gate will be opened for them.

Consequence of Collision

If the collision was to lead to complete failure of the gate then collision with the first gate would lead to the water flowing from the lock chamber down stream. As the second gate would be closed at this time the amount of flooding water is limited to the area of the chamber time the difference in water height. Collision with the second gate may lead to a larger amount of leakage, however due to large difference in sill height between the downstream and upstream gates collision will not take place between a vessel and the upstream gate but rather with the upstream sill. The consequences of such a collision are outside of the scope of this thesis.

Favourable Load Condition

In the case of downstream collision the higher water level will always be behind the door, this force helps the operating mechanism resist the collision force. It can thus be concluded that a larger gate, with potentially a larger water column will be a more favourable load condition.

Conclusion

The collision chance and load conditions would lead one to judge a collision with the second gate as governing. However due to there being no consequences for the gate to this collision a collision with the first gate is more critical. Note that a collision between a vessel and the upstream sill may still cause significant damage and must also be looked into for a complete design. This will not be done in this thesis.

2.5.3. Governing Collision Cases

From the four discussed it has been shown that a collision with the front for the second door from a upstream direction and a collision will the rear of the first door from a downstream direction will be the critical collision scenarios. These will be the collision cases that are considered in Chapter 3. In Chapter 3.4.1 it will be shown that it is not necessary for the rearward collision from the downstream direction to be modelled in more detail. Thus only the frontal collision with the second gate from the upstream direction will be discussed further in Chapters 4 to 6.

Another choice is whether to consider a single high energy collision, multiple low energy collisions or both. Low energy collisions may represent small vessels or low velocities and will make up the bulk of the collisions on the lock gate. The goal of this study is however to judge the cases capability to withstand the governing collision en examine the behaviour as reference for comparable lock gates. Examining low energy collision has no extra value in this respect. It is also not expected that multiple collisions will have any extra impact on the structure as the amount of collision will be too low to initiate any type of fatigue in the structure. For this reason only a single high energy collision is considered in this study.

2.6. Safety Factors

Conform the Eurocode two sets of safety factors will be applied during calculation. A set of load factors which can be obtained directly from the Eurocode[10] and a set of resistance factors which represent uncertainties in the structure. The structure meets the strength requirements when the following is valid:

$$Load * Load\ Factors < \frac{Resistance}{Resistance\ Factors} \tag{2.4}$$

As it is a rare and extreme case which is under consideration the load factors may to chosen as equal to 1, effectively removing them from the equations[10]. The resistance factors however still play an important role. For structure made from FRP there are multiple factors which must be taken into account with their roots is different uncertainties to do with a material. For FRP this is generally caused by the fact that the properties are strongly dependant on the production process and degree of curing. These factors are shown in Table 2.8 and an extensive explanation behind the choice of these factors is given in Appendix F.2.1.

Table 2.8: Applied resistance safety factors derived from material attributes [11]

Accounts For	Factor	Notes
Material Properties	1.35	Standard FRP practice
Production Method	1.2	Post Cured Vacuum Moulding
Temperature	1.1	Standard FRP practice
Moisture	1.3	Constant contact with water
Fatigue	1	Single Loading
Creep	1	Very Short Loading
Total	2.32	

3

Analytical Collision Analysis

The collision between a vessel and a lock gate is dependant on many aspects, making it a complicated event to model. A simple model, such as will be discussed in this chapter, will result in the basic behaviour. While in order to obtain more detailed results which take all the boundary conditions into account either a complicated and unwieldy analytical model or a finite element model should be used. The latter will be done in Chapter 4.

The model here serves to gain a basic understanding of the situation and as comparison for the results of the numerical analysis. This greatly reduces the chances of errors originating from modelling errors or misinterpretation. In this chapter the collision scenarios will be simplified to the point that they can be efficiently solved without the use of finite element software and preliminary conclusions will be drawn. Also any form of non-elastic deformation of the ship will be ignored. These deformations will be discussed in Chapter 6.

The first step which is taken, is defining the model which will be used. This model consists of geometrical assumptions, physical parameters (such as velocity and damping) en load scenario's and will be detailed in Chapter 3.1. Then in Chapter 3.2 the difference between the FRP design presented and a traditional steel design are elaborated on. The model which will be used is a series of two mass damper sets and is illustrated in Chapter 3.3. In order to gain some understanding of how the model reacts three sets of analyses are executed, static, differential and numerical. These are described in Chapter 3.4 along with the obtained results. Finally the conclusions that can be drawn from these results will discussed in Chapter 3.5.

Displacements are used as governing physical quantity as they can be easily related to the spring system and the stresses in the outer fibres. This is important as the failure point of the the laminate is known with regard to stresses, but the spring system does not give stresses as outputs. Converting both to displacements allows for easy comparison. This conversion will be explained further in Chapter 3.1.8.

3.1. Modelling Aspects

Because the real world collision is complicated in many ways some simplifications need to be made for the analytical calculations. In the following chapters multiple analysis types will be used to determine the collision behaviour, their analysis specific modelling aspects will be discussed then. The aspects which are shared by all analyses are treated in this chapter.

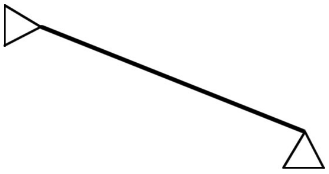

Figure 3.1: Simply Supported Beam

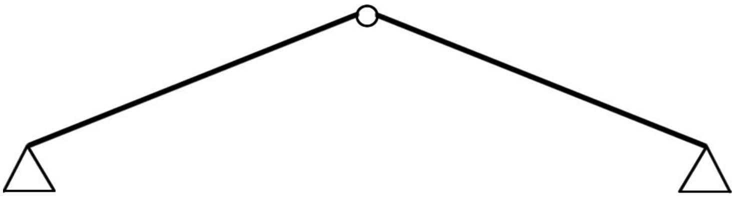

Figure 3.2: Three Hinged Beam

3.1.1. Static System

In order to quantify the behaviour of the gate after collision a static system of supports must be chosen from which values such as geometry and stiffness can be determined. This is done with the governing collision scenario from Chapter 2.5.3 in mind.

Mitre gates can also be seen as double leaf gates. The most simple static system for mitre gates is treating each gate separately as a beam on two hinged supports (see Figure 3.1). In this model the contact point between the two gates is said to be stationary and all load at the centre support is transferred to the other gate. The advantage of this model is the simplicity, making calculations brief. The disadvantage is that a degree of simplification is high. In reality the centre point will shift and won't act as a true hinge due to frictions.

A way to make this model slightly more accurate would be to model both gates together connected by a hinge (see Figure 3.2). In this composition the centre point is free to shift as long as the gate tips remain in contact with on another. This is an accurate representation for upstream collision and is preferred with regard to the beam on two supports. However the deformations of the gate which is not impacted will be relatively small due to the axial stiffness of the gate being larger the the bending stiffness, so the difference between the two models will be small. The minor increase in accuracy is not worth the added complexity of the model and thus a model with a beam on two supports will be satisfactory. For all the analytical calculations below this is the model of choice.

If it is desirable to examine the difference in displacements over the vertical axis then the gates must be modelled as plates instead of beams. The above considerations are still valid by means that the gates can either be modelled separately or with a connecting hinge. A third option is the introduction of a sill support along the bottom of the gates. This extra support was not included in the original calculations as this was a conservative choice, but seen as it could alter the stress and deformation pattern in the gates it can not simply be ignored. This system will be used for the calculation done with Ansys, in which the complexity is less of an issue. See Figure 3.4 for the static scheme which will be used for the numerical calculation. It is that which includes plate elements, has a sill support and the second gate has been modelled by a support. A noteworthy difference between this model and the model with beams is that the chamber wall is modelled as a fixed support. This is due to the fact that in reality there are two support points at a 90 degree angle from one another, this allows them to retain a moment at the support. This can be seen in Figure 3.3. The numerical model will be explained more in Chapter 4.

For the above models the assumption has been made that the gate will remain in contact at the centre point. However if collision takes place from the inside of the gates (see Chapter 3.1.2) this no longer holds. For such a collision from downstream the gates must be modelled separately because they will be pushed apart by the collision. The governing static scheme is shown in Figure 3.5 and is a beam supported by a hinge at one side and a spring part way down the beam. This spring represents the operating mechanism which is the only support preventing free rotation.

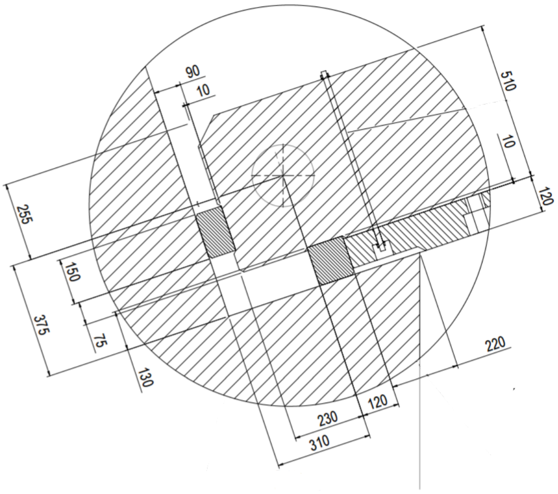

Figure 3.3: Detail of the chamber wall support, with two perpendicular support points

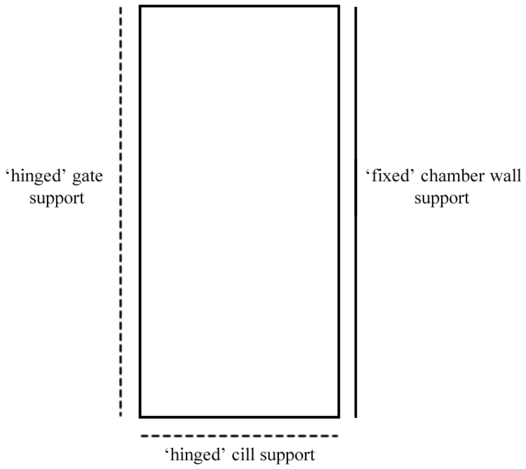

Figure 3.4: Static scheme including plates

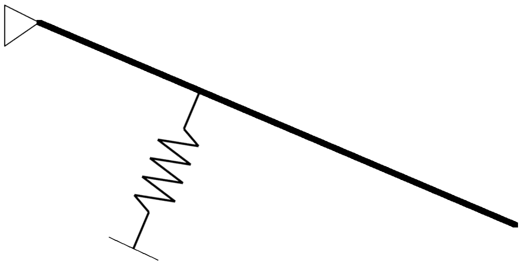

Figure 3.5: Static scheme for the rearward collision

3.1.2. Collision Orientation

The response from the structure is dependant on the magnitude, location and angle of the applied force. In essence there are six possible collision orientations:

1. Collision with the left gate from the front
2. Collision with the centre point from the front
3. Collision with the right gate from the front
4. Collision with the left gate from the back
5. Collision with the centre point from the back
6. Collision with the right gate from the back

Due to symmetry the collisions with the left and right gate are identical reducing the amount of collision scenario's to four. (see Figure 3.6)

These four scenario's have different normative vessels due to dimensional limitations. Simply said a vessel can only impact the gates at a distance from the walls of at least half of the ships breath. This is illustrated in Figure 3.7. In Chapter 2.5.1 it is discussed that the governing scenario is the case in which the ship has already entered the lock. These consideration leads to the following collision scenario's

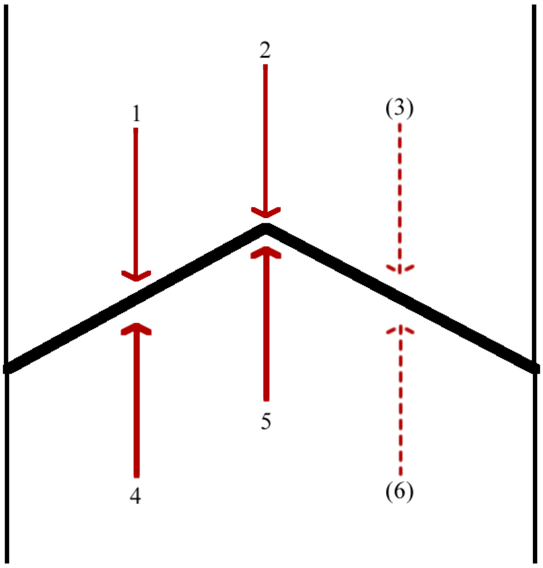

Figure 3.6: Overview of the collision scenario's. Number between brackets represent symmetrical loads

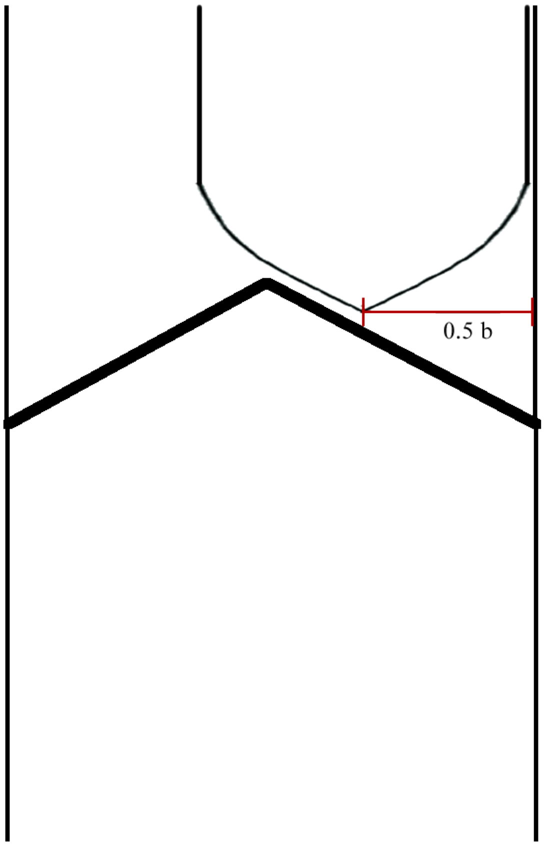

Figure 3.7: Top view showing the geometric limitations of collisions

for both frontal and backward collisions:

1. A Class IV ship in the chamber centre.
2. A Class III ship 1.15 metres from the chamber centre.
3. A Class II ship 1.95 metres form the chamber centre.
4. A Class I ship in the middle of the gate, at 2.62 metres from the chamber centre.

The angle of collision is limited by the geometry of the lock chamber. As the ship passes through a narrow section before colliding with a gate this angle will always be small and have little impact on the collision as a whole. If the ship were to collide at an angle the forces would cause it to rotate and the back of the ship would make contact with the chamber wall. Both the rotation and the additional impact will dissipate extra energy relieving the gate somewhat. For these reasons the governing scenario is assumed to be that with a vessel parallel to the lock chamber.

In scenario's in which the collision takes place with the first gate the angle of the ship may be slightly larger. It is however still limited by any guidance works installed to aid the ships approach. Such works are often constructed at an angle of 1:6 as illustrated in Figure 3.8 allowing for a collision angle of 9.5 degrees. Such a small angle will have little effect on the collision, but can be taken into account for cases in which the first gate is governing.

3.1.3. Hydrodynamic Added Mass

The amount of energy which needs to be dissipated during collision is linearly dependant on the mass of the colliding bodies. When given the class of the governing vessel the maximum mass of the vessel

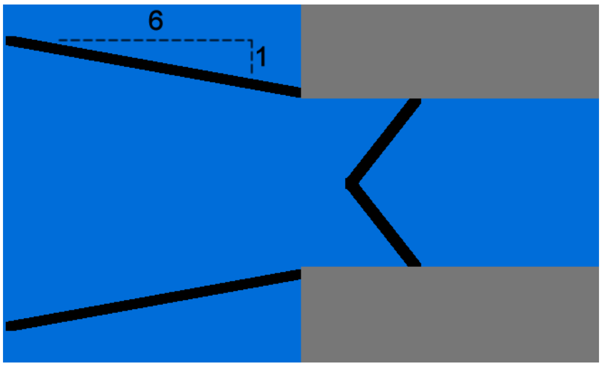

Figure 3.8: Overview of the first gate with guidance works

is a known quantity. The unknown aspect is the amount of water that is also moving towards the gate which needs to be slowed. This hydrodynamic added mass is a source of uncertainty in collision calculations on which much research has been done.

It is generally accepted that the hydrodynamic added mass can best be introduced as a factor on the mass of the ship, in literature the symbol C_m is often used. The magnitude of this factor is strongly dependant on the conditions surrounding the collision and can best be determined through (scaled) testing or through comparison to literature [12] en [13]. For example [14] found a factor of 1.4 for a vessel colliding frontally into the side of another vessel.

For frontal collision against structures, which is the most similar to the situation in question, the ROK 1.3 [15] prescribes a factor of 1.1. While [16] continues on this proclaiming that tests of frontal collisions with rigid structures show values of C_m ranging from 1.0 to 1.1, making 1.1 a conservative estimate.

Seen as the range of variation for the comparable case in literature is relative narrow a value of 1.1 will be assumed in the calculation to follow. The sensitivity of this factor will be examined to determine whether it is defensible to assume such a value or if scaled tests need to be executed to determine a more accurate value.

3.1.4. Collision Velocity

The collision velocity in all analyses will be taken as 3.33 m/s. This is the value defined by FibreCore for calculation of the gate in question and matches statistical data as found by Het Waterloopkundig Laboratorium. This is a high value, but serves to illustrate the worst of collisions. It is important that there is no loss of water retention due to collisions of this magnitude as the lock gate protects the centre of Tilburg from 7.9 meters of water. The statistics behind this value are discussed in Appendix A.3.3. This velocity must then be reduced to take the angle of the gate into account. The gate has an angle of 1:3 so the velocity perpendicular to the gate and parallel to the gate are respectively:

$$v_{perp} = 3.33 * \frac{3}{\sqrt{10}} \tag{3.1}$$

and

$$v_{para} = 3.33 * \frac{1}{\sqrt{10}} \tag{3.2}$$

These velocities will be used in any model in which energy is dissipated by both a bending and compression mode. These are frontal collisions in which the gate is not impacted at a support (Ship class 1-3 collisions). As such the collision velocity used later in this chapter represents v_{perp}.

3.1.5. Model Stiffnesses

In the considered models of a frontal collision between a vessel and a structure the elements will be simplified as spring to start off with. The details on this will be further discussed in Chapter 3.3. For now it will suffice to say each component of the collision will be represented as a spring with a given stiffness which is between zero and infinity.

Gate Stiffness

The stiffness given to the gates spring is dependant on both the gates properties as given in Chapter 2.4.2 and the collision orientation as given in Chapter 3.1.2.

For the cases in which the gates are loaded at their ends (the centre of the locking chamber) they will be primarily axially loaded. The stiffness of the spring is then dependant on the length of the gate [l] and the combined EA modulus of the inhomogeneous cross section. A weighted average can be used or the individual contributions can be summed up (See Chapter 2.4.2). The stiffness of the gate spring is then:

$$k = \frac{EA}{l} \tag{3.3}$$

For cases in which the gates are impacted part way along their length they will be loaded in bending. The stiffness of the gate spring is then dependant on the length of the gate [l] and the combined EI of the inhomogeneous cross section. See Chapter 2.4.2 for the calculation of this EI from the individual contributions. If the gate is impacted halfway along its length the gate spring stiffness will become:

$$k = \frac{48EI}{l^3} \tag{3.4}$$

If the collision is off-centre this expression become somewhat more complex. If we define the distance between the point of collision and the centre of the locking chamber as a, the gate spring stiffness will be:[17]

$$k = \frac{9\sqrt{3} * l * EI}{a(l^2 - a^2)^{3/2}} \tag{3.5}$$

With the maximum deflection being located at a distance x from the centre of the chamber. With x being:

$$x = \sqrt{\frac{l^2 - a^2}{3}} \tag{3.6}$$

Ship Stiffness

For this first set of analyses a ship shall be considered either as an infinitely stiff element or as a simple spring. If it is assumed to be infinitely stiff the gate will be forced to retain all the displacement energy which will result in a conservative solution for the gate displacements. If instead it is given a finite stiffness the vessel will also retain some of the introduced energy reducing the load on the gate. The amount of energy retained by the ship is dependant on the ratio between its stiffness and that of the gate. This ratio 'n' is calculated here by taking the elastic stiffness of the front portion of the ship and comparing to the the bending/compression stiffness of the gate. The obtained ratio's are shown in Table 3.1. In Chapter 6 this model will be refined to incorporate aspects such as ship failure and change of cross-section.

Spring theory dictates that if two springs are loaded in series, in this case the ship and the gate, the amount of energy they will each store will be related to their stiffness ratio. From the spring energy equation (Equation 3.7) it can be seen that the less stiff spring will contain more energy due to the

Table 3.1: Calculated stiffness ratio's per ship class (See Chapter 6)

Ship Class	I	II	III	IV
Stiffness Ratio	21.8	23.9	17.2	1.9

indentation being quadratic. It can be said that if the gate spring is 'n' time less stiff (ratio=n) it will retain $\frac{n}{n+1}$ of the energy.

$$Spring\ Energy = \frac{1}{2}k * x^2 \tag{3.7}$$

Operating Mechanism Stiffness

In the case that the gate is impacted from downstream the balancing force must come from the retained water level and the operating mechanism. This operating mechanism is generally a hydraulic system with limited flexibility. Instead of a stiffness being dictated there is a maximum accepted load after which the hydraulics give out voluntarily to prevent (expensive) damage. For the calculation the system can be assumed to have infinite stiffness while under its force threshold and no stiffness above this limit. In practice this will mean that the lock gate fails once this force is reached. For the gates in question this maximum load level is defined as 114kN [2].

3.1.6. Energy Dissipation Mechanisms

During collision the energy which is introduced to the system by the vessel is dissipated in many different ways. The collision can be said to be over once the amount of dissipated energy is equal to the amount of introduced energy. The most significant dissipation mechanisms for the collision in question are:

- Permanent deformation of the gate
- Permanent deformation of the ship
- Turbulence in the lock chamber
- Acceleration of the water behind the gate
- Friction at the 'hinged' supports
- Rotation of the ship
- Horizontal translation of the ship
- Permanent damage to the gate
- Permanent damage to the ship
- Friction between the ship and gate

In most cases the exact amount of energy removed by each mechanism is difficult to determine without detailed tests and so many of the above mentioned phenomena are summarised as a damping coefficient. This coefficient can only be estimated and will be varied during the analyses to follow to determine the sensitivity. If a more detailed value is desired physical experimentation is required.

3.1.7. Load

In most of the following analyses the load on the system in introduced as a source of energy which must be either dissipated of stored by the system. An exception to this is the solution via differential equations in which the system is loaded by boundary conditions, in this case an initial velocity. This case will be discussed separately below. Furthermore situations will be examined in which the ships motor has failed to be disengaged. The load which this introduced to the system will also be discussed here.

Load by Energy

The amount of energy is determined by the kinetic energy of the vessel and is thus dependant on the mass and velocity of the ship by the formula:

$$E_{ship} = \frac{1}{2} * m * v^2 * C_H * C_E * C_S * C_C \tag{3.8}$$

In which:

m	is the mass of the ship.
v	is the velocity of the ship.
C_H	is the hydrodynamic coefficient defined as $\frac{mass\ ship + water}{mass\ ship}$.
C_E	is the eccentricity coefficient.
C_S	is the softness coefficient.
C_C	is the configuration coefficient.

The four coefficients can be defined as follows:

- C_H represents the hydrodynamic mass which is moving together will the vessel. The Dutch codes[15] prescribe a value of 1.1 for this coefficient.
- C_E represents the yawing of the vessel during collision and the energy loss that accompanies it. As the collision considered here is considered to be frontal with minimal rotations a value of 1 can be used. This is also a conservative approximation.
- C_S represents the softness of the ships hull with respect to the structure. As the structure is made of FRP which is a relatively soft material this coefficient is taken as 1.
- C_C represents the energy dissipation due to water being squeezed away from the area between ship and lock gate. This effect will play a role in the collision considered but the effect will be combined with the other dissipation mechanisms. A value of 1 is chosen

With these coefficient defined the kinetic energy equation reduces to:

$$E_{ship} = 0.55 * m * v^2 \tag{3.9}$$

This energy is either stored in the gate and ship and elastic potential energy, or dissipated through the above mentioned mechanisms. The manner in which this happens is strongly dependant on the solution method and will be explained in the corresponding Chapter 3.4.

Load by Velocity

When a solution for the collision dynamics is obtained through use of the differential equation an energy input is not feasible. Instead the load must be introduced through a combination of initial conditions, displacement and velocity, and a load F(t). Seen as the input energy was directly derived from the velocity of the vessel it makes sense to input it into the differential equation as a initial velocity equal to the ships velocity at impact, taking into account the angle of impact with regard to the deformation model assumed.

Ships Engine Load

For cases in which the ships motor remains active during and after collision an extra force is introduced. This force is caused by a constant engine power pushing against the structure, this introduces energy to the system equivalent to the engines power. The choice was made to introduce this energy as an equivalent force. The force which coincides with such an influx of energy is dependant on the characteristics of both the ship and the structure. The derivation of this force is discussed here.

We consider a state of equilibrium in which the vessel is in contact with structure and all other sources of energy have been dissipated. The engine will exert its power onto the structure which in turn will be deformed a certain amount [w_{gate}]. The structure will in turn exert an equal amount of power on the ship to remain in equilibrium. If the structure is modelled as a spring, the force acting between the two bodies can be calculated through Hooke's Law as:

$$F = w_{gate} * k_{gate} \tag{3.10}$$

The engines power is a known quantity [W_{engine}] which, in order to maintain equilibrium will be equal to the theoretical power of the spring [W_{spring}]. A power by definition is an amount of work done per unit of time (often seconds). Work is in turn defined as a force acting over a certain distance. This leads to the following expression for W_{spring}:

$$W_{spring} = \frac{F_{spring} * \Delta x}{t} \tag{3.11}$$

Hooke's Law defines F_{spring} (Equation 3.10) and Δx represents the distance over which the spring would be able to exert the force F_{spring} if there was no resisting force. In this case the spring will apply an acceleration [a] to the influenced mass [m], which in accordance to the second law of Newton will be:

$$a = \frac{F_{spring}}{m} \tag{3.12}$$

As the bodies are in rest to begin with the distance an object is moved when subjected to an acceleration a is:

$$\Delta x = \frac{1}{2} a * t^2 = \frac{1}{2} * \frac{F_{spring}}{m} * t^2 \tag{3.13}$$

Bringing this all together an expression for the spring power is obtained which must be equal to the power from the engine for equilibrium. This leads to the following equilibrium:

$$W_{engine} = \frac{1}{2} \frac{F_{spring} * F_{spring} * t^2}{m * t} = \frac{1}{2} \frac{w_{spring}^2 * k_{spring}^2 * t}{m} \tag{3.14}$$

The power of the spring appears to be a function of time. As we are considering an equilibrium situation this should not be the case. The reason behind this is that the above formula allows the spring to accelerate at a constant rate, increasing its velocity and with it the amount of work that can be done. In reality the spring will not accelerate due to it being in equilibrium with the force exerted by the ships bow. If we were to allow the ship to also accelerate at a constant rate indefinitely its power would also increase the longer the time interval was taken. Effectively the ships power would become a function of t:

$$W_{engine} = W_{engine} * t \tag{3.15}$$

This model ignores all forms of friction as well as the fact that the spring force would also decrease as a function of time if allowed to accelerate. These assumptions only hold in the case of a kinematically stable situation between ship and gate. That being said this model is only an approximation, for an exact result collision mechanics should be applied. If the effects of the engine forces appear to be significant this should be done. The assumptions above lead lead to the following equilibrium:

$$W_{engine} * t = \frac{1}{2}\frac{F_{spring} * F_{spring} * t^2}{m * t} = \frac{1}{2}\frac{w_{spring}^2 * k_{spring}^2 * t}{m} \tag{3.16}$$

The indentation of the spring at equilibrium is then:

$$w_{spring} = \sqrt{\frac{2 * W_{engine} * m}{k_{spring}^2}} \tag{3.17}$$

Again using Hooke's Law (Equation 3.10) we obtain an expression for the force between the two bodies which can can be used for further calculations.

$$F = k_{spring} * \sqrt{\frac{2 * W_{engine} * m}{k_{spring}^2}} \tag{3.18}$$

3.1.8. Loading Capacity of the Gate

As the output of the models will be expressed as a displacement the loading capacity will be expressed as a maximum allowed displacement. This is possible as the the stress can be rewritten as displacements with the governing bending mode in mind. This is done in the following manner.

The amount of displacement that the gate is able to resist is directly related to the allowed stress in the material. This stress is determined with the known values for the E-modulus of the skin and the allowed strain of Glass Fibre laminates through Equation 3.19.

$$\sigma_{allowed} = E * \epsilon_{allowed} \tag{3.19}$$

The E-modulus for the skins in the direction that the load will be carried is equal to 32300 N/mm^2 for the bending cases and 27188 N/mm^2 for the axially loaded case. This second value is the results of the weighted average of the E-moduli of all the separate laminates. The allowed strain has two values depending the whether we are interested in damage or failure. Theses limits are 0.27% for damage and 1.2% for failure[18]. At a strain of 0.27% the first resin begins to crack, but the laminate maintains it's strength. This represents the SLS state of the material as surpassing it will decrease the durability of the material, especially with regard to moisture. The strain of 1.2% represents the ULS and the structure is considered to have failed once this level is reached.

Now that the allowed stress and the cross-sectional geometry are known along with the point of impact simple mechanics can be used to determine at which force the maximum stress level will be reached. The corresponding moment is obtained from:

$$\sigma = \frac{M}{W} \tag{3.20}$$

with

$$W = \frac{I}{\frac{1}{2} * h} \tag{3.21}$$

With the static scheme showed below in Figure 3.9 the load F which coincides with this moment is:

$$F = \frac{M * (a + b)}{a * b} \tag{3.22}$$

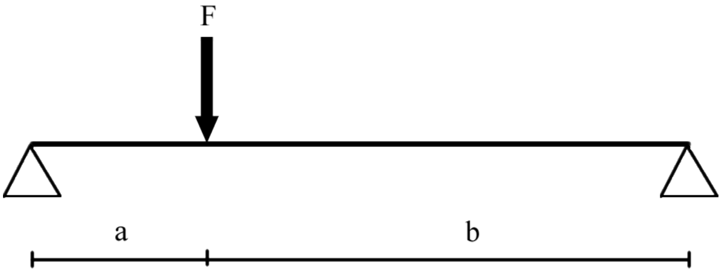

Figure 3.9: Static scheme for the case with non-central collision

Finally this F can be related to a displacement with the known spring stiffness of the gate. For the axially load condition the allowed force can be found directly through the EA modulus and again related to a displacement via a k factor.

The displacements found assume there are no safety factors applied to the structure or the materials. As this is not the case the governing safety factor must be applied to the allowed stresses before calculation. The governing safety factor is 2.32 as determined in Chapter 2.6. As we are interested in only the displacements due to collision the deformed state of the gate before the collision due to water pressures should be subtracted from this number.

$$w_{collision} = w_{total} - w_{water} \tag{3.23}$$

This reduction included creep behaviour for the long term water pressure and is equal to 15.3 mm. The resulting allowed displacements for each collision case, each $\epsilon_{allowed}$ and with/without safety factors are given in Table 3.2

Table 3.2: Allowed displacements for the gate during collision [mm]

Ship Class	Damage Limit (ϵ=0.27%)[18]		Failure Limit (ϵ=1.2%)[18]	
	No Safety Factor	With Safety Factor	No Safety Factor	With Safety Factor
Class I	105.3	45.4	468.2	201.8
Class II	114.3	49.2	507.8	218.9
Class III	110.6	47.7	491.4	211.8
Class IV	15.6	6.7	74.1	31.9

3.2. Difference to Steel Designs

When designing or evaluating a structure composed of FRP laminates the procedure is different than when compared to steel, which is by far the dominant choice for lock gates at present. Although there are a lot of differences both small and large they can be summarised in three main aspects.

Stress strain relationship

The shape of the force-displacement diagram is drastically different as can be seen in Figure 3.10. Especially for Glass-Fibre laminates it can be seen that its stiffness is much lower, but it lacks the yield point that steel has. Because of this a structure made of GFRP can be loaded to a higher level at failure, but will have much larger displacements for lower stress levels. Whether or not this is an advantage depends on what the limiting scenario is within the design. If displacements are expected to cause issues then extra precautions will have to be taken to prevent them. This effect is less pronounced for Carbon Fibre laminates but these have the disadvantage of being very expensive and susceptible to loads in the non-dominant direction (See Appendix D).

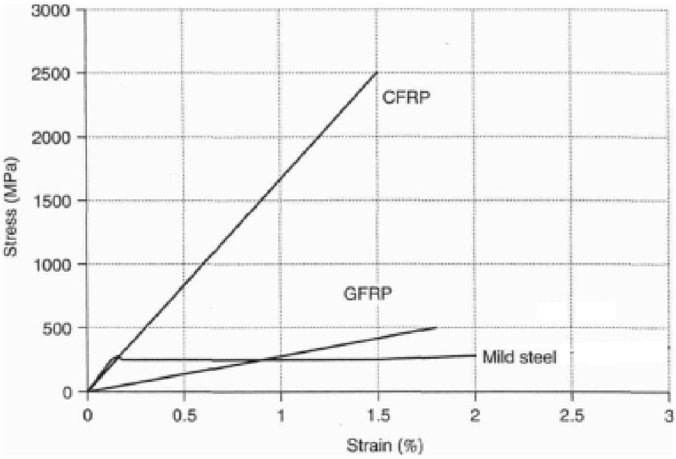

Figure 3.10: Typical FRP and mild-steel stress-strain curves[19]

A further effect of the lack of a yield point is that FRP structures show no plastic behaviour, they are elastic up to their failure point. Instead at a strain of 0.27%[18] the outer layer of the resin will start cracking, but the fibres will remain intact. This is considered as the first damage limit. As most of the laminate and all of the fibre are still functional further stresses can be resisted up to a limit of 1.2%[18] strain. At this point the outer fibres will begin failing and the structure is said to have failed.

The lack of the ability to form plastic hinges does change the design capacity significantly for a lot of structure types. For example the plastic analysis of lock gates suggested by Loïc Buldgem in his PhD work [20] in which the plate is assumed to develop plastic hinges allowing for model displacements becomes completely invalid. Instead elastic theory must be followed, which has a significant effect especially around joints and supports.

Orthotropic Behaviour

Steel in a uniform material which leads to strictly isotropic material properties. This makes many calculations a lot simpler as a direction of the loading doesn't affect material properties. With FRP structures the same cannot be said. The fact that fibres are significantly stiffer than resins makes the properties of a laminate dependant on their orientation. For calculations this means splitting the load scenario's per direction and may require more advanced software (if used). It is worth mentioning that even if the laminate is constructed in such a way that it's properties are roughly isotropic in its plane its strength would always be lower out of its plane where resin interfaces between fibre plys will have a carry large loads. For more information on this see Appendix D.

Customisability

The final difference is the ease with a FRP laminate can be customised to carry the desired load. Because every ply of the laminate can be chosen and these ply do not need to be constant through the entire structure the material can be adapted with the load field as a given factor. This is a complex procedure which requires a good understanding of the behaviour of FRP. In general having more fibre in the direction of the dominant load is beneficial and cross fibres can be added to retain concentrated loads of high levels of shear. More details on this is given in Appendices E, F and D.

3.3. Collision Model

For the analytical calculations the system will be represented by a mass connected to a reference stationary point via springs and dampers. Both the ship and the gate will each be modelled by a spring and a damper in parallel and these pairs themselves are set in series. In Figure 3.11 below this system is shown along with the spread of forces and energy. The interfaces between spring damper sets are considered infinitely stiff and irrotational. It can be seen that the load F which is introduced to the system will load both element pairs entirely while within each pair the load is spread over the spring and the damper. For energy in the other hand the total of all four elements will equal the input energy.

The masses of the gate and the ship with its added water mass are located together on the interface between the ship and the gate. This does not match the geometry of the real situation but as we are only interested in the deformation of the gate spring this model is sufficient. Water mass behind the lock which is activated by the collision is considered a damping process and incorporated in the gate damping factor.

The outputs of these analyses will be indentations of the springs, which coincide with the displacements of the gate. As the gate itself is isn't modelled directly, but used to determine the spring stiffness, no stress outputs are possible. However this isn't an issue if localised stresses are ignored, which is the case here, as the displacements can be converted to the stresses from pure bending through use of basic mechanics. As is discussed in Chapter 3.1.8.

The formulae with regard to the force and energy equilibrium are supplied in Figure 3.11.

3.4. Performed Analyses

In this chapter a series of analytical analyses will be performed based on three calculation methods: static analysis, differential equations and numerical programs. These analyses will be elaborated further on. Using these analysis types the collision will be examined to acquire values for the maximum displacements of the gate in question. in this manner a degree of failure can be determined. These analyses will be done for CEMT Class I-IV ships. Furthermore attention will be paid to the importance of the ships stiffness and the load supplied by the ships engine.

3.4.1. Static Analysis

The first analysis performed is a simple static analysis. In this case most of the complexities are removed from the model to obtain an idea as to the structures response. The results of such a static analysis give limited information about the deformation process as the output contains no time dependant information and consists of only a final deformation. The lack of information on velocities means the contributions of the systems dampers can not be determined except by adding a dissipation factor to the calculations. However because the level of dissipation is hard to predict it will be neglected completely for these first calculation, making it a very conservative upper limit of the displacements.

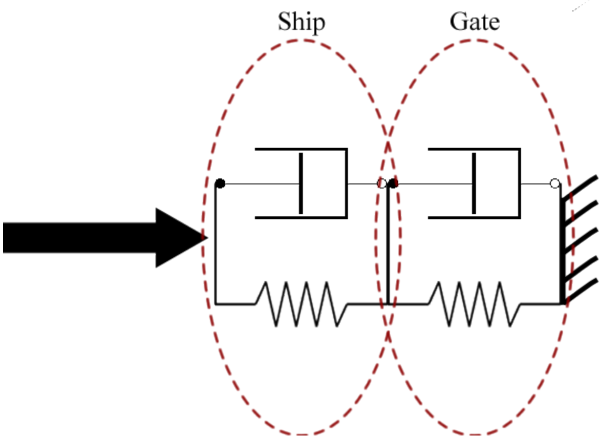

(a) Schematic System

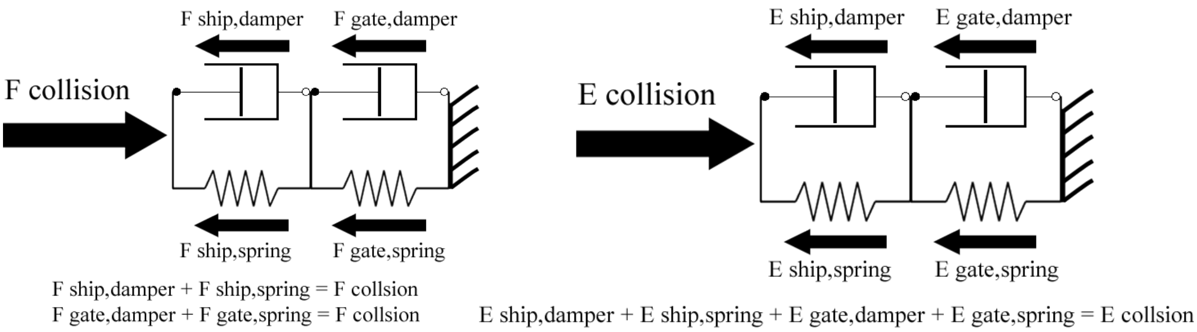
F collision
F ship,damper
F gate,damper
F ship,spring
F gate,spring
F ship,damper + F ship,spring = F collsion
F gate,damper + F gate,spring = F collsion
E collision
E ship,damper
E gate,damper
E ship,spring
E gate,spring
E ship,damper + E ship,spring + E gate,damper + E gate,spring = E collsion

(b) Force Distribution

(c) Energy Distribution

Figure 3.11: Spring Damper system used and the distribution of the physical quantities

Calculations

The ships attributes will be handled to two ways. First the calculation will be done assuming that a ship is infinitely stiff, second a ship stiffness will be added and the results will be compared. The results with a infinitely stiff ship will be the least favourable for the gate as all the energy will have to be taken by the gate. For the second calculation the complex buckling behaviour of the vessel will be ignored and the ships stiffness will be assumed to be that of the first buckling segment as given in Table 3.1.

As damping is not taken into account for the static calculation the systems from Chapter 3.3 reduce to the two systems from Figure 3.12:

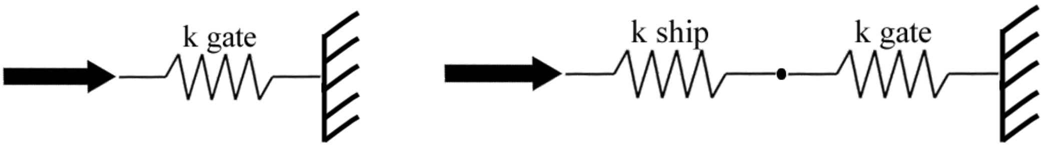
k gate
k ship
k gate

(a) Infinitely stiff ship

(b) Compressible ship

Figure 3.12: Static collision systems with and without ship deformations

For the first system the displacement can be calculated equating the ships energy to the springs energy.

$$\frac{1}{2} * m * v^2 = \frac{1}{2} * k * w^2 \tag{3.24}$$

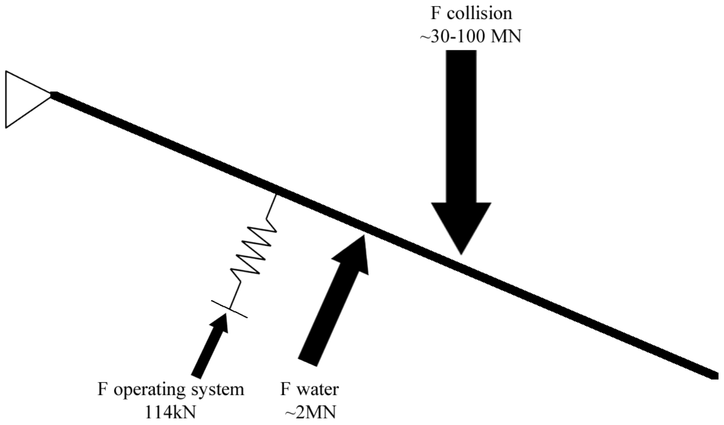

Figure 3.13: System of forces for a rearward collision, including order of magnitude

For the second system the same approach can be used but the left hand side must be multiplied by a factor $\frac{n}{n+1}$ in which n is the ratio between the ship stiffness and the gates stiffness. In both systems for the case in which a class IV vessel collides with the centre point the left hand side must be halved to account for the energy being spread over two gates.

The static calculations were also used to illustrate the dependencies between different physical entities. Diagrams showing the relationship between mass-displacement, mass-energy, velocity-displacement and velocity-energy are given in Figures I.1 to I.3 and discussed in Appendix I.

Results

The calculations described above result in the deflections shown in Table 3.3. The found deflections for classes I-III are higher than the damage limit but below the failure limit of the structure, however for class IV the failure limit is reached for the case n=∞.

Table 3.3: Results of the static analysis for the four classes of vessel with varying ship stiffness

Ship Class	Ratio n	Deflection n=∞[mm]	Deflection n≠∞[mm]	Force in Spring [MN]
Class I	21.8	68.0	65.9	37.6
Class II	23.9	90.2	87.6	61.5
Class III	17.15	86.9	84.5	91.3
Class IV	1.9	36.5	29.4	207

Failure of the Operating Mechanism

The magnitude of the load in the spring can be used to determine whether or not the operating mechanism will reach its load limit due to a collision with the back of the gate. We can see that the exact load depends on models properties but it will be in the order of magnitude of 30-200 MN. If we examine the static system with this applied force (as shown in Figure 3.13) it become clear that the operating mechanism will not be able to resist such a load and failure will occur unless extra measures are taken. The degree of failure is so large that the exact force and exact placement of the collision no longer matter, the operating system will give out nonetheless. This failure will result in the opening of the gates and possibly some local damage to the laminates. The consequences of this is that the chamber will empty and the water will flow over the ship, as this water column may be up to 7.9 metres in height this could cause major safety issues and secondary ship collisions. The effects of such a failure and possible prevention measures are outside the scope of this study.

Chapter Conclusions

The results of the static calculations form a point of reference and upper bound for the other more complex calculations which are to be done. They supply an order of magnitude for the deflections and forces while remaining simple to execute.

If the found displacements are compared to the allowed displacements found in Chapter 3.1.8 it becomes apparent that in all cases the damage limit of the structure be reached. This will mean the reparations will be needed but the structure doesn't critically fail except for the case with a collision with a Class IV ship for which the failure limit is also reached. Considering that this is a conservative approach ignoring damping it would seem that the lock gate in question is safe for collisions with all but the heaviest class of ship. However it is still worth using a more complex model to look at the collision to determine a scale for the degree of damage we an expect.

As a final note it is worth mentioning that the class IV collision would not cause failure in the case the the material safety factor is not applied. This bode well for the future when this safety factor will likely go down as familiarity with the material increases. A similar effect has taken place for steel and concrete to the point that these material factors approach 1.

3.4.2. Differential Equation

Executing the analysis in a dynamic manner instead of the aforementioned static approach allows for the inclusions of damping in the equations as well as an output of the collision progression as a function of time. The first series of dynamic calculations are executed via the differential equation defined as:

$$F(t) = m * \ddot{w}(t) + c * \dot{w}(t) + k * w(t) \tag{3.25}$$

In which:

F(t)	is the applied load as a function of time.
w(t)	is the displacement as a function of time
m	is the vibrating mass of the ship, the gate and the added water mass
c	is a factor representing the resistance of the damper.
k	is a factor representing the stiffness of the spring.
˙	represents the derivative with respect to t.

The mass m is the total vibrating mass and is defined by:

$$m = Mass\ of\ Ship * Factor\ for\ added\ water\ mass + Mass\ of\ Gate \tag{3.26}$$

The mass of the gate is known as 22 tonnes[2] and the factor for added water mass is 1.1 as discussed in Chapter 3.1.3. The mass of the ship can be determined by the amount of water it displaces as the dimensions and draught of the governing ship to known from Appendix B. The values of m is then dependant on the ship class and are shown in Table 3.4.

The damping of the system is represented by c. The value for this coefficient is calculated by choosing a relative damping factor ξ and calculating c with the equation:

$$c = 2 * \xi * \sqrt{k * m} \tag{3.27}$$

The analyses in this chapter are executed with a ξ value of 0.5 as will be discussed in Chapter 3.4.2. The c values that coincide with the ξ are dependant of ship class, due to the inclusion of m, and are given in Table 3.4.

The k-values are related to the stiffness of the gate and can be calculated with Equation 3.5 for classes I-III and by EA/l for class IV ships due to the compressive load condition. The gate responds in a much stiffer manner when loaded compressively which leads to the significantly larger value. The m, c and k values are also supplied in Table 3.4.

Table 3.4: Values used in the differential equation

Ship Class	m [kg]	c [Ns/m]	k [N/m]
I	$0.49*10^6$	$1.25*10^7$	$3.17*10^8$
II	$1.06*10^6$	$2.02*10^7$	$3.87*10^8$
III	$1.53*10^6$	$3.01*10^7$	$5.93*10^8$
IV	$2.24*10^6$	$11.02*10^7$	$54.13*10^8$

The load of the vessel onto the system in introduced through the initial conditions instead of through F(t), in this case that is an initial displacement of zero and an initial velocity of 3.16 as discussed in Chapter 3.1.4. This choice was made because the initial energy is a known quantity, while the force is a yet unknown function of time. Defining this force ahead of time would require assumptions to be made as to the displacements of the gate which is the quantity we are trying to determine. Using initial conditions instead remove some iteration steps in the process. The trade-off is that the gate is assumed to instantly reach the velocity of the vessel, which is not accurate and would cause the gate to be loaded by an infinitely high load for a infinitely small time period. This discontinuity is an error in the model at time t=0. This error is accepted for these analyses due to the fact that it has little effect on the global deformations of the gate, which is what is being examined here. For an analysis of the local deformation this model may not be acceptable and a different solution will have to be found.

The differential equation approach has many advantages over the static calculation, most important are the fact that it allows the introduction of resistances and applied forces and that data is acquired with respect to time. The complex ship behaviour will not be modelled in these analyses as the numerical methods later on are better suited to this. The obtained model is shown in Figure 3.14.

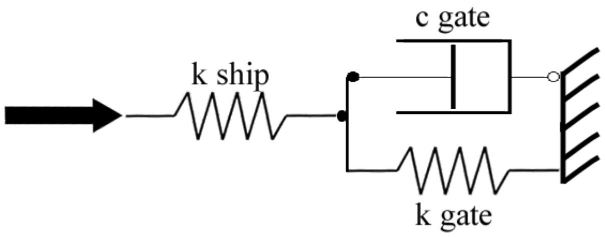

Figure 3.14: Collision system used for the differential equation, including damping for the gate structure

The differential equation will be used to examine three aspect of the collision, namely:

- The effects of varying levels of resistance.
- The effects of the application of an engine load to the system.
- The effects of ship stiffness to the collision behaviour.

Degree of Damping

The resistance that the gate and the surrounding water applies to the model in represented in the variable 'c' and is caused by many different aspects (as listed in Chapter 3.1.6). Calculating all these aspects is very difficult and physical test would need to take place to determine many of them. For this reason the resistance c is estimated in this study. To obtain an idea of the effects of the level of resistance it as varied in the differential equation and results were compared.

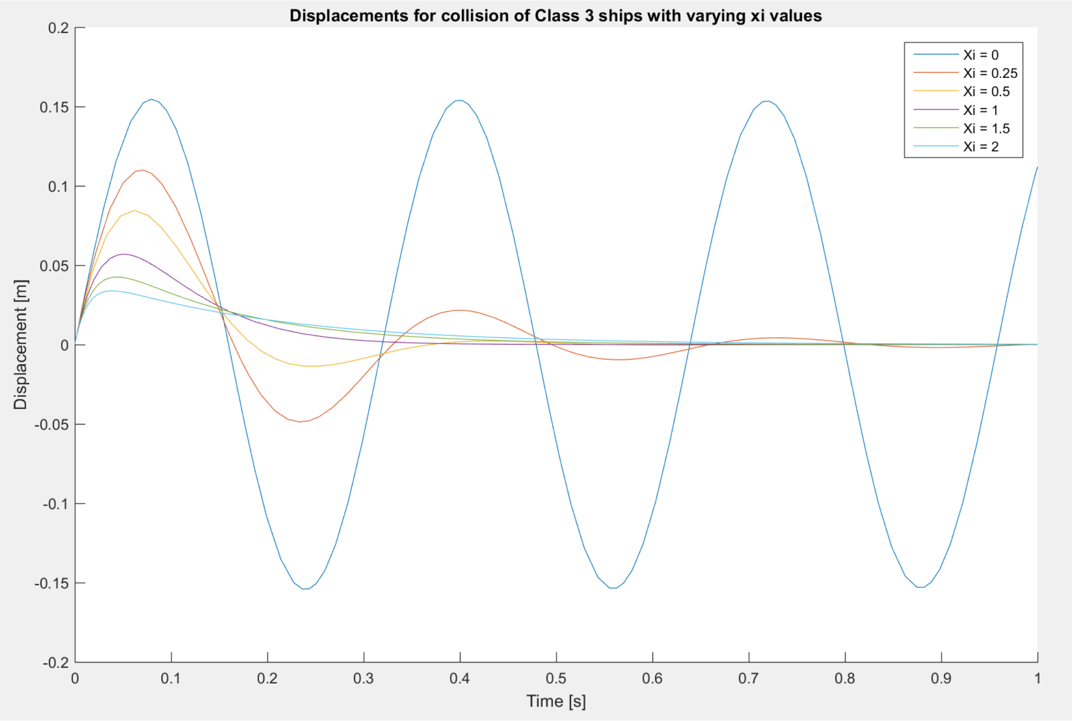

Figure 3.15: Displacements in time for varying Xi values

The gates properties such as the variable c are proportional to a ξ factor. This factor represents the relative amount of damping compared to the mass and stiffness of the structure. It is this variable which will be varied to easily determine the damping state (sub-, super- or critical damping). This ξ factor is defined as:

$$\xi = \frac{1}{2}\frac{c}{\sqrt{k * m}} \tag{3.28}$$

For which:

$\xi < 1$ represents sub-critical damping.
$\xi = 1$ represents critical damping.
$\xi > 1$ represents super-critical damping.

For the class 3 collision ξ was varied between 0 and 3 in 0.1 increments and it's effects on the energy dissipation and displacements were determined. Figures I.5 to I.7 in Appendix I show the results of this analysis.

The effects of the resistance in the model are found to be very large. For a ξ value of 0.1, which can be seen as lightly damped, the amount of energy dissipated is already ˜25% of the total kinetic energy applied and around critical damping this approaches ˜85%. This can in turn reduce the deflections by a factor 3. To illustrate this effect on the displacements Figure 3.15 shows the displacements as a function of time for some varying ξ values. It is clear that the choice for xi has a dramatic impact on the exact dynamic behaviour of the structure. The equation is solved using the ode23 command in MatLab.

For ξ values lower than 1 (sub-critical damping) the structure will enter a vibration in which it's displacement is negative at times. Because the ship is not stuck to the gate it will separate at this point and continue to travel backwards at the velocity it had when it's displacement was zero again. This is illustrated in I.8 in Appendix I. It can be seen the that sudden decrease in mass which comes from the separation damps the magnitude of the gates vibration and increase their frequency significantly. If this scenario was to take place it is possible that the vessel will collide with other obstructions due to it's reverse movement. The effects of this are outside the scope of this study.

A realistic value for the damping coefficient is difficult to determine because it is a combination of many different damping processes. Many of these processes are difficult to determine in themselves making the combination highly uncertain. The only way to substantiate an assumed ξ value is through physical experimentation which is expensive and takes time. For this study the ξ value will be assumed to be in the sub-critical region making vibrations a possibility. In illustrating the aspects in the following chapters a ξ value of 0.5 has been taken.

Engine Loads

The engine load applied to the systems is defined in Chapter 3.1.7 and can be inserted into the differential equation as F(t). In doing this we assume the engine is running at full power for the entirety of the collision and is thus constant in time. The engine powers for vessel of different classes[21] are combined with the stiffnesses of the springs for each collision scenario (as defined in Chapter 3.1.5) to obtain the engine forces for each collision. These values are given in Table 3.5.

Table 3.5: Engine forces for collision scenario's with ship classes 1-4

Ship Class	Max Engine Power [kW]	Gate stiffness [N/mm]	Engine Force [kN]
I	175	$16.76 * 10^6$	415.2
II	300	$19.95 * 10^6$	796.1
III	640	$21.21 * 10^6$	1400.7
IV	1070	$23.43 * 10^6$	2190.7

The addition of this force to the differential equation alternate the deformation pattern with respect to time. The maximum deflection is affected as well as the end displacement. The displacements graphs for a class 3 collision are shown below in Figure 3.16. The graphs for all four scenario's are given in Figures I.9 to I.12 and discussed in Appendix I.

Figure 3.16 represents the general aspects of all four collisions well even if the exact displacements differ. It can be seen that the maximum deflection increases only marginally (˜1%) and that the displacement at the end of the collision is a few millimetres. The extra deformations due to the application of the engine force can thus be said to be negligible. The collision duration and moment of maximal force remains unchanged. The fact that the engine only affects the collision to a minimal degree leads to believe that a more detailed calculation of the engine force is not necessary.

Ship Stiffness

In the current model the ship is seen as a spring which will deform a certain amount during collision. This deformation absorbs energy from the systems which then no longer had to be retained by the gate. The amount of energy which is removed from the gate in this way in dependant on the ratio between the stiffness of the gate and the ship. Spring theory states that if the ship is twice as stiff as the gate it will deform half as much and absorb half as much energy.

Calculation could be simplified by assuming the ship is infinitely stiff. This would be a conservative assumption as the gate would then have to retain all of the energy of the colliding vessel. In order to study whether or not significant gains could be obtained during design by taking the ships stiffness into account the differential equation is solved for both the case with an infinitely stiff ship and a flexible ship. This is done by reducing the amount of energy applied to the system by a factor $\frac{n}{n+1}$. As energy is not a direct parameter this is accomplished by reducing the initial velocity by the square root

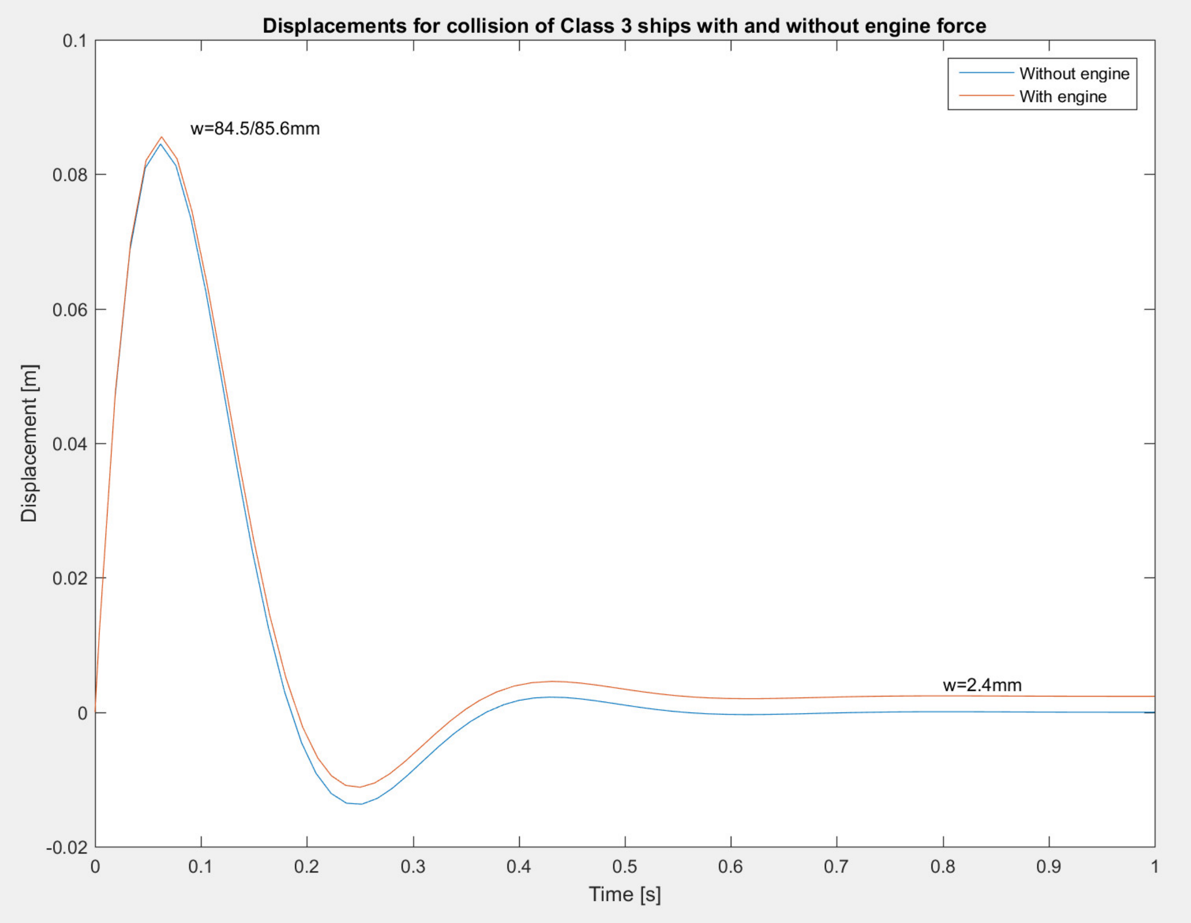

Figure 3.16: Displacement of the gate during a collision with a class 3 vessel, with and without engine force applied, as solved by the differential equation

of this factor. This can be done because the velocity in question is that of the gate and by indentation of the ship this will indeed be reduced.

The maximum deflections which are obtained from this analysis are shown below in Table 3.6. The resulting displacement graphs are given in Figures I.13 to I.16 and discussed in Appendix I.

Table 3.6: Displacement of the gate for collision with vessel from class 1-4 with varying n values

Ship Class	Ratio n	Displacement n=∞[mm]	Displacement n≠∞[mm]	% increase
I	21.76	38.1	37.0	2.4
II	23.91	50.6	49.1	2.6
III	17.15	48.7	47.4	1.0
IV	1.9	20.6	16.6	24.1

If can be seen that for the three scenario's in which the gate is loading in bending (class 1-3) the ship is relatively stiff in comparison to the gate. In these cases assuming the ship is infinitely stiff only affects the results in a minor manner and it can be said to be an acceptable model. However when the gate is loaded in compression it acts much stiffer and the deviations are significant. By adding the extra complexity of the ship stiffness to the model large savings can be made for the case of a central collision with a class 4 ship. For this reason it is valuable to take it into account.

Chapter Conclusions

From the analyses with the differential equation the following conclusions can be drawn:

- The level of resistance that is chosen has a large effect on the behaviour of the structure. Without physical experimentation it can only be estimated.
- The inclusion of the engine force, based op Chapter 3.1.7, has a negligible effect of the displacements of the gate and can be ignored.
- Including the stiffness of the ship as a spring can allow for a lighter design, but it only offers significant benefits for cases in which the gate acts stiff. For this case that is when it is loaded in compression due to a central collision.

3.4.3. Numerical Calculation

The final series of analytical analyses are executed numerically. Similarly to the differential equation this results in time based displacements which represent the entire collision duration. However instead of solving an equation that describes the motion the balance of energy and forces in examined at each point in time. Time steps of $1*10^{-5}$ seconds have been taken to assure precise results.

Analysis Methods

Two types of numerical calculations were executed in order to cross reference results and will discussed below. The first is an approach based around energy dissipation and the second focuses on the forces acting on the bodies in combination with Newtons second law. Each calculation consists of two time spans, namely the indentation of the gate and the returning to its original position.

The **Energy Approach** is based on the assumption that the system as a certain amount of energy in it as a resource and that it uses this energy to displace the mass. The amount of energy is equal to the kinetic energy of the ship. Each time step the spring and the damper do work which drains this energy supply. The velocity for the next time step is then determined based off the left over kinetic energy. Once the supply of kinetic energy reach zero the gate will stop moving forwards and the maximum displacement has been reached. Energy which has been absorbed by the damper is lost while energy absorbed by the spring will then exert a force which will return the gate to its original position, for this step the force approach is used.

The work done by the spring and the damper per time step are dependant on the displacement and the velocity respectively and have values of:

$$W_{spring} = \frac{1}{2} k * (w_1^2 - w_0^2) \tag{3.29}$$

and

$$W_{damper} = c * v * \Delta w \tag{3.30}$$

If a initial velocity is designated then the physical quantities (e.g. displacement, velocity, kinetic energy) of the system can be determined for each time step and plot can be made.

The **Force Approach** Assumes an initial velocity for the system and uses Newtons second law to determine the acceleration that the spring- and damper forces will cause for the mass. This acceleration then determines the velocity for the next time step.

The forces in the spring and damper are again dependant on the displacement and the velocity respectively. They are defined as follows:

$$F_{spring} = k * w \tag{3.31}$$

and

$$F_{damper} = c * v \tag{3.32}$$

In the first phase both and spring and damper exert a restoring force decelerating the mass until it is at rest. At this point the spring will begin pushing the mass back to its original position and will become the exciting force while the damper work to slow the mass down. If the system is sub-critically damped the spring and damper force may swap directions multiple times, with the the spring force reversing each time w=0 is passed and the damper force reversing each time $\dot{w}$=0 is passed. This will lead to a damped vibration pattern.

In **Comparison** these analysis types show very similar results. This is illustrated in Figure 3.17. It can be seen that the force approach gives a slightly higher maximum displacement. This is because with this method the gate is assumed to have an initial velocity and thus also be a source of kinetic energy. This is less accurate than the energy approach which has the kinetic energy as an initial value. The difference however are very small and are thus considered to be negligible.

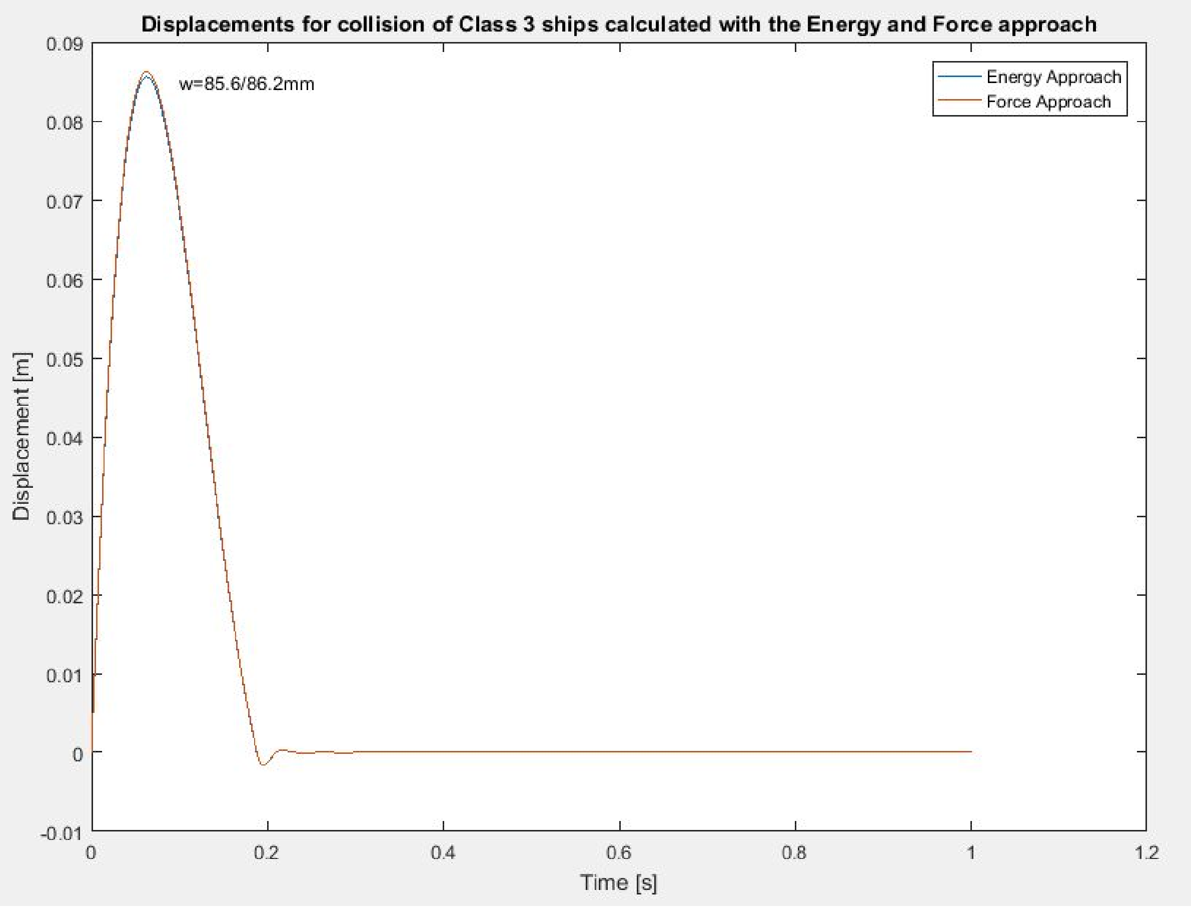

Figure 3.17: Comparison of the displacement of the gate for collision with a class 3 vessel solved with the Energy and Force methods

Each method has its own advantages and disadvantages with respect to calculating the contribution of different aspects. This is for a large part due to programming issues. Within the scope of this study the energy method is useful for modelling the complex behaviour of the ship, due to the ability to apply concentrated energy losses (see Chapter 6), and the force method can be used to examine aspects such as the engine force. The results acquired from the force method prove to be the same as those of the differential equation. This is to be expected considering that all the input is identical and serves mainly as a validation of the numerical code.

3.5. Discussion

The results for the displacements of the lock gate are summarised per analysis in Table 3.7.

Table 3.7: Displacements of the lock gate for each analysis type discussed in this chapter [mm]

Ship Class	Static Analysis		Differential Equation			Numeric Calculations	
	n=∞	n≠∞	n=∞	n≠∞	Engine Load	Energy approach	Force approach
I	120.7	118	68.0	65.9	66.5	64.9	66.4
II	161.9	158.7	90.2	87.6	88.5	87.1	88.1
III	158	153.6	86.9	84.5	85.6	85.6	86.2
IV	47.3	38.9	36.5	29.4	29.6	29.6	29.7

From these values we can reiterate some of the conclusions that have been drawn to this point:

- Within the analysis types (static, differential, numeric) the found displacements are all very similar, deviating only a few millimetres between results. From this three conclusions can be drawn:
  - With exception of the class IV collision there is no significant effect of assuming that the vessel in infinitely stiff. This can be used to simplify calculations. The class IV collision shows a larger deviation due to the displacement mode of the gate being axial and thus the gate acting much stiffer. The closer the stiffness of the gate is to the stiffness of the ship the larger the error will be by assuming the ship is infinitely stiff.
  - Whether or not the ship keeps its engine running during collision or not had next to no effect on the damage of the gate. This can thus be ignored to avoid complexities.
  - For the numerical calculation both the energy approach and the force approach are viable solution methods for such a collision. Which one is used can be dependant on what results one desires. If information on energy is required the energy approach will yield direct results and vice versa. The choice may also be dependant on which method is easier to code for the given situation. The slight difference is caused by the force approach assuming the gate has an initial velocity which adds slightly more energy to the system. However the analyses show that this difference is insignificant.
- As the solutions from the differential equation and the numerical calculations are based on the same theory there results are also very similar. In essence the numerical calculations as done are the same as the differential equation with n≠∞. Which solution method is chosen is again dependant on factors such as desired results.
- The found displacement for the static analysis or much higher than those of all the other methods. This is due to damping not being included. This makes the static calculation a very simple but very conservative solution. It may be used during design but in almost all cases a lighter structure would then also satisfy the needs of the project. It would thus be worthwhile to see how much could be saved with a more advance method.

Now the found displacement can be compared to the allowed displacements of the gate from Table 3.2 and a series of unity checks can be performed. A unity check is defined as the found value of a variable divided by the allowed value of the same variable:

$$Unity\ Check = \frac{Found}{Allowed} \tag{3.33}$$

A value below 1 means the structure satisfies the criteria and a value above 1 means failure will occur. Teh unity check for the displacements of the gate during collision are given in Table 3.8. To cut back on calculations two values will be taken for each collision case, the static and differential equation results for n=∞, as these represent the values well. The values will be compared to the allowed deformation for both the damage and the failure limits with material safety factors included. For cases I - III the 9.4 mm of deformation due to the governing water pressure has be subtracted from the allowed deformations.

Table 3.8: Unity checks for the static and dynamic collision for class I - IV ships.

Ship Class	Analysis Type	Damage Limit $(\epsilon = 0.27)$[18]	Failure Limit $(\epsilon = 1.2)$[18]
I	Static	2.87	0.64
	Dynamic	1.70	0.38
II	Static	3.47	0.78
	Dynamic	2.02	0.45
III	Static	3.51	0.79
	Dynamic	2.02	0.45
IV	Static	8.45	1.78
	Dynamic	6.84	1.44

From the unity checks it can be seen that no matter which collision type or calculation method the gate will always be stressed to above its damage limit so reparation will be needed. If the failure limit is examined however only the collision with a class IV vessel will cause failure, all others seem to be safe. For the case with a class IV ship it can be calculated that the material safety factor would have to reduce to 1.5 or lower in order for the unity check to go below 1. This is a scenario which is not impossible in the future when more experience with FRP has been obtained.

These results serve as a good first impression of the degree to which the gate will be loaded during collision from here they will be expanded on in two ways. First a full numerical calculation of the collision will be done in Chapter 4 as a verification step. Then in Chapter 6 a model will be suggested in which some of the conservative issues may be removed from the analysis by allowing the ship to fail in a non-elastic manner. It is expected that this will decrease the displacement of the gate and possibly allow for a lighter structure.

4

Global Gate Behaviour - Numerical Analysis

The analytical calculations from Chapter 3 give a good first impression of the gate displacements but are strongly simplified with regard to certain aspects.

- The load is considered as a point load, which is a decent assumption for the first point of impact, but will become less accurate as the displacements increase.
- The situation has been considered as two dimensional which enforces both equal deformations over the entire height of the gate and the entire gate cross section being activated by a local force.
- The final deformation is given as a single value for the maximum deflection, the general shape of the deformation is not determined.
- The gate is modelled as just a spring-damper so it's exact geometry has no effect. This disregards any form of local deformations.

These aspect will be elaborated in the following two chapters through use of both implicit and explicit numerical finite element models. These analyses will be done with version 16.2 of the Ansys software packet. The classic variant of Ansys will be used instead of the graphical Workbench variant as it allows more control over the parameters which will make modelling a FRP structure easier.

Ansys was chosen due to the experience within IV-Infra which was available to me as well as the ease in which such a model can to converted to LS-Dyna for a dynamic analysis.

The global behaviour of the lock gate during collision will be modelled in two ways:

- A static calculation will be done in which the ship load is modelled as a distributed force applied to the structure. This manner of loading is comparable to the ROK codes[15]. Such an analyse is quick to complete and gives a good idea of the deformation shape, but has no values s a function of time.
- A dynamic calculation in which LS-Dyna will to used to simulate a rigid ship bow colliding with the gate. In this analysis the bow is physically implemented in the model and the load distribution is thus more accurate.

The model aspects used, such as constraints and loads, will be discussed in Chapter 4.1. After which the results will be shown in Chapter 4.2. These will then be compared to the static results and discussed in Chapter 4.3.

4.1. Collision Model

An Ansys Classic model is a series of commands saved in a text file which is then read by the Ansys client. Such a model consist of different aspects which will be discussed in the following sections namely: element data (such as type, material and real constants), geometry, constraints and loads. These are followed by a solver and finally post-processing to obtain quantified results and images.

4.1.1. Element Data

The gate structure consists of a series of relatively thin laminate elements in combination with solid cores. To ensure a balance between computation times and accuracy of the calculations it was chosen to model the laminates as orthotropic shell elements and the cores as isotropic solid elements. For the global calculations first order elements will used, consisting of 4-noded shells and 8-noded cubes.

For the static analysis SHELL181 and SOLID45 elements were used. These implicit first order elements have degress of freedom at each of their nodes. Six per node for the shell elements (3 translations and 3 rotations) and 3 per node for the solids (3 translations). The Ansys User Guide images of these elements are shown in Figure 4.1.

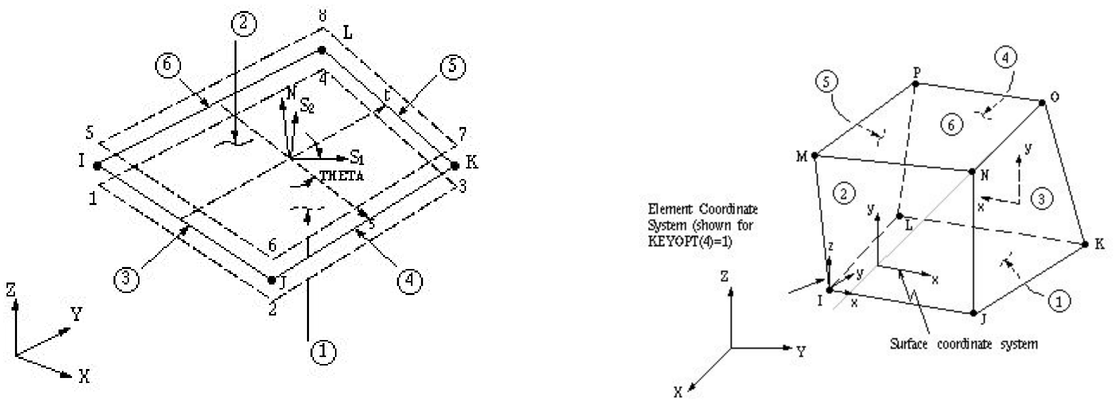
②
8
L
⑥
⑤
4
N
S2
5
I
S1
K
7
THETA
3
1
6
③
④
J
2
①
Z
Y
X
⑤
P
④
O
⑥
M
N
②
③
Element Coordinate System (shown for KEYOPT(4)=1)
L
K
Z
I
J
①
Y
X
Surface coordinate system

(a) SHELL181 Finite Strain Shell

(b) SOLID45 3-D Structural Solid

Figure 4.1: Chosen implicit elements for the static analysis

When this model is converted to LS-Dyna to execute a dynamic analysis explicit elements are necessary. The explicit versions of the chosen elements are SHELL163 and SOLID164 which have three additional degrees of freedom at each node in the form of accelerations. The Ansys Digital User Guide images of these elements are shown in Figure 4.2.

4.1.2. Geometry

The geometry of a finite element mesh consists of two aspects, the locations of the areas en the chosen mesh size. As these aspects are different for the static and dynamic calculations they will be handled separately in the chapter below. I large simplification which is made for all geometries is ignoring the presence of valves in the bottom of the door. These valves are large a may affect the stability of the region around them, however they are also at a great distance from the impact that they will likely have no influence. This will have to be checked after the calculations have been run.

Static

The area placement for the static calculation serves as a base for all further calculations. The geometry of the physical gate is known through project files [2] and can be accurately simulated. The axis origin

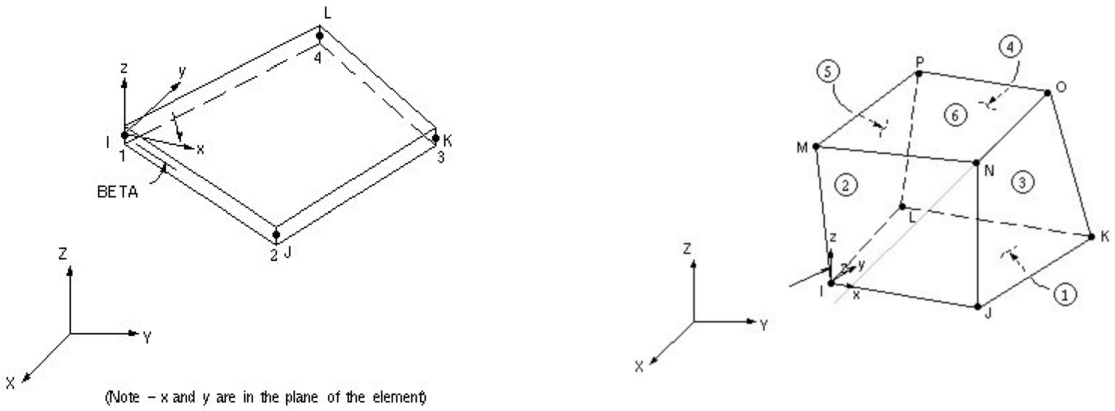

(Note – x and y are in the plane of the element)

(a) SHELL163 Explicit Thin Structural Shell

(b) SOLID164 Explicit 3-D Structural Solid

Figure 4.2: Chosen implicit elements for the static analysis

is chosen in the centre of the chamber at sill level in the middle of the thickness of the gate. The gate is modelled in its own local axis with the x-axis along the length of the gate, the y-axis upwards and the z-axis towards the upstream retention side as can be seen in Figure 4.3. With this coordinate system the elements can be modelled without having to take the angle of the gate into account.

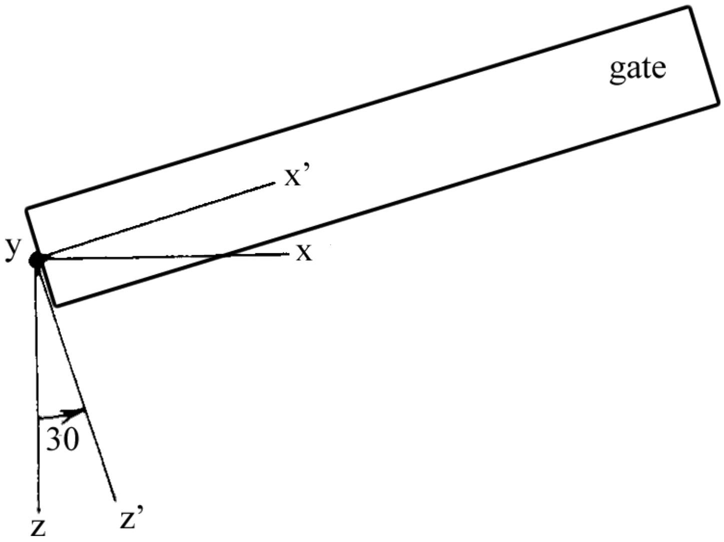

Figure 4.3: Schematic of the gate and its local axis

The model then consists of two skins shell of 30 mm thick in the xy-plane surrounded by edge plates of 60 mm thick in the zx and yz planes. Within there are internal flanges in the zx plane, these are 5mm thick and spaced every 100 mm up the entire height of the gate. The enclosed areas are filled with a structural foam. The properties of all these elements are given in Chapter 2. The core material is modelled even though it is much weaker than the surrounding laminates as in provided internal support and prevent laminate buckling. Some area are sliced to allow for constraints or loads, the locations of these extra areas will be discussed later.

Area are subdivided into elements with a certain mesh density. A finer mesh will allow for more accurate calculation and acquisition of data at more points, but smaller elements also increase calculation times. For the static calculation it was chosen to take a relatively fine mesh in the region in which the gate is loaded and a less fine mesh in other regions. Attention was paid to making sure there were always multiple elements over important stretches of the model, such as the thickness. The mesh which was used in visualised in Appendix J, Figures J.2 and J.3.

Dynamic

The dynamic geometry is similar is many ways, but some aspects are worth mentioning. All areas placed for the static analysis are kept for the dynamic mesh with the same locations and thicknesses. In an attempt to reduce calculation time the volume elements which represent the foam core were ignored in the first run of calculations as they are a factor thousand weaker. However it became clear that this simplification had significant impact on the failure modes, thus the volume elements were included in the second run. This will be discussed in Chapter 4.2.

Also areas which represent the ship are added so that collision can take place. These are modelled to be close to the gate so that there are few wasted time steps before impact. The mesh for the ship is imported from a Workbench file. The gates area placement with ships bow can be seen in Figures 4.4 and 4.5. It becomes apparent that the point of impact will be a lot closer to the centre of the chamber than originally assumed. This will lead the gate to respond stiffer than expected.

The element density is also different for the dynamic calculation, a finer mesh has been chosen in almost all regions. This would normally be inefficient as it would drastically increase calculation times, however it is both necessary and not too detrimental for three main reasons:

- It is important that the elements are roughly square otherwise they will tend to act stiffer than they are in reality, or the generated matrix may become unsolvable. Because the size of an element in the vertical can not become larger than the distance between two internal plates, a mesh size is dictated.
- During dynamic calculation each node in the gate is related to nodes in the ship. If the mesh sizes are too different from one another this can cause errors due to mapping failures.
- A LS-Dyna calculation works differently from a static finite element calculation in that the smallest element always defines the required time step and thus the calculation time. Making the mesh less fine outside the region of interest has no effect of the calculation time except for that of the meshing itself, which is insignificant with respect to the calculation phase.

For the reasons above a uniform mesh was chosen of 100 mm square elements. This mesh in shown in Appendix J, Figures J.4 and J.5

4.1.3. Constraints

The gate is support horizontally by the sill support and three wooden fenders by which the gate rests on the chamber wall and the other gate and vertically by the pivot in the chamber wall. The horizontal supports are represented as line supports in the centre of their contact area, while for the vertical support all nodes within the pivot area are constrained. Modelling the fender as line supports instead of elements supports will lead to stress concentration around the supports. Considering however that the region of interest is not near constrained regions this is a valid simplification. The disadvantage of this is that no conclusions can be drawn around the supports.

The locations of the support constraints are based on the detailing of the constructed gate. In Figure 4.6 this detailing can be seen and the way this represents itself in the Ansys model is shown in Figures 4.7 and 4.8. All supports except the centre gate support are orientated in the local axis which coincides with the direction of the fender. The centre support is in the global axis to prevent the create of a cantilever beam, this would greatly increase the displacements and be inaccurate with regard to the real behaviour of the gate.

in the dynamic calculation an extra constraint has to be applied. In this case the mesh of the ships bow is constrained in every direction and against every rotation except movement in the direction of the waterway. This coincides with the the global z-axis.

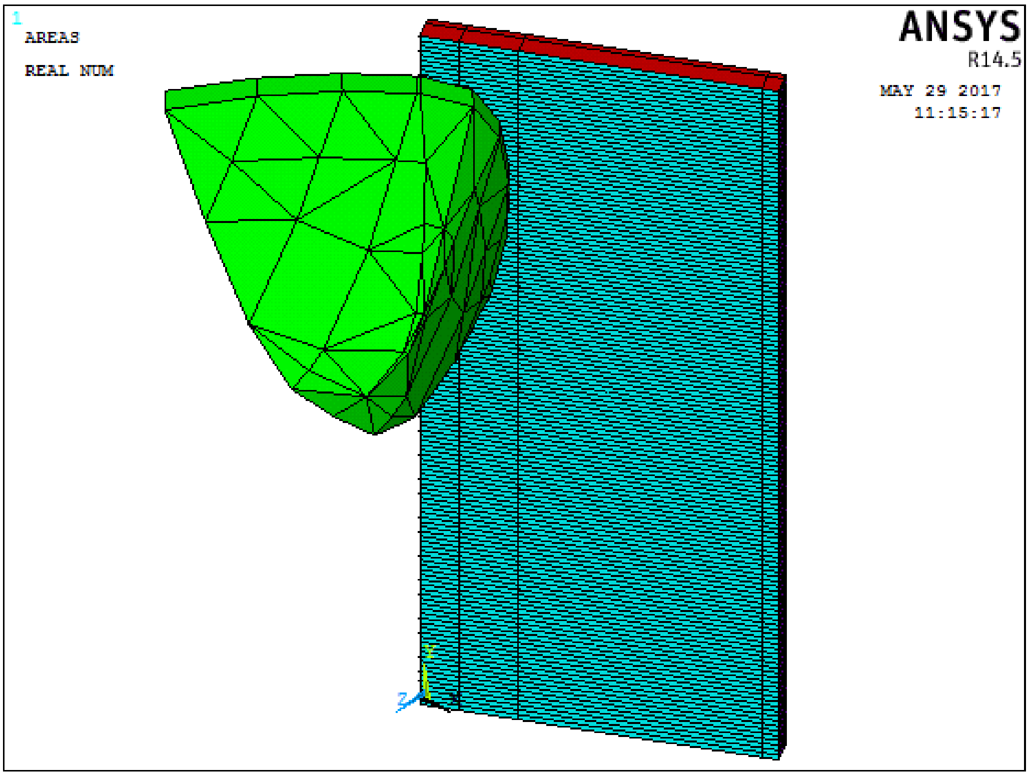
1
AREAS
REAL NUM
ANSYS
R14.5
MAY 29 2017
11:15:17
Y
Z
X

Figure 4.4: Overview of the area geometry including the ship bow

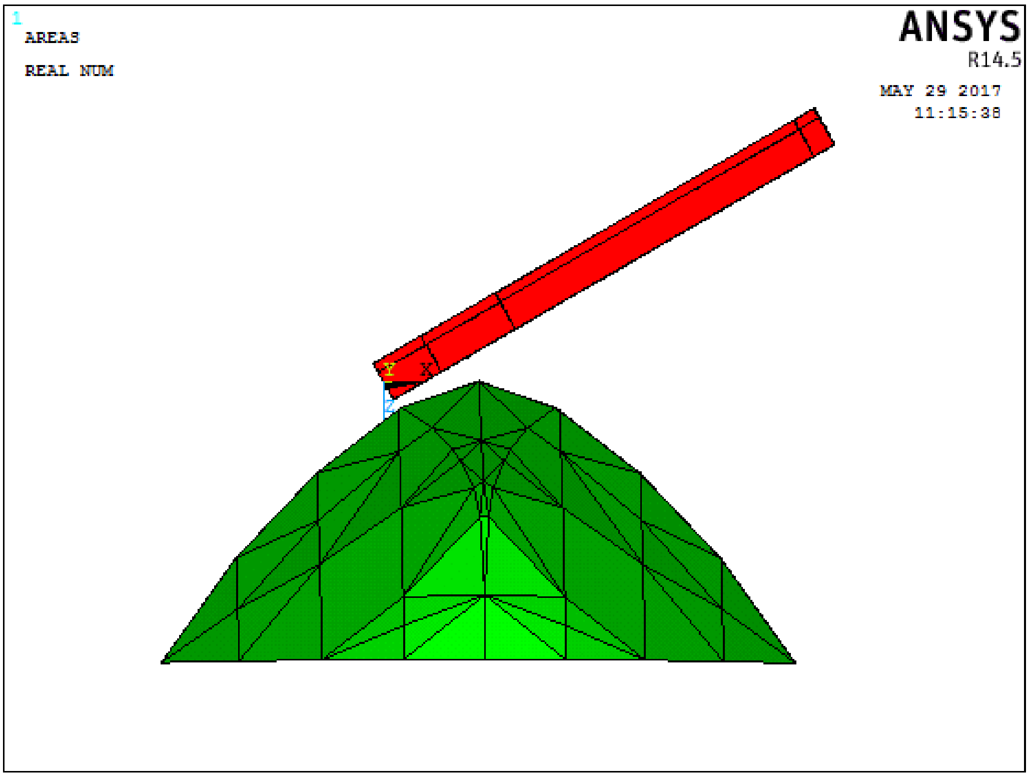
1
AREAS
REAL NUM
ANSYS
R14.5
MAY 29 2017
11:15:38
Y
X
Z

Figure 4.5: Top view of the area geometry including the ship bow

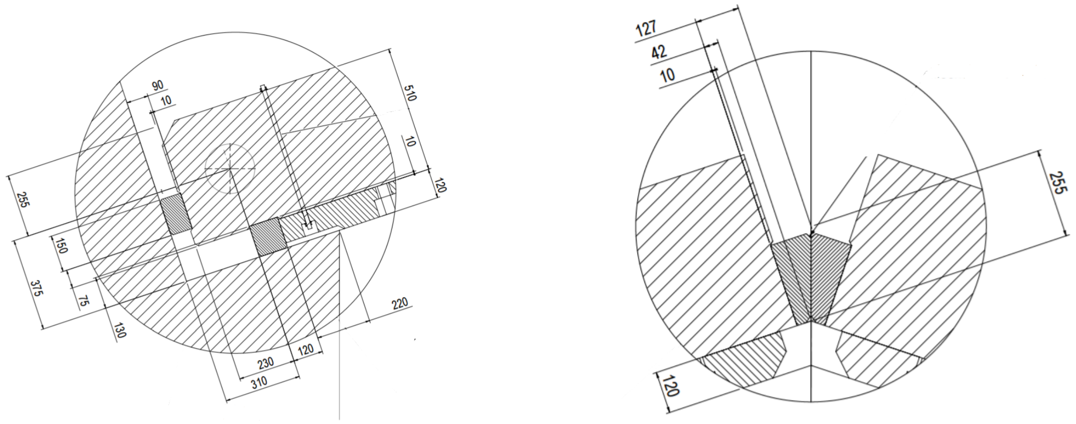

(a) Chamber wall support and pivot (b) Chamber centre support

Figure 4.6: Dimensions of the gate around its supports

4.1.4. Load conditions

The manner of loading is the main point in which the static and dynamic calculations differ. For the static analysis the approach suggested in the dutch codes (ROK 1.3[15]) is followed using Ansys whereas for the dynamic calculation the force is applied by physically colliding modelled elements with LS-Dyna. These approaches will be discussed below:

Static

During the static calculation two loads will be applied. First is the impact load from the ship, which is the governing load that is of interest. Second is the water pressure from the coinciding water levels. The results of the analysis will be examined with and without this water load to determine if it has a significant contribution to the displacements. If this is not the case then the calculation time for the dynamic calculation can be reduced by not taking it into account.

The ROK 1.3 suggests assumed a colliding ship subjects a lock gate to a load spread evenly over a small area. This area is 1 metre wide, 0.5 metres high and is located 1 - 1.5 metres above the water line. Seen as the point of collision in the width of the lock and the governing water level are known the location of this loaded rectangle can be determined. Within the element geometry slices are made to assure that elements coincide with this region. Then the force which has been determined during the analytical calculation is decomposed into a perpendicular pressure and pressure parallel to the gate to account for the angle between the movement of the ship and the gate. These decomposed loads are then spread evenly over this region and applied as an element pressure loads. The location and magnitude of the pressure are given in Table 4.1

Table 4.1: Values concerning the application of the static load condition

X coordinate left of load region	650 mm
X coordinate right of load region	1650 mm
Y coordinate bottom of load region	12950 mm
Y coordinate top of load region	13450 mm
Perpendicular pressure	11.52 MPa
Parallel pressure	106 kPa

The water pressure is applied as an element pressure with a value of zero at the water level and increasing with the depth. Figures J.6 and J.7 which show this pressure can be found in Appendix J.

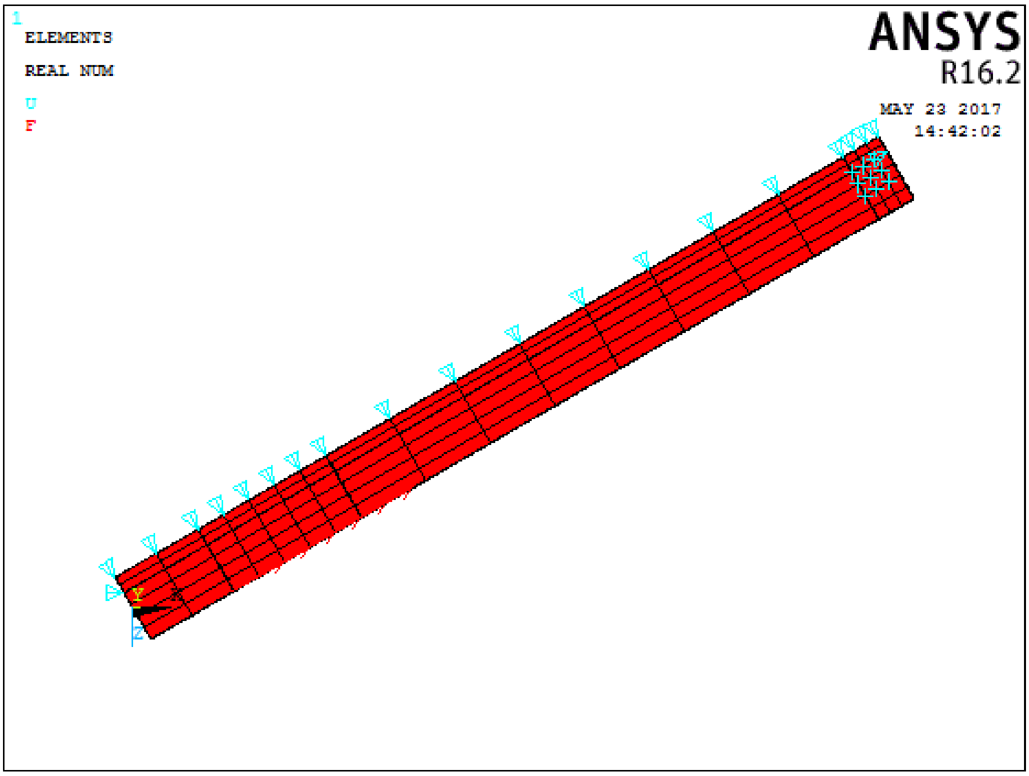
1
ELEMENTS
REAL NUM
U
F
ANSYS
R16.2
MAY 23 2017
14:42:02
Y
Z
X

Figure 4.7: Top view of the structure with constraints made visible

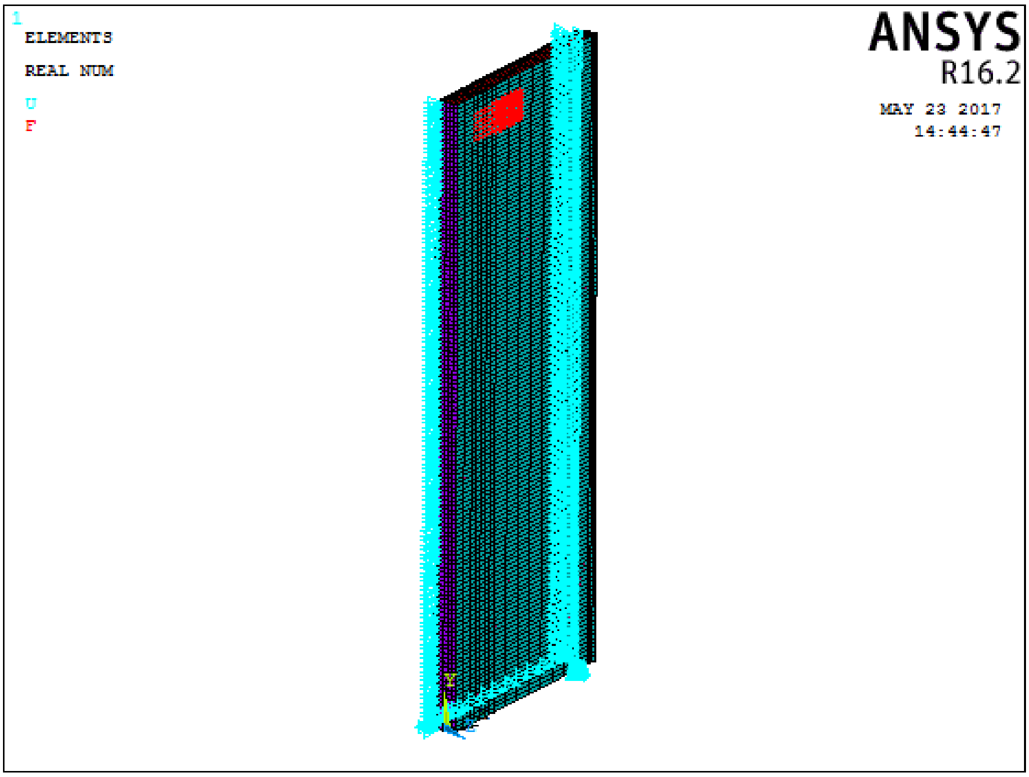
1
ELEMENTS
REAL NUM
U
F
ANSYS
R16.2
MAY 23 2017
14:44:47
Y

Figure 4.8: Profile view of the structure with constraints and loads made visible. Blue: Constraint, Red: Load

Dynamic

The dynamic load conditions is executed with the help of the LS-Dyna environment for Ansys. In it the modelled ship bow which is discussed in Chapter 4.1.2 is given a velocity and allowed to collide with the gate mesh. The software then records the displacements in each node for each small time step and in doing so models the collision behaviour. This is a relatively time consuming process, but it makes it possible to apply a realistic load and see the displacements in time.

The level of loading is determined by the velocity, which was taken as 3.3 as with the analytical calculations, and the mass of the ship. The velocity is taken in the global z-axis which implies a collision angle of 30 degrees. The mass is determined by the density of the ship elements. As only part of the ship is modelled the density of the ships elements must be proportionally increased so that the total colliding mass is equal to that of the vessel. The required density can be determined by constructing a model in which the ships bow is simply supported, given a dummy density and subjected to a gravity load. The reaction forces which occur allow one to calculate the volume of the modelled bow. The density used in the final model is then equal to the ships mass divided by this volume and results in $1.57*10^6$ kg/m^3.

4.2. Analysis Results

All the inputs for the global numerical analyses have been given above. In this chapter the results which are obtained from the finite element calculation will be shown. They will be split into the results from the static and the dynamic calculation en then compared in Chapter 4.3.

4.2.1. Static

The static calculation was run with and without water pressure to determine whether the contribution is significant enough to be deemed as necessary during dynamic calculations. Diagrams showing the deformation in the local z-axis perpendicular to the span the the gate without and with water are shown in Figures 4.9 and 4.10.

It can be seen from these plots that the water pressure has very little effect on the maximum displacements within the gate. The fact that the water pressures, per definition, act outside the region of the collision in the ROK codes lends to this effect. The difference it makes is a mere 2.6 mm on a ˜85 mm deflection, so it is safe to say no extreme errors will occur if it is not added to the dynamic calculation, this is beneficial for the calculation times. For the sake of comparison the water pressure will also not be taken into account for the static response.

Now that an idea has been obtained as to the deformation confirmation can be made whether the simplifications to the model were just. These simplifications were the removal of the valves and modelling the supports as lines. The deformation figures (4.9 and J.8) and stress figures (J.9 and J.11) show no response at all around the valves and no concentrations around the constraints. This is a sign that the results aren't being affected by the imposed simplifications. Both the removal of the valves and not applying the hydro static water pressure will not be valid simplifications if the collision load was applied below the water level as would be the case if the ship had a bulb. This scenario is likely for sea locks.

It might be expected that the parallel stress due to the angle between impact and gate might cause deformations in the x direction and pull the gates apart. This deformation is constrained along the line constraint at x=0, z=-0.1275 which makes it difficult to draw conclusions. In Figure J.8 it can be seen that the front of the gate has a displacement of 21 mm away from the other gate. Without the constraint this will likely be larger. However the deformation is still relative small in comparison to the size and flexibility of the gates so it isn't unreasonable to expect that the other gate, loaded by the water pressure, will displace as well to fill this gap. Furthermore if a gap was to appear between the

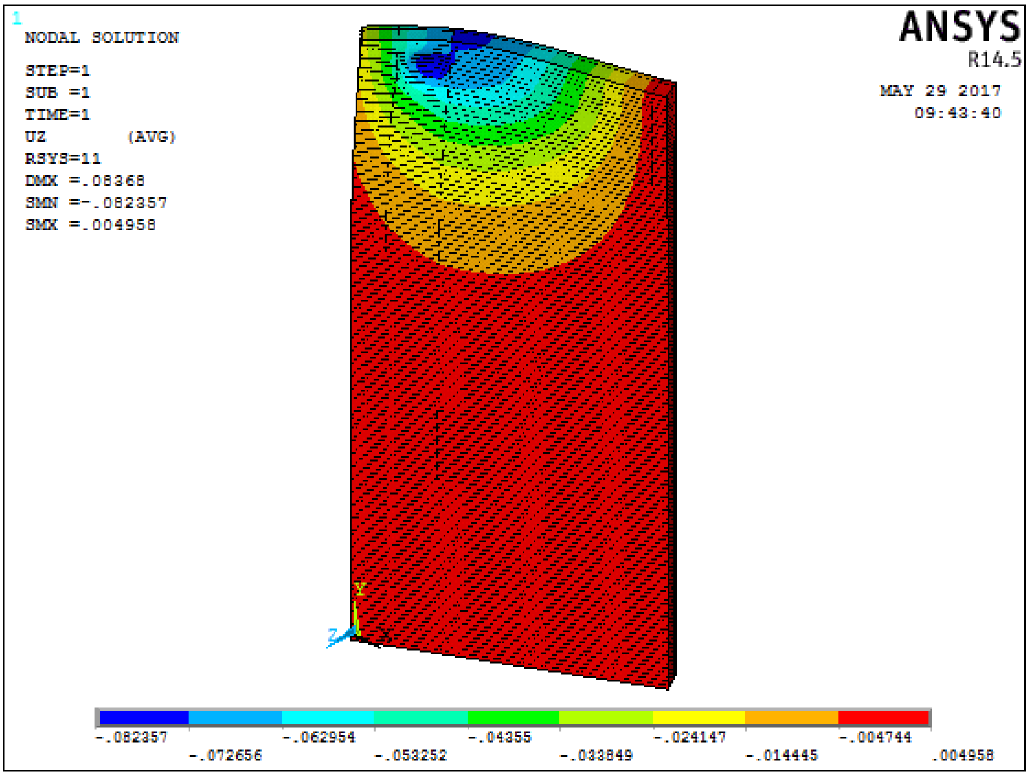

Figure 4.9: Displacements of the lock gate under static load condition without water pressure

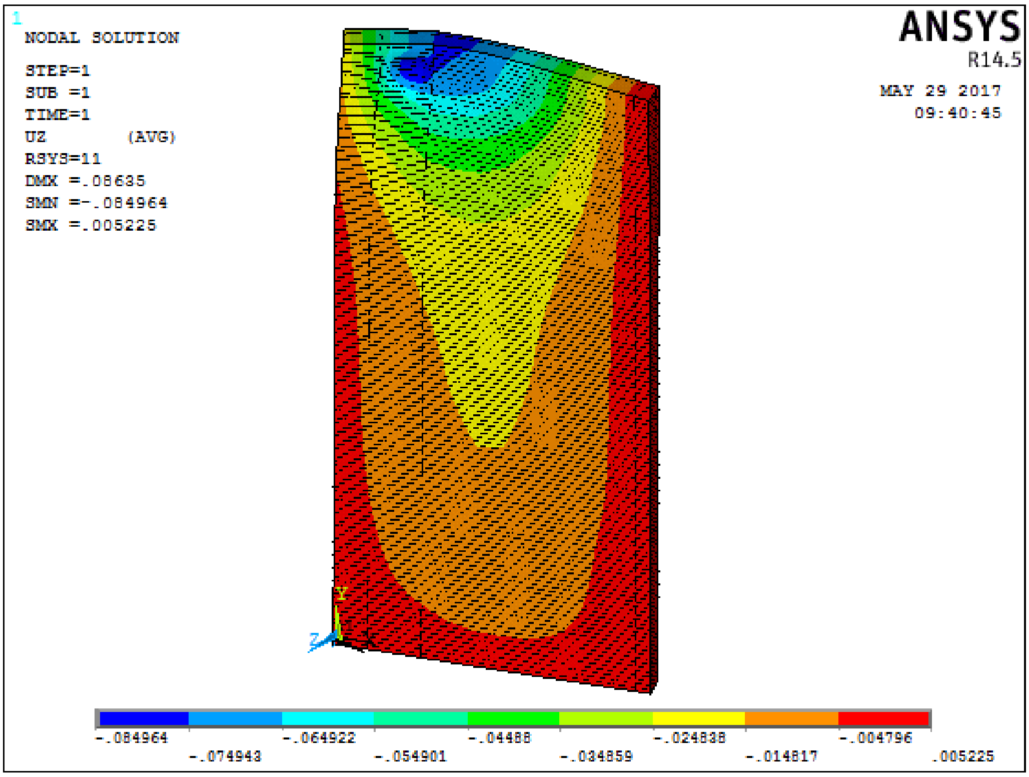

Figure 4.10: Displacements of the lock gate under static load condition with water pressure

gates at this point it is above the governing waterline and will not be a risk factor for leakage.

The manner in which an InfraCore Inside gate, or any other form of multi-bow gate carries its loads can be found with this model. The results of the stresses in the x and z-direction are used to illustrate this. The stresses in the x-direction, which are in the plane of the skins, are carried almost exclusively by the skins themselves. The internal flanges serve only as a connection between the front and back skin allowing them to share the load effectively. The flanges fulfil this purpose well, as it can be shown that the front skin carries 60% of the load and the back skin the other 40%. Meanwhile the stresses int he z-direction, which is out of plane of the skins is carried by the internal flange laminates.

4.2.2. Dynamic

The dynamic calculations, executed with LS-Dyna, output physical properties (displacements, stresses, strain etc.) as a function of time. It was chosen to model the first 1.2 seconds the the collision as the analytical calculation shows that by then the impact will be over, save perhaps a lingering vibration. After calculation it was discovered that the collision was much shorter than this.

As mentioned in Chapter 4.1.2 the dynamic analysis was run twice, once without core elements and once with them. These analyses showed that core elements are required to prevent unrealistic buckling of the skin elements. This is shown in Appendix J.1.5. Only the realistic situation with core elements will be discussed here.

Model with Core Elements

For the analysis with core elements we are interested in the progression of the displacements as well as their maximum values. At the beginning of the deformation the point of impact displaces away from the ship while further along the gate axis the gate displacement is towards the ship. The point of maximum deflection in the z direction is shown in Figure 4.11 and takes place at t=0.15. At this point in time the maximum deflections in both directions (at the point of impact and along the body) is reached in the z direction. As can be seen there is no obvious buckling and the displacements are around 145mm.

For the displacements in x-direction a slightly different phenomenon is observed with regard to the time at which maximums are reached. At the point of impact the maximum absolute displacement is reached at the same time as the maximum z displacement, as shown in Figure J.15. The maximum displacement in the body however isn't reached until t=1.75, as can be seen in Figure J.16. This suggests the friction from the vessel takes time to travel down the length of the gate in the form of a translational wave.

From the analysis it become clear that the gate acts like a spring and reversed the direction of the ship. Once the gate is back in its original position the ship disconnects from the gate and the gate itself enter a state of vibration. This vibration is not the simple first-mode vibration that has been assumed during analytical calculation but has a component is both x and z directions as well as a weaker one in the y-direction. Figure J.17 show the progression in time from a complex vibration field to the first order vibration once the higher order modes damp out.

4.3. Comparison and Discussion

In this chapter the results for the different analysis types, analytical and numerical, will be compared and conclusions will be drawn as to the effectiveness of each analysis type. This will be done on the basis of maximum displacements which is the only output which is given by all analyses.

After that a closer look will be taken at the numerical calculations and the gates ability to resist the

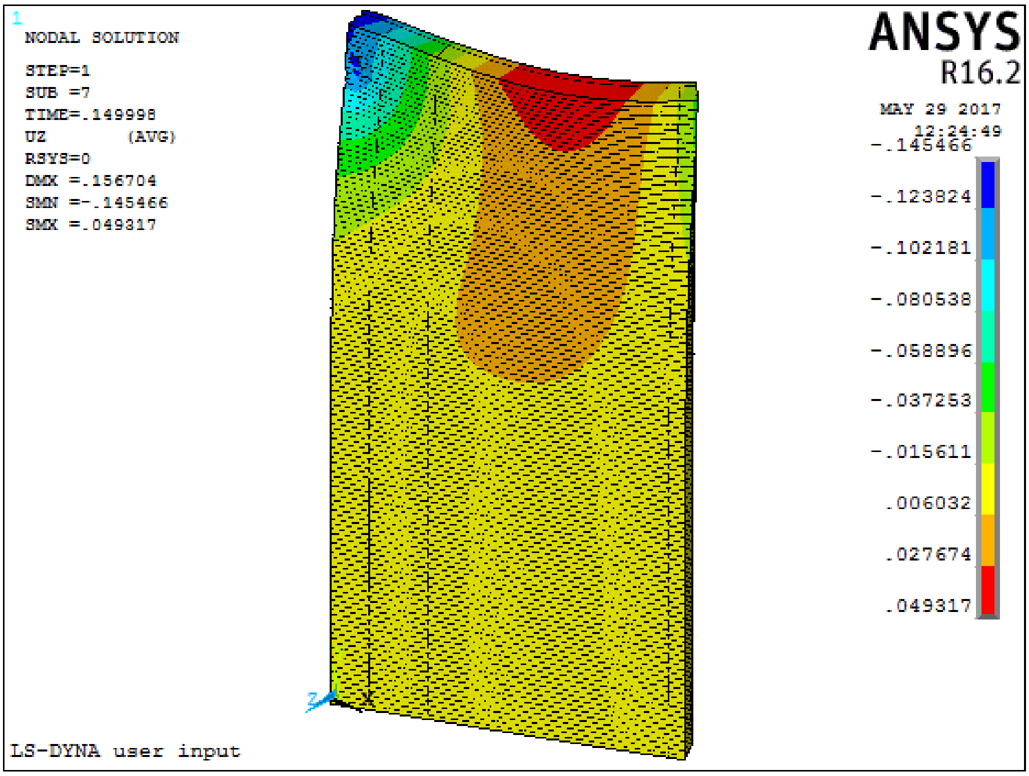

Figure 4.11: Z-displacements of the lock gate for the dynamic analysis including core elements

governing collision load in a global sense will be discussed in depth.

4.3.1. Comparison of Analyses

Below in Table 4.2 the results for the maximum deflections of the gate are given for the four main analysis types treated in this study.

Table 4.2: Found maximum displacements for the gate from the analytical and numerical calculations

	Analytical		Numerical	
	Static	Dynamic	Static	Dynamic
Maximum displacement [mm]	158	86.9	82.3	145.5

There are three aspects which effect the comparison between the results, namely the way the load is applied, the stiffness of the model and the amount of damping. Table 4.3 compares these aspects for the four analysis types in a quantitative manner.

Table 4.3: Quantitative comparison of the modelling aspects per analysis type

Analysis Type		Load application	Resistance of the model	Amount of damping
Analytical	Static	Concentrated	Low	None
	Dynamic	Concentrated	Low	High
Numerical	Static	Distributed	High	Low
	Dynamic	Concentrated	High	Low

From this table it becomes apparent that any similarities between solutions are coincidental as they are caused by different aspects. It can not be guaranteed that these similarities will be true for all gates.

If the real situation is considered the numerical dynamic collision is the closest match, as it has the real geometry en real load application however the finite element model doesn't take most of the damping mechanisms into account. The sloshing of water, or friction between vessel and gate for examples are not modelled. So in reality the displacement will be somewhat lower making it a conservative solution. In the general case however one can not rely on there been a strong enough damping as a mechanism of protecting the gate. That way if for whatever reason the damping is lower than expected or removed due to a rare scenario the gate would no longer be able to be considered safe.

We can conclude that no guarantee can be given that the simpler analytical models will provide accurate results for all cases. Although a dynamic analytical approach will give an estimate of the degree of deformation it is of import to execute a full numerical calculation whenever possible as this will supply the most reliable results.

When a comparison is made between the two numerical analyses one can see that the dynamic load condition leads to 75% more displacements than the load condition suggested in the codes. This in turn means that applying the load condition form the ROK 1.3 would lead to an unsafe structure. The reason for this is likely that the ROK was formed with steel lock gates in mind. The possibility that plastic deformation can take place will spread the loads more evenly and make the distributed load case suggested more accurate. For FRP structures however this theory does not apply due to the strictly elastic nature of the material.

4.3.2. Results and Discussion

The results obtained from the global analysis can be separated into two main categories which will be discussed in this chapter. Firstly we have general conclusion as to the deformation behaviour of the structure. These conclusion will often be qualitative and serve to better understand what happens during the collision. Secondly we have quantitative data as to displacements and stresses in the gate elements. Using this data conclusions will be drawn as to the structural soundness of the gate during collision.

Qualitative Results

The numerical analyses show very little deformation of the internal structure of core and plates and as an effect of this the front and back skins have similar displacements and stress levels. This would indicate that a three dimensional model may not be necessary in order to obtain reliable results of the gates behaviour. A more time efficient method may be a model consisting of a single orthotropic plate element of which the properties are derived from the gate geometry. The displacements of this plate could then either be solved using p[late mechanics formulae. As the gate is constructed of FRP plastic behaviour must be ignored which limits the failure modes. Executing this approach is an interesting step, but outside of the scope of this study.

As discussed previously the core elements have significant influence on the behaviour of the structure even though they are multiple orders of magnitude less stiff. Being fully confined they resist compression enough to be of structural aid. The buckling process of the gate without core elements is shown in Figures J.13 and J.14, in which the gate is shown just before and just after failure respectively. If these images are compared to those in which the core elements are taken into account (Figure 4.11) the effects become clear. It would be possible to construct the gate using fibre reinforced foams which would be able to carry more loads, or by filling the core areas with resin. However it appears that the weak foam chosen is sufficient to restrain the buckling modes so this is not necessary. Only if concentrated loads are expected at a certain location would extra reinforced be required. An example of such a location is the connection to the pivot structure.

Quantitative Results

As discussed the main physical quantity that will be examined is the maximum displacement, which will be compared to the allowed displacements of the gate here. The found maximum displacements for all the performed analyses are given in Table 4.2 and the allowed displacements are found in Table 3.2. These value are compared in Table 4.4 and each combination of load and resistance is checked for failure. Although the codes require the use of safety factors the cases without these factors are also included. This is done because it is expected that the material safety factors will decrease as more familiarity is gained with FRP structure, thus the unfactored scenario´s represent a possible future case.

From the results is can be concluded that for the current situation in which the safety factors are applied the structure will surpass its damage limit but remain below its failure limit for every performed analysis. As the case examined is a dramatic collision at high speeds this result is satisfactory. The outer laminates will take damage but not to such an extent that the gate will fail and lose all water tightness. Repairs will have to made, the degree of which depends on the exact impact region and if the pivot is damaged in any way.

Table 4.4: Performed analyses compared to the known deformation limits, judged to pass or fail for a Class III ship

			Analytical		Numerical	
			Static	Dynamic	Static	Dynamic
Found displacement [mm]			158	86.9	82.3	145.5
Damage Limit [mm]	No safety factors	95.3	Fail	Pass	Pass	Fail
	With safety factors	32.5	Fail	Fail	Fail	Fail
Failure Limit [mm]	No safety factors	476.2	Pass	Pass	Pass	Pass
	With safety factors	196.9	Pass	Pass	Pass	Pass

By using the displacements as a indicator of the stresses in the gate the assumption is made that all the stresses are those that coincide with the displaced form and locally introduced stresses are ignored. For large scale failure phenomena this is reasonable, but with the finite element model it is possible to have a closer look at the stresses around the point of impact. This is done for the stresses in the x-direction and the z-direction, while the y-direction is ignored as it is not a main load axis. The stress fields are illustrated in Appendix J with Figures J.9 and J.10 showing the stresses in x-direction for the skins and the flanges respectively and Figures J.11 and J.12 doing the same for the z-direction.

As FRP laminates respond equally to compression and tension the largest absolute value of the stress is taken to judge if failure will take place. The maximum found stresses and the stress limits of the laminate are listed in Table 4.5. Comparison leads to the conclusion that the skins will be stress to just below their failure limit. This combined with the fact the the rear skin is stressed to a lower level gives cause to expect the gate will not lose its ability to retain water although it will suffer considerable damage. The results for the internal flanges are however less positive. The failure limit is surpassed for both the stresses in x- and z-direction which symbolises crushing of the flanges.

If Figures J.10 and J.12 are examined more closely it can be seen that the stress peaks for the x-direction are located in the edge panel while the rest of the internal flanges are stressed to a much lower level. For this case the failure is thus very localised and far above the governing water level. For the stresses in the z-direction however the flanges directly next to the load will be the ones to fail. This could lead to a chain reaction which would cause put the water retention at risk.

Table 4.5: Allowed and found stresses for the skins and internal flanges in the x and z directions

	Allowed Stress [MPa]		Found Stress [MPa]	
	Damage Limit	Failure Limit	X-direction	Z-direction
Skin Laminate	87.2	387.6	376	20
Internal Flange	37.3	165.8	188	228

To summarise the finite element model has given quantitative data to back-up the qualitative understanding of the model. The values obtained have shown that the gate will be able to retain the collision load without failure, save for crushing of the internal flanges directly under the load. This crushing is a risk to the ability of the gate to retain water and may put the area behind the lock at risk of flooding. If this issue is addressed the rest of the gate meets the requirements although large scale damage will take place in the form of damaged resin layers due to too large strains. This will further weaken the laminates as water will be able to penetrate more easily. Because of this the damage will have to be repaired before the gate can be put back into use.

5

Local Delamination Analysis

Up to this point the gate has been considered as being made up of skin plates, internal plates and edge plates. Globally this is correct and serves as an accurate model when gate behaviour is considered at a global level. In reality however the gate is not constructed from straight laminate panels but overlapping Z-shaped elements as is discussed in Appendix H. In this chapter the model from the previous analysis will be refined to include the manner in which the panel in layed-up in practice. By doing so the failure modes which coincide with the gates design can be examined to check for failure. The main failure mode which will be analysed is macro level delamination of the Z-shaped laminate due to extreme stresses in the connecting resin layers. The model is not constructed to such a level that micro level delaminations within the laminates themselves can be analysed or that cracking pattern can be determined.

In this chapter the chosen model, with its geometry, loads and constraints will be discussed in Chapter 5.1. For this model some assumptions and simplifications were made. In order to determine whether these are acceptable assumptions they will be authenticated in Chapter 5.2. Finally in Chapter 5.3 the results will be shown and discussed.

5.1. Collision Model

The collision model is the combination of the gate geometry with its constraints and loads. The model used here differs from the model from Chapter 4.1 in the fact that the skin panels consist of multiple layers instead of a simple shell element. Doing so allows more data to be collected as to the behaviour and loading of the laminate while also making the model more difficult to comprehend and increasing calculation times. Even when analysing local behaviour the global constraints and the rest of the structure will have a large effect. This can be handled either by modelling the entire structure or by modelling only a section of it and changing the constraint loads to create an equivalent situation. For this case the choice was made to continue modelling the entire structure. This will lead to higher solving times, but there are counter acted by the model being simpler to make. In the following sections the geometry, constraints en load conditions are discussed.

5.1.1. Geometry

Modelling the geometry of the gate can be separated into two aspects. The first represents the gross of the gate and consists of the 140 overlapping Z-shaped laminates which together form the internal flanges and the skins. The second is the manner in which the edge panels and cores can be added to this skeleton of laminates. The aspects themselves will be discussed in the following two sections.

As the exact manner in which the gate is constructed is patent owned and not discussed in detail in the project files for the case, so some simplifications have been applied:

- FRP laminates which support the internal flanges in cross direction are mentioned in passing in the project files. But there is no way of knowing how many there are or where they are located. For this reason the gate is modelled assuming they are not added.
- As for the cross supports of the internal flanges mention is also made to FRP blocks which replace the core elements at locations where large local forces are introduced. The exact locations are not given, but it is likely that they are mainly around the supports, which are not in the direct region of interest. For this reason these blocks are also assumed non-existent for the sake of this model.

Both these simplifications are conservative in that they weaken the gates structure. This makes them safe assumptions but it is worth keeping them in mind while analysing the results.

Internal Flanges and Skins

Both the internal flanges and the skin laminates are formed by the overlapping Z-laminates and their connecting resin. In total 140 Z-laminates are modelled with a spacing of 100mm. The vertical body of the Z-laminate forms the internal flange while the layered horizontal sections form the skins. The length of these horizontal sections is not supplied by FibreCore however it is known that the skin is 30 mm thick and the Z-laminates are 5 mm thick. From this we can conclude that 6 laminates will overlap in order to form the skin. This is the case when the horizontal sections are 600 mm long, which will be the assumption for the rest of the analysis. This can be seen in Figure 5.1.

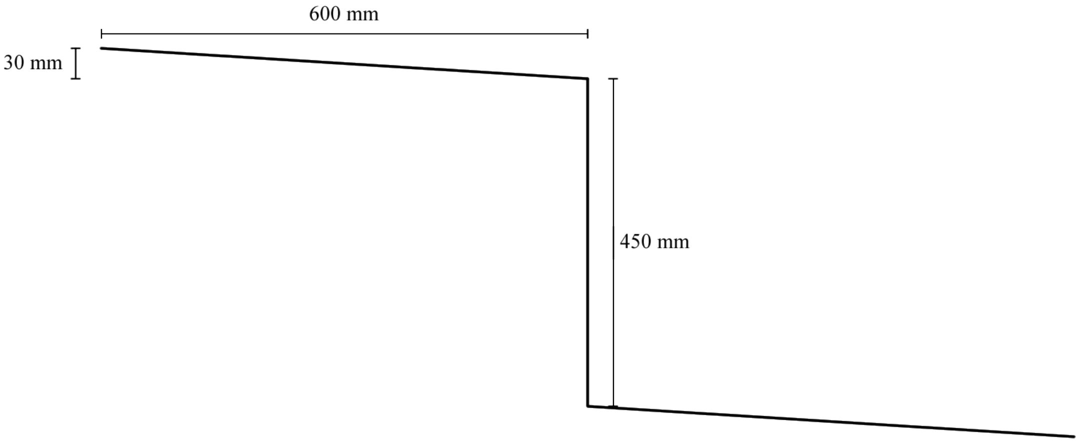

Figure 5.1: Schematic of a Z-laminate with its measurements

The Z-laminates are modelled as shell elements located in their centre of gravity. As an effect of this the overlapping elements share no nodes in Ansys. The connection between the different laminates is enforced by solids which represent the interconnecting resin in the gate. The manner in which this resin is modelled is shown in Figure 5.2.

As we are interested in local forces it is important to keep the measurements of the skin laminates the same as for the real situation. In order to accomplish this the resin layers are modelled as 5 mm thick while in reality they will be compacted to minimal thickness. A workable estimate would be 1 mm. The thicker resin layer will displace more than the structure would in reality which will affect the behaviour of the structure. In order to minimise this effect the properties of the resin will be changed such that the gate behaviour remain the same. The manner in which this is done will be discussed in Chapter 5.2.1. The resulting properties are dependant on the whether stresses of displacements are desired as output. With the E-modulus for the resin being increased by a factor 5 and 14 respectively

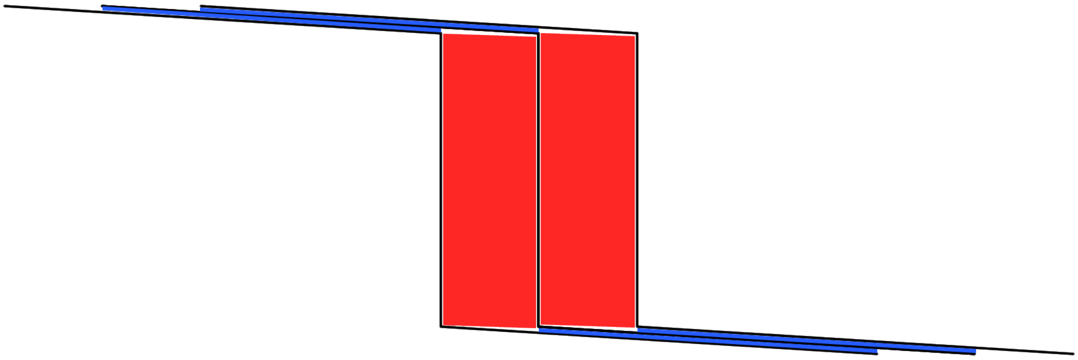

Figure 5.2: Element build-up for a series of overlapping Z-laminates. Black: Laminate Shell, Blue:Resin, Red: Core Foam

for this properties.

Cores and Edge Panels

The network of skins and internal flanges is supplemented by a frame of edge plates with a thickness of 60 mm and foam cores between the flanges. The edge plates along the top and bottom of the gate can be modelled using the same key points as the Z-laminates and given them a larger thickness. More difficult to model are the side plates and the cores due to the uneven shape and key point placement caused by the Z-laminates. As noted in Chapter 4 these cores may not be ignored as they help the skin laminate resist buckling failure.

The geometry of the Z-laminates leaves an open space between the internal flanges which must be filled with a solid element representing the foam. However if we examine the key point locations around this open area we see that there are 6 key points around the circumference which does not allow for simple inclusion of first order solid elements. Attempting to do so would mean creating a rectangular solid and two narrow triangular volumes. Due to the dimensions of these triangular volume very fine meshing would be required to model them accurately which would significantly increase calculation times. Instead it is decided to model only the rectangular volume as a solid and leave the triangular areas open. This process is shown in Figure 5.3.

The core now supports the internal flanges against buckling, but not the skins. This is solved by not allowing any nodes in the skin between the locations of the internal flanges. Because buckling is represented by large displacements of point between supports, it will not be taken into account if there are no points at which displacement data is collected (nodes) between two supported points. This model will be confirmed in Chapter 5.2.2. The vertical elements of the edge frame follow the same geometry as the cores but are modelled as shell elements.

Mesh dimensions

The mesh dimensions chosen are 100mm in all directions for all elements, although this is sometimes limited by geometry. These measurements are based on the following considerations:

- 100 mm is the distance between two internal flanges, so in choosing the elements so no intermediary nodes will be generated along the core widths.
- Ansys has trouble working with elements which have a ratio of more than 1:20 between their dimensions in each direction. As the resin layers have a thickness of 5 mm, as described by the skin geometry, a maximum dimension of 100 mm is set.

As can be concluded, 100 mm elements are the only viable option for this specific model.

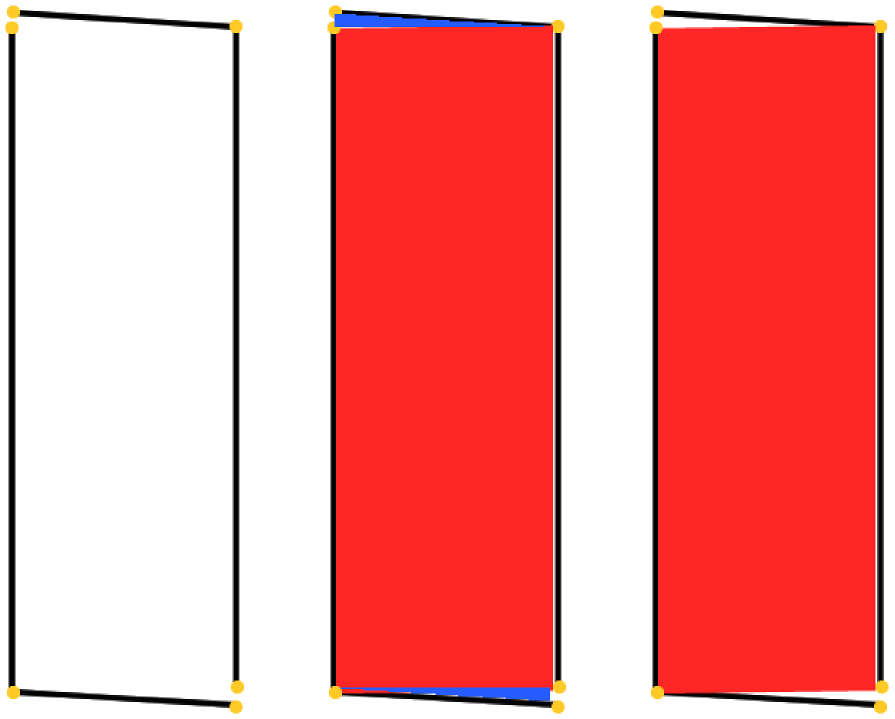

(a) Key point lay-out around a single core element

(b) Required core areas to fill the space

(c) Modelled core areas disallowing thin elements

Figure 5.3: Schematic overview of the manner of modelling core elements

5.1.2. Constraints

As with the global model from Chapter 4 the entire gate is modelled here so the real constraints in the locking chamber can be reproduced. These consist of horizontal support against the chamber walls, other gate and cill as well as vertical support from the pivot. The locations and direction of these are identical to those given in Chapter 4.1.3

5.1.3. Load conditions

The manner in which the load is applied to the gate will determine the size of the stresses and their spread over the skins. A more concentrated load will cause larger peaks in the stress levels in the resin layers which may lead to delamination and failure of the laminates. In general there are four ways in which the load can be applied:

- As a distributed load over an area. This is identical to the load pattern described in the ROK and used for the static calculation from Chapter 4. It had the best spread of the stresses of the loads described here, with likely the lowest stress peaks.
- As a vertical line load coinciding with the front of the ship bow. This is an accurate approximation as the ships bow has a vertical line at its tip with a height of 35cm. However in reality the region of loading will always have a width, especially if the ship deforms. Stress peaks are expected around the area of loading.
- As a point load. This is a very conservative approach which will lead to large stress concentrations en almost certain failure of the gate.
- As a dynamic load with LS-Dyna. this would likely give the realistic results however because the model consists of very small elements, which cannot be made larger due to the geometry, the calculation time would be very large. Reducing the area of the gate which is modelled would only

marginally reduce this as calculation time is mainly decided by the element size.

The most realistic load scenario which can also be calculated in a reasonable time will be combination of the first two loads mentioned. It will take the form of a vertical strip load which is comparable to the line load mentioned before but with a quantifiable width. This reduces stress peaks from directly introducing load at single nodes. The height and width of the strip are chosen with regard to the ship bow shape and the chosen element mesh. As the ships bow has a vertical surface of 350 mm and the mesh size is 100 mm it is chosen to apply the load over a strip of 400 mm high and 100 mm wide. This loads four element faces. For the sake of comparison the scenario in which the gate is loaded in accordance with the ROK will also be executed.

5.2. Model Authentication

While constructing the finite element model two points came to light for which it was necessary to make simplifications, namely the thick resin layers and the core geometry as discussed in Chapter 5.1.1. In the following sections these two aspects will be further discussed and authenticated. For the resin layers this means determining the properties which they must be given to mimic realistic gate behaviour, while for the core geometry it takes the form of a check against unexpected behaviour.

5.2.1. Resin Layers

As discussed in Chapter 5.1.1 in order to maintain the known skin thickness while modelling the laminates as shell elements the resin layers have been thickened in comparison to the real scenario. In the model they are 5 mm thick whereas in reality this thickness is much lower. The exact thickness is unknown, but considering that the elements are created with vacuum moulding (See Appendix D) a thickness of 1 mm in reasonable [5].

This increase in thickness will change both the displacements and the stresses of the model if all properties are kept the same. For this reason it is important to determine to what degree the properties must be changed to mimic realistic behaviour. This will be done by performing tests on a simple structure modelled both with the assumed model and a more realistic model and calibrating results.

Test Structure

In order to compare two model types a simple structure is designed in which the expected mode is isolated and tested. In this model the mode of interest is inter-laminar shearing. The tests are performed on a structure that consists of two laminate plates of 1 by 1 meter connected with a layer of resin. The bottom plate is constrained at one end, while the top plate is loaded at the other end. This load scenario is shown in Figure 5.4.

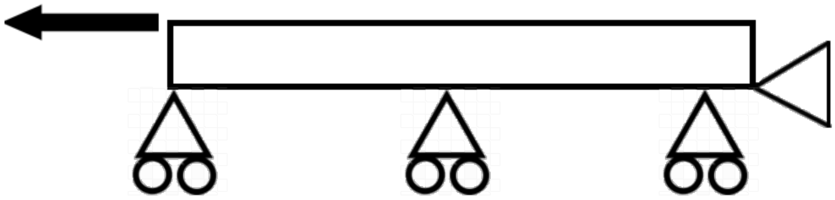

Figure 5.4: Static scheme for the loading of the test structure

The first model will be set up where the resin in modelled as a solid with 5mm thickness and the top and bottom face of this solid are given the properties of the laminates as shells elements. This represents the simplified model which will be used for the local analysis. The second model will be constructed as three solid elements atop one another of which the middle one has a thickness of 1 mm and represents the resin and the top and bottom solids are the laminates with a thickness of 5mm. These model can be seen in Figure 5.5, for the sake of visibility of the details a cut out section is presented.

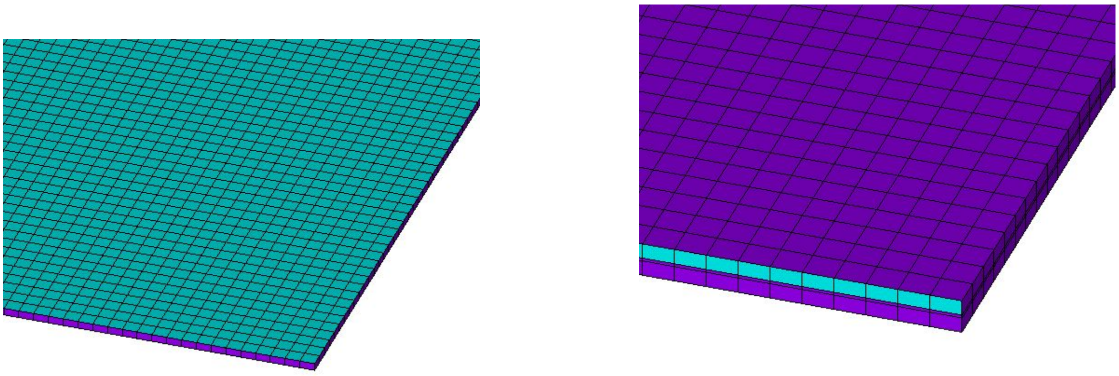

(a) Detail of the layers of the first model, with solid resin and shell laminates

(b) Detail of the layers of the second model, with solid resin, solid laminates and a shell to apply pressure loads

Figure 5.5: Area layouts for the resin property comparison model

The properties of the resin of the first model are varied, while all other elements are given their real values. In this manner the required resin properties can be determined. The load which is applied is arbitrary as long as it is the same for both models. For the first model it is a line load and for the second an area pressure.

Theory

Although the model is quick enough to run multiple times and obtain results through trail-and-error it is valuable to understand the process which takes place.

In the case described above the resin layer is loaded by in-plane shear. This deformation mode is illustrated in Figure 5.6. The deformation angle γ is related to the shear stress via the shear modulus [G] as follow:

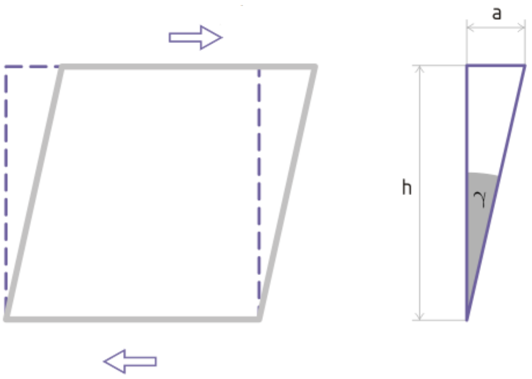

Figure 5.6: Schematical shear deformation behaviour

$$\tau = G\gamma \tag{5.1}$$

The expected deformations are small, thus the expression for γ can be written as:

$$\gamma = arctan\left(\frac{a}{h}\right) \approx \frac{a}{h} \tag{5.2}$$

If the same resin properties were used for both models τ and G would not change, thus γ would also remain the same. The resin layer thickness [h] is five times as high and so the shear deformation [a] would also be five times as high.

Instead we aim to keep the deformation [a] the same by changing the resin properties, represented here by G. Now a remains the same while h is multiplied by five, this leads to a five times as low γ. For the same stress level [τ] we now require a five times larger G-modulus of the resin. As the G-modulus is given by Equation 5.3 this can be accomplished by increasing the E-modulus. Decreasing the Poisson ratio is not an option here as it always has a value between 0 and 0.5 which will never result in a increase by a factor 5.

$$G = \frac{E}{2(1+\nu)} \tag{5.3}$$

Results and Chapter Conclusions

The theory would suggest that increase the E-modulus of the resin by a factor five would equalise the displacements. However when the model is executed with these parameters the displacements and stresses do not coincide. This suggests that there are other aspects which affect the structural behaviour such as the fact that the case does not represent pure shear. This means that trail-and-error will be necessary in order to calibrate the model.

This process of trail-and-error in which the E-modulus is varied leads to an increase of the E-modulus by a factor 2.3. The results of the displacements and peak stresses for the two structure with and without the scaling factor of 2.3 are given in Table 5.1.

Model	Max Displacement [mm]	Peak Stress [GPa]
Reference Model (Thin Resin)	3.04	1.17
Simple Model (Thick Resin), No Scaling	3.22	0.51
Simple Model, With Scaling of 2.3	2.93	1.17

Table 5.1: Displacements and stress peaks for the two model used to authenticate the resin model.

As the stresses are the aspect that is most interesting for a case of delamination this is the property the scaling was based on. When this is done the displacements of the scaling model are slightly too low, this is partly due to the fact the shear deformation of the laminate is not taken into account when they are modelled as shells. This deformation mode is not expected to have a serious impact on the behaviour of the structure as a whole which makes this a satisfactory model. We can thus conclude that the E-modulus of the resin should be increased by a factor 2.3 (from 3.7 to 8.5 GPa) for calculation of the local stresses.

5.2.2. Core Geometry

In Chapter 5.1.1 it became clear that the real core geometry would require too small elements to be represented in the finite element model. For this reason an approximation was made in which the internal flanges were supported by core elements and the buckling of the skins was artificially restrained by disallowing intermediary nodes. In order to ascertain whether this model is accurate two aspects must be checked, namely whether the skin buckles and if internal flange behaviour is comparable to other analyses.

In Figure 5.7 a detail in shown from the results of the final local analysis and in Figure 5.8 the same detail is shown for the global analysis. From these images conclusions can be drawn as to the accuracy of the model.

The first point of interest, the skin buckling behaviour, can be examined for the local model. It can be seen that the core edges parallel to the skins remain straight and at a distance from the skins. This is the behaviour which was desired and it can be concluded that not filling the entire core with solid does not affects the gates behaviour.

The second point of interest is the behaviour of the internal flanges which can be compared for the local and global models. It can be seen that for both case the flanges remain primarily straight, with a slight wave pattern. These waves differ slightly due to there not being the same amount of elements in both models. The behaviour as a whole to the same and thus it can be concluded that the model meets the requirements.

5.3. Results and Discussion

The value of the model described in this chapter is the ability to discern the stresses between the Z-laminates. This is impossible in the more simple model from Chapter 4, where the skin laminate is formed by a single shell element. A discussed previously the results that are of interest are these stresses and thus the model in which the resin has been modelled as 2.3 times as stiff is executed (see Chapter 5.2.1).

In Figures 5.9 and 5.10 the stress levels in the resin layers are shown for the distributed ROK load and the strip load discussed in Chapter 5.1.3 respectively. It can be seen that the general spread of the stresses is comparable with 4 peaks around the corners of the loads, 2 positive and 2 negative. They primarily differ in the level of stress around these peaks. For the ROK load a stress of 27.4GPa is found while for the strip load a larger stress of 55.5GPa is found. It makes sense that the loads increase as the area of loading decrease as it approaches the situation with a concentrated force.

As it is known that the structure makes use of polyester resins we can compare the stresses to the resistance of these layers. Polyester resin has an ultimate stress level of 40-75 GPa[5]. This means that as long as high quality resin is used and attention is paid to the production and curing the stresses which occur during the governing collision can be resisted. It is important that the peak stress does not cause failure because, due to the nature of delamination the peak stresses will translate down the laminate boundary as they come apart causing the delamination to progress for as long as load is applied.

There are two mechanisms which are not taken into account in the current model which may have become important if failure occurred:

- If tearing of the resin layer takes place a model in which cracking could occur will yield better results. This mechanism is hard to model and will always be an approximation.
- Because failure will progress for as long as a high load is applied the progression of the load in time plays a role in the final amount of damage. This can be taken into account in the model either by estimating a load progression from the analytical calculations and applying it to the model or by executing an LS-Dyna calculation.

However because the load can be retained without risk of delamination it was a satisfactory assumption to ignore these mechanisms. Furthermore there are some general points to be made as to the manner in which the gate would fail:

- Delamination of the skins does not instantly remove their water tightness. Damage will have to

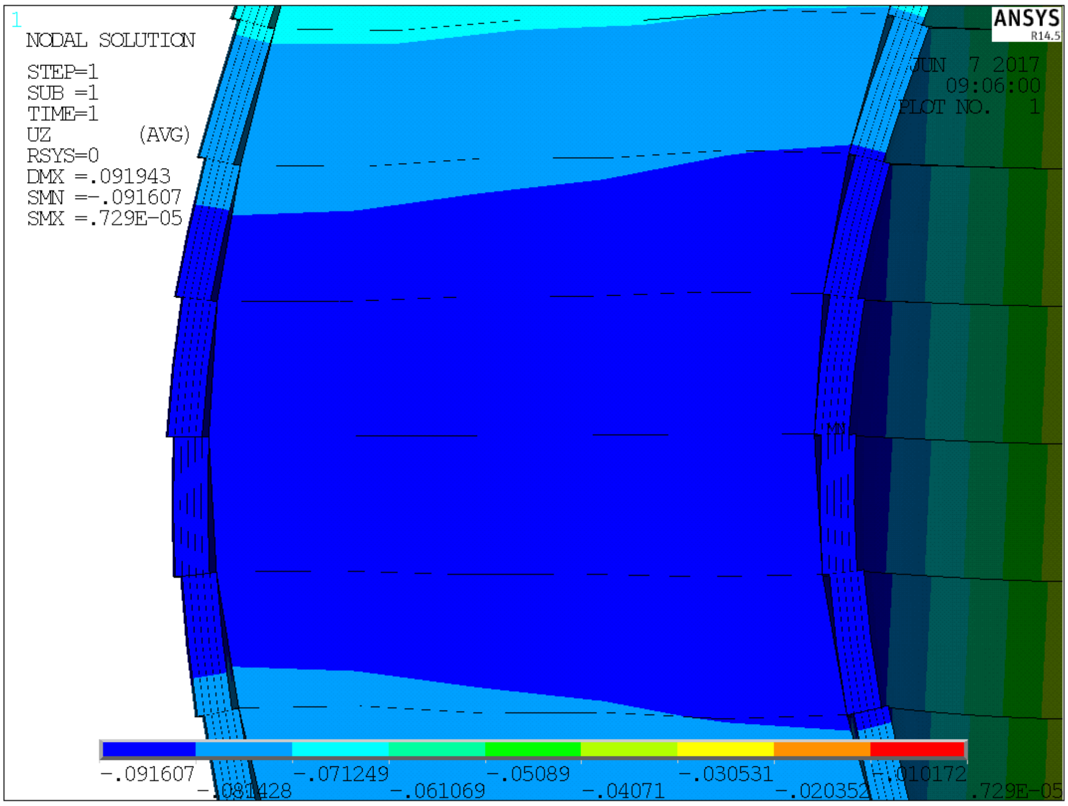

Figure 5.7: Detail of the core region in the local analysis model

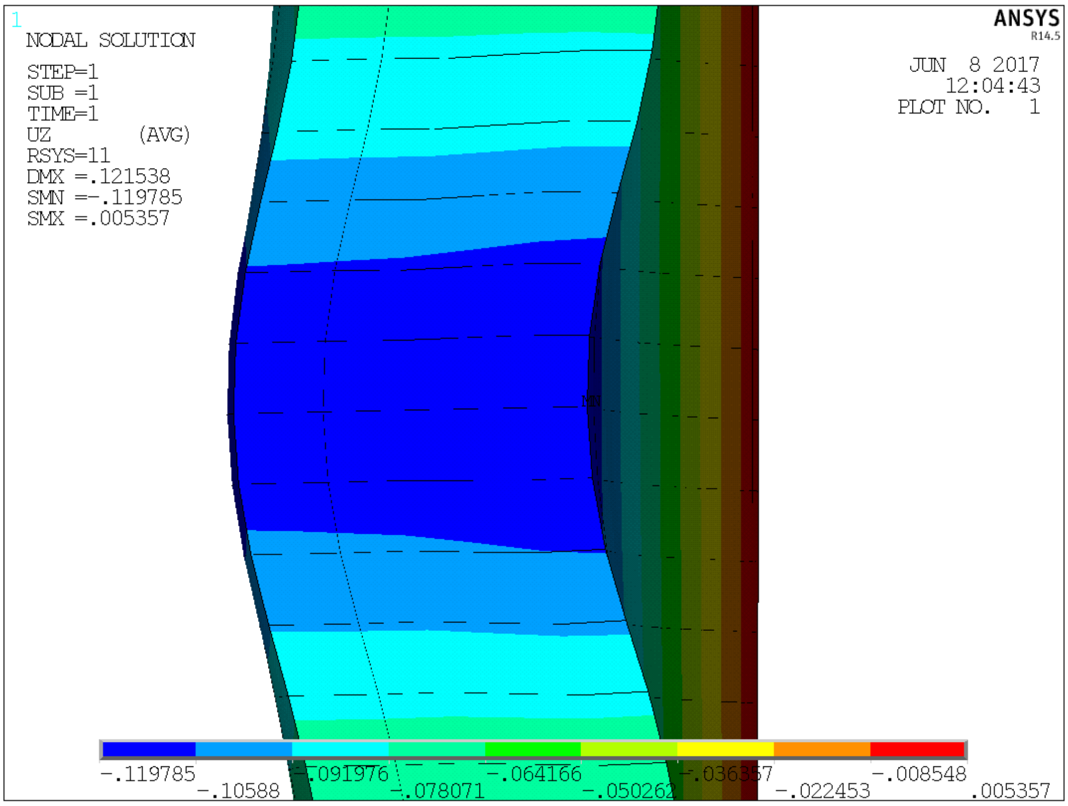

Figure 5.8: Detail of the core region in the global analysis model, as reference

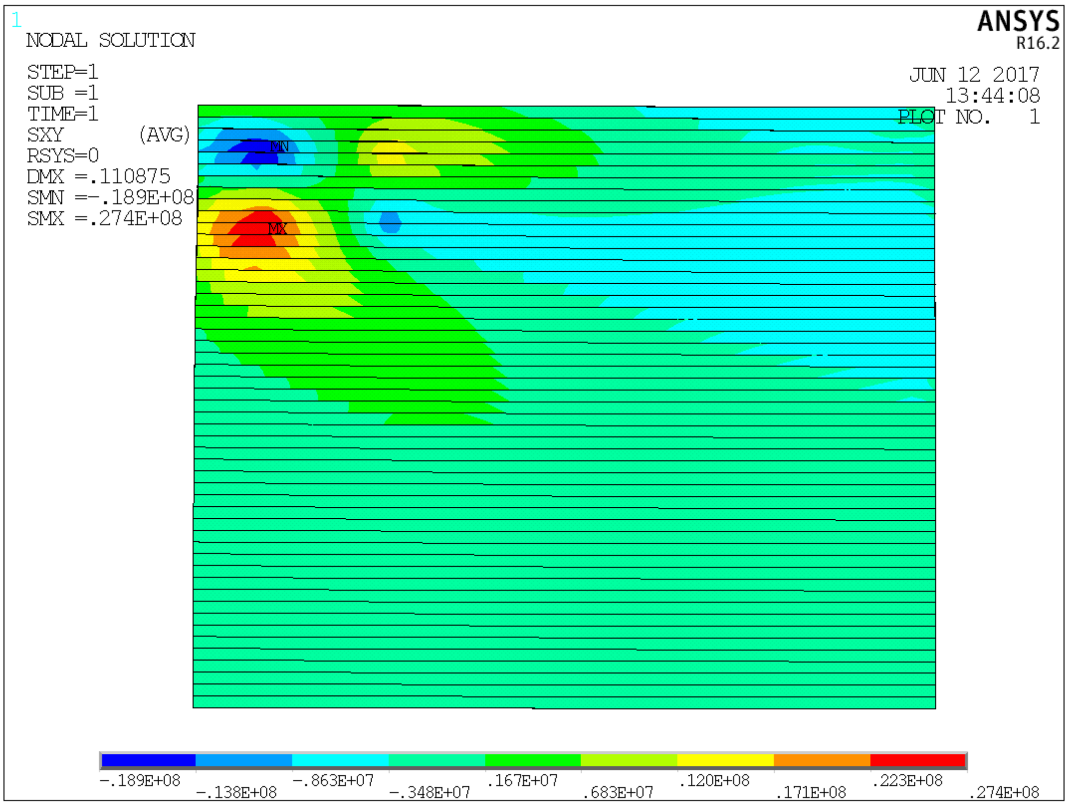

Figure 5.9: Stresses in the resin layer of the gate with scaling factor included and loaded by a distributed load (ROK)

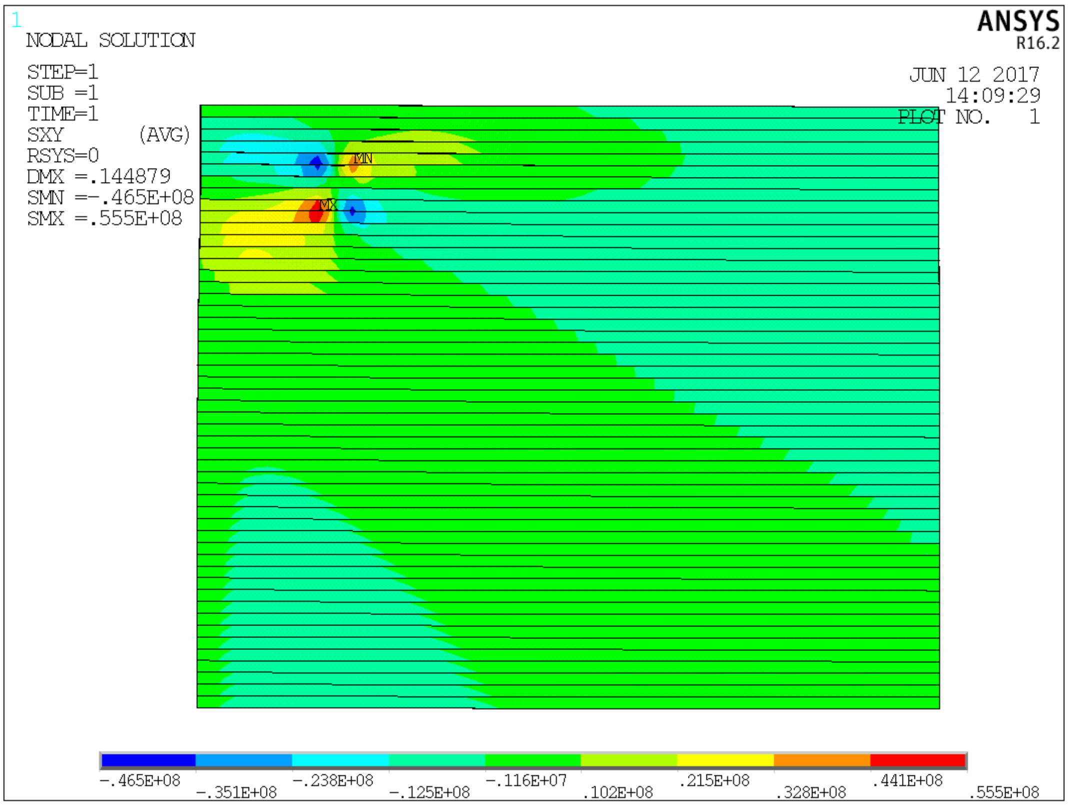

Figure 5.10: Stresses in the resin layer of the gate with scaling factor included and loaded by a strip load

be repaired but the degree of damage to the surrounding area may not be high. The rear skins are capable of retaining water even if the front skin ruptures and the stress peaks in this rear skin are lower, as illustrated in Figures J.18 and J.19 the stresses in the rear skins of the laminate are significantly lower.

- The collision takes place above the water level and the stress peaks are also above the water level. Depending on the progression of the tear the gate may still be structurally sound with regard to water retention.
- The collision discussed here is a very rare and destructive collision due to the high velocity assumed for the ship. The majority of collisions will produce stresses far below the results found here.
- Whether the gate fails appears to be dependant on the load model. If the ship bow deforms before the peak stress is reached the loaded area will increase which is beneficial for the stress field. This possibility will be further discussed in Chapter 6.

The four points discussed above are all advantageous for the resistance and safety of the gate. From this it can be concluded that the gate as designed will not fail due to macro delamination if subjected to the governing collision load.

6

Non-Elastic Ship Behaviour

In Chapter 3 the assumption was made that a behaviour of the ship was relatively simple and easy to predict. This was done by assuming either linear stiffness or infinite stiffness. This is common practice as suggested by structural codes and leads to valuable results for the design of a lock gate. These results are all on the conservative side, thus there is reason to believe that a more efficient design could be obtained if this behaviour was modelled in a different way.

In reality ships are more complex than a simple spring. They consist of sheets of steel stiffened by girders and welded together into non prismatic elements and may contain internal partitions or other irregularities. These imposed simplifications will be discussed in Chapter 6.1. In order to fully determine the behaviour of such a vessel during collision an elaborate analysis would have to be done with finite elements. This is a too time-consuming solution for this research. Instead a simplified model is suggested in the form of a spring with a non-constant k-value with concentrated damping due to damage. This model is first discussed in Chapter 6.2 en then applied to a collision scenario from the previous chapter. In Chapter 6.3 the different effects of the parameters on which the model is dependant are discussed. The parameters are varied in order to gain a better understanding of the model. Finally in Chapter 6.4 the obtained results will be summarised and their value will be discussed.

6.1. Simplifications in the Current Model

Although modelling the ship as a simple spring is sufficient to obtain an idea of the deformations of the gate, such a simple model will always be different from reality. In essence the problem with the model can be brought back to the fact that the ship, and thus the steel, is assumed to be perfectly elastic independent of the force applied to it. This reasoning is flawed for two reasons:

- Steel is only elastic up to a certain point. At a certain stress level the steel will yield and suddenly deform large amounts without extra application of force. The stiffness can be said to be zero in this region. After this the steel regains some stiffness but it is far from linear. In assuming that the ship responds purely elastic it is automatically assumed that the vessel will undergo no plastic deformation or other forms of failure such as buckling. One need only look at a vessel after a collision to see this is not true. In ignoring ship failure and non-elastic deformations the material model is simplified in a a manner which is not accurate, due to lack of yield point and failure point. This is shown in Figure 6.1.
- Even if the material behaviour of steel is ignored the stiffness of the ship as a whole will change during collision. As the collision progresses a large portion of the ships hull will be activated. This

includes wider cross-section, which will in turn have larger stiffnesses.

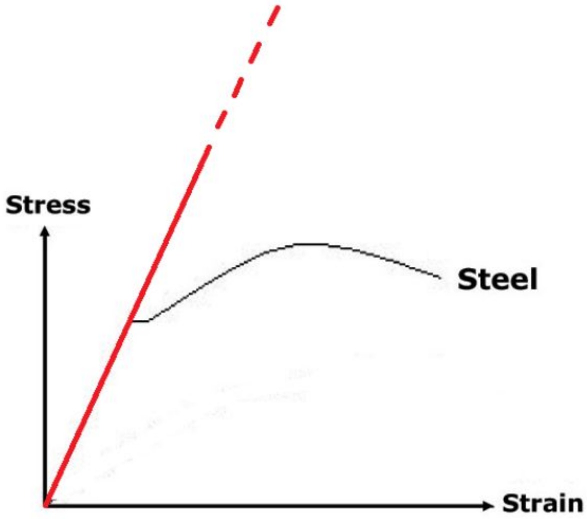

Figure 6.1: Real stress/strain relationship for steel (Black) compared to the simplified model (Red)

If forces are small the simple model will likely be quite accurate due to the steel still being loaded in its elastic stress region. During collision however there is no reason to believe that the forces will be small. Once a vessel starts deforming it will dissipate a large amount of energy through work which will have a significant effect on the energy balance during collision. For this reason a model which can take this energy dissipation into account is desirable.

6.2. Non-Elastic Ship Behaviour Model

In this chapter a deformation model for the colliding ship is suggested which attempts to solve the two issues described in the previous chapter. First the solutions to each issue are discussed a then they are brought together in one model.

6.2.1. Changing Cross-section

The cross-section of the bow increases from zero at the tip to a certain value for the mid-span of the ship. It does so non-linearly which makes describing the cross-sectional area as a function of the distance from the point difficult. The exact bow shape for a typical V-bow is given in [22] for a class III ship. Other ship classes are assumed to have the same shape but scaled to match the global dimensions. These bow shapes are given in Appendix C. In order to simplify these shapes to make them workable they shall be linearised over short spans. It would make sense to choose the supporting cross-beams as edges of these spans. The exact heart-to-heart distance these cross beams depends on the vessel type, but a reasonable assumption is 0.5m[16]. For each linear stretch the average cross-section is said to apply over the entire stretch. This is shown in Figure 6.2. For these calculations the hull shape can be found in Appendix C and can be interpolated over the segments to obtain the average cross section. Then a hull thickness of 8mm is chosen and the effective deck thickness (included lateral support beams) of 10mm, which together lead to the steel cross section of the bow.

Stiffness Ratio's

The distribution of energy between the gate and the ship can be calculated by using the ratio between their stiffnesses. If, for example, the ship was five times as stiff as the gate (ratio 5) the gate would

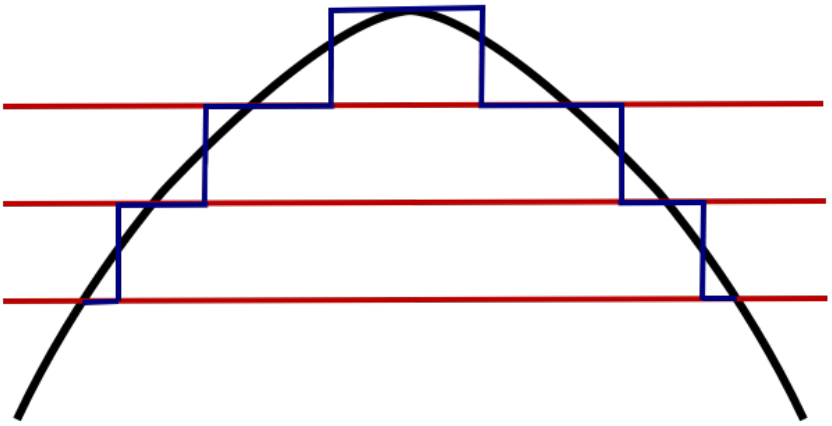

Figure 6.2: Assumed bow shape during calculations. Black: Real bow, Red: Segment edges, Blue: Averaged bow shape

absorb $\frac{ratio}{ratio+1} = \frac{5}{6}$ of the energy. This can be used to simplify calculation later on. The ratio's between the stiffness's of ships of classes I-IV are related to the gate stiffness from the collision scenario's in Table 6.1. The stiffness ratios are calculated from there.

Table 6.1: Stiffness's and stiffness ratio's between ships and gate for classes I-IV[22]

Ship Class	Span from Bow Tip [m]	Ship stiffness [N/mm]	Gate Stiffness [N/mm]	Ratio
I	0 - 0.5	$6.89 * 10^6$	$3.17 * 10^5$	21.76
	0.5 - 1	$16.76 * 10^6$		52.91
II	0 - 0.5	$8.17 * 10^6$	$3.42 * 10^5$	23.91
	0.5 - 1	$19.95 * 10^6$		58.40
III	0 - 0.5	$8.67 * 10^6$	$5.06 * 10^5$	17.15
	0.5 - 1	$21.21 * 10^6$		41.95
IV	0 - 0.5	$9.83 * 10^6$	$51.74 * 10^5$	1.90
	0.5 - 1	$23.43 * 10^6$		4.52

6.2.2. Non-Elastic Behaviour and Failure

Once the force between the gate and the vessel exceeds a certain limit the ships bow will begin to deform in a plastic manner. This deformation may be caused by yielding of the steel or by buckling of the plates. Which mode takes place depends on the exact shape of the bow and is difficult to compute. For the global behaviour of the collision however it is not important which mode leads to failure only at which stress this occurs.

In order to simplify the failure path a model is used based on [16] in which the vessel consists of a series of segments which will fail independently one after another. These sections are bound by the supporting cross beams as these stiffen the ship and help prevent deformation. This is another reason why the choice was made to average the cross-section over these spans in the previous chapter. Each section will first deform elastically up to its failure load after which it will fail completely and deform all the way to the next cross beam. Following this the next section will deform elastically and then fail and so forth. This is shown schematically in Figure 6.3

The exact failure mode is dependant on the assumed segment length and the failure stress. The sensitivity of these variables is examined in Chapter 6.3

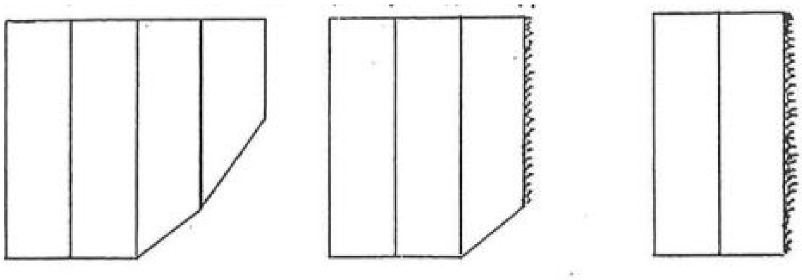

Figure 6.3: Schematic overview of a vessel failing segment by segment [16]

6.2.3. Resulting Model

If the above simplifications are combined we obtain a model with a quantifiable cross-section and a simplified displacement mode. This makes it possible to construct a force-displacement diagram as shown in Figure 6.4.

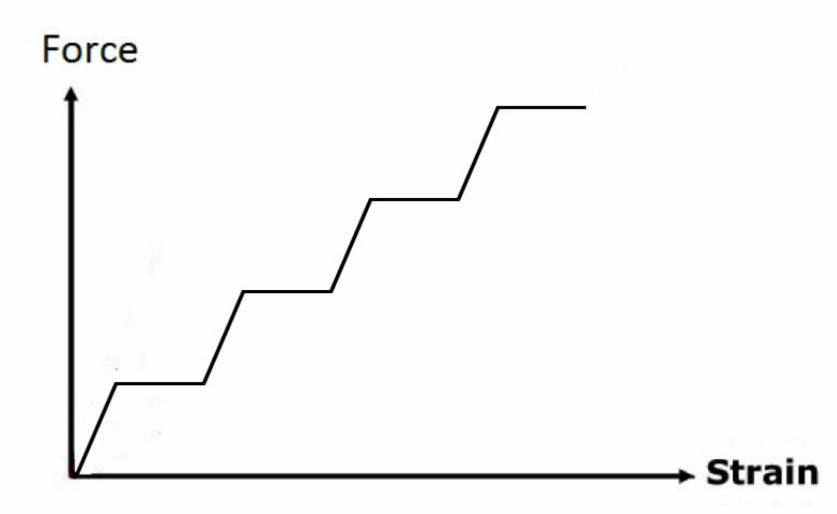

Figure 6.4: The force-displacement diagram for the non-linear ship spring model

The loads at which the force plateaus are located are equal to the failure stress multiplied by the average cross-sectional area for each segment. The stiffnesses for each span of each ship class are given in Table 6.1 in the following section.

6.2.4. Collision Force

To be able to work with the model suggested in this chapter it is necessary to know what the force is which is applied to the ships hull. The force equilibrium at the time of impact is illustrated in Figure 6.5.

Using this equilibrium the collision force can be defined as:

$$F_{collision} = F_{damper} + F_{gate,spring} \tag{6.1}$$

With the known definitions for the damper force and the gate spring force, this can be written as:

$$F_{collision} = k_{gate} * w + c_{gate} * v \tag{6.2}$$

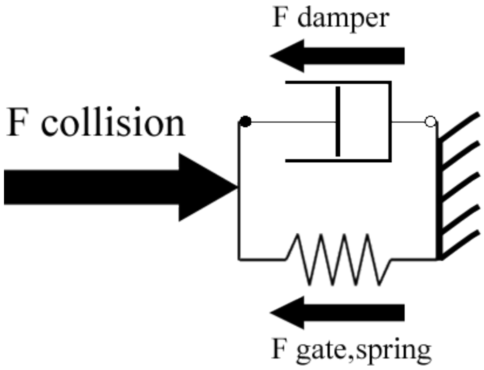

Figure 6.5: Force equilibrium during collision

This equilibrium assumes that all the dissipation mechanisms which are bundled in the damper force are situated at the tip of the ships bow and thus directly contribute to the collision force in the ship. In reality this is not the case, as many of the dissipation mechanisms and listed in Chapter 3.1.6 are located at different points such as the gate hinges. The placement of these dissipation mechanisms can not be portrayed accurately in a 1D model.

In order to determine a solution for how to express the collision load, the effects of this damper force on the gates displacement must be determined. If the collision force at which the first segment fails is a known constant, which is the case for a known vessel, the equilibrium can be written as:

$$F_{segment,failure} = F_{damper} + k_{gate} * w_{gate} \tag{6.3}$$

Because the expression on the left of the equilibrium is a constant it can be concluded that the larger the value of F_{damper} is the lower the value of the gates displacement [w_{gate}] will be. This suggests that assuming the total damping force to be applied at the tip of the ships bow would lead to unrealistically small gate displacements. This is undesirable as it makes the gate seem more resistant to collisions than it really is.

Instead a conservative approach would be to assume the opposite and remove F_{damper} from the equilibrium equation. In doing so it is being said that none of the damping forces are applied at the ships hull, instead they are carried by the gates supports. This is also not a realistic model, but it can be said to be conservative and thus safe. It also has the added benefit of simplifying the equation for the collision force, which then becomes:

$$F_{collision} = k_{gate} * w \tag{6.4}$$

The effect this will have on the displacement of the gate as a function of time is sketched in Figure 6.6. Not that at the point at which the kinetic energy of the ship is completely dissipated and the direction of the velocity reverses the two expressions give the same results. This is due to the velocity being zero at this point and thus the factor [c * v] also being zero. In effect the maximum displacement of the gate doesn't change by removing the damping from the expression of the contact force. The amount of energy dissipated by the non-elastic deformation of the ships hull also remains the same, as it is defined as [$F_{segmentfailure}$ * segment length] which has not changed.

6.2.5. Example Calculation

The model described above will now be used to calculate the displacements of the gate due to a collision with a class III vessel in order to compare it to the simple model. In order to run the calculation four

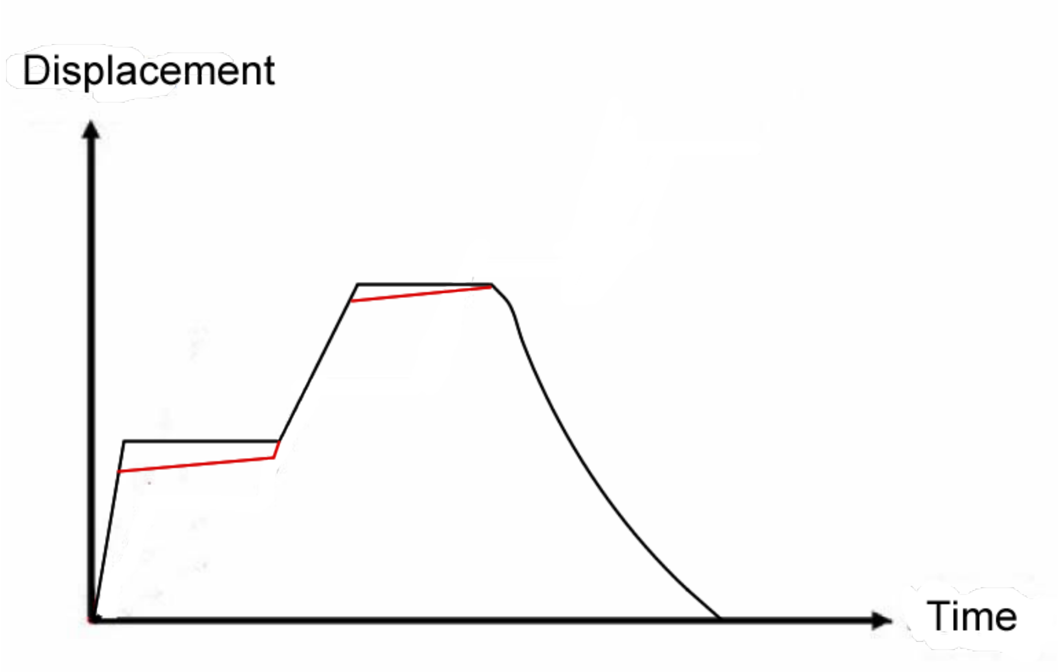

Figure 6.6: Sketch of the effects of removing the damping force from the calculation of the collision force. Black:Without damping, Red:Changes by including damping.

variables must be chosen. these are the segment length, the failure stress, the damping factor and the collision velocity.

It has been discussed in Chapter 3.4.2 that the damping factor will be chosen as 0.5. This is a large value but it represents multiple damping processes. The collision velocity is discussed in Chapter 3.1.4 and a value of 3.3 m/s is taken. The segment length is the amount the ship hull displaces once a failure load is reached. This is will be discussed in Chapter 6.3.2 and is visible in Figure 6.4 as the length of the horizontal stretches. Finally the failure stress is the average stress in the steel of the cross section at the point of failure. When this is multiplied by the steel cross section as discussed in Chapter 6.2.1 the failure loads of the segments are found. These loads are the seen in Figure 6.4 as the height of the horizontal stretches.

To summarise the variables chosen to do this are:

- Segment Length - 0.5 meters
- Failure Stress - 270 N/mm^2
- Damping Factor ξ - 0.5
- Collision Velocity - 3.3 m/s

The calculation is run numerically using MatLab in the following manner:

1. The ship and gate are considered to have the same displacement during the collision and are given an initial velocity equal to the collision velocity.
2. For every time step op 0.00001 seconds the displacement of the ship and gate are determined. Taking into account the work done by the gate spring and damper. The velocity after each step is calculated assuming all remaining energy is kinetic energy.
3. The force which would be required to acquire this displacement is calculated by multiplying the displacement by the stiffness of the gate. As long as this force in below the failure load the situation is treated as with the cases from Chapter 3.
4. Once the force between the gate and the ship reaches the failure load of the first segment the force (and with it the displacement of the gate) remains constant while the ship segment crushes

dissipating energy equal to the work required (Force * Displacement).

5. During each time step in which the ship bow is failing the ship is moving forwards with a certain velocity which decrease each step due to there being less energy available. Once the entire segment has displaced the gate begins to deform again.
6. This process repeats for the following ship bow segments until the kinetic energy reaches 0. At this point the gate spring becomes the driving factor returning to its original position in the same manner as in the simple system from Chapter 3.

This MatLab code used for this analysis is supplied in Appendix K.

The results of this calculation are shown in Figure 6.7, giving maximum deflection for the simple model and complex model of 86 and 23 millimetres respectively. This coincides with roughly 50% of the ships kinetic energy is dissipated by the non-elastic deformation of the ships hull. The graph of the contact force has the same shape, but all displacements should be multiplied by the gate stiffness k.

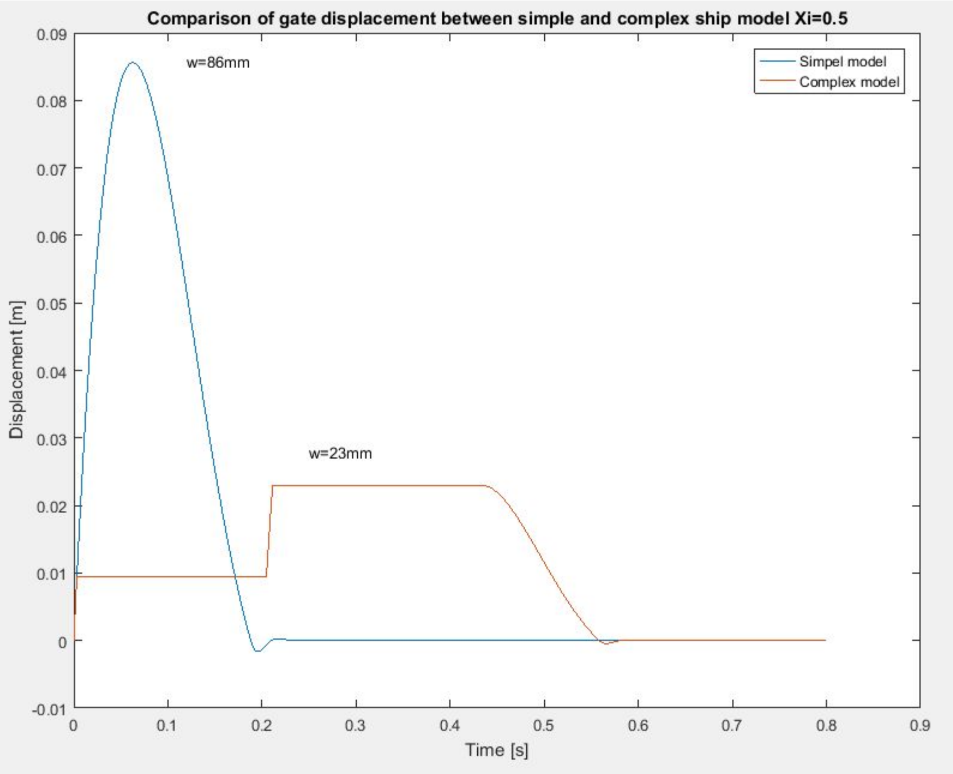

Figure 6.7: Comparison of gate displacement between simple and complex ship model, Xi=0.5

6.2.6. Discussion

The first thing that can be seen from the previous calculation is the large difference in maximum deflection. This reduction is caused solely by the amount of energy dissipated by deforming the ships bow. This seems strange considering that is is regular practice to consider a ship infinitely stiff even for steel designs. With FRP having lower moduli than steel it would increase the relative stiffness of the ship and bring it closer to the 'infinitely stiff' region. However what this image shows is that even though the elastic deformation of the ships bow is insignificant the forces between vessel and gate are high enough to cause failure of the ships cross-section. The plastic deformation which coincides with this will still have an impact on the energy balance.

In the example from Chapter 6.2.5 five regions can be distinguished in the complex models graph.

1. The first part of the line follows the same path as the simple solution. Here the ship is deforming elastically which has no visible effect of the deflection of the gate.
2. The second part is horizontal, this means that during this 0.2 of a second the gate does not deform. The reason for this is that the first segment of the ship has reached its failure load and is collapsing. During this collapse the force between vessel and gate remains constant and thus the gate spring remains at the same displacement. Energy is being dissipated in the form of the work needed to deform the ship. This region lasts as long as it take the vessel to move its segment length (in this case 0.5m).
3. The third part once again represents deformation of the gate. The ship has now deformed exactly one segment length and is now reinforced by a cross beam. The following segment is now deforming elastically.
4. The forth part is again horizontal, as the failure load for the second ship segment has been reached. Just like in the second section the ship is now crushing against the gate and dissipating energy equal to the work required. The section does not necessarily end when the entire ship segment has deformed. It is possible that the kinetic energy is all dissipated before this point in which case the ship will stop crushing.
5. The final section begins when all the kinetic energy has either been dissipated by the deformation of the vessel and other damping terms or stored in the gate spring. At this point the gate begins returning to its equilibrium position pushing the ship with it. This happens in an identical manner to the simple model.

Depending on the systems input variables the deformation may consist of fewer of more sections. These variables and their effects will be discussed in Chapter 6.3.

The amount of energy dissipated by the ships deformation is equal to the sum of all the work components.

$$Dissipated\ Energy = \sum Work = \sum F_i * u_i \tag{6.5}$$

The loads F are the failure loads for each segment and the displacements u are the amount the ship deforms within that segment. As the amount that the final segment deforms is not known before the calculation this equation will be solved numerically.

The results of this analysis are that 77.8% of the total kinetic energy of the ship if dissipated through plastic deformation. At this point the ship will have deformed 0.71 meters.

6.3. Effect of the Influencing Parameters

In the numerical calculations for the complex ship model there are five parameters that can be distinguished. All other aspects are either directly proportional to one of the five or known constants such as material properties. These five variables are:

- Failure Load
- Segment Length
- Gate Stiffness
- Input Energy
- Damping Factor

In order to examine the effects of each of these values they will each be varied in turn while all others remain at their standard value. By standard value the value is meant which was assumed during the analytical calculations. These values are shown in Table 6.2. The failure load in represented by an equivalent failure stress and the input energy is represented by the ships velocity. This will be discussed in Chapters 6.3.1 and 6.3.4 respectively.

Table 6.2: Standard Values for model influencing parameters

Parameter	Standard Value
Segment Length [m]	0.5 m
Failure Load (Failure Stress)	270 N/mm^2
Gate Stiffness	1.65*10^9 Nmm^2
Input Energy (Ship Velocity)	3.3 m/s
Damping Factor ξ	0.5

6.3.1. Failure Load

The load at which the ship fails is directly proportional to the amount of energy dissipated when failure of a segment takes place via the segment length. If the steel cross-sectional area of each segment is known then this can be represented as an equivalent failure stress by dividing the load by the steel cross-sectional area. With this in mind the energy dissipated when a segment fails completely is:

$$Work = \sigma_{failure} * A_{steel} * segment\ length \tag{6.6}$$

In which:

$\sigma_{failure}$	is the failure stress.
A_{steel}	is the steel cross section of the current hull segment

The effects of an increase in $\sigma_{failure}$ are twofold. Firstly an increase failure stress makes it less likely that a segment of the ship reaches the load at which it would fail. Secondly when a segment fails it will dissipate more energy due tot the increased load. These two aspects have opposite effects on the displacement of the gate, increasing and decreasing it respectively. Furthermore the fact that higher strength steel will dissipate more energy is based on the assumption that the load remains constant during failure of a segment. It is also possible that the ultimate strain of the material will be reached and the material will tear. The effects this will have on the progressions of the collision force can not be taken into account in this model without experimental data on ship hull failure. For these reasons it can not be said whether or not a large $\sigma_{failure}$ is beneficial or not without further testing.

In order to determine the effects the numeric analysis was run multiple times with standard values while varying the failure stress with each run. The largest displacement during each run was recorded and plotted as a function of $\sigma_{failure}$. The results are shown in Figure 6.8. It is worth noting that the graph goes up to much higher failure stresses than would ever be realistic. For low quality steel and a buckling mechanism a lower bound of around 100 N/mm^2 could be expected. While for very high quality steel which can be stressed to its yield stress a upper bound of roughly 460 N/mm^2 can be estimated. The higher values in the graph serve to illustrate the extremes of the model.

The horizontal part of the graph for very high $\sigma_{failure}$'s in the region in which no plastic deformation takes place. Therefore the displacement is independent from the ship strength and the vessel can be said to be infinitely stiff. This is the region which is used for calculation in practice. As can be seen this is only a valid theory for stress levels which are far outside the realistic region and will thus always be very conservative. If we look at the range in which be expect to find our failure load it can be seen that the displacements are 50-90% lower. This is a huge difference which could potentially save a lot of material on the gate structure.

Another point which stands out is the saw-tooth shape of the graph. This pattern consist of regions in which there is a positive derivative and a negative derivative. this in essence means that whether making the ships structure stronger will have a positive or negative effect on the gates displacement is dependant on which region of the graph the values are in. This is caused by the fact that the displacements are influence by two factors which have opposite effects of the energy balance:

1. The height of each of the plateaus is increased as the ship become stiffer as it is defined by
$$w_{gate} = \frac{F_{failure,ship}}{k_{gate}} \tag{6.7}$$
and the force at which the ship fails is increase as the failure stress goes up.
2. The high force at which the ship fails requires more energy in the form of work to deform the ship the given segment length. This means that after such a segment was to fail there is less energy left for further gate deformation and the ultimate deformation will be decreased.

The first point discusses the situation in which the final gate deformation takes place on a plateau, as that is what is changed. The second point discusses the situation in which there is still energy left after a segments deformation and further elastic gate deformation takes place. These cases coincide with the front (upward) en back (downward) sides of the saw teeth respectively.

In the region of interest there seems to be a linear relationship between failure stress/load and displacement, because in all cases the kinetic energy will be fully dissipated during the failure of the second segment. However the exact location of this peak is also dependent on the other influencing variables. For example, in Figure 6.9 a Xi value of 1.5 is taken and now the peak is right in the middle of the region of interest. This is not a positive thing as the xi value is hard to determine and has a significant effect on what the most beneficial failure load would be.

In reality the failure stress of the vessel is not a variable as is presented here, but a ship constant which can be calculated. In those cases it can be inserted into the model presented here as a known constant. The images here have value for the cases in which the failure stress is not known exactly. in these cases a safe assumption would be the value that coincides with the highest saw tooth which is located in the region you expect the value to be found.

6.3.2. Segment Length

The energy dissipated when a ship segment fails is determined by the combination of the failure load and the segment length as it is defined by the displacement times the force. In order to illustrate the effects of varying the segment length Figure 6.10 show two lines. The blue line represents the case in which the four other variable are kept as their standards and the red line is a situation with a higher level of damping (xi=1.3). The pattern shown makes it clear that the response of the gate only changes if lengthening the segments leads to a situation in which the second segment no longer reaches it's failure load due to there no longer be enough energy. This suggests that as longer as the failure load (and with it the plateau height) is known the segment length isn't a very sensitive parameter. However the fact that the jump between plateaus moves as the damping is increased means that this will not be true for all cases and a closer look must be taken for each case with the parameter discerned from the local conditions.

Another note-worthy point is that the line from Figure 6.10 assume that the failure load (and thus the plateau height) is constant even as the segment length grows. In reality this is not the case as the failure load is dependant on the average cross-section of the ship which increases as a larger segment is taken. In reality the graph should look like the red line in Figure 6.11 in which the failure load in increased by a factor as the segment length increases. This factor is dependant on the ship cross-section as the function of distance from the tip of the bow and is an unknown at this point making the graph shown purely qualitative. For the case in which a specific ship is detailed this value could be calculated to make quantitative graph of the displacements.

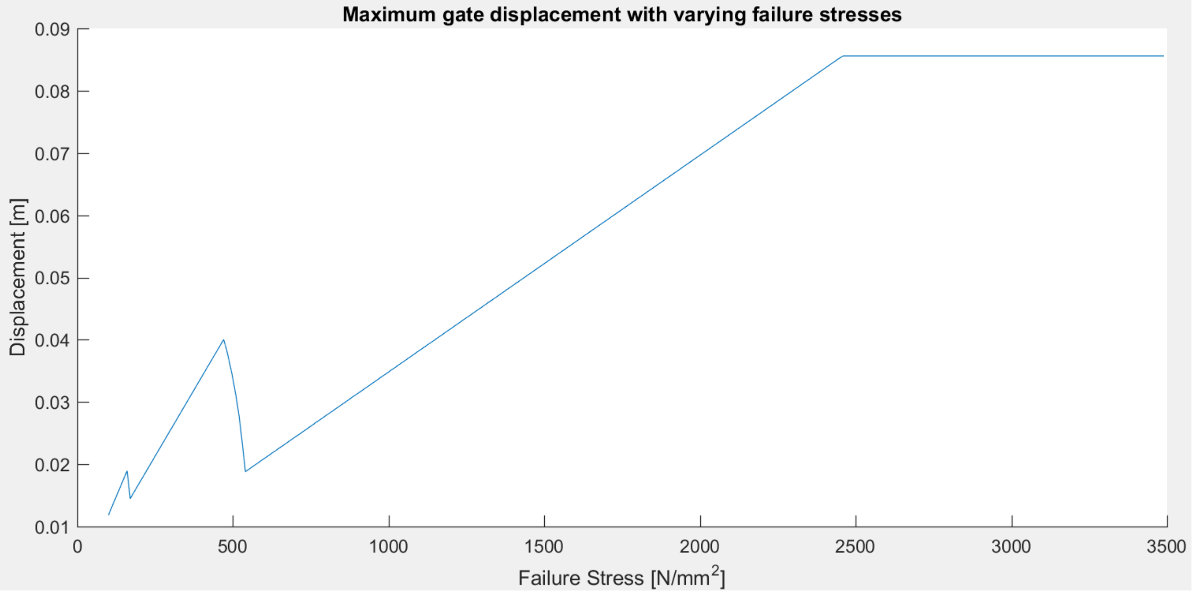

Figure 6.8: Maximum displacement of the gate as a function of failure stress

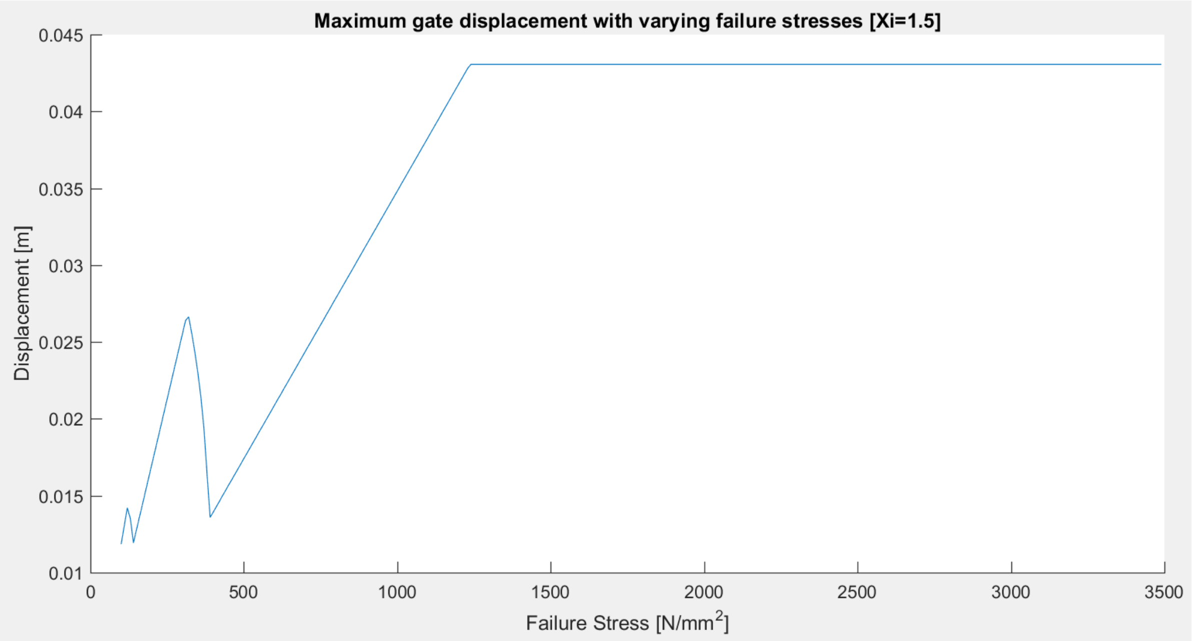

Figure 6.9: Maximum displacement of the gate as a function of failure stress with a higher xi value such that the peak falls in the region of interest

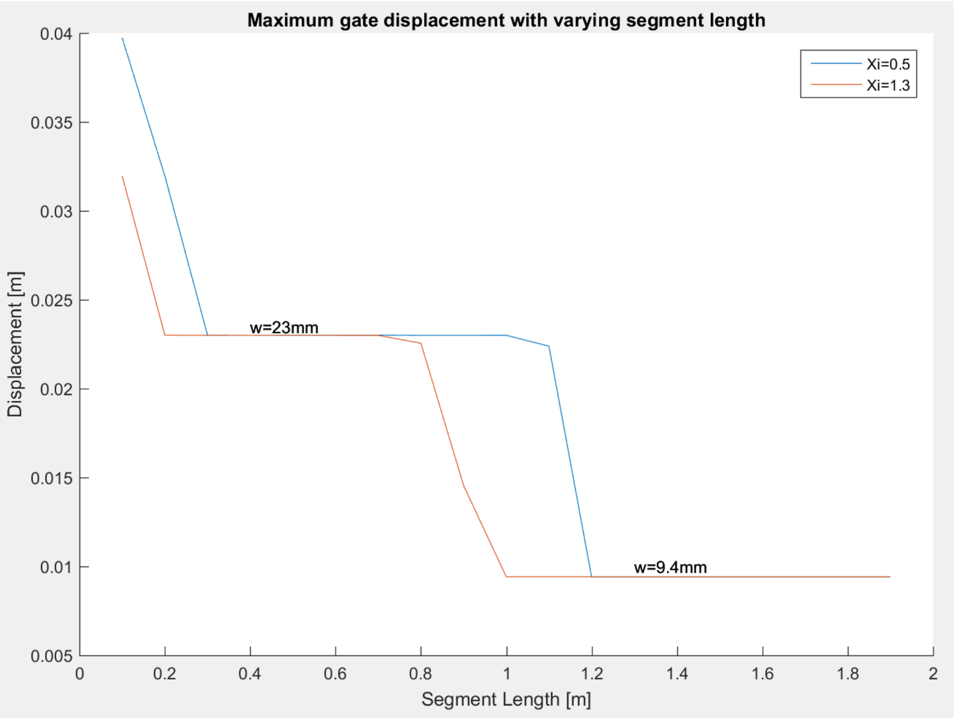

Figure 6.10: Maximum displacement of the gate as a function of failure stress, assuming no change in cross-section

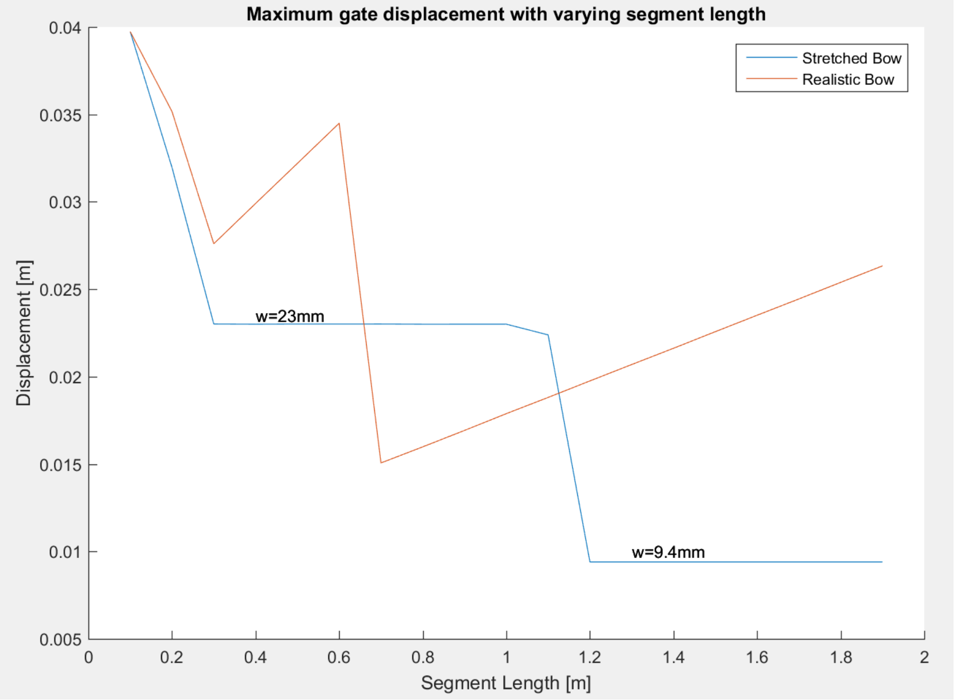

Figure 6.11: Maximum displacement of the gate as a function of failure stress, including change in cross-section

6.3.3. Gate Stiffness

The gate stiffness has two effects in the numerical model. Firstly it determined the stiffness value for the gate spring which in turn dictates the gates displacement at the moment the the ship starts failing. Secondly it is indirectly used to calculate the amount of damping due to the c value being a function of the spring stiffness. In the simplified situation in which the gate is only represented as a spring-dashpot system the EI is the only attribute of the gate which effects the calculation. In effect changing this value is testing a different gate. Still it is interesting to see the effect and a plot is made in which the maximum deflection is plotted as a function of the EI of the gate. This is shown in Figure 6.12.

Seen as the gate stiffness k is linearly proportional to the EI it is expected that the deflections are reversely proportional to the EI of the gate. Apparently the plastic model has no effect on this aspect of the calculation as this response is what would be expected of a displacement problem.

6.3.4. Input Energy

The input energy is directly related to the mass and velocity of the ship. The mass is known and the velocity is a statistical value which is dependant on a great many factors as discussed in Appendix A. For this reason there is a large degree of uncertainty in its exact value and one would like to know how sensitive the results are to the choice of velocity. In Figure 6.13 the velocity is varied while the other four variables are kept the same. It can be seen that there are regions is which the gates displacement remain equal independent of the chosen velocity. In these region the extra extra added as the velocity increases is dissipated through deformation of the ship, in other words the energy runs out in the plastic region of the collision.

For the specific case shown in Figure 6.13 the expected value is located in the middle of such a plateau and the model is mostly insensitive to the velocity. The plateau lower can also be said to represent a lower degree of collision caused, for example, by a vessel being slightly too late slowing down and gentle making contact with the gate. It must however be said that the exact location of the jumps in displacement are dependant on the choices made for the other four variables. One can not simply assume that an estimated velocity will give an accurate result, but must examine the sensitivity with the other variable known.

6.3.5. Damping Factor

As mentioned before in Chapter 3 the damping factor has a large influence on the amount of energy which remains in the system to be dissipated by the gate and ship. It is also notoriously difficult to predict without laboratory tests which are difficult and expensive. In order to estimate how sensitive the solution is to the assumed damping factor the numerical analysis is run multiple times with a series of xi values between 0 and 5. 0 is the undamped case which is even less favourable than just the internal material damping for FRP, which is 4-8%, and 5 is far above any realistic value. This way the extremes are visible. Figure 6.14 shows this plot.

In becomes apparent that for a Xi value of lower than ˜2 the maximum deflection of the gate does not change. This is unexpected due to the fact that it represents a difference of almost 90% of the kinetic energy. The reason behind this is that in all cases up to a Xi value of ˜2 the energy is completely dissipated during the failure of the same segment. Apparently the choice of Xi is much less important than originally expected when accounting for ship deformation.

To further verify this conclusion the same plot is made while also varying the failure load (in the form of the equivalent failure stress). This multi-plot is shown in Figure 6.15. It becomes apparent that the failure load has an impact on the location of the stable regions with regard to Xi. This is not unexpected seen as it strongly influence the energy dissipation during failure. What is interesting however is that within the region we expect Xi to be in, 0-1 (sub-critically damped), the choice of Xi still seems to be

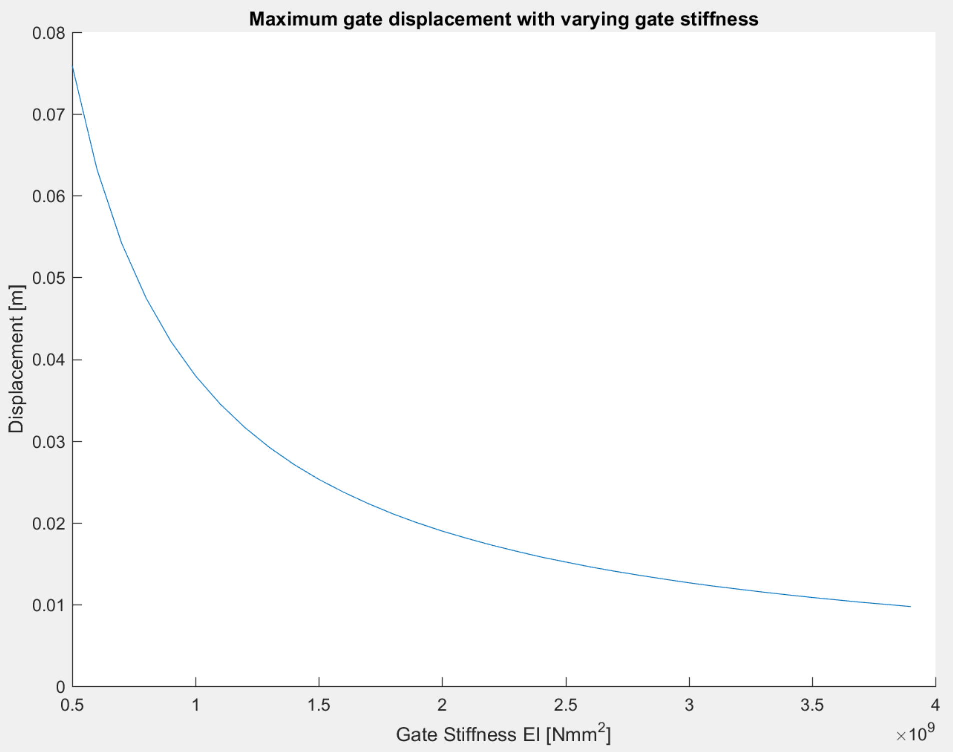

Figure 6.12: Maximum displacement of the gate as a function of gate stiffness

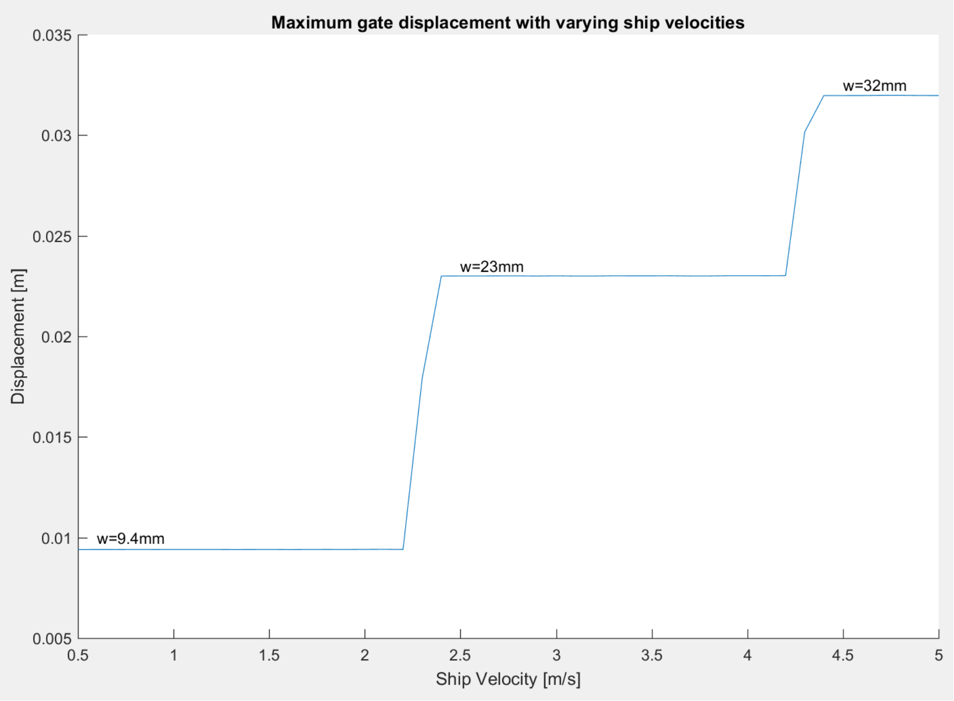

Figure 6.13: Maximum displacement of the gate as a function of ship velocity

arbitrary. In fact Xi could simply be chosen as 0 and damping ignored completely without it altering the results. This will likely not be true for all values of $\sigma_{failure}$, but if ignoring damping would alter the results it will always be in a conservative manner.

6.4. Conclusions and Discussion

From the findings in this chapter we can conclude that the common simplifications of the case in which a ship collides with a lock gate are too conservative. A comparison of the force on the ships bow and it's geometry is enough to show that the assumption that it will not deform at all is a highly conservative simplification which could lead to over-dimensioning of the lock gates in cases where collision is considered the governing load case.

The effect the collision will have on the considered lock gate is dependant on the manner in which the ship will fail. The findings above are based on a segmented failure model, which is somewhat crude but serves to illustrate the effects of ship failure as a whole. In order to create a more accurate model more information is needed about the exact structure of the colliding vessel, preferably backed up by physical tests. Obtaining this information is outside the scope of this study and thus only qualitative conclusions can be drawn.

Although the degree to which the effects of the collision on the gate are reduced is dependant on a series of variables, all cases in which variables within the realistic region are chosen will lead to less deformation than the traditional case. This means that the non-elastic dissipation mechanism will be relevant for all constructed lock gates. The degree to which the results will be affected will increase as the gate becomes stiffer. Seen as steel gates are generally stiffer than FRP gates it is expected that this mechanism will be even more important for steel gates.

The governing variables as described in the previous chapters are Failure Load, Segment Length, Gate Stiffness, Input Energy and Damping Factor. Of these five variables four of them are functions of the physical geometry of either the ship or the gate and can thus be calculated before a calculation is done. This leaves the Damping Factor which is a function of the collision scenario are very hard to predict. In order to gain some notion as to the level of this damping factor normally scaled tests would be performed. The results from Chapter 6.3.5 however show that, due to the segmented behaviour of the ship, the system become insensitive to the damping factor within certain regions. It also shows that the region of interest will coincide with these stable regions for the other variable as assumed here. This has the potential to remove the need for scaled tests in the future.

If determining the value of one of the variables proved difficult it is possible to plot the reaction of the gate as a function of this variable and graphically determining a safe estimate. Doing so requires an estimation of the damping factor, or multiple plots with a series of damping factors. With these plots the value which coincides with the largest gate deformation within the range of interest is a good conservative estimate and may safely be used.

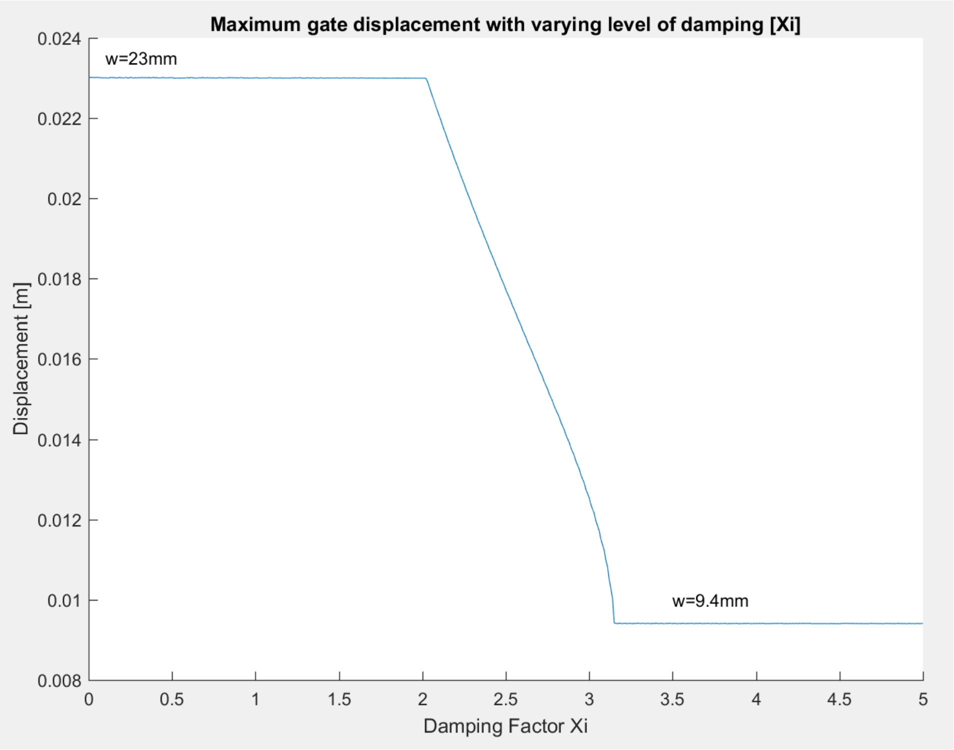

Figure 6.14: Maximum displacement of the gate as a function of Xi

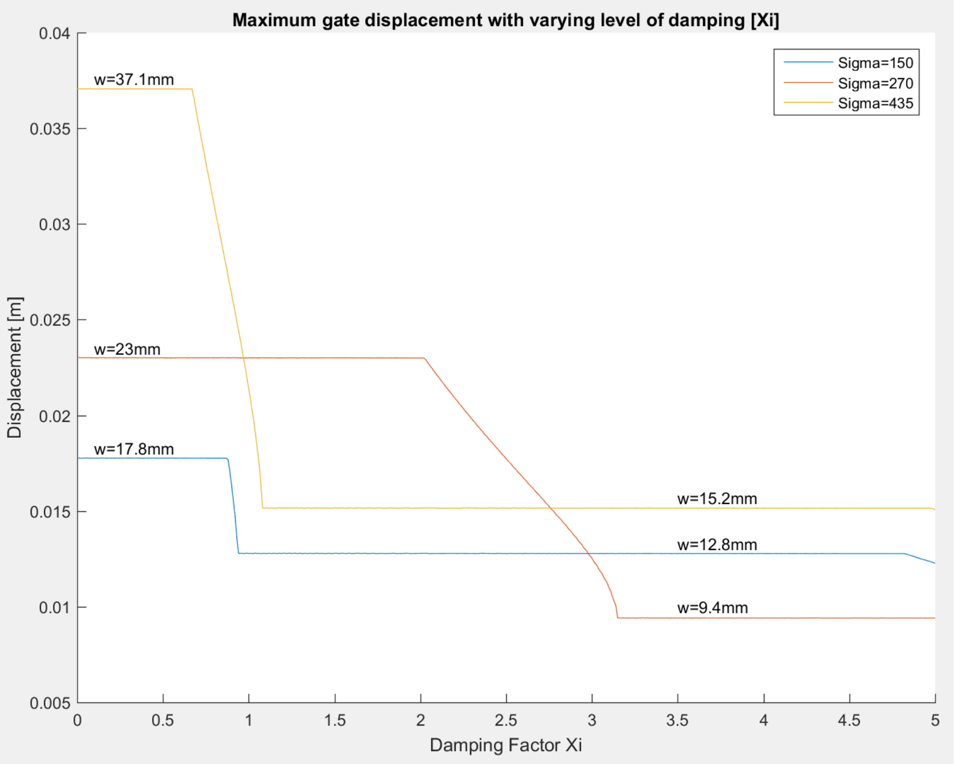

Figure 6.15: Maximum displacement of the gate as a function of Xi for multiple sigma's

7

Conclusions

The goal of this study was to develop a model, which can be used to simulate the collision behaviour of a vessel and a lock gate constructed of Fibre Reinforced Polymers. This has been accomplished by applying a series of calculation methods to the existing FRP lock located in the Wilhelminakanaal in Tilburg, Sluis III, and using the results to draw general conclusions.

In order to gain insight into the reaction of the ship and gate as a whole an analytical model was constructed. This model consists of a one dimensional system in which the gate in represented by a spring damper system. All forms of failure of the gate and non-elastic deformations of the ship were neglected for this first look at the collision. Using this model it was shown that it was not important whether or not the ships engine remained engaged during the collision, as only minimal extra displacements were caused. It was also shown that the often used approach in which the ship is considered infinitely stiff is a valid estimation which is somewhat on the conservative side, but only in the order of 2%. The manner in which this simple system was solved, be it by differential equation or numerical code, was of no importance to the results. However an accurate estimation of the amount of expected damping is necessary to acquire accurate results.

Using a finite element model constructed in Ansys 16.2 more detailed information on the stresses in the gate elements was obtained. Preliminary runs of the model to check its behaviour lead to the conclusion that both the hydrostatic water pressure and the cavities for the valves could be ignored during calculation. This is due to the collision being above the water level and away from the valves. For other cases in which the governing vessel has an underwater bulb, as is common in sea locks, this will not be true. Simulating the collision with a static or dynamic load made a significant difference to the displacements of the gate, with 75% larger displacements being found for the dynamic collision, due to more concentrated load application. This shows that the load condition suggested by the ROK leads to a gross underestimate of the damages and that the result may lead to an unsafe structure. The lack of plastic deformation in FRP structures requires a more accurate load case.

When the gate is subjected to a dynamic load applied via a rigid model of the ships bow, it can be shown that the gate will surpass its damage strain of 0.27% over a large region of the gate, but it will remain under its failure limit. This means that were such a collision to take place the gate would not fail and will remain able to retain water, but substantial repairs will have to take place to restore the gate to full working order. The gate will become less resistant to moisture or further loading, because the protective resin layer is damaged. It may be possible that these reparations will not be necessary once more experience is gained with the material and the safety factor are reduced. However this is not expected due to the fact that this damage limit is surpassed by a large amount around the collision area. Furthermore it was shown that the internal flanges directly around the point of collision will be subjected to crushing. This damage will not lead to loss of water retention, but will increase the degree of repairs required to restore the gate to serviceability.

The gate is designed as an InfraCore Inside panel, which is a patent owned by FibreCore. This design has multiple overlapping laminates interconnected with resin which together form the skin panels of the gate. This structure is strong due to the long failure paths but susceptible to macro level delaminations. An analysis in which each sub-laminate was modelled separately was used to determine if this mode would lead to failure. It became clear that the manner in which the load in applied is important for the magnitude of the stresses in the resin layers, but that for a realistic load case the ultimate failure stresses will not be surpassed.

If the assumption that the ship will not fail and deform is removed and the load between the ship and the gate is compared to the resistance of the ships bow it becomes clear that the front end of the ship will deform. The manner is which this will take place is dependant on the exact structure of the vessel and is hard to predict. In order to account for this deformation and the energy that will be dissipated through it a segmented failure model is introduced. The outputs of this model are dependant on multiple variables, however if the structure of the vessel is known most of these can be calculated prematurely. The remaining variable is the degree of damping during the collision, which is a difficult issue to estimate. However it is shown that sensitivity to this variable is low within certain regions. The exact locations of these regions is dependant on the other input variables. For the case handled here the stable regions coincide with the realistic regions for the governing variables. This would lead us to believe that for realistic cases the choice of the damping factor is not very important.

The model shows large degrees of energy dissipation for all realistic choices of input variables and suggests that the calculation method which is commonly used today is very conservative. This leads to believe that a large portion of the collision energy (˜50%) is dissipated through non-elastic deformation of the ships hull. If more research is done into ship bow failure large savings could be made for lock gates in which collisions are considered the governing load. The model presented here is still in a very crude form and is thus not suitable to draw quantitative conclusion, but further refinement may change the way collision deformations are calculated in the future.

8

Recommendations

During execution of this research aspect came to light for which no direct information was available. Due to time constraints it was not possible to answer all these questions and thus follow up research is necessary to fully understand the behaviour of ship collisions and the response of a Fibre Reinforced Polymers to them. Below a list of topics is found for which follow up research in suggested:

- **The chance and consequence of a rearward collision**. It was shown in Chapter 3.4.1 that is a vessel were to collide with the back of the mitre gates the operating mechanism would fail and the gates would be pushed open. Were this to occur for the peak locking level a water column of 7.9 metres will pass through the gates, hit the ship and flow further downstream. The consequences of this may be damage to the ship, severe downstream flooding or loss of life. The degree to which this should be taken into account or prevented should be determined.
- **The ships behaviour post collision**. If a sub-critical damping scenario is assumed the vessel will have a velocity away from the gate after collision. This may lead to secondary collisions with the chamber, guidance works or the other gate. If this will occur and the effects of such a collision are interesting topics.
- **The effects of lesser collisions to the structure**. The collision handled in this report is one of high velocity made to represent the worst possible scenario. The gross of the collision which take place are of a far lesser degree, thus a documentation of the structural response to these collision has practical value. Of special importance is which collisions can take place with no damage occurrence and the effects of multiple lesser collisions.
- **Two dimensional analytical calculations**. In Chapter 3 a one dimensional analysis was used to represent the gate. However the results of Chapter 4 gave cause to believe that a two dimensional model, making use of plate elements, would be better suited and may be able to replace the lengthy three dimensional calculation all together.
- **Determine a realistic level for the damping factor**. As discussed in Chapter 3 determining a value for the damping factor xi which will lead to realistic results is a difficult matter. One which can only be accomplished through experimentation.
- **Response in the support due to the collision**. In this report the response of the gate itself was thoroughly treated, but the effect of this loading on the pivot and supports was not taken into account. There is however a decent chance that a weak point may be found there. This merits further examination.

- **Describe the effects of collision with the upstream sill**. A vessel travelling upstream runs the risk of colliding with the upstream sill due to the large height difference. The effects of such a collision on ship and structure may be significant.
- **Cracking patterns in the resin layers**. In Chapter 5 the loads in the resin are used as a measure of their failure and the coinciding delaminations. This method assumes the there is no crack formation due to the peak stresses which occur during loading. If a crack were to form in may propagate along the resin layer a cause large scale failure and total delamination. In order to determine whether this failure mode will occur a more detailed finite element mesh will be necessary in which this mode can occur.
- **Delaminations within the laminates**. In Chapter 5 the stresses in the resin layers between laminates were examined, however the laminates themselves were considered as single shells. In reality these laminates each consist of multiple plys interconnected with resin. In a similar manner to how macro level delamination was checked in this report the micro level delamination can be examined. For this a very fine mesh is necessary, which will only be possible if a segment of the gate is isolated.
- **Determine the exact ship properties through precise modelling**. In Chapter 6 the properties of the colliding vessel were estimated by assuming an effective plate thickness and multiplying this by the cross section. As the stiffness of the bow is of interest this is a crude approximation. In order to better understand the behaviour of the ship during collision and to have correct value to insert into the plastic ship model a finite element calculation should be executed in which the bow is allowed to fail. The model of this vessel should be made based off blue prints to ensure a realistic representation.
- **Refine the plastic ship model presented in Chapter 6**. The model presented assumes each segment fails separately and abruptly, in reality this will not be true. The manner in which a ship will fail will follow one of two modes. Either the segmented approach is realistic, in which case the forces during segment failure should be determined, or the segments are less noticeable, in which case the model should be changed for infinitely small segments.
- **Determine the degree of deterioration of the material properties due to moisture**. In this study this is taken into account by a factor to the stress resistance as suggested in the CUR recommendation[11]. Laboratory tests for the laminates used will give a better understanding of which properties deteriorate and by how much.
- **Devise methods to repair the damage FRP laminates after collision**. As this report shows the gate will suffer damage even if the collision can be retained. Part of this damage will be external in the skin and part will be internal in the flanges. Ways to repair FRP laminate without recasting them are still under development. If such a method were devised the damage allowance for the gate would be increased. The fact that the damage is above the water line will make repair easier.

List of Figures

1.1 Flowchart of the report structure 3

2.1 Schematic of a sample lock. Top- and side view 6

2.2 Visual representation of the locking process 7

2.3 Top view of a lock with mitre gates. Left: Uni-lateral retention. Right: Bi-lateral retention 7

2.4 Schematic representation of a laminate structure 9

2.5 Aerial view of the Sluis III complex 9

2.6 Location of Sluis III in the Wilhelminakanaal - Tilburg 10

2.7 Schematic sideview of Sluis III in the Wilhelminakanaal - Tilburg, including sill and water levels 11

2.8 Image of the gate being lifted into place 12

2.9 Overview of the gate elements 12

2.10 Cross section of the gate structure 13

2.11 Overview of the collision between a vessel and the second gate from a upstream direction 15

3.1 Simply Supported Beam 20

3.2 Three Hinged Beam 20

3.3 Detail of the chamber wall support 21

3.4 Static scheme including plates 21

3.5 Static scheme for the rearward collision 21

3.6 Overview of the collision scenario's. Number between brackets represent symmetrical loads 22

3.7 Top view showing the geometric limitations of collisions 22

3.8 Overview of the first gate with guidance works 23

3.9 Static scheme for the case with non-central collision 29

3.10 Typical FRP and mild-steel stress-strain curves 30

3.11 Spring Damper system used and the distribution of the physical quantities 32
3.12 Static collision systems with and without ship deformations 32
3.13 System of forces for a rearward collision, including order of magnitude 33
3.14 Collision system used for the differential equation, including damping for the gate structure 35
3.15 Displacements in time for varying Xi values 36
3.16 Displacement of the gate during a collision with a class 3 vessel, with and without engine force applied, as solved by the differential equation 38
3.17 Comparison of the displacement of the gate for collision with a class 3 vessel solved with the Energy and Force methods 40

4.1 Chosen implicit elements for the static analysis 44
4.2 Chosen implicit elements for the static analysis 45
4.3 Schematic of the gate and its local axis 45
4.4 Overview of the area geometry including the ship bow 47
4.5 Top view of the area geometry including the ship bow 47
4.6 Dimensions of the gate around its supports 48
4.7 Top view of the structure with constraints made visible 49
4.8 Profile view of the structure with constraints and loads made visible 49
4.9 Displacements of the lock gate under static load condition without water pressure . . . 51
4.10 Displacements of the lock gate under static load condition with water pressure 51
4.11 Z-displacements of the lock gate for the dynamic analysis including core elements . . . 53

5.1 Schematic of a Z-laminate with its measurements 58
5.2 Element build-up for a series of overlapping Z-laminates 59
5.3 Schematic overview of the manner of modelling core elements 60
5.4 Static scheme for the loading of the test structure 61
5.5 Area layouts for the resin property comparison model 62
5.6 Schematical shear deformation behaviour 62
5.7 Detail of the core region in the local analysis model 65
5.8 Detail of the core region in the global analysis model, as reference 65

5.9 Stresses in the resin layer of the gate with scaling factor included and loaded by a distributed load (ROK) . . . 66

5.10 Stresses in the resin layer of the gate with scaling factor included and loaded by a strip load . . . 66

6.1 Real stress/strain relationship for steel compared to the simplified model . . . 70

6.2 Assumed bow shape during calculations . . . 71

6.3 Schematic overview of a vessel failing segment by segment . . . 72

6.4 The force-displacement diagram for the non-linear ship spring model . . . 72

6.5 Force equilibrium during collision . . . 73

6.6 Sketch of the effects of removing the damping force from the calculation of the collision force . . . 74

6.7 Comparison of gate displacement between simple and complex ship model, Xi=0.5 . . . 75

6.8 Maximum displacement of the gate as a function of failure stress . . . 79

6.9 Maximum displacement of the gate as a function of failure stress with a higher xi value such that the peak falls in the region of interest . . . 79

6.10 Maximum displacement of the gate as a function of failure stress, assuming no change in cross-section . . . 80

6.11 Maximum displacement of the gate as a function of failure stress, including change in cross-section . . . 80

6.12 Maximum displacement of the gate as a function of gate stiffness . . . 82

6.13 Maximum displacement of the gate as a function of ship velocity . . . 82

6.14 Maximum displacement of the gate as a function of Xi . . . 84

6.15 Maximum displacement of the gate as a function of Xi for multiple sigma's . . . 84

A.1 Top view of a lock with mitre gates. Left: Uni-lateral retention. Right: Bi-lateral retention 102

C.1 Visualisation of the shape of a V-bow . . . 113

C.2 Reference points for the shape of a V-bow . . . 114

D.1 Schematic representation of a laminate structure . . . 122

D.2 Graphical representation of a fibre roving . . . 123

D.3 Weave Patterns . . . 123

D.4 Polar diagrams for a selection of reinforcements . . . 124

D.5 Percentage of FRP market share per industry in the USA, 1998 129
D.6 Example Cross-sectional diagram of a double web beam as produced by the Strongwell Corporation 131
D.7 Honeycombed core sandwich panel 132
D.8 FRP components of a Airbus 320 subdivided by fibre type 133

E.1 Stresses and their orientations for the 3D situation 136
E.2 Image of the angle between the element x-y axis and the fibre 1-2 axis 138
E.3 Graphical representation of the coupling mechanisms in the constitutive equation . . . 142

G.1 Preliminary design U-shaped shell 152
G.2 Location of the Spieringssluis lock 153
G.3 Preliminary design - Sandwich panel (Polymarin) 154
G.4 Preliminary design - Pultruded Corrugated Sheet (Koninklijke Schelde Scheepsbouw) . 155
G.5 Preliminary design - Curved Shell Structure (Grontmij Verkeer & Infrastructuur) 156
G.6 Final design of the Spieringssluis 157

H.1 Schematic overview of a sandwich panel and the coinciding failure paths and modes . . 160
H.2 Examples of multi beam panels and the coinciding failure paths and modes 160
H.3 Build-up of a Infracore Inside panel 161
H.4 Fibre orientation in a InfraCore Inside panel 161

I.1 Displacement of the gate as a function of the mass of the vessel 164
I.2 Energy absorbed by the gate as a function of the mass of the vessel 164
I.3 Relationship between the velocity of a vessel and its energy 165
I.4 Relationship between the velocity of the colliding vessel and the displacement of the gate 165
I.5 Energy absorbed by the gate as a function of the assumed damping factor 166
I.6 Percentage of the total energy which is dissipated by damping mechanisms as a function of the assumed damping factor 167
I.7 Maximum displacement of the gate structure during collision as a function of the assumed damping factor 168
I.8 Comparison of the behaviour of the ship and gate for the case with and without ship-gate separation 168

I.9 Displacement of the gate with and without the application of an engine load for a Class I vessel . . . 169

I.10 Displacement of the gate with and without the application of an engine load for a Class II vessel . . . 169

I.11 Displacement of the gate with and without the application of an engine load for a Class III vessel . . . 170

I.12 Displacement of the gate with and without the application of an engine load for a Class IV vessel . . . 170

I.13 Displacements of the gate due to a collision with a flexible and rigid vessel of Class I . 171

I.14 Displacements of the gate due to a collision with a flexible and rigid vessel of Class II . 171

I.15 Displacements of the gate due to a collision with a flexible and rigid vessel of Class III 172

I.16 Displacements of the gate due to a collision with a flexible and rigid vessel of Class IV . 172

I.17 Comparison of the displacements of the gate due to a collision with a Class I ship, as calculated with the energy and force approaches . . . 173

I.18 Comparison of the displacements of the gate due to a collision with a Class II ship, as calculated with the energy and force approaches . . . 173

I.19 Comparison of the displacements of the gate due to a collision with a Class III ship, as calculated with the energy and force approaches . . . 174

I.20 Comparison of the displacements of the gate due to a collision with a Class IV ship, as calculated with the energy and force approaches . . . 174

J.1 Geometry of the finite element areas for the static global calculation . . . 176

J.2 Geometry of the finite element mesh for the static global calculation . . . 176

J.3 Internal geometry of the finite element mesh for the static global calculation in which the flanges are visible . . . 177

J.4 Geometry of the finite element mesh for the dynamic global calculation with a 100 mm square mesh . . . 177

J.5 Front view of the geometry of the finite element mesh for the dynamic global calculation with a 100 mm square mesh . . . 178

J.6 Water pressures on the upstream side of the gate . . . 178

J.7 Water pressures on the downstream side of the gate . . . 180

J.8 Displacements in the x-direction (along the gate axis) . . . 180

J.9 Stresses in the x-direction as carried by the gate skins . . . 181

J.10 Stresses in the x-direction as carried by the internal flanges . . . 181

J.11 Stresses in the z-direction as carried by the gate skins 182

J.12 Stresses in the z-direction as carried by the internal flanges 182

J.13 Displacements in the z-direction for the dynamic analysis without internal core elements pre-buckling 183

J.14 Displacements in the z-direction for the dynamic analysis without internal core elements post-buckling 183

J.15 X-displacements when their maximum is reached at the point of impact 184

J.16 X-displacements when their maximum is reached in the body of the gate 184

J.17 Progression of the vibration in the gate after ship separation 185

J.18 Stresses in the resin layer of the rear skin of the gate with scaling factor included and loaded by a distributed load (ROK) 186

J.19 Stresses in the resin layer of the rear skin of the gate with scaling factor included and loaded by a strip load 186

List of Tables

2.1 Pros and Cons of FRP in the construction industry 8

2.2 Gate properties of the up- and downstream lock gates 10

2.3 Laminate build-ups for 'Sluis III' in the Wilhelminakanaal, Tilburg 11

2.4 Laminate properties for 'Sluis III' in the Wilhelminakanaal, Tilburg 12

2.5 Values for the calculation of the gates EI modulus 14

2.6 Comparison of the collision scenario's for upstream collision 14

2.7 Comparison of the collision scenario's for downstream collision 15

2.8 Applied resistance safety factors derived from material attributes 17

3.1 Calculated stiffness ratio's per ship class 25

3.2 Allowed displacements for the gate during collision 29

3.3 Results of the static analysis for the four classes of vessel with varying ship stiffness . . 33

3.4 Values used in the differential equation 35

3.5 Engine forces for collision scenario's with ship classes 1-4 37

3.6 Displacement of the gate for collision with vessel from class 1-4 with varying n values . 38

3.7 Displacements of the lock gate for each analysis type discussed in Chapter 3 41

3.8 Unity checks for the static and dynamic collision for class I - IV ships 42

4.1 Values concerning the application of the static load condition 48

4.2 Found maximum displacements for the gate from the analytical and numerical calculations 53

4.3 Quantitative comparison of the modelling aspects per analysis type 53

4.4 Performed analyses compared to the known deformation limits, judged to pass or fail for a Class III ship 55

4.5 Allowed and found stresses for the skins and internal flanges in the x and z directions . 55

5.1 Displacements and stress peaks for the two model used to authenticate the resin model. 63

6.1 Stiffness's and stiffness ratio's between ships and gate for classes I-IV 71
6.2 Standard Values for model influencing parameters 77

A.1 Characteristic values for the measures distribution of ship speeds towards locks 106

B.1 Translations of Dutch words in Appendix B 109

C.1 x, y and z coordinates of a V-bow for a class III ship with reference to Figure C.2 . . . 115
C.2 x, y and z coordinates of a V-bow for a class IV ship with reference to Figure C.2 . . . 116

D.1 Characteristics of Glass Fibre Types 118
D.2 Achievable fibre volume percentages for production methods 125

F.1 Load factors as dictated by the Eurocode 144
F.2 Partial material factor derived from production and cure 145
F.3 Use of conversion factors during different calculation types 145
F.4 Nominal values for stiffness properties of unidirectional plies 147
F.5 Nominal values for stiffness properties of weave plies 147
F.6 Nominal values for stiffness properties of mat plies 147
F.7 Values for the inter-laminar strengths of glass fibre reinforced resins 148

G.1 Laminate build-ups for the final design of the Spieringssluis 157

Bibliography

[1] D. M. Kolstein, *Fibre-reinforced polymers (FRP) composites in structural applications* (Faculty of Civil Engineering and Geosciences - TU Delft, 2008).

[2] J. Peeters, *Series of project documents on the frp gate design for the lock in the wilhelminakanaal,* (2015), confidential Project Files.

[3] *Lock (water navigation),* https://en.wikipedia.org/wiki/Lock_(water_navigation), access Date: 02/05/17.

[4] A. Vrijburcht, *Ontwerpen van schutsluizen*, Tech. Rep. (Rijskwaterstaat Bouwdienst, 2000).

[5] R. Nijssen, *Composieten Basiskennis* (Hogeschool Inholland, 2013).

[6] http://www.fibre-reinforced plastic.com/, *Fibre reinforced plastic - the fibre reinforced plastic & composite technology resource centre,* http://www.fibre-reinforced-plastic.com/2010/12/lamina-and-laminate-what-is-that.html (2010), access date: 8/7/2016.

[7] Google Maps, *Sluis III satellite, 51.5818631 N, 5.0342971 E,* https://www.google.nl/maps/@51.5818631,5.0342971,205m/data=!3m1!1e3?hl=en (2017), access date:19/7/2017.

[8] Google Maps, *Sluis III 51.5754947 N, 5.0469584 E,* https://www.google.com/maps/@51.5754947,-5.0469584,13z (2017), access date:31/1/2017.

[9] M. Dalman, https://beeldbank.rws.nl.

[10] B. En, *2005 eurocode 1,* (1991).

[11] Stichting CUR, *CUR-Aanbeveling 96 ,* Vezelversterkte kunststoffen in civiele draagconstructies (2003).

[12] J. Blok, L. Brozius, J. Dekker, *et al.*, *The impact loads of ships colliding with fixed structures,* in *Offshore Technology Conference* (Offshore Technology Conference, 1983).

[13] A. Vrijburcht, *Loads on fender structures and dolphins by sailing ships*, Tech. Rep. (Rijkwaterstaat, Dienst Getijdewateren, 1991).

[14] M. Petersen, *Dynamics of ship collision,* Ocean Engng. **Vol 9**, 295 (1982).

[15] *Richtlijnen Ontwerpen Kunstwerken, ROK 1.3*, Tech. Rep. (Rijkswaterstaat, 2015).

[16] N. J. . R. Pater, *Aanvaarbelasting door schepen op starre constructies*, Master's thesis, Technical University Delft (1993).

[17] B. J.M.Gere, *Mechanics of Materials*, 8th ed. (Cengage Learning, 2013).

[18] R. Seracino, *FRP Composites in Civil Engineering-CICE 2004: Proceedings of the 2nd International Conference on FRP Composites in Civil Engineering-CICE 2004, 8-10 December 2004, Adelaide, Australia* (Taylor & Francis, 2006).

[19] J. Teng, J.-F. Chen, S. T. Smith, and L. Lam, *Frp: strengthened rc structures,* Frontiers in Physics , 266 (2002).

[20] L. Buldgem, *Simplified analytical methods for the crashworthiness and the seismic design of lock gates*, Ph.D. thesis, Université de Liège (2014).

[21] *Richtlijnen Vaarwegen 2011, RVW 2011*, Tech. Rep. (Rijkswaterstaat, 2011).

[22] *Europese overeenkomst voor het internationale vervoer van gevraalijke goederen over de binnen wateren (ADN), Bijlagen Editie 2013*, Tech. Rep. (Verenigde Naties - Economische Commissie voor Europa, 2013).

[23] ir. W.F. Molenaar, *Hydraulic Structures - Locks* (Faculty of Civil Engineering and Geosciences - TU Delft, 2011).

[24] A. Vrijburcht, *Aanvaarrisico's voor sluisdeuren*, Tech. Rep. (Waterloopkundig laboratorium, 1992).

[25] Bureau Voorlichting Binnenvaart, *Scheepstypen,* http://www.bureauvoorlichtingbinnenvaart.nl/inland-navigation-promotion/basic-knowledge/waterways?searched=cemt&advsearch=oneword&-highlight=ajaxSearch_highlight+-ajaxSearch_highlight1.

[26] Build-on-Prince.com, *Glass fiber types used in structural frp reinforcement,* http://www.build-on-prince.com/glass-fiber.html#sthash.SChFSHTF.dpbs (2016), access date: 24/6/2016.

[27] T. R. Gentry et al., *Accelerated test methods to determine the long-term behavior of composite highway structures subject to environmental loading,* Journal of Composites Technology and Research **20**, 38 (1998).

[28] F. Ellyin and C. Rohrbacher, *Effect of aqueous environment and temperature on glass-fibre epoxy resin composites,* Journal of reinforced plastics and composites **19**, 1405 (2000).

[29] Case Western Reserve University, *Thermal properties of polymers,* Online tutorial, access date: 6/7/2016.

[30] R. G. Weatherhead, *FRP Technology - Fibre Reinforced Resin Systems* (Applied Science Publishers LTD, 1980).

[31] http://www.corrosionresistant.org/, *What materials are used to make composites?* http://www.corrosionresistant.org/composites-101/what-materials-are-used-to-make-composites/, access date: 1/7/2016.

[32] Strongwell Corporation, *Extren dwb design guide,* https://www.strongwell.com/wp-content/uploads/2013/03/EXTREN-DWB-Design-Guide.pdf (2003), access date: 1/8/2016.

[33] www.globalspec.com, *Honeycomb materials information,* http://www.globalspec.com/learnmore/-materials_chemicals_adhesives/composites_textiles_reinforcements/honeycombs_honeycomb_-materials, access date: 1/8/2016.

[34] P. Mallick, *Fiber-Reinforced Composites - Materials, Manufacturing, and Design*, 3rd ed. (Taylor & Francis Group, 2007).

[35] D. Zenkert, *Lecture slides - kth, stockholm, sweden,* Department of Aeronautical and Vehicle Engineering, Division of Lightweight Structures.

[36] Stichting CUR, *Achtergrondrapport bij CUR-Aanbeveling 96,* Vezelversterkte kunststoffen in civiele draagconstructies (2003).

[37] W. A. Stein, *A summary of classical lamination theory,* http://wstein.org/edu/2010/480b/projects/-05-lamination_theory/A%20summary%20of%20Classical%20Lamination%20Theory.pdf, access Date: 22/08/16.

[38] G.N.Wells, *The Finite Element Method: An Introduction* (Faculty Electrical Engineering, Mathematics and Computer Science - TU Delft, 2009).

[39] D. M. Kolstein, *Fibre reinforced polymer (FRP) structures - Case studies* (Faculty of Civil Engineering and Geosciences - TU Delft, 2004).

[40] Google Maps, *Spieringssluis 51.778515 N, 4.762273 E,* https://www.google.co.uk/maps/place/-Spieringsluis/@51.7785704,4.7601472,17z/data=!4m5!3m4!1s0x47c42821b50e536d:0x415f99a-2fb4f7632!8m2!3d51.7785705!4d4.7623358 (2016), access date:3/8/2016.

[41] J. Peeters, *Frp, cie5128, lecture 3 frp in civil structures: design for robustness,* (2016), lecture slides for a guest lecture given by FibreCore.

A

Locks and Collisions

In this appendix expands on the introduction to locking structures given in Chapter 2.1. Appendix A.1 discusses the parts which make up a standard lock after which Appendix A.2 discussed the lock gates in more detail as they serve as the focus for this report. Finally in Chapter A.3 collision in locks are detailed, including their causes and governing velocities.

A.1. Lock Parts

In order for a lock to function many different parts are needed. Without going into minute detail these parts can be summarised into the following categories:

- **Chamber** - The chamber is the area in which the water level can be raised or lowered. It consists of a floor, also called the sill, and walls which are watertight. Most often these are constructed from concrete or masonry. The size of the largest vessel which can be locked is directly proportional to the dimensions of the chamber, taking into account that some leeway is required to allow for water displacement and to reduce collision probability. Important dimensions for the chamber capacity are the width, length and sill depth. Also capstone height is of importance for the maximum water level which can be retained by the walls.
- **Gate** - At both sides of the lock the chamber is closed off by a gate. These gates serve to close off the chamber during levelling and to retain high water at one side of the lock. More information on gates will be given below in Chapter A.2
- **Filling/Emptying System** - In order to change the water level in a lock a filling/emptying system is installed. For lifts up to roughly 6 meters this is most commonly done through the inclusion of valves in the gates. For larger lifts a more complex system is needed, such as a system of culverts or a stilling chamber.
- **Drive System** - In order to open and close the gates and to control the filling/emptying system and drive system is required. The amount of power needed depends strongly on the types of systems which need to be controlled. A heavy gate for instance will require a more powerful drive system.
- **Guide Works** - Outside the lock chamber a series of guide rails and potentially dolphins are installed to guide ships into the chamber at the correct speeds. The quality of these works has a strong effect on the likelihood of collisions.
- **Other Facilities** - Apart from all the parts mentioned above many locks also have other facilities. To name a few of these a lock may of may not have a control tower, mooring facilities or (temporary) harbour.

A.2. Lock Gates

For this thesis the important part of the lock design is the gate. This will be further elaborated on in the chapter below.

A.2.1. Gate Functions

Generally speaking a lock gate has two main functions to fulfil, namely:[23]

- **Water retention** - When the gate is in its closed position it should stop water from flowing from the high water side to the low water side. This includes keeping leakage at an acceptable level for the project at hand. Furthermore the gate should be able to retain the hydrostatic force from the side, or sides for bilateral retaining gates, for which it is designed.
- **Separation/Connection** - For a lock to function one gate must completely close off the waterway while the other gate is moved completely out of the waterway to allow passage. A gate must have the capability to be in both these states.

A.2.2. Gate Types

The functions described above can be fulfilled by multiple different design types. In this chapter the most important gate types will be discussed along with their distinguishing features and is based on [4] and [23].

Mitre Gates

Mitre gates are commonly used for locks in the Netherlands up to widths of roughly 24 meters. They consist of two gates which rotate around a vertical axis, each spanning half the lock width, which come together at an angle in the middle of the lock. This angle is often chosen as 1:3[4]. The gates point towards high water so that the excess water pressure from the locks lift pushes the gates closed. The loads are then carried through a combination of normal forces and bending in the gates to the chamber walls. Effectively each gate functions as a beam on two supports with potential extra support where the gate leans against the sill.

This design makes mitre gates only function as a unilateral retention systems, although with some extra precautions small negative water pressures can also be retained allowing a certain amount of leakage. Where bilateral retention is necessary and mitre gates are desired two sets of gates are needed at each end of the lock. A schematic top view for both uni- and bilateral retention is shown in Figure A.1.

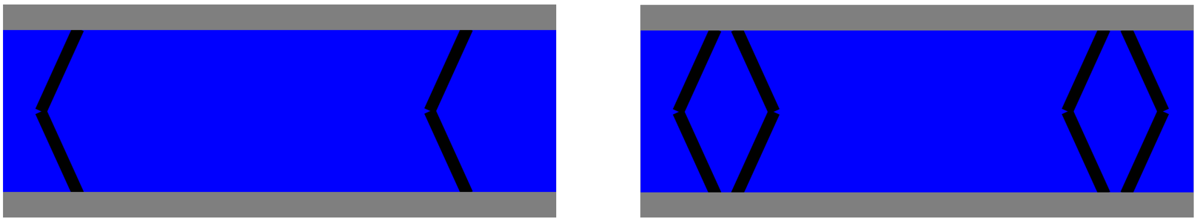

Figure A.1: Top view of a lock with mitre gates. Left: Uni-lateral retention. Right: Bi-lateral retention

Briefly summarised the advantages and disadvantages are as follows:

Advantages:

- Due to the design which carries loads as normal forces, instead of pure bending, an economic use of materials is obtained.

- The opening mechanism is relatively simple when compared to other gate types.
- When open the gates can be stored in a shallow recess in the chambers side.

Disadvantages:

- Precise dimensions are required to ensure water tightness.
- The gates are susceptible to waste and ice formation.
- A vessel colliding with the gates form the low water side may push the gates open.
- Collision is possible even when the gates are open due to their being stored in the side of the lock chamber.

Rolling Gates

Rolling gates are most commonly flat gates which close off the waterway perpendicularly. The gate is stored in a deep chamber in one the the lock sides and rolled out to close off the lock on roller carriages which in turn are mounted on a guiding rail in the cill.

When open the gate is pushed against the supports in the cill and chamber walls. and is equally capable of retaining high water is both directions. When only unilateral retention is required rolling gates are seldom used as mitre gates will be more economical, with the exception of very wide locks.

Briefly summarised the advantages and disadvantages are as follows:

Advantages:

- The gate is capable of bilateral retention.
- A light operating mechanism is sufficient.

Disadvantages:

- A lot of space is required to house the large gate chamber. This can be reduced by using a curved gate and chamber, but this will in turn increase the complexity of the design.
- The guidance system with roller carriages is expensive and complex. Many moving parts increase the amount of maintenance required.
- The system and gate chamber are sensitive to floating waste such as silt.

Lift Gates

A lift gate is a gate which is opened by lifting the gate vertically out of the waterway. In raised position the gate hangs between two towers which contain counter weights to aid in the lifting procedure.

The gate itself is often flat, but may also be lens shaped, and capable of bilateral retention. When closed the gate differs little from a rolling gate structurally. It is supported by gate guides in the chamber sides and acts as a beam across the entire waterway.

Briefly summarised the advantages and disadvantages are as follows:

Advantages:

- The gate is capable of bilateral retention with only one sided cladding.
- Inspection and maintenance is easier as a gate is completely free of the waterway is opened state.
- There is little sensitivity to waste or ice formation.
- The locking structure is relatively narrow.

Disadvantages:

- There is limited shipping clearance, which may be a problem is certain waterways.
- Complicated gate guides and operating mechanisms are required.
- The super structure is large and expensive.

A.3. Collisions in Locks

A collisions in a locking complex can take place in different ways:

- Collisions between two vessels.
- Collisions between a vessel and a leading jetty.
- Collisions between a vessel and the lock itself.
  - Frontal Collision between a vessel and a closed gate.
  - Sideways Collision between a vessel and a open (mitre) gate.
  - Sideways Collision between a vessel and the chamber wall.

For this thesis the situation in which a vessel collide frontally with a closed gate is the interesting scenario because it is the collision with both the largest required energy dissipation and the largest consequences if failure was to occur.

By confining the research to frontal collisions the most dangerous situations are isolated for calculations. This however does not in itself specify the exact collision scenario. Collision may still take place between different vessels and there are two lock gates, which often have different heights and coinciding water levels, to be taken in to account. Both these points are discussed in the main report, the differences in gates in Chapter 2.4 and the collision specifics in Chapter 3.1.2.

To further complicate matters the vessels have complex bow shapes, may be loaded or unloaded and may have a range of different velocities when approaching the lock gates. As we are interested in the governing collision the ships will be considered loaded as this equals more collision energy. The other aspects will be discussed elsewhere: Bow shapes in Chapter 3.1.5 and collision velocities in Chapter A.3.3.

A.3.1. Causes of Lock Collision

A collision between a vessel and one of the lock gates may have many different causes. These causes can be be split up into five categories as shown in the list below:[24]

1. Caused by Vessel
   - Too large dimensions
   - Too high speeds
   - Too heavily loaded
   - Slow screw reversal
   - No bow screws
   - Low reliability of ship
2. Caused by Human Failure
   - Poor steering
     - Shift engine in the wrong direction
     - Poor use of bow screws
     - Manual steering error
   - Poor evaluation of the situation
     - Poor estimate of the distance to the gate
     - Poor estimate of the entrance speed
   - Communication error between vessel and lock personnel
3. Caused by External Influences

    - High winds
    - Low vision
    - Currents and waves
        - Harbour current
        - Wind waves
        - Translation waves
        - Waves from other ships
4. Caused by Traffic Intensity
    - Many other ships
5. Caused by Waterway
    - Waterway geometry
        - Diagonal lock chamber
        - Narrow lock entrance
        - Short length/width of the waterway in front of the lock
        - Bend in the waterway in front of the lock
    - Location
        - Coastal locks have increased collision chance.

Because the degree of damage during a potential collision is governed by the mass and velocity of the vessel, with the latter being more important, some of the above collisions are worse than others. Which type will be the governing collision depends on the combination of the collision energy and the probability of collision (as discussed in the follow chapter). Although it can be said that it is likely that the cases in which a ship collides at full entering speed will be governing. This may be cause by either human or vessel failure. Other collisions will likely be of a much smaller magnitude, and will be ignored.

A.3.2. Probability of Lock Collision

In this study the effects of a collision are examined, that implies that a collision takes place. However to obtain an idea of the collision scenario and the coinciding risks a short look at collision probability is desirable. The main source for this chapter is a report by the 'Waterloopkundig Laboratorium' (currently known as Deltares) on collision with guidance structures around locks [24]. Although this data does not look into lock gate collisions the causes are similar so some conclusions can still be drawn on for example the order of magnitude.

In 1992 the Waterloopkundig Laboratorium collected data on collision over the past 11 years and measure a series of approaches in the field. From this, relatively small, set of data they determined collision probabilities and compared them to error-trees. To do this they generated data sarcastically with distribution functions that they derived from expert opinions, measurements and casuistics.

To determine the return period that be expected for a lock gate collision two value are needed, the amount of passes per year [n] and the chance of collision per pass [P$_{collsion}$]. The first value is determined from the size and profile of the lock. The lock is made for a single vessel which can be seen as an acceptable choice up to 12.000 passes per year [21]. The value 12.000 will be assumed to remain on the conservative side of the calculation. The chance of a collision which causes measurable damage is calculated in [24] as $6.9*10^{-6}$ per approaching ship. This value however is determined using 15 year old data and was meant for guidance works not the gate itself. For this reason it can only be seen as a rough estimate.

Assuming the values above the expected return period of a significant collision can be said to be:

$$T_{collision} = \frac{1}{n * P_{collision}} = \frac{1}{12000 * 6.9 * 10^{-6}} = 12.07 years \tag{A.1}$$

With a lifespan for the structure of 100 years 8 or 9 significant collisions can be expected. This is an estimate which will be used to determine what velocity should be taken into account for the collision in the following chapter. In reality many of the aspects which cause collisions (e.g. weather, chamber width, approach) are dependant on the actual lock and using generalised data is unreliable.

A.3.3. Velocity of Lock Collision

The degree to which a structure is loaded is strongly dependant on the vessel velocity at the moment of collision because the energy is quadratically dependant on it. The velocity of a vessel is influenced by its size and whether it is loaded or not as well as less deterministic issues such as the captains sailing style and the condition of the ships machinery. Because of this it can vary wildly even for identical vessels. For this reason it isn't realistic to see the ships velocity as a deterministic value, but it should be handled as a statistical variable. To be able to do this data is needed.

Velocity Data

The 'Waterloopkundig Laboratorium' (now known as Deltares) measured ship velocities when approaching locks. They measured the speeds at 400, 200 and 10 metres from the lock and used these to determine averages and standard deviations. These values are shown in Table A.1. The final column (the $v_{95\%}$) is extrapolated from the given distributions (see Chapter A.3.3).

Table A.1: Characteristic values for the measures distribution of ship speeds towards locks[24]

Distance from lock [m]	(Un)Loaded	Speed [m/s]				
		Average	Sta. Dev.	Max	Min	$v_{95\%}$
400	Loaded	2.50	0.87	4.00	0.70	3.93
	Unloaded	2.64	1.08	4.40	0.35	4.42
200	Loaded	1.90	0.80	3.60	0.07	3.22
	Unloaded	2.20	0.99	4.50	0.08	3.83
10	Loaded	1.54	0.53	2.90	0.66	2.41
	Unloaded	1.98	0.67	3.60	0.97	3.08

These values were measured in seven locks in the Netherlands and represent approaching speeds of vessels of classes IV, V and VI but are further undiscriminated by class. Some noteworthy points based in the data:

- Unloaded vessels have higher velocities than loaded vessel. This is not unexpected as their mass is lower and they have less water to displace. But because the collision energy is dependant on both mass and velocity this means it is not directly clear which vessel will be governing.
- Both the average and the standard deviation drop as the ship approaches the lock. This is likely because not every captain starts slowing down at the same distance, but they are all expected to reach a certain speed by the time they reach the lock. The maximum and minimum values do not show such a strong trend, but they are affected by outliers had have only qualitative value. Especially with so few measurements.

Correlation between Cause and Velocity

It would seem logical that a larger velocity would lead to a larger chance of collision and to a certain extent this is true. In this study the critical collision is considered and in Appendix A.3.1 it is concluded that these will be caused by either human failure (not slowing down) or mechanical failure (unable to slow down) and these have equal chance of occurring at all velocities. Other causes which are more directly correlated to velocity such as steering errors or not being able to slow down on time all include the captain attempting to stop the vessels, thus decreasing the collision velocity.

Chance Distribution

The Waterloopkundig Laboratorium[24] states that the velocities are normally distributed and gives these distributions for loaded and unloaded ships at three distances from the lock. This gives 6 distributions which can be used. In using these distribution line is kept with the Eurocode standards in which values are used with 95% chance of being met. For a standard distribution this the a value of:

$$v_{95\%} = \mu + 1.645\sigma \tag{A.2}$$

The final column of Table A.1 shows these values.

Conclusion

Two conclusions have to be drawn:

1. Whether the loaded or unloaded vessels are governing.
2. What distance should be chosen as governing distribution.

The first point can be determined by comparing the decrease in velocity to the increase in mass when loading a vessel. Keeping in mind that the velocity is quadratic in the energy function. For a class IV vessel (such as the one which will be used in the case study) the draught, and with it the mass, increases by a factor three when loaded. The velocity however only decreases by between 10% and 25%. This indicates that the situation in which collision takes place with a loaded vessel will always be governing.

The second point is somewhat more subjective. Comparison is made to the velocities which were chosen by FibreCore to be used on the Wilhelminakanaal project (see Chapter 2) namely an average collision velocity of 0.83m/s (3 km/h) and a maximum collision velocity of 3.33 m/s (12 km/h)[2]. Because the critical collision is more interesting the higher of these two value will be taken as a benchmark. When this is compared to the values in Table A.1 it becomes clear that the value of 3.33 m/s as chosen by FibreCore is well within the correct range, being very much comparable to the 200m velocities. This would coincide with a ship failing to slow down its engine at this point. For this reason a value of 3.33 m/s is chosen for the rest of this study as suggested by FibreCore.

A.3.4. Ship Classes

Vessels are divided into categories dependant on the dimensions. This way it is easy to determine whether or not a waterway is sufficient for a certain type of vessel. Within these categories a distinction is made between inland vessel and sea vessels. An overview of the different shipping classes is given in Appendix B.

B

Shipping Categories

In this appendix the governing properties of ships from the different shipping categories as defined by the dutch authorities are given. The values for length, width and draught are of utmost importance when designing a lock and the maximum allowed tonnage induces the largest expected collision force. The following two pages are an extract from the website of the 'Bureau Voorlichting Binnenvaart' (Bureau of inland navigation information)[25].

Although the pages are in dutch only minimal words are used. Translations for these words are given below in Table B.1:

Table B.1: Translations of dutch words in Appendix B

Dutch	English
Klasse	Class
Lengte	Length
Breedte	Width
Diepgang	Draught
Laadvermogen	Loading capacity

Scheepstypen

Bureau Voorlichting Binnenvaart

Klasse				
I	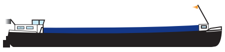	**Spits** Lengte 38,5 meter - breedte 5,05 meter - diepgang 2,20 meter - laadvermogen 350 ton	🚛	14 x
II	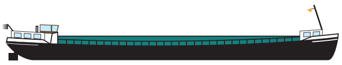	**Kempenaar** Lengte 55 meter - breedte 6,60 meter - diepgang 2,59 meter - laadvermogen 655 ton	🚛	22 x
III	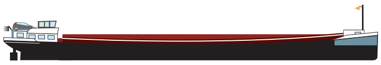	**Dortmund-Eemskanaalschip (Dortmunder)** Lengte 67 meter - breedte 8,20 meter - diepgang 2,50 meter - laadvermogen 1.000 ton	🚛	40 x
IV	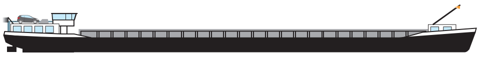	**Rijn-Hernekanaalschip (Europaschip)** Lengte 85 meter - breedte 9,50 meter - diepgang 2,50 meter - laadvermogen 1.350 ton	🚛	54 x
Va	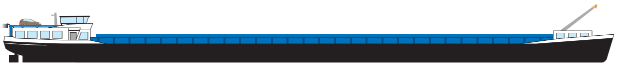	**Groot Rijnschip** Lengte 110 meter - breedte 11,40 meter - diepgang 3,00 meter - laadvermogen 2.750 ton	🚛	120 x
Vb	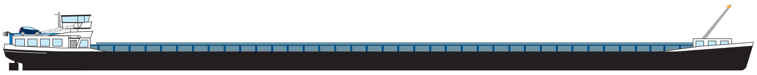	**Groot Rijnschip** Lengte 135 meter - breedte 11,40 meter - diepgang 3,5 meter - laadvermogen 4.000 ton	🚛	160 x
VIa	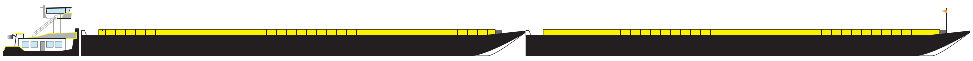	**Tweebaksduwstel** Lengte 172 meter - breedte 11,40 meter - diepgang 4 meter - laadvermogen 5.500 ton	🚛	220 x
VIb VIc	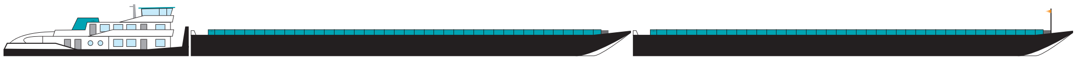	**Vier- of zesbaksduwstel** Lengte 193 meter - breedte 22,80 / 34,20 meter - diepgang 4 meter - laadvermogen 11.000 / 16.500 ton	🚛	440 / 660 x
Va	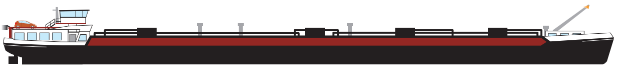	**Standaard tanker** Lengte 110 meter - breedte 11,40 meter - diepgang 3,50 meter - laadvermogen 3.000 ton	🚛	120 x

Vormgeving: © Stephan le Sage

Scheepstypen

Bureau Voorlichting Binnenvaart

Klasse		
Vb	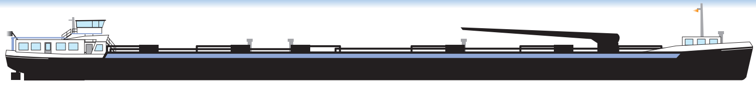 **Grote tanker** Lengte 135 meter - breedte 21,80 meter - diepgang 4,40 meter - laadvermogen 9.500 ton	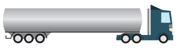 380 x
Va	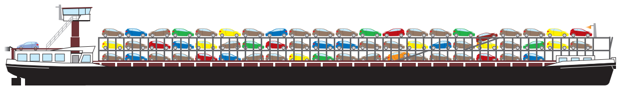 **Autoschip** Lengte 110 meter - breedte 11,40 meter - diepgang 2,00 meter - laadvermogen 530 auto's	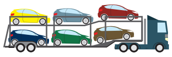 60 x
III	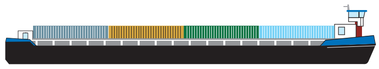 **Containerschip Kempenaarsklasse** Lengte 63 meter - breedte 7 meter - diepgang 2,50 meter - laadvermogen 32 TEU	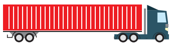 16 x
Va	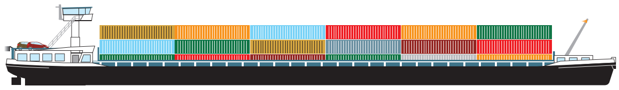 **Standaard containerschip** Lengte 110 meter - breedte 11,40 meter - diepgang 3,00 meter - laadvermogen 200 TEU	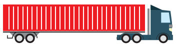 100 x
Vb	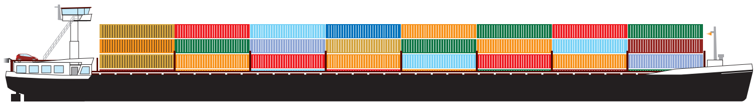 **Groot containerschip** Lengte 135 meter - breedte 17 meter - diepgang 3,50 meter - laadvermogen 500 TEU	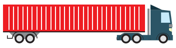 250 x
Va	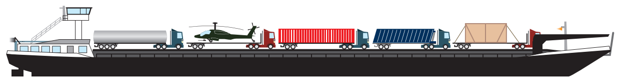 **Ro-roschip** Lengte 110 meter - breedte 11,40 meter - diepgang 2,50 meter	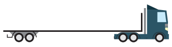 72 x
VIb	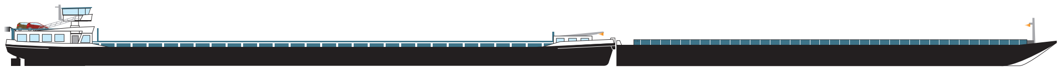 **Koppelverband (schip met duwbak)** Lengte gemiddeld 185 meter - breedte 11,40 meter - diepgang 3,50 meter - laadvermogen 6.000 ton	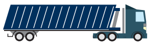 240 x
VIb	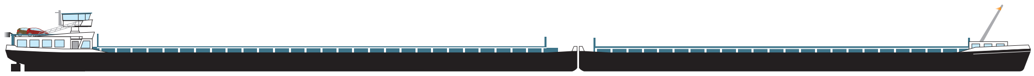 **Koppelverband (schip met schip)** Lengte gemiddeld 185 meter - breedte 11,40 meter - diepgang 3,50 meter - laadvermogen 6.000 ton	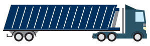 240 x

the Blue Road
duurzaam vervoer over water

Vormgeving: © Stephan le Sage

C

Ship Bow Shapes

The ships considered in this study have so called V-bows. This type of bow is illustrated in detail in this Appendix. A visual representation of such a bow is given in Figure C.1.

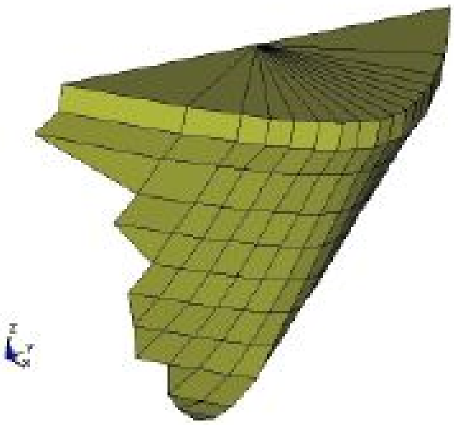

Figure C.1: Visualisation of the shape of a V-bow[22]

Figure C.2 shows an overview of reference points for such a bow shape. These reference points coincide with the values in Tables C.1 and C.2 which are for CEMT class III and IV ships respectively.

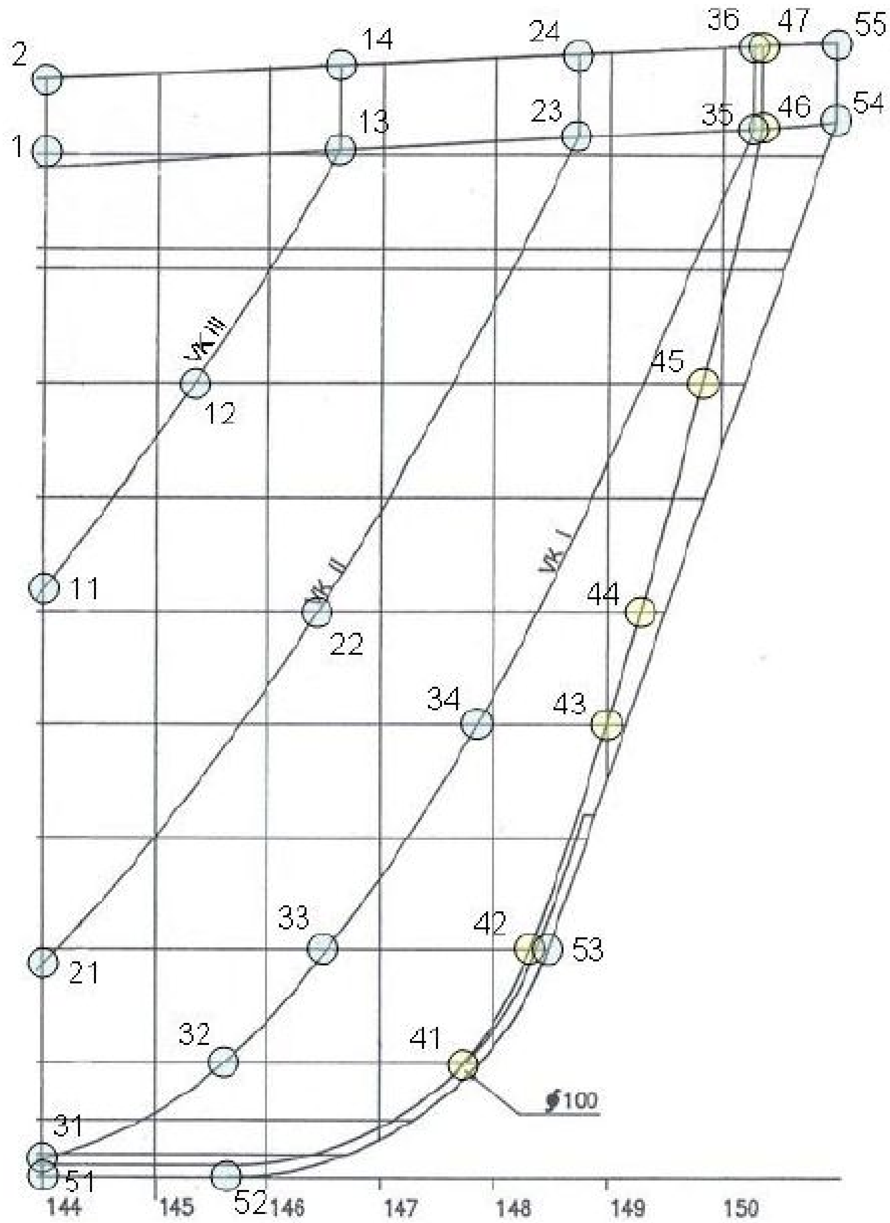
2
14
24
36
47
55
1
13
23
35
46
54
VK III
45
12
11
VK II
VK I
44
22
34
43
33
42
53
21
32
41
ϕ100
31
51
52
144
145
146
147
148
149
150

Figure C.2: Reference points for the shape of a V-bow[22]

Table C.1: x, y and z coordinates of a V-bow for a class III ship with reference to Figure C.2 [22]

Reference number	x	y	z
1	0	3.923	4.459
2	0	3.923	4.852
11	0	3	2.596
12	0.652	3	3.507
13	1.296	3	4.535
14	1.296	3	4.91
21	0	2	0.947
22	1.197	2	2.498
23	2.346	2	4.589
24	2.346	2	4.955
31	0	1	0.085
32	0.42	1	0.255
33	0.777	1	0.509
34	1.893	1	1.997
35	3.123	1	4.624
36	3.123	1	4.986
41	1.765	0.053	0.424
42	2.131	0.12	1.005
43	2.471	0.272	1.997
44	2.618	0.357	2.493
45	2.895	0.588	3.503
46	3.159	0.949	4.629
47	3.159	0.949	4.991
51	0	0	0
52	0.795	0	0
53	2.212	0	1.005
54	3.481	0	4.651
55	3.485	0	5.004

Table C.2: x, y and z coordinates of a V-bow for a class IV ship with reference to Figure C.2 [22]

Reference number	x	y	z
1	0	4.75	5.975
2	0	4.75	6.501
11	0	3.632	3.478
12	0.789	3.632	4.699
13	1.569	3.632	6.077
14	1.569	3.632	6.579
21	0	2.421	1.269
22	1.449	2.421	3.347
23	2.840	2.421	6.149
24	2.840	2.421	6.639
31	0	1.210	0.113
32	0.508	1.210	0.341
33	0.940	1.210	0.682
34	2.293	1.210	2.675
35	3.781	1.210	6.196
36	3.781	1.210	6.681
41	2.137	0.064	0.568
42	2.580	0.145	1.346
43	2.991	0.329	2.675
44	3.169	0.432	3.340
45	3.505	0.711	4.694
46	3.824	1.149	6.202
47	3.824	1.149	6.687
51	0	0	0
52	0.962	0	0
53	2.678	0	1.346
54	4.214	0	6.232
55	4.219	0	6.705

D

Additional Information on Fibre Reinforced Polymers

This appendix aims to supply the reader with a good understanding of Fibre Reinforced Polymers as a material set and expands on the introduction given in Chapter 2.2. In Appendix D.1 the composition of FRP laminates will be discussed. In Appendix D.2 the means of production are elaborated further and in Appendix D.3 the applications throughout the different fields are discussed.

D.1. Composition

A FRP element consists of two main components namely the fibres and a resin. The fibres act as the load bearing elements while the resin is responsible for four main functions, namely: [1]

- Fixing the fibre in their geometrical arrangement
- Transferring forces between fibres
- Preventing buckling of the fibres
- Protecting the fibre from external damage from humidity, UV etc.

The role of fibres in the FRP can be fulfilled by multiple materials, this will be further elaborated on in Chapter D.1.1. Likewise the different resin types will be discussed in Chapter D.1.2.

FRP elements are most often formed through the lamination of multiple plies each with their own fibre orientation. By tweaking the direction, order, amount and fibre density of these plies a custom laminate is formed. The properties of the formed laminate depends on the properties of the components as well as their mutual bonding and compatibility. Also the orientation of the fibres plays an an important role in defining the orthotropic behaviour of the laminate. These properties can be calculated using the theory given in Appendix E.

D.1.1. Fibres

As mentioned previously the fibres within a FRP are responsible for the strength of stiffness of the material. Due to their strongly isotropic behaviour not only the fibre properties are important but also their orientation. Unlike most materials the density of fibres is not expressed in kg/m^3 but in ”tex” which is g/km.

Table D.1: Characteristics of Glass Fibre Types [26]

Glass Type	Characteristics
E-Glass	Alkali-free glass High electrical resistance Decent mechanical and chemical resistance
A-Glass	Alkali glass used when E-Glass is not needed
C-Glass	High corrosion resistance
D-Glass	Low dielectric constant
ECR-Glass	E-glass with increased corrosion resistance
R-Glass	Reinforced, high strength glass
S-Glass	High strength High stiffness Extreme temperature resistance
SR-Glass	Further improved S-glass

In the following sections the most commonly used fibre types will be briefly discussed, these are glass fibres, polyaramid fibres and carbon fibres. Of these three types glass fibre are by far the most common in the construction industry. This mainly due to the fact that they are roughly fifteen times cheaper than polyaramid fibres and forty times cheaper than carbon fibres.[1] That being said, specific applications may require the superior properties offered by other fibre types.

Glass Fibre

Although having the worse properties than the other types of fibre, glass fibre is the most commonly used fibre in the construction industry. It is formed by melting SiO_2 (sand) and combining it with additives to give it the necessary properties. The melted glass is then wound at high speeds to stretch the fibres and, in doing so, decrease their thickness.

Different additives can lead to a wide variety of glass fibre which can be used depending on the application. The most commonly used in the construction industry is E-glass for it's all-round performance and reasonable price. For specialised application other type may be chosen, but S-glass and R-glass are rarely used outside of the aerospace industry due to their costs. Table D.1 shows the main glass fibre types and their distinguishing characteristics.

Glass fibres are often applied in structural elements in the formed of mats or weaves. This is be further elaborated on in Chapter D.1.5.

Polyaramid Fibre

Well known examples of polyaramid fibres are Kevlar™and Twaron™. They are high quality man-made fibres which are five times stronger than steel on a weight for weight basis.[1] They have good heat and wear resistance and good dimensional stability. They differ greatly from glass- or carbon fibres by their failure mode. Where glass- and carbon fibre fail in a brittle manner, polyaramids show ductile behaviour and fibre deformation before collapse. Polyaramid fibres are susceptible to failure in their compressive mode and attention should be paid to this during design.

Production take place by keeping the ingredients in a solution with the help of a solvent between -50°C and -80°C followed by extrusion in a hot walled cylinder at 200°C. This forms thin fibre which are very strongly directional. The heat from the cylinder also removes any excess solvent.

Carbon Fibre

Carbon fibre is an expensive fibre type, but one which is still commonly used in many different industries due to its high strength. Within the construction industry they are often used as suspension cables for bridge for example. Currently their costs outweigh their advantages for most construction projects, making them a good choice only when other fibre types are not sufficient. In the future the production costs are expected to decrease significant which may lead to their use becoming more common.

They can be produced from multiple raw materials as long as they have a high carbon atom content such as polyacrylnitrill (PAN) or naturally occurring pitch or cellulose. Of these carbon fibre formed from PAN will have better properties, but pitch will lead to a cheaper production process. The production itself take place in three steps:[5]

- Oxidation at 200°C
- Carbonisation at 800-1600°C
- Grafitisation at >2000°C

During production they are stretched to form a unidirectional anisotropic material. These fibre can be used to form mats of weaves like with glass fibres, but the greatest tensile properties will be obtained from unidirectional, twist-free tows.

Other Fibres

Apart from these commonly used fibre there are also other options which may be used depending on the application considered.

Basalt Fibres are produced in a similar manner to glass fibre, but with basalt rock as raw material. Unlike glass fibres no extra additives are needed, as the basalt can be seen as an ”all-inclusive” package. Because of this the exact composition of the rock is of great importance which limits the amount of suitable material.

Natural Fibres such as flax, hemp, bamboo and wood offer cheap alternatives to man-made products. However their fibre are limited in length and are sensitive to moisture and rotting effects. When compared to other fibre type they are weaker and lighter, but have comparable strength to weight ratios.

Boron Fibres are high quality but expensive fibres often used in the aerospace industry.

D.1.2. Resins

Although it is often said that fibre reinforced polymers derive their strength and stiffness from the properties of the fibres, the importance of the chosen resin must not be understated. As mentioned in Chapter D.1 the resin functions as to fix the fibre matrix composition, to transfer forces between the fibres, to resist buckling of the fibres and to protect the fibres from outside influences. When a structural element is subjected to shear the resin become especially important when it comes to transferring the loads.

Traditional resins can be subdivided into two categories namely thermosets and thermoplastics. Most of the commonly used resins to date are thermosets. These resins consist of short molecular chains which lead to a low viscosity when fluid. This low viscosity makes processing the resin into the desired shape relatively easy. Once solidified these resins will not return to liquid form when heated, instead they will burn once there ignition temperature has been met. Within the range of application for most civil engineering structure however this is not of importance and thermosets will have preferable thermal behaviour at higher temperatures.

Thermoplastics, or remeltable resins, are still a relatively new addition to the possibilities. They consist of long molecular chains and have a high viscosity in their liquid form. To compensate for this either high temperature or high pressure is needed to fully impregnate the fibres and this is not always practical. However is has been shown that polymerisation of the reactant monomers can take place during curing This may drastically increase the situations in which thermoplastics can be used by making production through infusion possible.[5]

Regardless of their classification into thermosets and thermoplastics all resin are affected by temperature to a certain extent. Properties will change as temperatures rise and deterioration from environmental causes will be accelerated[27][28]. All resins also have a glass transition temperature (Tg) which is a measure for what state the molecules will be in at a certain service range. Below Tg a resin will act as a amorphous solid and be glassy and rigid. When subjected to temperatures above Tg the molecules gain enough energy to move from their original matrix and the resin becomes flexible and rubbery. This change is accompanied by a change in properties such as heat capacity and thermal expansion. Depending on the resin Tg can be below 0°C or over 100°C making it possible to choose a resin depending on the regarded service temperature and desired properties.[29]. Thermoplastics also have a melting point (Tm) at which they revert to their fluid form.

Polyester

Polyester is a thermoset resin which has found many applications in a multitude of sectors, such as yachts, cars, piping and infrastructure. One of the main reasons for this is that it is cheap and easily formed, but it lacks some of the better properties of other resins. Most polyesters are susceptible to moisture if not properly coated. An exception to this is isoftaal acid polyester[5].

Polyester is formed from a mixture of roughly 65% polyester monomers and 35% styrene with a catalyst (such as peroxide) and an accelerator. The cure of this mixture takes place in four steps:[1]

- **Induction period**, in which nothing seems to happen while free radicals are being formed.
- **Gelation**, in which the cross-linked network begins to form.
- **Exotherm**, in which there is an energy build-up.
- **Final hardening**, which may take days or weeks.

It is worth noting that if the best possible properties are to be obtained then it is necessary to apply a post-cure at increased temperatures.

Vinyl-ester

Vinyl-esters are comparable to polyesters in many ways. Both resin are produced and are cured in a similar manner and like polyester an polyvinyl element also requires a post-cure at increased temperature to obtain the best properties.

The main difference between the two is in the length of the molecular chains. This as well as the specifics types of esters often used give vinyl-esters a higher level of chemical and moisture resistance and increased toughness once cured. The disadvantages however are that vinyl-esters cost more and have the tendency to degrade aesthetically through discolouration. In many cases it can be advantageous to apply a vinyl-ester top layer to enjoy the increased resistances, but if aesthetics are important an extra top layer will also be necessary.

Epoxy

Epoxy is one of the highest quality and most expensive resins which often finds use in sectors which value quality over price such as aerospace and sports. Epoxy resins are stiff resins with strong bonding, low shrinkage and high moisture, chemical and electrical resistances. They are formed through combination of an amine- and a epoxy group in combination with a curing agent. A good example of this are the well known epoxy two-component glues.

Others

In addition to these three common resins there are many other which may be used when the situations allows. A few of these are discussed below.

Phenolic resins are thermosets which are especially beneficial with regards to heat en spark resistance. They are brittler than other resins but will not burn or melt, only singe slightly under thermal influences. They are often used for computer ship or interior design.[5]

Silicone resins have not found wide scale acceptance due to the fact that they are expensive and have relatively poor mechanical properties. They are interesting though because they have an inorganic backbone based in silicon rather than carbon. This gives them a good resistance to elevated temperatures, but poor moisture resistance[30].

Polyimide resins are moulded and cured at high temperatures (300°C and 400°C respectively) during which all water is removed. As a result of their chemical build up and curing process polyimide resins very thermally stable resins but have a high water absorption.[30]

Furan resins are different from other resins in the fact that they are cured through reaction with an acidic catalyst. The curing process release water and must take place slowly to avoid delamination of the ply. Furan resins have excellent resistance to strong alkalis and acids and are superior to the three common resins in their solvent resistance. They can be used up to about 120°C is corrosive environments as long as no oxidising chemicals, chromic acids, nitric acids, peroxides or hypochlorites are present.[31]

D.1.3. Gel Coats

An advantage of FRP is that they can be aesthetically pleasing without requiring painting or post-coating. To accomplish this a smooth, and sometimes decorative or coloured layer is applied as a top layer of the laminate. This layer can also serve as protection of the fibres in the otherwise top layer. Because this layer can visible throughout the lifetime of the component and is not reinforced only the highest quality resins are used for gel coats. Great care is taken when design such as coat, attention is paid to which catalysts and additives are used as well as the viscosity and thixotropy (i.e. the increase in viscosity due to applied stresses) to guarantee the coating can resist sagging in the mould. A low quality gel coat can lead to uneven or rough top layers, decreased adhesion with the structural laminates and increased risk of osmosis which may cause damage to the laminate during it life.

One side of the gel coat is often applied to the mould by brush, although increasing the amount of styrene in the mixture allows for a spray coat by reducing the viscosity and compensated for the extra evaporation. The other side, which is also called the flow coat, is applied quickly after the final laminate in order to improve the adhesion. The coating requires a short gelation tie when compared to other resins to decrease the mould cycle times and prevent styrene evaporation which would be detrimental to the adhesion. Sometimes gel coats are used in combination with surface veils. Surface veils are lightweight (swirl)mats which can serve as decoration or as support for the gel coat.

Colour is added to a gel coat by adding pigments to the mixture. Apart from the colour these pigments may also change other properties of the coating such as viscosity and curing process. Proper dispersion of the pigment is important for the quality of the finish and is, for a large part, dependent of the processing.

D.1.4. Additives

The properties of resins can be changed in a multitude of ways through addition of other substances during curing. This can be done either by adding particulates or by dissolving in the resin itself.

A common reason for additives is the reduction of costs, clay or carbonates are good examples of this which can be added up to 30% in weight[1]. When this is done the resulting resin must be well tested as such price reducing additives will generally have negative effects on the properties of the resin, such as increased viscosity, more voids or less environmental resistance.

When a gel coat is not desired, but a coloured end product is still required pigments can be added to the structural resins instead. This concerns such small quantities of additives that no significant adverse effects on the resin properties are to be expected. It is possible however that the curing process will change, which must be checked. In addition some pigments will be beneficial for the resin by absorb some incoming UV radiation.

Because FRP consists of materials which are vulnerable to elevated temperatures fire retardance is an important properties. Additives that can increase a components resistance to fire are for example phosphate esters, halogenated hydrocarbons or halogen compounds[1]. Of these the latter is combined chemically while others are added at particulates. Polyesters and poly-vinyls can be significantly improved in this manner but smoke formation will remain an issue, making them less well suited for application in enclosed spaces. As with other additive flame retardants can alter resin properties. They can lower strength, effect colouration, increase weathering and increase viscosity.

Some resins, especially polyesters, are known for their shrinkage during curing be it in the mould or during early lifetime. This deformation may cause unexpected problems such as internal stresses, elements no longer fitting or even cracking. To solve this so called 'low-profile' additives have been developed to reduce shrinkage. This is greatly useful for precise parts and has found use for elemental formed through hot moulding.

D.1.5. Laminate build-up

It is common for FRP elements to be executed as laminates. Such as laminate consists of multiple structural layers called plies, each with their own thickness, fibre ratio and fibre orientation consolidated together to function as a single element. This is very much comparable with multiplex wood panels. A schematic representation of a laminate is given in Figure D.1, the fibre angle is clearly visible. The properties of the element as a whole is dependant on the properties and position of each ply and can be adjusted dependant on the load situation. To simplify matters it is often chosen to vary only the fibre orientation and to keep a laminate symmetrical around its middle plain (to avoid torsion), but this is by no means compulsory.

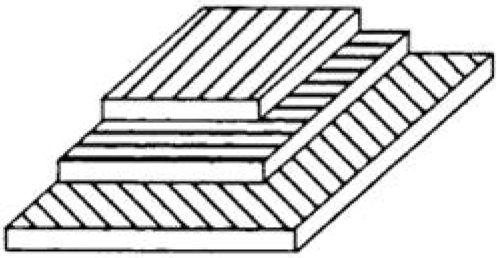

Figure D.1: Schematic representation of a laminate structure[6]

Calculations with laminates are more complex than for an element with uniform properties and for this reason classical laminate theory is used to determine how the element as a whole behaves. Traditional laminate theory is elaborated on in Appendix E.

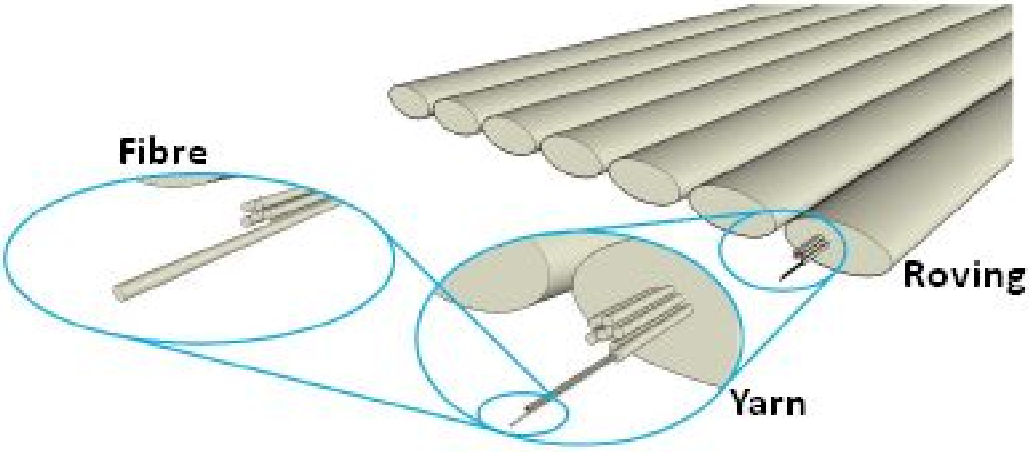

Figure D.2: Graphical representation of a fibre roving[5]

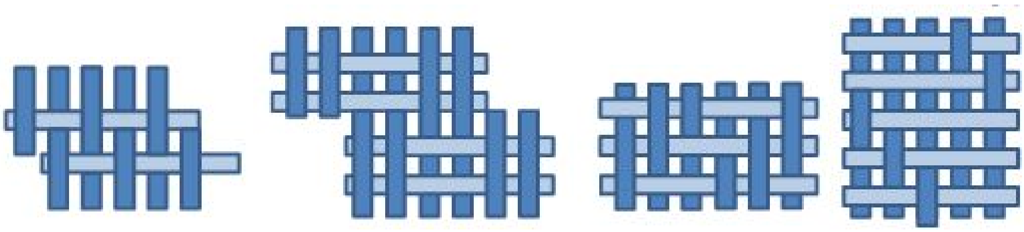
(a) Plain Weave (b) Basket Weave (c) Twill Weave (d) Satin Weave

Figure D.3: Weave Patterns (increasing drapeability and decreasing crimp from left to right) [5]

Mats and Fabrics

The fibres used in FRP are in the order of tens of micrometres thick and too fine to be applied separately. To be of use they are processed into mats and fabrics which can then be impregnated and used as reinforcement.

Mats are thin sheets of fibres which are randomly distributed. They come in two main types namely, chopped strand mats and continuous strand mats. The former consisting of short fibres and the latter of long fibres. Mats can vary in weight from a few hundred to about 1200 g/m^2 [1], the lighter of which are sometimes referred to as fleeces.

Fabrics are weaved in a similar manner to e.g. cotton fabric. The thin fibre strands are bundled into yarn, which in turn is bundled into rovings. These rovings are comparable to cotton thread and can be weaved into fabrics with properties depending on the requirements. A graphical view of this is given in Figure D.2.

A fibre fabric has two main properties which are dependant on the weave pattern, crimp and drapeability. Crimp is the extent to which the rovings are angled in the weave, with sharp angles being high crimp. A large crimp can be linked to a low stiffness to tensile forces [5]. Drapeability is a measure for how easily a fabric will lie in a desired shape. A fabric with a higher drapeability will be more flexible and can be used in more complex moulds, but will be less stable. An example of some weaves is given in Figure D.3 with increasing drapeability and decreasing crimp from left to right.

Apart from the weave pattern above there are also so-called stitched fabrics in which almost all rovings are in the same direction, with only a few cross stitches to keep them together. Such a fabric is sometimes also known as a non-crimp fabric or NCF. Because almost all of the fibre are uni-directional the fabric will display very good properties in its longitudinal direction, and poor properties perpendicular

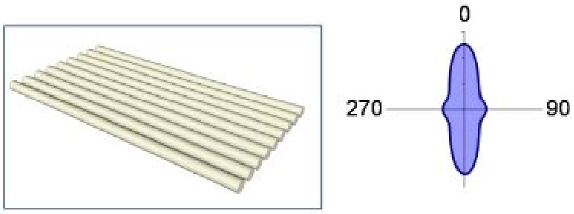

(a) Unidirectional Fabric

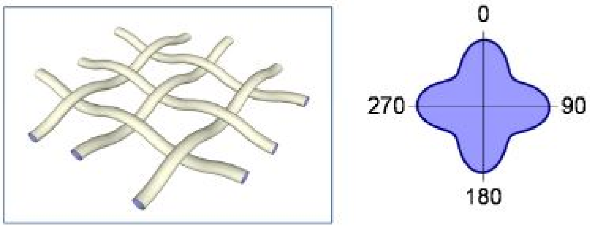

(b) Plain Weave

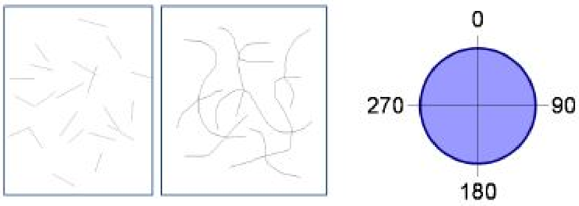

(c) Strand Mats (Chopped and Continuous)

Figure D.4: Polar diagrams for a selection of reinforcements[5]

to this. Schematised polar stress diagrams are shown below in Figure D.4.

D.2. Production of FRP elements

Fibre reinforced polymers are a set of materials whose properties can be strongly affected by their means of production. For this reason it's important to have at least a basic understanding of the many production methods available.

Every method consists of the same five production steps, the differences are in the execution of each step and the mould types. The steps are as follows:[1]

1. Mix the resin and activator.
2. Positioning reinforcement.
3. Impregnating reinforcement with resin.
4. Dispense the resin into the mould.
5. Curing.

In the following sections the commonly used production methods will be briefly discussed and their differences mentioned. Both health and safety during production and tooling after production play an important role in the manufacturing of FRP as well, but these issues are outside the scope of this thesis.

A large factor when choosing a production method is the fibre percentage which can be achieved. An indication of the fibre volume percentages which can be expected are given in Table D.2

Table D.2: Achievable fibre volume percentages for production methods [11]

Production Method	Mat	Weave	Unidirectional or Lay-up
Spray-up	10-20%	-	-
Hand Lamination	10-20%	25-40%	40-50%
Vacuum- or Pressure injection	20-30%	40-50%	50-60%
Filament winding	-	-	50-70%
Prepregging	-	40-55%	50-70%
Pultrusion	20-30%	40-55%	50-70%

Fibre weight percentages can be calculated from the fibre volume percentage and vice versa as shown below in Equations D.1 and D.2.

$$G_{\mathrm{f}} = \frac{V_{\mathrm{f}} \cdot 100}{\frac{\rho_{\mathrm{r}}}{\rho_{\mathrm{f}}} \cdot (100 - V_{\mathrm{f}}) + V_{\mathrm{f}}} [\%] \tag{D.1}$$

$$V_{\mathrm{f}} = \frac{G_{\mathrm{f}} \cdot 100}{\frac{\rho_{\mathrm{f}}}{\rho_{\mathrm{r}}} \cdot (100 \cdot G_{\mathrm{f}}) + G_{\mathrm{f}}} [\%] \tag{D.2}$$

In which:

G_{f}	is the fibre weight percentage.
V_{f}	is the fibre volume percentage.
ρ_{r}	is the specific weight of the resin.
ρ_{f}	is the specific weight of the fibres.

D.2.1. Open Mould Production

Open mould techniques are generally the most simple. They have either a female or a male mould which will produce a smooth finish and the other side is not covered.

Hand Lamination

Hand lamination is the most simple method of fabrication of FRP. It is labour intensive and has a relatively low precision because it is strongly operator dependant. Yet still it is widely used because it requires no machinery, and is very flexible both in the size and shape of the produced components. The main principal is a open mould in which the operator alternately lays down fibres and resin to form a laminate. The resin used is often mixed by hand in a bucket. This four step process is described below:

1. Application of a gel coat if desired.
2. Apply laminating resin with a brush or soft roller.
3. Lay down a pre-cut layer of reinforcement fibres.
4. Consolidate with a ribbed metal roller.

Steps 2 - 4 can be repeated as often as necessary to create a laminate of the desired thickness and properties. After each ply has been consolidated it is left briefly to gel to improve the adhesion between plies. Also if ribs, a core or (metal) inserts are required as a part of the laminate they can be applied during lamination between the relevant plies.

Spray-Up

Spray-up techniques are characterised by the application of resin with a spray gun. This only works with resin with a low viscosity. Three types of spray-up processes are distinguished and discussed below.

Saturation is very similar to hand lamination in the sense that an operator lays the required reinforcement fibre down in their desired orientation by hand, but instead of brushing on resin it is applied with a spray gun. The main advantage of this is that the resin mixture is formed within the pump in a more controlled environment.

Hand Spray-up uses a mixture of low viscosity resin and short chopped fibres ready mixed throughout the resin. After the gel coat has been applied the rest of the component is simply sprayed on and later consolidated by hand to remove air bubbles. This method is still very much operator dependant as thickness difference can occur. It also has the down side that it can only be applied with random fibres orientation limiting the flexibility of the components made. It is commonly used for high volume, non-critical applications.

Auto Spray-up is in essence the same as hand spray-up apart from the fact that the human element has been completely removed by controlling the spray gun by computer. For simple shape the movements and speed of the gun can easily be programmed, whereas for most complex elements robots often 'learn' operators through AI, which again introduces a human error factor. Still it can be said that the components formed this way are of a higher precision and quality.

Rotational Techniques

These techniques are used to create tubes and function by rotating the mould (male or female) on a lathe. They are often used for producing pressure vessels or structural hollow sections.

Filament winding is a technique in which fibre from a spool and impregnated by being drawn through a resin bath and then wound around a male mould. The mould rotates while a mandrel moves along the mould. By adjusting the relative speeds of the lathe and mandrel the fibre angle can be changed and the desired fibre content can be acquired by applying more or less tension to the fibres. Multiple mandrel can also be used if a combination of fibre angles is desired. Elements made with filament winding are well suited for high strength and stiffness applications such as structural beams and high-pressure vessels because they can have high fibre content and precisely tailored properties.

Spray winding is very similar to filament winding in its execution except for that the spool with long fibres is replaced with a spray gun with a low viscosity resin and short shopped fibres. This process is cheaper and quicker but fibre will always be randomly distributed. This techniques is often used for low-pressure vessel for which the lower properties do not matter.

Centrifugal casting can be seen as the reverse process of spray winding. In this case a female mould is used with the spraying gun mounted on the inside. As the fibre resin mixture is being sprayed the mould rotates around the gun forming a component on the inside of the mould. Because the mould rotates at high speed centrifugal forces will consolidate the resin preventing voids. However these centrifugal forces will create thickness differences in non-circular elements and will also partially separate the fibres from the resin. Fibres are more dense than the resin and will be pushed to the outside of the element, while a lighter resin layer will form on the inside.

D.2.2. Closed Mould Production

Closed mould techniques have moulds on both sides of the elements which are being produced. This makes it possible to have a high quality surface finish on both sides, but requires more moulds increasing the price.

Pressure Methods

Methods in this category use either over- or under-pressure to consolidate and form the components.

Vacuum bag moulding is a variation on hand lamination in which, after the fibres and resins have been placed in the mould as described earlier, a rubber bag is attached over the mould. This bag is sealed to be air tight and then vacuum is applied to the mould. The air pressure then consolidates the resin, although it may be desirable to further consolidate by hand. This method gives a better top layer finish than hand lamination and is very efficient in bonding cores and skins in sandwich panels (see chapter D.3.1).

Pressure bag moulding is very similar to vacuum bag moulding except that the rubber bag is replaced with a balloon which can be inflated. After the hand layup the balloon is inflated to an overpressure to consolidate the resin. Further hand consolidation is not possible, but because the applied pressure is not limited to 1 bar as with vacuum bag moulding this is not necessary. The balloon can be filled with hot air or steam for a hot cure if desired. The high pressure does call for a more robust mould which if often made of metal.

Autoclave moulding is in essence a combination of vacuum bag- and pressure bag moulding. The process is identical to vacuum bag moulding but the component is cured in a heated and pressurised vessel to allow for even higher consolidation pressures. The conditions in the vessel are ideal for full consolidation and cure of the component, but the size of the vessel does limit the constructable component size.

Matched Mould Methods

Matched mould methods make use of two moulds, male and female, which together form the exact shape of the component which is to be constructed. This paths the way for highly accurate elements with a high quality finish on both sides. The cost for making the mould however are significantly higher so mould have to be able to be used many times to make it cost-effective.

Leaky mould is the most simple matched mould method. The laminate is built up by hand lamination in the female mould and the male mould in pressed into place as consolidation. The mould are made to be a loose fit so that any excess resin is pushed out from between them during the press.

Cold press is similar to leaky mould in the fact that the male mould is pressed as consolidation and excess resin is pushed out. The difference is that, instead of hand lamination of the laminate, the fibres are placed in the female mould and the resin mixture is poured over it. Under the pressing force, which must be at least 2 bar to avoid air bubbles, the resin is spread throughout the entire mould.

Hot press has the advantage over cold press that the cycle times of the moulds are lower, because the heat speeds the curing. For the highest output a temperature of at least 140°C is required which requires metal moulds. While the same layup procedure as cold press is possible it is more common to use a prepreg, which is a half cure mixture of resin and chopped fibres. The heat from the press makes the mixture malleable and pushes it throughout the mould. Components produced in this manner are very accurate but have variable properties due to the random distribution of the fibres.

Resin injection moulding starts by laying the reinforcement fibre in the female mould in the desired configuration. After this the male mould is clamped over the female mould and resin in pumped in under pressure. By applying vacuum to the mould before resin injection the process can be improved further. Resin injection is limited to low fibre counts, but can form more complex shapes than cold press at a similar production rate.

Injection moulding is a process derived from the, capital-intensive, high volume process used for thermoplastic production. A male and female mould pair are clamped together and heated. Prepreg resin mixture is inserted into the mould by a feed screw in a heated barrel. As with other prepreg processes it is limited to short randomly distributed fibres.

D.2.3. Continuous Production

When a large amount of the same components are needed it may be worth setting up a production line. These processes are fit for mass production where components are formed and cured as they move along a track and can be sawed to the needed length. Three production methods are discussed below.

Continuous laminating can be used to create wither flat sheets of corrugated plates. Reinforcement fibres and resin are combined between two layers of release film which functions as a carrier to transfer the laminate past rollers for consolidation and through a curing oven. After passing through the oven the film are peeled away and the plates is sawed to length. Fibre and reinforcement are either combined through a resin bath or by applying resin to the film and sandwiching the fibres. This process is highly productive but can only form a limited number of shapes.

Pultrusion is a process in which long yarns, cloths or mats from multiple spools are impregnated and formed into a profile of the desired shape. With the use of guides and alignment tools the fibres are put in the correct shape and then lead through a heated clamp. Upon exiting this clamp they are fully cured and ready to be sawed to size. Impregnation can take the form of a resin bath, or resin can be directly injected into the heated clamp. Pultrusion can create components with a very high fibre content and consistent longitudinal properties to close tolerances, but can not apply fibre in any other directions.

Continuous Filament Winding is in essence the same as filament winding, multiple spools of fibres rotate around the mould while the mould itself moves at a constant rate past them and then though a curing oven. The mould is designed in such a way that after the curing oven it can collapse upon itself and reform at the beginning of the conveyor.

D.3. Current Applications

The ability to shape them freely, and control their properties combined with light weight en low maintenance make them obvious choices for a large number of products. For this reason FRP has found applications in many different sectors. The percentage of the total FRP output of the USA in 1998 used in these sectors is shown below in Figure D.5. The use of FRP in some of the larger sectors will be elaborated here.

D.3.1. Civil Engineering

Contrary to other sectors weight reduction is not the largest advantage of FRP in the construction industry. Although lower weight can decrease loads, improve craning and allow for larger elements, the main advantage is corrosion resistance and reduced maintenance needs. Some examples of the civil engineering projects in which FRP was used are given in Appendix G.

The most commonly used FRP in construction is E-glass fibre polyester due to its low costs and decent strength properties. However depending on the application and specific project other reinforcement resin combination may also be used. For example reinforcements and cables and often constructed from carbon fibres, because of their superior longitudinal strength. The most prominent FRP element types are discussed in the following sections.

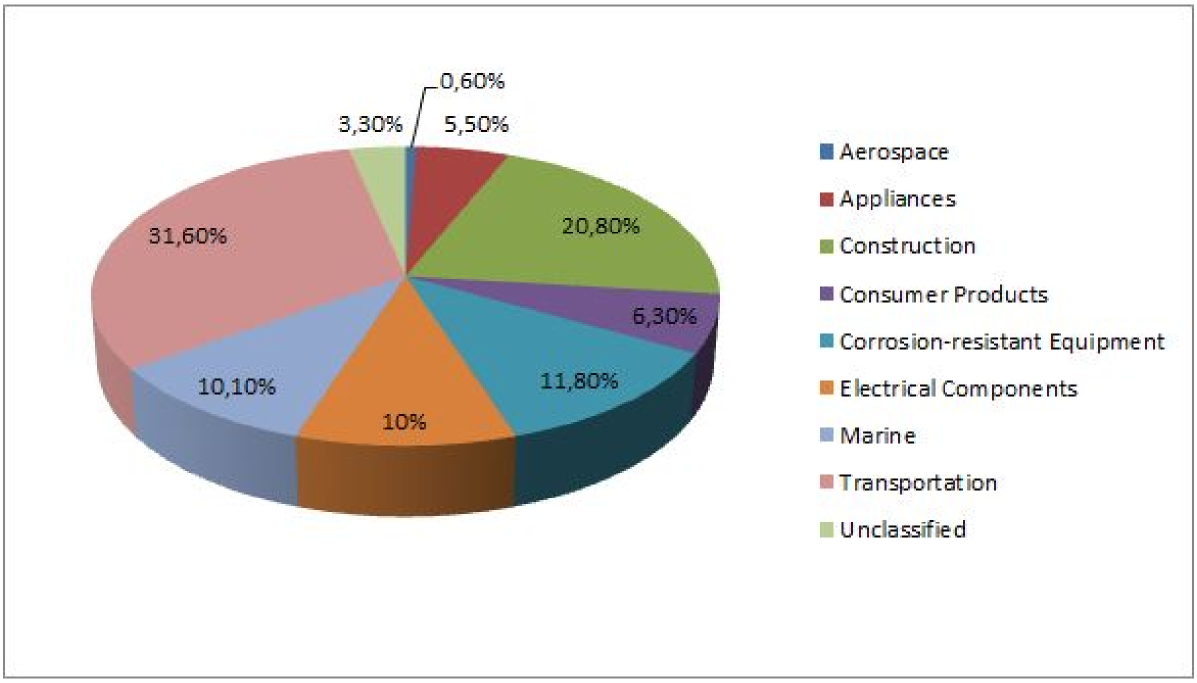

Figure D.5: Percentage of FRP market share per industry in the USA, 1998[1]

Cables and Tendons

The high strength and stiffness of FRP strands in their principle direction makes them a good choice for cables and tendons which, by their design, are primarily subject to tensile forces. As such FRP elements are often found as stays, prestressing cables or external reinforcement. They are often formed through pultrusion and unlike steel are not twisted to maintain the most strength.

The popularity of FRP cables and tendons started to grow in the early 1980's. The steel which was the norm up until then, had the tendency to corrode causing damage to the concrete it reinforced and the combination of fatigue and corrosion lead to cable-stays needing replacing, which is a costly endeavour. The combination of good corrosion and fatigue resistance, low weight and high strengths lead to field testing of FRP elements.

When choosing whether to use steel of FRP cables it is important to consider the lifetime costs, not just construction. Glass fibre cable are 2.5 times as expensive as steel cable and when carbon fibre is used it may cost as much as five times what steel was cost. To offset this it FRP cables will likely not need replacing during their 80-100 year lifespan, whereas steel cable have a lifespan of 20-30 years due to corrosion and fatigue. Also the handling costs are significantly lower for FRP cables owing to their low weight (15-20% of that of steel cables).

When designing a structure with FRP cables attention must be paid to the anchorage. Where the cables bend in order to fasten then to the structure lateral forces are introduced which can be damaging to the cables which are unidirectional. Care must also be taken that carbon fibre are not in contact with metal fasteners as this may cause galvanic corrosion of the steel. Much research has gone into this and current designs retain up to 90% of the tensile strength of the cables[4].

There are a lot of examples of bridges in which carbon fibre cables are used. A few examples are:[1]

- Storchenbrücke in Winterthur, Switzerland
- Bridge of the Kleine Emma River, Switzerland
- Verdasio Bridge, Switzerland
- Herning Footbridge, Denmark

FRP cables are also often used in large antennae, stadiums, roofs, offshore tie-downs and ground anchors.

When it comes to FRP reinforcement of concrete there are two types which can be distinguished, reinforcement with short fibres and with bars or tendons. Reinforcement though use of short fibres is a method in which chopped fibres are added to the concrete mix to limit cracking and does not add any significant load bearing capacity. Reinforcement with bar or tendons is comparable to steel reinforcement. Because the FRP won't corrode the concrete doesn't run the risk of being damaged over time, but there are also distinct disadvantages:

- The ribs needed for the bond between reinforcement and concrete are expensive to produce
- Large temperature strains caused by differences in thermal coefficients
- More concrete cover is needed
- The reinforcement bars are more fragile on site
- Precautions are needed to avoid the reinforcement floating in unset concrete.

Despite these problems FRP reinforcement can still be a viable option in many situations.

Beams

FRP beams can be constructed in many shapes and sizes and can be used to fill the same roles as steel beams. Similarly to other applications the main advantages are the corrosion resistance and the light weight which reduces dead loads en handling costs. In some application it is also beneficial that FRP causes no electromagnetic interference. They are often formed by pultrusion and thus have very good longitudinal properties. As when working with steel beams, FRP beams must be designed to meet both strength and stiffness criteria, but the properties of FRP mostly make stiffness the governing criterion. Extra attention must also be paid to the joints between beams, as these pose extra challenges when compared to steel.

Often FRP beams are pultruded to the same shape as steel beams, such as I-beam or U-beams. However the company Strongwell have developed a beam profile specially designed for use of FRP. It is shaped like an I-beam, but with two webs internally connected by flanges. Such a beam has a 8 to 10 fold better torsional resistance and is still easily pultruded.[32] See Figure D.6 for an example of a cross-sectional diagram.

As is the case with steel beams, FRP beams are often combined to form trusses. The reasoning behind this is also the same, namely that the moment of inertia can be drastically increased without having to use a lot more material. For FRP beams this is more advantageous as it compensates for their lower stiffness.All loading is also in the form of compressive and tensile forces which can easily be carried by the unidirectional fibres in pultruded beams. The disadvantage of FRP trusses is the large amount of joints which may be very complex.

Sandwich Panels

Sandwich panels are elements which consist of thin but relatively stiff and strong skin panels which are separated from each other by a lighter core. The skins are core are fastened to each other either through mechanical connections of some form of adhesive. The skins have the highest contribution to the moment of inertia of the element due to their stiffness and distance from the centre line. They are mainly subjected to normal forces in their plane. The core is mainly a spacing element to improve the efficiency of the skins, but also serves to carry shear forces and improve the buckling resistance of the skins.

In he composite industry the skins mostly consist of FRP laminates customised to meet the requirements for the given application while the core is made from a different material attached through adhesives. The core normally consists of either a light-weight material (e.g. balsa-wood), a foam (e.g. polystyrene, PVC) or a honeycomb structure. If a foam is chosen fibre may also be added to increase properties.

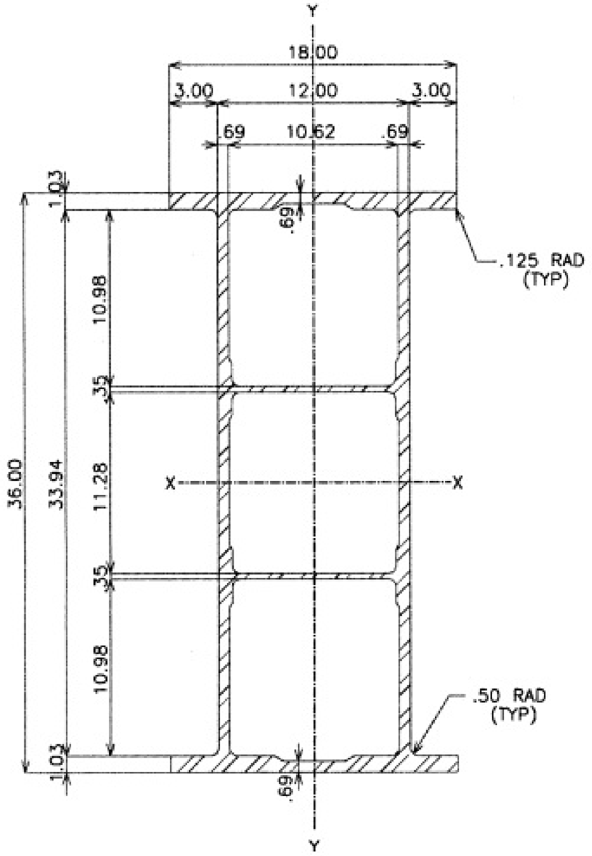

Figure D.6: Example Cross-sectional diagram of a double web beam as produced by the Strongwell Corporation[32]

A honeycomb core is a core made up of thin-sheet material connected in such a way that it resembles a honeycomb. The large empty areas keep the weight low even if the material itself is not. Honey comb cores can be produced from a lot of different materials such as metals (e.g.aluminium, steel of titanium), FRP sheets (e.g. aramid sheets, Kevlar™) or others (e.g. cardboard, fibreglass). The chosen core type is based on the loads it must be able to carry. A schematic representation of a honeycomb cored sandwich panel is shown below in Figure D.7, but any other core system would have a similar build-up.

Laminates and Wraps

Whereas the previous sections described structure which can be produced from FRP, laminates and wraps are used to repair and strengthen structures which have already been produced from other materials. They take the form of either laminate plates and strips of thin FRP sheets which are connected to existing structures through use of adhesive in areas where increase properties are needed. Most often applied to reinforced concrete structures or concrete steel bridges they solve problems such as environmental exposure, inadequate design, increased loads or seismic vulnerability.

The main advantages of using FRP additions as opposed to concrete or steel reparation are that very little weight is added and that the dimensions to not need to increase much to be significant. A FRP layer of 25mm can already add strength where needed and significantly increase the lifespan of a structure[1].

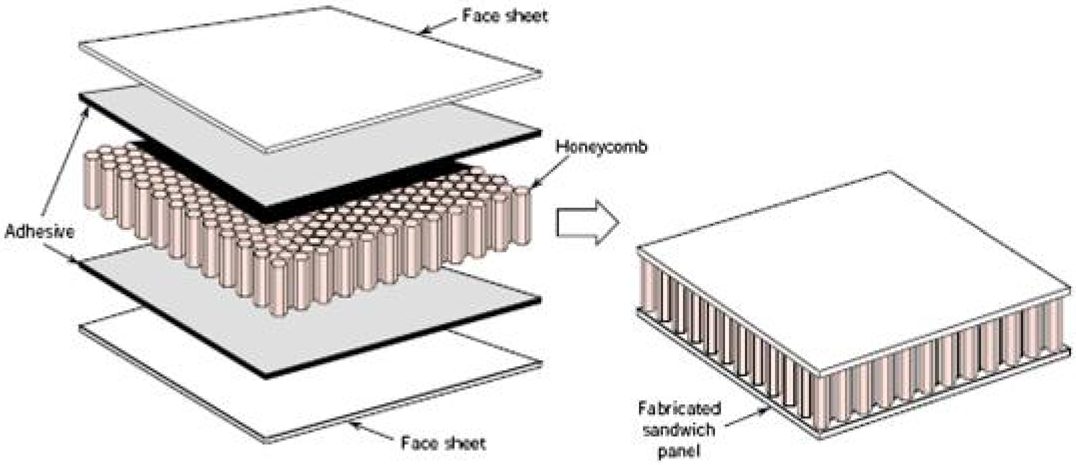

Figure D.7: Honeycombed core sandwich panel[33]

D.3.2. Aerospace

In aerospace engineering every weight reduction that can be achieved can have a large impact on the final product and fuel consumption. This makes FRP a natural candidate for many aircraft components. As one of the first large industries to apply FRP and the need for a high level of understanding of the material there is a large theoretical base on FRP originating from aerospace research.

The use of FRP in the aerospace industry goes back to the 1960's when the military started experimenting in order to reduce aircraft weight. In 1969 boron fibres were used in the horizontal stabilisers of the F-14 plane. After 1970 carbon fibres with epoxy resins were adopted and nowadays military aircraft consist of 25% percent FRP. An interesting application is the outer skin of stealth aircraft where the high vibration damping and the texture improve the stealth properties. In 1987 a small amount of components were installed in commercial aircraft as the test group. When after a year no unexpected degradation had occurred the A310 was outfitted with 10% FRP. Like military aircraft, commercial aircraft also consist of about 25% weight percentage nowadays.[34]

There are numerous advantages other than weight reduction to using FRP in the aerospace industry. Because FRP can be formed in almost any shape required more efficient wing shapes can be realised. This also allows complex elements to be constructed from less components. For example the Lockheed L-1011 has 72% less components and 83% fewer fasteners since being constructed using FRP instead of aluminium[34]. The corrosion resistance and fatigue life has lead to FRP helicopter blades which no longer need to be replaced every few years due to corrosion pitting. Limiting factors are the low impact resistance, high costs and vulnerability to lightning strikes.

FRP has also proved useful in space applications where it is used for truss structures, pressure vessels, structural plates and a multitude of smaller components. The main reason for this is that FRP can be designed to be thermally stable in the large temperature range that space vessels are subjected to (approx -100°C to +100°C).[34] Disadvantages are the susceptibility to atmospheric oxygen and possible embrittlement due to the overpressure of sealed gasses due to the vacuum of space.

D.3.3. Automotive

In the automotive industry FRP elements have been applied as part of the body, chassis and engine. Body and chassis parts have shown to have great promise due to their high stiffness and quality surface finish and reduced tooling costs (40-60% less when compared to steel stamped parts). Epoxy isn't an option because the high rate of production needed for automated component production requires a shorter curing time. For this reason vinyl-ester or polyester are often used. Many vehicles are outfitted

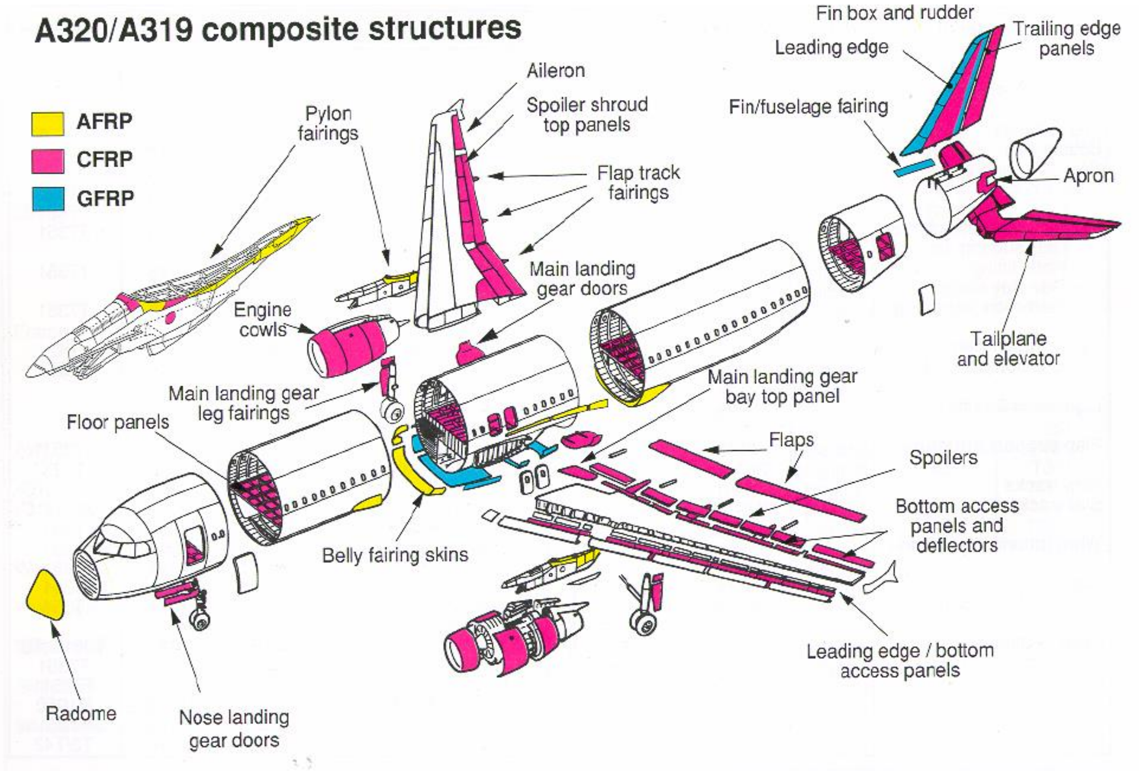
A320/A319 composite structures
AFRP
CFRP
GFRP
Pylon fairings
Aileron
Spoiler shroud top panels
Flap track fairings
Fin box and rudder
Leading edge
Trailing edge panels
Fin/fuselage fairing
Apron
Engine cowls
Main landing gear doors
Tailplane and elevator
Main landing gear leg fairings
Floor panels
Main landing gear bay top panel
Flaps
Spoilers
Bottom access panels and deflectors
Belly fairing skins
Leading edge / bottom access panels
Radome
Nose landing gear doors

Figure D.8: FRP components of a Airbus 320 subdivided by fibre type (AFRP=aramid, CFRP=carbon, GFRP=glass)[35]

with E-glass polyester body parts, springs or shafts for example. For engine parts FRP has had less success. The combination of high fatigue loading and high temperature can lead to damage in FRP elements.

Although one would expect that the weight reduction would prove very beneficial for fuel consumption, this has been shown to only be the case if carbon fibres are used[34]. This leads to expensive production costs which are often only accepted for sports cars where performance is more important than costs.

D.3.4. Maritime

In the maritime sector FRP has conquered a large part of the market. 90% of recreational vessels nowadays are constructed from glass fibre polyester or glass fibre vinyl-ester by means of contact moulding, making large components with precise shapes realisable. Recently however polyaramid fibre such as Kevlar™have started taking their place. Large naval vessels, such as the 72m long Visby-class corvette owned by the Swedish Navy, are also being constructed of carbon fibre epoxy. The weight reduction which comes with the use of FRP in ships increase their speed, acceleration, manoeuvrability and fuel efficiency, making it especially favourable.

D.3.5. Other

Apart from the industries mentioned above FRP can be found in many other products. A list of them is below although it is in no way a complete list.[34]

- Sporting Goods (such as golf clubs, hockey stick, pole vault poles)
- Electronics (such as printed circuit boards)

- Furniture (such as chair springs)
- Power industry (such as transformer housing)
- Oil industry (such as offshore oil platforms and oil suckerrods used in lifting underground oil)
- Medical industry (such as bone plates for fracture fixation, implants, and prosthetics)
- Gas tanks(such as oxygen tanks)

E

Classical Laminate Theory

E.1. Introduction

The following chapter derives and explains classical laminate theory as it is often used to determine properties of FRP laminates. The information for this chapter was obtained from [36] and [37].

Classical laminate theory is a method and a set of assumptions which allows a complex laminate to be expressed in a matrix form which can be used for calculations. For especially complex laminates with, for example, different materials and ply thicknesses the response calculations may become rather difficult. In these case classical laminate theory still has its uses seen as its systematic approach makes it compatible with software packets such as Kolibri or PLAMOR.

E.1.1. Definition of a Laminate

A laminate is a material which is built up from multiple thin plies. It is often beneficial for the laminates properties to vary the fibre orientation of the plies. For FRP laminate this is even compulsory according to the CUR [11].

Classical laminate theory can be used to determine the properties of the laminate as a whole from the properties of the separate plies. The properties needed for this calculation are as follows:

E_{11}	The modulus of elasticity in the direction of the fibres.
E_{22}	The modulus of elasticity perpendicular to the direction of the fibres.
G_{12}	The shear modulus.
v_{12}, v_{21}	The Poisson ratio's.
t	The ply thickness.
θ	The fibre angle with respect to the global axis.
build-up	The order in which the plies are laid.

E.1.2. Area of Validity

Classical laminate theory is based on a set of assumptions, if these are not valid then the theory can not be used.

- Both the plies and the laminate as a whole are assumed to be thin and have a constant thickness.

- The Euler-Bernoulli beam theory is assumed to be valid, meaning that cross-sections perpendicular to the centre line of the plate remain straight and perpendicular during displacements. This is valid for small displacements in which shear deformations are not dominant [38].
- It is assumed that slip between plies can be neglected.
- A two dimensional stress situation is dominant within a laminate. This is partially derived from the first assumption.
- Each ply is treated as having fibre only in one direction. Weaves and mats require extra calculation steps.

E.2. Derivation of the Classical Laminate Theory

The following pages describe the derivation of the laminate level constitutive relationship through use of the classical laminate theory. The basis for this is Hooke's law applied in multiple dimensions on a ply level while taking fibre angle into account. From here the theory will be scaled up to the laminate level through integration.

E.2.1. Classical Laminate Theory on Ply Scale

Hooke's law

The basis for the classical laminate theory is Hooke's law. In it's most simple form for a 1D situation it is well recognised and given by $\sigma = E \cdot \epsilon$. If this is expanded to a 3D anisotropic situation the more general form of Hooke's law can be given as:

$$\sigma_{ij} = E_{ijkl} \cdot \epsilon_{kl} \quad (i, j, k, l = 1, 2, 3) \tag{E.1}$$

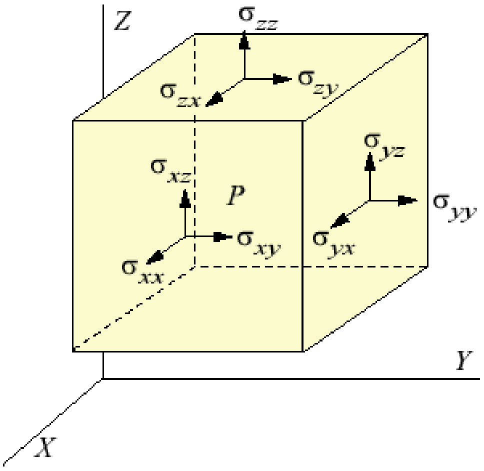

Figure E.1: Stresses and their orientations for the 3D situation

The stress orientation is shown in Figure E.1. Each of the nine stresses is related to nine strains and thus the stiffness matrix **Q** is 9x9 and has 81 entries. Because of the conservation of angular momentum we can say that $\sigma_{ij} = \sigma_{ji}$ reducing the number of entries to 36 as shown in Equation E.2. Furthermore it is assumed that there is no coupling between normal stresses and shearing angles. This introduces a large number of zeroes to the matrix.

$$\begin{Bmatrix}\sigma_{11}\\\sigma_{22}\\\sigma_{33}\\\sigma_{23}\\\sigma_{31}\\\sigma_{12}\end{Bmatrix}=\begin{bmatrix}Q_{11}&Q_{12}&Q_{13}&0&0&0\\Q_{21}&Q_{22}&Q_{23}&0&0&0\\Q_{31}&Q_{32}&Q_{33}&0&0&0\\0&0&0&Q_{44}&0&0\\0&0&0&0&Q_{55}&0\\0&0&0&0&0&Q_{66}\end{bmatrix}\begin{Bmatrix}\epsilon_{11}\\\epsilon_{22}\\\epsilon_{33}\\\epsilon_{23}\\\epsilon_{31}\\\epsilon_{12}\end{Bmatrix}\tag{E.2}$$

This equation can be further simplified by taken into account that the plies are thin and that thus the forces perpendicular to their plane will be negligible. Also is can be said that $Q_{ij} = Q_{ji}$. This reduces above formula to the following:

$$\begin{Bmatrix}\sigma_{11}\\\sigma_{22}\\\sigma_{12}\end{Bmatrix}=\begin{bmatrix}Q_{11}&Q_{12}&0\\Q_{12}&Q_{22}&0\\0&0&Q_{66}\end{bmatrix}\begin{Bmatrix}\epsilon_{11}\\\epsilon_{22}\\\epsilon_{12}\end{Bmatrix}\tag{E.3}$$

The inverse of this formula has the form $\epsilon_{ij} = S_{ijkl} \cdot \sigma kl$ in which **S** is called the compliancy matrix as shown in Equation E.4.

$$\begin{Bmatrix}\epsilon_{11}\\\epsilon_{22}\\\epsilon_{12}\end{Bmatrix}=\begin{bmatrix}S_{11}&S_{12}&0\\S_{12}&S_{22}&0\\0&0&S_{66}\end{bmatrix}\begin{Bmatrix}\sigma_{11}\\\sigma_{22}\\\sigma_{12}\end{Bmatrix}\tag{E.4}$$

The values for **S** can be derived from simple material property relationships and are as follows:

$$\begin{gathered}S_{11}=\frac{1}{E_{11}}\\S_{22}=\frac{1}{E_{22}}\\S_{12}=-\frac{v_{12}}{E_{11}}=-\frac{v_{21}}{E_{22}}\\S_{66}=\frac{1}{G_{12}}\end{gathered}\tag{E.5}$$

The values fro **Q** can then be determined by inverting the compliance matrix. This gives:

$$\begin{gathered}Q_{11}=\frac{S_{22}}{S_{11}S_{22}-S_{12}^2}=\frac{E_{11}}{1-v_{12}v_{21}}\\Q_{22}=\frac{S_{11}}{S_{11}S_{22}-S_{12}^2}=\frac{E_{22}}{1-v_{12}v_{21}}\\Q_{12}=\frac{S_{12}}{S_{11}S_{22}-S_{12}^2}=\frac{v_{12}E_{22}}{1-v_{12}v_{21}}\\Q_{66}=\frac{1}{S_{66}}=G_{12}\end{gathered}\tag{E.6}$$

Fibre orientation angle

With Hooke's law we have a method of determining the stress and strain of a ply with respect to its fibre orientation. The main advantage of a laminate system however, is that the fibre need not always be in the same direction in each ply, and not in the same direction as the global coordinate system. To account for this difference in angle a transformation matrix **T** is used. in which the variable θ represents the angle between the x-y and 1-2 coordinate systems. This is illustrated in Figure E.2

$$\begin{gathered}\begin{Bmatrix}\sigma_{11}\\\sigma_{22}\\\sigma_{12}\end{Bmatrix}=[T]\begin{Bmatrix}\sigma_{xx}\\\sigma_{yy}\\\sigma_{xy}\end{Bmatrix}\\\begin{Bmatrix}\epsilon_{11}\\\epsilon_{22}\\\epsilon_{12}\end{Bmatrix}=[T]\begin{Bmatrix}\epsilon_{xx}\\\epsilon_{yy}\\\epsilon_{xy}\end{Bmatrix}\end{gathered}\tag{E.7}$$

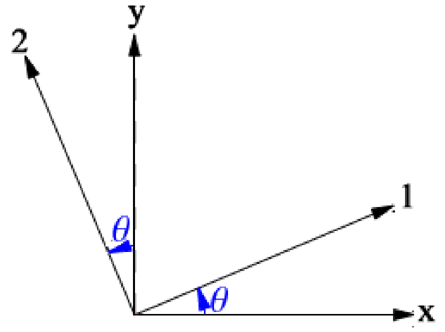

Figure E.2: Image of the angle between the element x-y axis and the fibre 1-2 axis

The values of **T** are derived from trigonometry and contain combinations of sines and cosines. Below the matrices **T** and **T^{-1}** are given as functions of c and s which represent cos(θ) and sin(θ) respectively.

$$\begin{aligned}[T] &= \begin{bmatrix} c^2 & s^2 & 2sc \\ s^2 & c^2 & -2sc \\ -sc & sc & c^2-s^2 \end{bmatrix} \\ [T]^{-1} &= \begin{bmatrix} c^2 & s^2 & -2sc \\ s^2 & c^2 & 2sc \\ sc & -sc & c^2-s^2 \end{bmatrix}\end{aligned} \tag{E.8}$$

The relationship between stress and strain for a ply with arbitrary fibre angle can now be written by combining Equations E.3, E.7 and E.8.

$$\begin{Bmatrix} \sigma_{xx} \\ \sigma_{yy} \\ \sigma_{xy} \end{Bmatrix} = [T]^{-1}\,[Q]\,[T] \begin{Bmatrix} \epsilon_{xx} \\ \epsilon_{yy} \\ \epsilon_{xy} \end{Bmatrix} \tag{E.9}$$

or:

$$\begin{Bmatrix} \sigma_{xx} \\ \sigma_{yy} \\ \sigma_{xy} \end{Bmatrix} = \begin{bmatrix} \overline{Q}_{11} & \overline{Q}_{12} & \overline{Q}_{16} \\ \overline{Q}_{12} & \overline{Q}_{22} & \overline{Q}_{16} \\ \overline{Q}_{16} & \overline{Q}_{26} & \overline{Q}_{66} \end{bmatrix} \begin{Bmatrix} \epsilon_{xx} \\ \epsilon_{yy} \\ \epsilon_{xy} \end{Bmatrix} \tag{E.10}$$

The values for $\overline{\mathbf{Q}}$ are as follows:

$$\begin{aligned}\overline{Q}_{11} &= Q_{11}c^4 + Q_{22}s^4 + 2(Q_{12} + 2Q_{66})s^2c^2 \\ \overline{Q}_{22} &= Q_{11}s^4 + Q_{22}c^4 + 2(Q_{12} + 2Q_{66})s^2c^2 \\ \overline{Q}_{12} &= (Q_{11} + Q_{22} - 4Q_{66})s^2c^2 + Q_{12}(c^4 + s^4) \\ \overline{Q}_{66} &= (Q_{11} + Q_{22} - 2Q_{12} - 2Q_{66})s^2c^2 + Q_{66}(c^4 + s^4) \\ \overline{Q}_{16} &= (Q_{11} - Q_{12} - 2Q_{66})sc^3 - (Q_{22} - Q_{12} - 2Q_{66})cs^3 \\ \overline{Q}_{26} &= (Q_{11} - Q_{12} - 2Q_{66})s^3c - (Q_{22} - Q_{12} - 2Q_{66})c^3s\end{aligned} \tag{E.11}$$

The same things can be done for the compliance matrix **S**. The relationship is then:

$$\begin{Bmatrix} \epsilon_{xx} \\ \epsilon_{yy} \\ \epsilon_{xy} \end{Bmatrix} = \begin{bmatrix} \overline{S}_{11} & \overline{S}_{12} & \overline{S}_{16} \\ \overline{S}_{12} & \overline{S}_{22} & \overline{S}_{16} \\ \overline{S}_{16} & \overline{S}_{26} & \overline{S}_{66} \end{bmatrix} \begin{Bmatrix} \sigma_{xx} \\ \sigma_{yy} \\ 0.5\sigma \end{Bmatrix} \tag{E.12}$$

The values for $\overline{\mathbf{S}}$ can be obtained wither the same way as for $\overline{\mathbf{Q}}$, or by inverting matrix $\overline{\mathbf{Q}}$.

$$\begin{aligned}\overline{S}_{11} &= S_{11}c^4 + S_{22}s^4 + (2S_{12} + S_{66})s^2c^2 \\ \overline{S}_{22} &= S_{11}s^4 + S_{22}c^4 + 2(2S_{12} + S_{66})s^2c^2 \\ \overline{S}_{12} &= (S_{11} + S_{22} - S_{66})s^2c^2 + S_{12}(c^4 + s^4) \\ \overline{S}_{66} &= 2(2S_{11} + 2S_{22} - 4S_{12} - S_{66})s^2c^2 + S_{66}(c^4 + s^4) \\ \overline{S}_{16} &= 2(2S_{11} - 2S_{12} - S_{66})sc^3 - 2(2S_{22} - 2S_{12} - S_{66})cs^3 \\ \overline{S}_{26} &= 2(2S_{11} - 2S_{12} - S_{66})s^3c - 2(2S_{22} - 2S_{12} - S_{66})c^3s\end{aligned} \tag{E.13}$$

E.2.2. Expansion to Laminate Scale

Now that the stresses and strains have been related to one another on a ply level we can take it a step further to determine the properties of the entire laminate. Up until now material aspects and fibre orientation have been taken into account. When scaling to the laminate level other aspects come into play such as the ply thicknesses, laminate build-up and the applied loads.

Stress and strain variations in a laminate

If we consider a part of a laminate subjected to bending we can discern that the displacement is not equal at all points on a plane perpendicular to the centre axis. The displacement in the x-direction of a point on the plane is given by:

$$u = u_0 - z\alpha \tag{E.14}$$

In which:

u_0 is the displacement in the x-direction at the centre line.
α is the rotation angle of the laminate.

Because the rotation angle can be defined as $\alpha = \frac{\partial w_0}{\partial x}$, with w_0 being the displacement in z-direction of the centre line, we can express the displacement in x-direction of a point as:

$$u = u_0 - z\frac{\partial w_0}{\partial x} \tag{E.15}$$

The same reasoning in the y-z plane gives an expression for the displacement in y-direction.

$$v = v_0 - z\frac{\partial w_0}{\partial y} \tag{E.16}$$

Assuming the strain is much smaller than the displacement in the z-direction the system simplifies to a 2D situation with three strains which must be taken into account: $\epsilon_{xx}, \epsilon_{yy}$ and ϵ_{xy}. Using the above two equations for u and v the strains can be defined as:

$$\begin{aligned} \epsilon_{xx} &= \frac{\partial u}{\partial x} = \frac{\partial u_0}{\partial x} - z\frac{\partial^2 w_0}{\partial x^2} \\ \epsilon_{yy} &= \frac{\partial v}{\partial y} = \frac{\partial v_0}{\partial y} - z\frac{\partial^2 w_0}{\partial y^2} \\ \epsilon_{xy} &= \frac{\partial u}{\partial y} + \frac{\partial v}{\partial x} = \frac{\partial u_0}{\partial y} - \frac{\partial v_0}{\partial x} - 2z\frac{\partial^2 w_0}{\partial x \partial y} \end{aligned} \tag{E.17}$$

This can also be written in matrix notation:

$$\begin{Bmatrix} \epsilon_{xx} \\ \epsilon_{yy} \\ \epsilon_{xy} \end{Bmatrix} = \begin{Bmatrix} \epsilon^0_{xx} \\ \epsilon^0_{yy} \\ \epsilon^0_{xy} \end{Bmatrix} + z \begin{Bmatrix} k_{xx} \\ k_{yy} \\ k_{xy} \end{Bmatrix} \tag{E.18}$$

In which:

$$\begin{Bmatrix} \epsilon^0_{xx} \\ \epsilon^0_{yy} \\ \epsilon^0_{xy} \end{Bmatrix} = \begin{Bmatrix} \frac{\partial u_0}{\partial x} \\ \frac{\partial v_0}{\partial y} \\ \frac{\partial u_0}{\partial y} + \frac{\partial v_0}{\partial x} \end{Bmatrix} \quad and \quad \begin{Bmatrix} k_{xx} \\ k_{yy} \\ k_{xy} \end{Bmatrix} = - \begin{Bmatrix} \frac{\partial^2 w_0}{\partial x^2} \\ \frac{\partial^2 w_0}{\partial y^2} \\ 2\frac{\partial^2 w_0}{\partial x \partial y} \end{Bmatrix} \tag{E.19}$$

This shows that the strain varies linearly over the thickness of a laminate. To obtain a relationship for the stress distribution over the laminate this is combined with Equation E.10.

$$\begin{Bmatrix} \sigma_{xx} \\ \sigma_{yy} \\ \sigma_{xy} \end{Bmatrix} = \begin{bmatrix} \overline{Q}_{11} & \overline{Q}_{12} & \overline{Q}_{16} \\ \overline{Q}_{12} & \overline{Q}_{22} & \overline{Q}_{26} \\ \overline{Q}_{16} & \overline{Q}_{26} & \overline{Q}_{66} \end{bmatrix} \begin{Bmatrix} \epsilon^0_{xx} \\ \epsilon^0_{yy} \\ \epsilon^0_{xy} \end{Bmatrix} + z \begin{bmatrix} \overline{Q}_{11} & \overline{Q}_{12} & \overline{Q}_{16} \\ \overline{Q}_{12} & \overline{Q}_{22} & \overline{Q}_{26} \\ \overline{Q}_{16} & \overline{Q}_{26} & \overline{Q}_{66} \end{bmatrix} \begin{Bmatrix} k_{xx} \\ k_{yy} \\ k_{xy} \end{Bmatrix} \tag{E.20}$$

Contrary to strains one can see that stresses do not vary linearly over the thickness of a laminate. There are discontinuities at the transition between plies where the $\overline{\mathbf{Q}}$ matrix changes. These sudden changes in stress cause interface shear.

Laminate stiffness matrix

When working with stresses at laminate level it is easier to work with normal forces and moments rather than stresses. Doing so removes the difficulty of nonuniform stress distribution over the plies. Normal forces are calculated through summation of the ply stresses while taking into account their thickness. Moments are calculated similarly, by also taking the distance from the centre line into account.

$$\begin{aligned} N_{xx} &= \int_{-h/2}^{h/2} \sigma_{xx} dz \qquad & M_{xx} &= \int_{-h/2}^{h/2} \sigma_{xx} z dz \\ N_{yy} &= \int_{-h/2}^{h/2} \sigma_{yy} dz \qquad & M_{yy} &= \int_{-h/2}^{h/2} \sigma_{yy} z dz \\ N_{xy} &= \int_{-h/2}^{h/2} \sigma_{xy} dz \qquad & M_{xy} &= \int_{-h/2}^{h/2} \sigma_{xy} z dz \end{aligned} \tag{E.21}$$

If a laminate consists of n layers these relations can be written in vector notation as follows:

$$\begin{Bmatrix} N_{xx} \\ N_{yy} \\ N_{xy} \end{Bmatrix} = \sum_{k=1}^{n} \int_{h_{k-1}}^{h_k} \begin{Bmatrix} \sigma_{xx} \\ \sigma_{yy} \\ \sigma_{xy} \end{Bmatrix} dz \qquad \begin{Bmatrix} M_{xx} \\ M_{yy} \\ M_{xy} \end{Bmatrix} = \sum_{k=1}^{n} \int_{h_{k-1}}^{h_k} \begin{Bmatrix} \sigma_{xx} \\ \sigma_{yy} \\ \sigma_{xy} \end{Bmatrix} zdz \tag{E.22}$$

If we now combine Equation E.22 with the relationship on ply level Equation E.20 we obtain the following two matrices relating forces directly the strains:

$$\begin{Bmatrix} N_{xx} \\ N_{yy} \\ N_{xy} \end{Bmatrix} = \sum_{k=1}^{n} \left\{ \int_{h_{k-1}}^{h_k} \begin{bmatrix} \overline{Q}_{11} & \overline{Q}_{12} & \overline{Q}_{16} \\ \overline{Q}_{12} & \overline{Q}_{22} & \overline{Q}_{26} \\ \overline{Q}_{16} & \overline{Q}_{26} & \overline{Q}_{66} \end{bmatrix} \begin{Bmatrix} \epsilon^0_{xx} \\ \epsilon^0_{yy} \\ \epsilon^0_{xy} \end{Bmatrix} dz + \int_{h_{k-1}}^{h_k} \begin{bmatrix} \overline{Q}_{11} & \overline{Q}_{12} & \overline{Q}_{16} \\ \overline{Q}_{12} & \overline{Q}_{22} & \overline{Q}_{26} \\ \overline{Q}_{16} & \overline{Q}_{26} & \overline{Q}_{66} \end{bmatrix} \begin{Bmatrix} k_{xx} \\ k_{yy} \\ k_{xy} \end{Bmatrix} zdz \right\} \tag{E.23}$$

and

$$\begin{Bmatrix} M_{xx} \\ M_{yy} \\ M_{xy} \end{Bmatrix} = \sum_{k=1}^{n} \left\{ \int_{h_{k-1}}^{h_k} \begin{bmatrix} \overline{Q}_{11} & \overline{Q}_{12} & \overline{Q}_{16} \\ \overline{Q}_{12} & \overline{Q}_{22} & \overline{Q}_{26} \\ \overline{Q}_{16} & \overline{Q}_{26} & \overline{Q}_{66} \end{bmatrix} \begin{Bmatrix} \epsilon^0_{xx} \\ \epsilon^0_{yy} \\ \epsilon^0_{xy} \end{Bmatrix} zdz + \int_{h_{k-1}}^{h_k} \begin{bmatrix} \overline{Q}_{11} & \overline{Q}_{12} & \overline{Q}_{16} \\ \overline{Q}_{12} & \overline{Q}_{22} & \overline{Q}_{26} \\ \overline{Q}_{16} & \overline{Q}_{26} & \overline{Q}_{66} \end{bmatrix} \begin{Bmatrix} k_{xx} \\ k_{yy} \\ k_{xy} \end{Bmatrix} z^2dz \right\} \tag{E.24}$$

To make these equations slightly more workable a few more assumptions need to be made. If we state that the strains at the neutral line and curvature of each ply is equal (which is a decent assumption for small displacements) we get the following:

$$\begin{Bmatrix} N_{xx} \\ N_{yy} \\ N_{xy} \end{Bmatrix} = \begin{bmatrix} A_{11} & A_{12} & A_{16} \\ A_{12} & A_{22} & A_{26} \\ A_{16} & A_{26} & A_{66} \end{bmatrix} \begin{Bmatrix} \epsilon^0_{xx} \\ \epsilon^0_{yy} \\ \epsilon^0_{xy} \end{Bmatrix} + \begin{bmatrix} B_{11} & B_{12} & B_{16} \\ B_{12} & B_{22} & B_{26} \\ B_{16} & B_{26} & B_{66} \end{bmatrix} \begin{Bmatrix} k_{xx} \\ k_{yy} \\ k_{xy} \end{Bmatrix} \tag{E.25}$$

and

$$\begin{Bmatrix} M_{xx} \\ M_{yy} \\ M_{xy} \end{Bmatrix} = \begin{bmatrix} B_{11} & B_{12} & B_{16} \\ B_{12} & B_{22} & B_{26} \\ B_{16} & B_{26} & B_{66} \end{bmatrix} \begin{Bmatrix} \epsilon^0_{xx} \\ \epsilon^0_{yy} \\ \epsilon^0_{xy} \end{Bmatrix} + \begin{bmatrix} D_{11} & D_{12} & D_{16} \\ D_{12} & D_{22} & D_{26} \\ D_{16} & D_{26} & D_{66} \end{bmatrix} \begin{Bmatrix} k_{xx} \\ k_{yy} \\ k_{xy} \end{Bmatrix} \tag{E.26}$$

In which:

$$\begin{aligned} A_{ij} &= \sum_{k=1}^{n} \left(\overline{Q}_{ij}\right)_k (h_k - h_{k-1}) \\ B_{ij} &= \frac{1}{2} \sum_{k=1}^{n} \left(\overline{Q}_{ij}\right)_k (h_k^2 - h_{k-1}^2) \\ D_{ij} &= \frac{1}{3} \sum_{k=1}^{n} \left(\overline{Q}_{ij}\right)_k (h_k^3 - h_{k-1}^3) \end{aligned} \tag{E.27}$$

Finally Equations E.25 and E.26 can be combined to obtain the complete constitutive relationship for the laminate.

$$\begin{Bmatrix} N_{xx} \\ N_{yy} \\ N_{xy} \\ M_{xx} \\ M_{yy} \\ M_{xy} \end{Bmatrix} = \begin{bmatrix} A_{11} & A_{12} & A_{16} & B_{11} & B_{12} & B_{16} \\ A_{12} & A_{22} & A_{26} & B_{12} & B_{22} & B_{26} \\ A_{16} & A_{26} & A_{66} & B_{16} & B_{26} & B_{66} \\ B_{11} & B_{12} & B_{16} & D_{11} & D_{12} & D_{16} \\ B_{12} & B_{22} & B_{26} & D_{12} & D_{22} & D_{26} \\ B_{16} & B_{26} & B_{66} & D_{16} & D_{26} & D_{66} \end{bmatrix} \begin{Bmatrix} \epsilon^0_{xx} \\ \epsilon^0_{yy} \\ \epsilon^0_{xy} \\ k_{xx} \\ k_{yy} \\ k_{xy} \end{Bmatrix} \tag{E.28}$$

Or as often simply written:

$$\begin{Bmatrix} N \\ M \end{Bmatrix} = \begin{bmatrix} A & B \\ B & D \end{bmatrix} \begin{Bmatrix} \epsilon^0 \\ k \end{Bmatrix} \tag{E.29}$$

In which:

A = Axial stiffness matrix
B = Coupling matrix
D = Bending stiffness matrix

Simplified Cases

Although the matrix in Equation E.28 is relatively complex there are cases in which major simplifications can be applied. The largest is if the laminate is symmetrical around its centre line. Is this case there is no coupling and matrix **B** becomes zeroes. In the case of orthotropic materials, where normal forces have no effect on the shear angles, A_{16} and A_{26} become zero. Similarly D_{16} and D_{26} also become zero if bending moments do not affect torsion. Graphical representations of these coupling mechanisms are shown in Figure E.3.

C

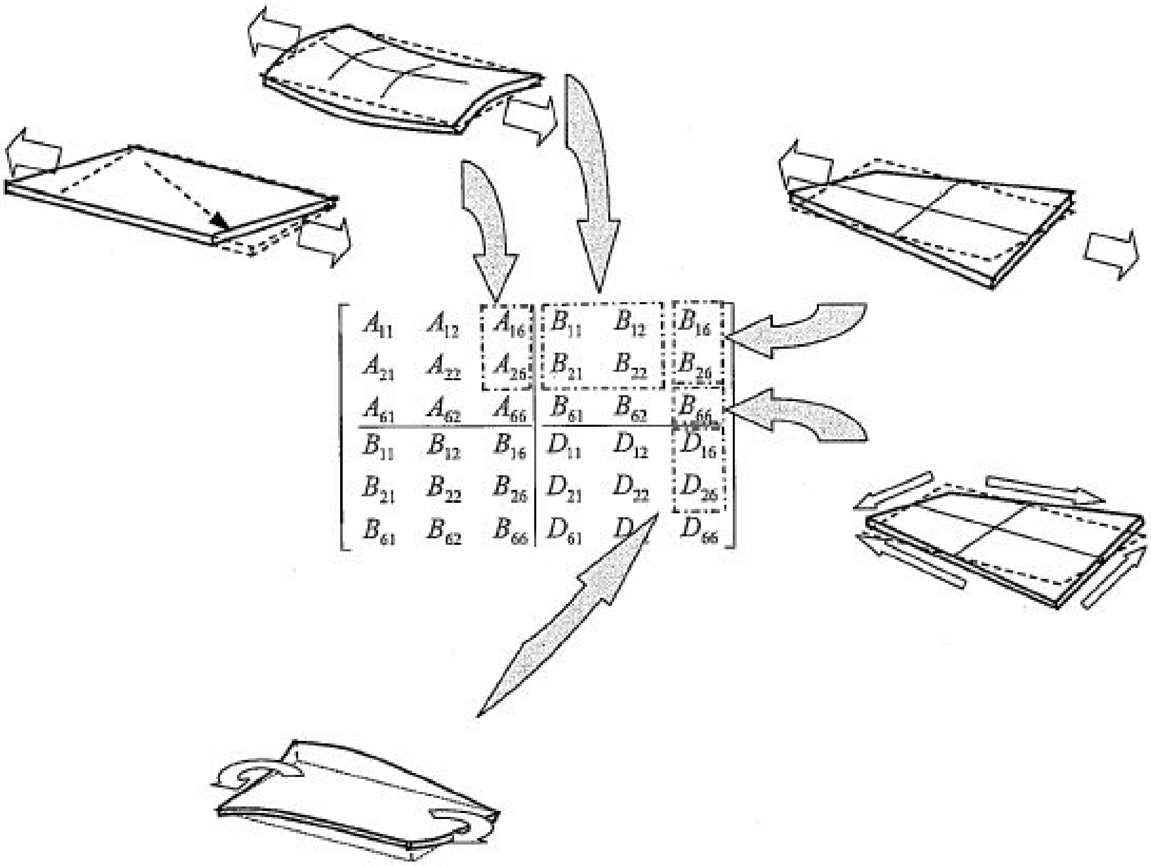
A11 A12 A16 B11 B12 B16
A21 A22 A26 B21 B22 B26
A61 A62 A66 B61 B62 B66
B11 B12 B16 D11 D12 D16
B21 B22 B26 D21 D22 D26
B61 B62 B66 D61 D D66

Figure E.3: Graphical representation of the coupling mechanisms in the constitutive equation [36]

F

CUR Recommendations

There is no official code of conduct for constructing with FRP owing to the short period that they have been considered a serious contender within the civil engineering market. Many companies which regularly work with FRP have developed their own codes, or use those provided by the manufacturers whom have the deepest understanding of the material. An exception to this rule is the recommendation provided by the CUR, which is an independent board of professionals. As stated it is a recommendation, not a code, and thus it is not compulsory to follow its guidelines. The dutch government has however declared that structures which follow the CUR recommendation 96 are considered to be safe.

The following chapter is a summary of the main points of the CUR recommendation 96 [11] and the background report supporting it [36].

F.1. Introduction in the CUR Recommendation 96

The CUR (Centrum Uitvoering Research [Centre of execution of Research]) Recommendation 96 was put together by CUR-committee C 124 named ”FRP in civil supporting structures” to give engineers working with glass fibre reinforced polymers guidelines by which to design structures. The safety philosophy behind the guidelines is analogous to that of the Eurocode which is widely accepted.

The code is only valid for glass fibre reinforced structures with at least 20% fibre volume percentage and may not be used if a laminate consists completely of mats. However a separate ply may have a lower fibre ratio or be a mat. A laminate must also contain at least 15% of the used fibres in each main direction to account for unpredicted forces and to prevent fatigue, creep of impact being taken only by the resin.

Within the recommendation FRP as a material is assumed to respond in a linear elastic manner until rupture and thus the elasticity theory is applied. Because of this no redistribution of forces will take place for statically indeterminate structures. There may also be a level of coupling between normal forces and bending due the asymmetry in the laminate. This must be accounted for when applicable.

F.2. Safety Calculations

As mentioned before the CUR follows the same safety philosophy as the Eurocode. Conservative values for the loads and resistance of the structure are assumed as characteristic values and these value are further adapted through use of safety factors which account for uncertainties. The basic form of this equation is given in Equation F.1.

$$S \cdot \gamma_\mathrm{f} \leq \frac{R}{\gamma_\mathrm{m} \cdot \gamma_\mathrm{c}} \tag{F.1}$$

In which:

S	is the characteristic force applied.
R	is the characteristic resistance of the structure.
γ_f	is a load factor.
γ_m	is a material factor.
γ_c	is a conversion factor.

These factors are further explained in the following sections.

F.2.1. Load Factors

The load factor γ_f is independent of the material which is used to construct the structure in question and is solely dependant on the nature of the load. For this reason the procedure for FRP structures does not differ from that of, for example, steel and the governing norms may still be used. For the case in the Netherlands this means the Eurocode and the NEN-norms. The load factors dictated by the aforementioned norms are given in Table F.1.

Table F.1: Load factors as dictated by the Eurocode[10]

Load Type	Load Factor γ_fW
Permanent Loads	1.2
Variable Loads	1.5
Self Weight (Detrimental)	1.2
Self Weight (Beneficial)	0.9

In addition to the factor mentioned above there are special cases (e.g. snow loads) for which other factors are governing. For those cases reference is made to [10].

F.2.2. Material Factors

The uncertainties with respect to material properties can be separated into two categories as shown in Equation F.2.

$$\gamma_\mathrm{m} = \gamma_\mathrm{m,1} \cdot \gamma_\mathrm{m,2} \tag{F.2}$$

In which:

$\gamma_\mathrm{m,1}$	is a partial material factor derived from uncertainties in material properties.
$\gamma_\mathrm{m,2}$	is a partial material factor derived from uncertainties in the production and cure.

The factor $\gamma_\mathrm{m,1}$ is taken to be equal to 1.35 in all cases in which no tests have been preforms on the laminate in question. The factor $\gamma_\mathrm{m,2}$ is dependant on the production process and level of curing. Value of $\gamma_\mathrm{m,2}$ are given in Table F.2.

Table F.2: Partial material factor derived from production and cure[11]

Production method	Partial material factor $\gamma_{m,2}$	
	With post-cure	Without post-cure
Spray-up	1.6	1.9
Hand Lamination	1.4	1.7
Vacuum or Pressure Moulding	1.2	1.4
Filament Winding	1.1	1.3
Pre-pregs	1.1	1.3
Pultrusion	1.1	1.3

A requirement which is always valid despite the actual value of the factors $\gamma_{m,1}$ and $\gamma_{m,2}$ is that γ_m must be at least 1.5 when testing the ultimate limit state for safety reasons.

$$\gamma_m = max(\gamma_{m,1} \cdot \gamma_{m,2}; 1.5) \tag{F.3}$$

F.2.3. Conversion Factors

Conversion factors are used to represent uncertainties with regard to the environment and loading conditions in which a structure must function. They can be separated into four categories as shown in Equation F.4.

$$\gamma_c = \gamma_{ct} \cdot \gamma_{cv} \cdot \gamma_{cf} \cdot \gamma_{ck} \tag{F.4}$$

In which:

γ_{ct}	is a partial conversion factor derived from temperature effects.
γ_{cv}	is a partial conversion factor derived from moisture effects.
γ_{cf}	is a partial conversion factor derived from fatigue effects.
γ_{ck}	is a partial conversion factor derived from creep effects.

Unlike other factors not every conversion factor needs to be taken into account for every calculation. This depends on factors such as the time scale of the contributions. Which factors are needed when is shown in Table F.3.

Table F.3: Use of conversion factors during different calculation types[11]

	Ultimate Limit State			Serviceability Limit State		
	Strength	Stability	Fatigue	Deformation	Vibrations	First Crack
γ_{ct}	yes	yes	yes	yes	both	yes
γ_{cv}	yes	yes	yes	yes	both	yes
γ_{cf}	no	yes	no	yes	both	yes
γ_{ck}	yes	yes	no	yes	no	yes

Note that vibration calculation should be performed twice, once with and once without conversion factors. This is because it is hard to predict whether or not the use of conversion factors will prove beneficial for the natural frequencies.

The values of the conversion factors are given below.

γ_{ct} **Temperature effects**
The conversion factor for temperature effects is taken to be γ_{ct} = 1.1 in all cases.

γ_{cv} **Moisture effects**
The conversion factor for moisture effects depends on the conditions for which the structure is designed:

- For a structure which is almost constantly in dry conditions: γ_{cv} = 1.0.
- For a structure which is exposed to alternating wet and dry conditions γ_{cv} = 1.1.
- For a structure which is almost constantly in wet conditions (e.g surface water, ground water, sea water, water tanks) γ_{cv} = 1.3.

γ_{cf} Fatigue effects
The conversion factor for fatigue effects is taken to be γ_{cf} = 1.3 in all cases.

γ_{ck} Creep effects
The conversion factor for creep effects must be taken into account for long term loading effects. It can be calculated from:

$$\gamma_{ck} = t^{n} \tag{F.5}$$

In which:

t is the length of the loading in hours.
n is a factor dependant on the type of fibre reinforcement.

If the fibres are in the direction of the main loading the following n-factors can be used:

- n = 0.01 for uni-directional reinforcement
- n = 0.04 for a weave
- n = 0.1 for a mat

If the fibres are not in the direction of the main loading the n-factor can be determined with the following steps:

1. Determine which plies have fibres in the main loading direction.
2. Determine the long term deformation of the entire laminate.
3. Determine the long term deformation of the laminate with only the plies which are orientated in the main loading direction.
4. Calculate the ratio between the deformations calculated in 2 and 3.
5. Multiply the n-factor from the list above by this factor.

F.3. Laminate Properties

Laminate properties can be determined by testing the end product. If however the material is regularly tested during production and proved to meet certain criteria representative values for the laminates plies can be taken from design tables. The properties of the laminate as a whole can then be determined through use of classical laminate theory as described in Appendix E.

F.3.1. Stiffness Properties

The relevant stiffness properties are the Young's modulus in the direction of the fibres, the Young's modulus is traverse direction, the shear modulus and the Poisson ratio. These are denoted as E_1, E_2, G_{12}, v_{12} respectively and given as a function of the fibre content v_f. Intermediary values may be determined through linear interpolation.

Properties for unidirectional plies, weave plies and mat plies are given in Table F.4, Table F.5 and Table F.6 respectively.

Table F.4: Nominal values for stiffness properties of unidirectional plies[11]

V_f	E_1 [GPa]	E_2 [GPa]	G_{12} [GPa]	v_{12} [GPa]
40%	30.8	8.9	2.8	0.30
45%	34.3	10.0	3.1	0.29
50%	37.7	11.3	3.5	0.29
55%	41.1	12.8	3.9	0.28
60%	44.6	14.6	4.5	0.27
65%	48.0	16.7	5.1	0.27
70%	51.4	19.3	6.0	0.26
Reduction factor for UD-stiffness properties (except v_{12}): 0.97				

Table F.5: Nominal values for stiffness properties of weave plies[11]

V_f	E_1 [GPa]	E_2 [GPa]	G_{12} [GPa]	v_{12} [GPa]
25%	13.4	13.4	2.1	0.21
30%	15.5	15.5	2.3	0.20
35%	17.6	17.6	2.5	0.20
40%	19.8	19.8	2.8	0.19
45%	22.1	22.1	3.1	0.19
50%	24.5	24.5	3.5	0.19
55%	27.0	27.0	3.9	0.18
Reduction factor for weave-stiffness properties (except v_{12}): 0.93				

Table F.6: Nominal values for stiffness properties of mat plies[11]

V_f	E_1 [GPa]	E_2 [GPa]	G_{12} [GPa]	v_{12} [GPa]
10%	6.2	6.2	2.3	0.33
12.5%	6.9	6.9	2.6	0.33
15%	7.6	7.6	2.9	0.33
17.5%	8.3	8.3	3.1	0.33
20%	9.1	9.1	3.4	0.33
25%	10.6	10.6	4.0	0.33
30%	12.2	12.2	4.6	0.33
Reduction factor for mat-stiffness properties (except v_{12}): 0.91				

Table F.7: Values for the inter-laminar strengths of glass fibre reinforced resins[11]

Resin Type	Inter-Laminar Tensile Strength [MPa]	Inter-Laminar Shear Strength [MPa]
Polyester	10.0	20
Vinylester	12.5	25
Epoxy	15.0	30

F.3.2. Strength Properties

The strength of a glass fibre reinforced laminate is determined by the maximum allowed strain. The laminate is said to fail once the maximum strain is surpassed in the outermost ply. The level of the maximum strain depends on whether or not cracks are allowed in the laminate. If a structure is allowed to crack to a certain extent then a strain of 1.2% is allowed in the ultimate limit state. However for structure which must resist cracks altogether or which is at risk of damage from moisture (through prolonged contact with water) the maximum strain is 0.27% in the serviceability limit state. With a known laminate build-up and these strains the failure load can be determined.

To avoid delamination of the composites the inter-laminar forces must also be tested. The inter-laminar tensile strength and the inter-laminar shear strength are dependant on the resin type chosen and given in Table F.7.

F.3.3. Other Properties

There are tables similar to those for the stiffness properties for other attributes of glass fibre reinforced polymers such as thermal coefficients and electrical resistance. For these you are referred to the CUR Recommendation 96 [11].

F.4. Calculations

In many ways calculations for a FRP structure are similar to those of steel structures. However their layered build-up together with their anisotropic character changes how some calculation must be made. Basic guidelines as to the execution of the main calculations are given in the chapters below.

F.4.1. Stiffness Calculations

When working with FRP instead of traditional steel and concrete one must be aware that displacements are more likely to be the decisive factor during design due to the relatively low modulus of elasticity compared to strength.

The allowed displacements are the same as for steel or concrete structures as stated in the Eurocode and both bending and shear displacements must be taken into account. The CUR Recommendation 96 [11] gives a few examples of these calculations.

F.4.2. Stability Calculations

When parts of a FRP structure are subjected to compressive or shear forces they must be checked on stability in the ultimate limit state. For these checks the product of the material factor γ_m and the load factor γ_f must be at least 2.5.

These calculations are identical to those for steel save the different method of determining the material properties. The CUR Recommendation 96 [11] gives a few examples of these calculations.

F.4.3. Strength Calculations

In general there are six values which need to be checked with strength calculations. These are:

- Tensile stress/strain in the main fibre direction, $\sigma_{1,t}/\ \epsilon_{1,t}$.
- Compressive stress/strain in the main fibre direction, $\sigma_{1,c}/\ \epsilon_{1,c}$.
- Tensile stress/strain perpendicular to the main fibre direction, $\sigma_{2,t}/\ \epsilon_{2,t}$.
- Compressive stress/strain perpendicular to the main fibre direction, $\sigma_{2,c}/\ \epsilon_{2,c}$.
- Shear stress/strain between these two directions,$\sigma_{12}/\ \epsilon_{12}$.
- Interlaminair shear stresses, σ_{ILSS}.

These calculations can be done in the stress or strain domains. For calculations in the strain domain the strain criterion of 1.2% (or 0.27% for non crack resistant structures) should be used. For stresses the nominal values in combination with the classical laminate theory may be used if it has been proven that the material meets all requirements. Otherwise properties results from tests should be used.

Strain Domain

In the strain domain values should be tested with the criterion given in Equation F.6.

$$\frac{\epsilon_S}{\epsilon_R} \leq \frac{1}{\gamma_f \cdot \gamma_m \cdot \gamma_c} \tag{F.6}$$

In which:

ϵ_S is the applied strain.
ϵ_R is the maximum strain which can be resisted by the structure.

If there is a constant strain field the criterion may be used over the entire laminate. If not then each ply should be tested separately, especially the outer plies.

Stress Domain

In the stress domain values should be tested with the criterion given in Equation F.7.

$$\frac{\sigma_S}{\sigma_R} \leq \frac{1}{\gamma_f \cdot \gamma_m \cdot \gamma_c} \tag{F.7}$$

In which:

σ_S is the applied stress.
σ_R is the maximum stress which can be resisted by the structure.

One can only assess the laminate as a whole if it is a uniform laminate (i.e. consists of equal plies with the same orientation), otherwise the stresses will not be equal in the different plies and each must be assessed separately. This is due to the fact that each ply will fail at the same strain, but their stiffness's vary with the fibre orientation.

When stresses applied is multiple directions their coupling effects must be taken into account. This can be done with the two equations below, F.8 for tensile stresses and F.9 for compressive forces.

Tension:

$$\left(\frac{\sigma_{1,t,S}}{\sigma_{1,t,R}}\right)^2 - \left(\frac{\sigma_{1,t,S}\cdot\sigma_{2,t,S}}{\sigma^2_{1,t,R}}\right)^2 + \left(\frac{\sigma_{2,t,S}}{\sigma_{2,t,R}}\right)^2 + \left(\frac{\sigma_{12,S}}{\sigma_{12,R}}\right)^2 \leq \frac{1}{\gamma_f\cdot\gamma_m\cdot\gamma_c} \tag{F.8}$$

Compression:

$$\left(\frac{\sigma_{1,c,S}}{\sigma_{1,c,R}}\right)^2 - \left(\frac{\sigma_{1,c,S}\cdot\sigma_{2,c,S}}{\sigma^2_{1,c,R}}\right)^2 + \left(\frac{\sigma_{2,c,S}}{\sigma_{2,c,R}}\right)^2 + \left(\frac{\sigma_{12,S}}{\sigma_{12,R}}\right)^2 \leq \frac{1}{\gamma_f\cdot\gamma_m\cdot\gamma_c} \tag{F.9}$$

In which:

$\sigma_{1,i,S}$	is the applied stress in the fibre direction.
$\sigma_{1,i,R}$	is the maximum stress which can be resisted by the structure in the fibre direction.
$\sigma_{2,i,S}$	is the applied stress perpendicular to the fibre direction.
$\sigma_{2,i,R}$	is the maximum stress which can be resisted by the structure perpendicular to the fibre direction.
$\sigma_{12,S}$	is the applied shear stress.
$\sigma_{12,R}$	is the maximum shear stress which can be resisted by the structure.

Note: 'i' represents the stress direction and can be both 't' for tensile stresses or 'c' for compressive stresses.

The above equations assume that the principal stresses are known. If instead there is a stress in a arbitrary direction with an angle Ψ from the fibre direction the principal stresses $\sigma_{1,S}, \sigma_{2,S} and \sigma_{12,S}$ can be determined with the set of equations F.10.

$$\begin{aligned} \sigma_{1,S} &= \left(\cos^2\Psi\right)\sigma'_{\Psi,S} \\ \sigma_{2,S} &= \left(\sin^2\Psi\right)\sigma'_{\Psi,S} \\ \sigma_{12,S} &= \left(\sin\Psi\cdot\cos\Psi\right)\sigma'_{\Psi,S} \end{aligned} \tag{F.10}$$

In which:

$\sigma_{1,S}$	is the applied principle stress in the fibre direction.
$\sigma_{2,S}$	is the applied principle stress perpendicular to the fibre direction.
$\sigma_{12,S}$	is the applied shear stress.
Ψ	is the angle between the applied stress and the fibre orientation.

G

Reference Projects

A large portion of this Appendix is based on [39]. In this Appendix two projects in which FRP was used will be discussed to serve as a reference. In Appendix G.1 a pedestrian bridge in Harlingen which serves as a boarding bridge for a ferry will be discussed. Appendix G.2 discusses a set of FRP mitre gates fitted in the Spieringssluis near Dordrecht. This project closely resembles the case considered in this study.

G.1. Pedestrian bridge - Koegelwieck

On the 4th of December 1997 a footbridge fully constructed from FRP (the first in the Netherlands) was opened in Harlingen. It serves as a boarding bridge for the ferry 'Koegelwieck' and must be able to support pedestrians and postal carts and make boarding possible at all tidal levels. This brings with it the requirement that one side of the bridge must be able to move to accommodate the current level of the ferry. In the original design it was planned to do this by mounting the one side on a floating pontoon, but later it became apparent that this wasn't possible and a manual lifting system was installed.

Originally designs were made in steel aluminium and FRP. There were a few reason why FRP was chosen, the main on being that maintenance costs were anticipated to be high for metallic structures due to stricter environmental guidelines. Each time the structure would need to be sanded down and repainted all the dust would have to be caught so as not to end up in the surface water. The other reason was that it was seen as beneficial to gain experience with FRP as a potentially useful material of which there was little knowledge to date. Monitoring and measurements during the life of the bridge would supply useful research data.

The bridge was designed and constructed through cooperation of Composieten Team BV, Bouwdienst Rijkswaterstaat and Poly Products BV. They came up with three global designs which were compared to select the most fitting design. The three options were a bridge formed from standardised pultruded elements, a bridge with custom designed pultruded elements and a self-supporting shell structure. In all three designs it became clear that the vertical displacement requirement which is normally used for a steel bridge must be relaxed to reach a economically attractive solution. Although global analysis showed that the standardised pultruded elements bridge would be the cheapest to construct the team choose the self-supporting shell. The reasoning behind this was that the design contained less bolted connections which could become problematic when it is considered that they are subjected to alternating torsion.

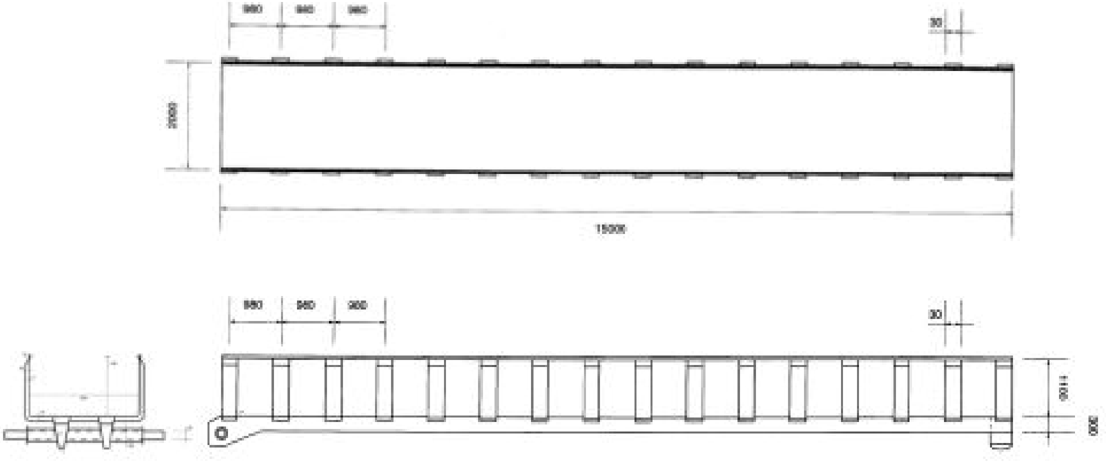

Figure G.1: Preliminary design U-shaped shell[39]

Was the choice for a shell structure was made, three more detailed design were made and a final design was chosen. The three options were:

- A stiffened shell with a n-shaped cross section
- A stiffened shell with a u-shaped cross section
- A shell with a tension cable running beneath it

The second options, a stiffened shell with a u-shaped cross section turned out to be the cheapest option. The preliminary design is shown in Figure G.1. Aesthetics was not a major issue in the design, the most important point when deciding on a shell shape was the expected costs which would be paired with the mold. Camber was applied to compensate for the sagging due to creep effects.

Because the design is stiffness dominated glass fibre reinforced polyester was originally chosen, because it has the highest stiffness per weight per cost ratio. However the contractor had experience working with vinylester resin and decided to use this instead. In hindsight this proved unwise as the resin proved hard to handle and there was difficulty when forming the laminates causing too much air to remain between the fibres. Eventually polyester was used after all, but the failed attempt lead to extra costs.

The used laminates came in 15 thicknesses and were all constructed from three layup types: a 0/±45°fabric (75/25%, 600 g/m^2) and two unidirectional tapes of 500 and 1250 g/m^2.

After construction the assumptions and computer models were tested to see if the design method was accurate. The quality control of the laminate were tested by applying test plates during construction which could be removed for tests. Test results showed that the computer models had a decent accuracy and that the wear and tear of the structure of of an acceptable level. Most of the maintenance which was needed was for aesthetic reasons (cleaning and such).

G.2. Mitre Gates - Spieringssluis

In 1999 a set of FRP mitre gates were installed in the Spieringssluis near Dordrecht as replacements for two wooden doors. The Spieringssluis is a lock in a branch of the Nieuwe Merwede connecting it to the Gat van Den Hardenhoek (see Figure G.2). The project was a cooperation between the Nederlandse Corrosie Centrum, Rijkwaterstaat and Stichting Materiaal Onderzoek in de Zee. It was seen as a pilot

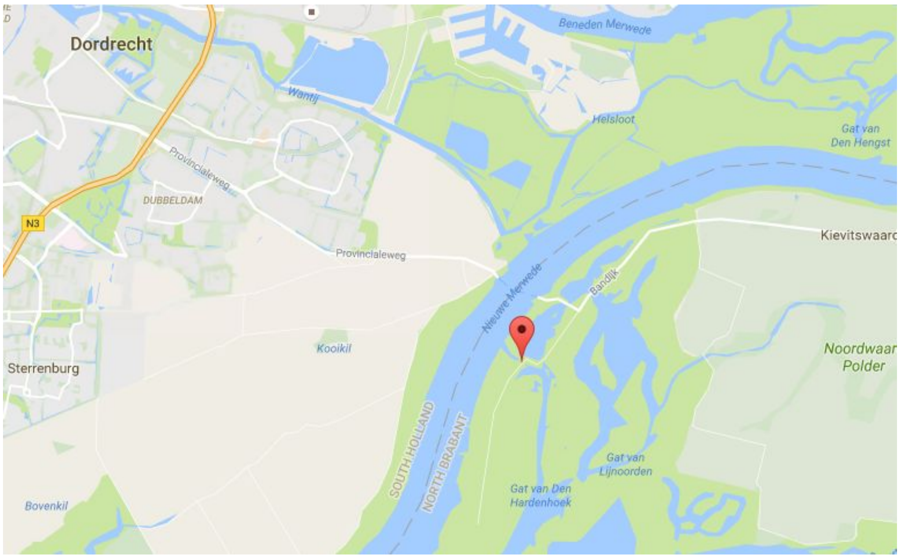
Dordrecht
Beneden Merwede
Wantij
Helsloot
Gat van
Den Hengst
Provincialeweg
DUBBELDAM
N3
Provincialeweg
Kievitswaar
Bandijk
Nieuwe Merwede
Kooikil
Sterrenburg
Noordwaar
Polder
SOUTH HOLLAND
NORTH BRABANT
Gat van
Lijnoorden
Gat van Den
Hardenhoek
Bovenkil

Figure G.2: Location of the Spieringssluis lock[40]

project and was accompanied by a lot of tests and research.

Some of the main aspects and requirements of the lock are listed below:

- The lock in located in brine water.
- The lock must last 50 years of which at least 20 without maintenance.
- Local damage above the water line must be able to be repaired without removing the lock door.
- The doors must resist a fatigue load of 5500 lockings per year over its entire life time.
- The gates must have walkways above them to allow crossing.
- As the old doors are being kept as reserve door, the gate geometry must remain the same as in the old design.
  - Doors must be 3,6m wide and 6,4m high.
  - The hinges, foot and bumpers must remain at the same locations.
  - The lock chamber must remain the same to reduce costs.
- From statistical data and considering that the situation may change somewhat a positive fall of 1.3m at high and low water was found. The negative fall is limited to 0.25m and is caused by waves from ships.
- No leakage due to positive water fall.
- Leakage due to negative fall is allowed, because it is very temporary in nature.
- Extra requirements for an FRP design due to its lower stiffness than steel.
- Safety will be guaranteed through use of material and load factors.
  - Vertical displacement of the walkways must be limited.
  - Horizontal displacement of the handrails must be limited.

From this list of requirements three design were made which will be discussed in the following section.

G.2.1. Preliminary Design Concepts

Three companies came up with designs for the FRP lock gates namely: Polymarin, Koninklijke Schelde Scheepsbouw and Grontmij Verkeer & Infrastructuur. Each company worked on a different type of door so that comparison was possible. Even in this early stage of design attention was paid to some constructive details such as hinge points, closure en valve location. The three designs were:

- A sandwich panel door (Polymarin)

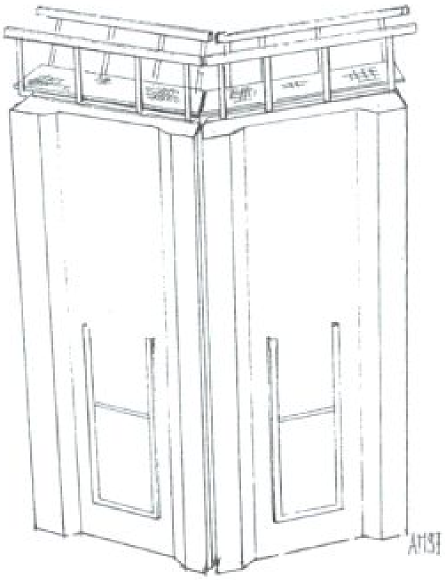

Figure G.3: Preliminary design - Sandwich Panel (Polymarin)[39]

- A pultruded corrugated sheet door (Koninklijke Schelde Scheepsbouw)
- A curved shell section (Grontmij Verkeer & Infrastructuur)

Sandwich Structure

The design thought up by Polymarin consists of a sandwich panel door fitted with U-shaped stiffeners. A sketch of which can be seen in Figure G.3. The skin is made from glass fibre reinforced polyester and is spaced by a core of structural foam. This construction method is easily scalable to larger doors. All steel parts needed can be added during lamination and the flat topside makes it relatively easy to add a walkway.

A disadvantage is that the structure is very light and at rick on floating up. This wouldn't be a problem is the rest of the lock and the hinges were designed to accommodate this, but because the existing geometry is enforced measures would have to be taken to weight the door down. Also when adding the lock valves extra stiffening elements will need to be added around the openings to protect the foam core.

Pultruded Corrugated Sheet

The design by Koninklijke Schelde Scheepsbouw is based on large pultruded sheets which resemble traditional sheet piling. Four such sheet are used per door with the inner two being aligned vertically and the outer two horizontally. Each ply is responsible for the strength and stiffness in the direction of its fibres. A sketch of this design is shown in Figure G.4.

Pultruded sheets of this size are hard to construct because they require large machinery and a lot of fibre spools. This may cause issues during production and will make up-scaling very difficult.

Once the elements are made this design is relatively easy to construct as long as attention is paid to the gluing process, which must be resistant to freezing and thawing. Valves can be sawed out of the plates and the sides can be sealed with disks made to fit. Also, being a hollow structure, floatation isn't expected to be a problem.

On the down side this design strongly resembles a design as it would be made for a steel gate. From

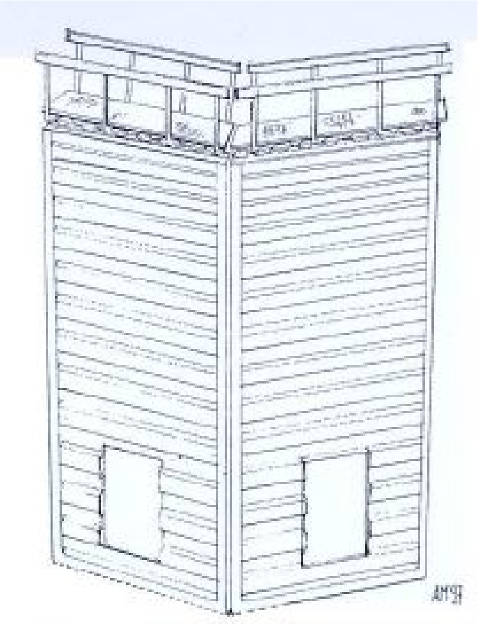

Figure G.4: Preliminary design - Pultruded Corrugated Sheet (Koninklijke Schelde Scheepsbouw)[39]

an aesthetic point of view this isn't preferable. From a structural view it also means that the material usage is sub optimal as it is not design while taken the unique character of FRP into account.

Curved Shell Structure

Grontmij Verkeer & Infrastructuur came up with a design which consists of the curved shell structure as shown in the sketch in Figure G.5.

The shape of the structure causes mostly normal forces in the FRP plates. This leads to very efficient material usage. During positive fall the entire plate will be subjected to compression and during negative fall tension. The thrust forces which are caused by this push the doors together which is good when it comes to preventing leakage. The curved shape make detailing more complex and the walkway would have to bend along with the door. Normal valves also become impossible, making it necessary to use rotational valves.

Comparison

The three designs were compared by costs, feasibility, producibility and aesthetics with attention being paid to technical aspects such as floatation, freeze resistance and damage susceptibility. Because this was a pilot project it was also of value if important lessons could be learnt from design and construction.

The sandwich panel door was seen as a good compromise between innovation and producibility and costs, but the light weight may cause floatation issues.

The corrugated plate was easy to produce and detail, but didn't have the FRP character that the commissioning party wished to radiate.

The curved sheet was the best FRP design, with optimal material usage, but it was seen as too high-tech and was less compatible with the existing lock geometry.

For these reasons the sandwich plate design made by Polymarin was chosen for further detailing.

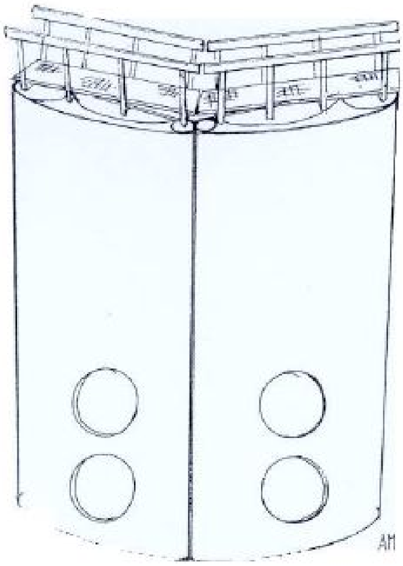

Figure G.5: Preliminary design - Curved Shell Structure (Grontmij Verkeer & Infrastructuur)[39]

G.2.2. Final Design

A lot of changes were made to the design between the preliminary and final steps. During detailing the floatation problem turned out to be greater than expected so fundamental changes were made to the sandwich panel build-up. The front of the gate was changed to be a solid FRP laminate plate and the core was replaced by a single corrugated plate as described in the design made by Koninklijke Schelde Scheepsbouw, the ribs of which were orientated horizontally. The skin at the back of the door is removed completely and the sides of the gates and valves are fitting with FRP U-shaped profiles. The final design can be seen in Figure G.6.

The thicker front plate improves collision resistance and the resistance to freezing while the corrugated plate removes the risk of the gate floating up. Seen as there is now only one sheet with ribs in only the horizontal direction the vertical stiffness of the gate is lower. This is partially solved by the U-shaped profiles around the edge and partially by producing the corrugated sheet through hand lamination instead of pultrusion, allowing for fibres perpendicular to the ribs. Hand lamination also solves the issue with a size of the sheets as no extra machinery is needed and makes scaling of the project in the future possible. Connections with the walkway, hinges etc. are more easily detailed due to the flat surfaces formed by the U-shaped profiles.

From calculations as to the necessary bending stiffness of the elements dimensions were determined. For this glass fibre reinforced polyester with a fibre percentage of 32% was assumed (which is 50% in weight), which is a realistic amount for hand lay-up elements. The corrugated sheet was determined to be 10mm thick with a corrugation angle of 60°. The U-shaped profiles, which give the vertical stiffness, required a thickness of 20mm with 2mm of glue to attach them. Although possible to vary the thickness of the sheet depending in the exact loading conditions it was proved that the amount of material saved was too small to be worth the extra effort during production. The walkway will be constructed from pultruded elements and all stainless steel parts fastened with glue and bolts.

Laminate build-up

All elements were constructed as laminates of glass fibre reinforced polyester plies with a fibre percentage of 32%. As a resin Sinolite 1573-I-1 (by DSM.BASF Structural Resins) was used which is a polyester with especially good moisture resistance. Before construction the elements were tested to

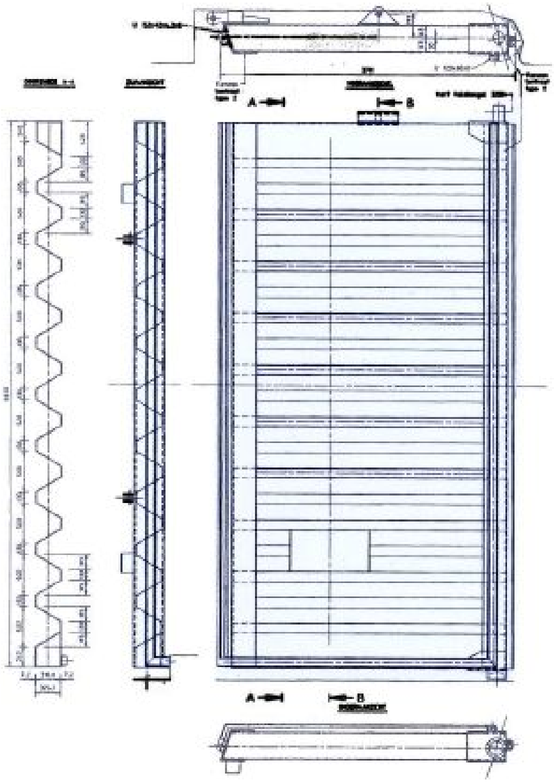

Figure G.6: Final design of the Spieringssluis[39]

guarantee that the assumed value during design were accurate.

During laminate design the basic design rule that at least 15% of the fibres must be orientated in every direction with major loads. Considering that water pressure causes a uniform stress field, all principal directions (0°/90°/±45°) must contain 15% of the fibres. This leaves 40% of the fibres which can be used to optimise the laminate. In most elements they will be applied in the direction in which the element carries the largest load. For the valve stiffeners they will be spread evenly over the principle directions.

Three different ply types were used in the laminates: a unidirectional tape, a 0°/90° weave and a ±45° weave. All of which were formed from 800 g/m^2 E-glass fibres and were 1mm thick. Attention was paid to keep the laminates as symmetrical as possible to avoid internal torsional force. Complete symmetry proved impossible for the chosen fibre orientation, but the deviations were minimal and had no significant structural effects. The different laminate build-ups are displayed below in Table G.1.

Table G.1: Laminate build-ups for the final design of the Spieringssluis [39]

Element	Fibre Percentages	Ply Build-up	Thickness
Corrugated sheet	$0_{55}/90_{15}/+45_{15}/-45_{15}$	$UD_4/(0\text{-}90)_3/\pm45_3$	10 mm
U-shaped profiles	$0_{55}/90_{15}/+45_{15}/-45_{15}$	$UD_8/(0\text{-}90)_6/\pm45_6$	20 mm
Valve stiffeners	$0_{25}/90_{25}/+45_{25}/-45_{25}$	$(0\text{-}90)_7/\pm45_7$	14 mm

H

InfraCore Inside

InfraCore Inside as designed by FibreCore is in essence a combination of a sandwich panel and the multi beam plate. Both these plate types have distinct issues which often limit their properties. By combining the two a plate is obtained in which these known failure modes are reinforced to increase the ultimate strength. These two types of plate will be discussed in the following chapters along with their shortcomings, followed by the InfraCore design which attempts to solve the issues.

H.1. Sandwich Panels

Sandwich panel have already been briefly discussed in Chapter D.3.1, but considering their resemblance to the case at hand they deserve some further explanation, especially into their failure modes.

In a general sense a sandwich panel consists of two skins, which are structurally strong, with a light, and structurally weaker, core material in between. The core serves as a cheap and lightweight manner to increase the section moduli of the panel. The skins and the core are connected through a form of adhesive. Section mechanics tells us that, in this configuration, the skins will be mainly stressed by normal forces which counteract present moments by the internal arm formed by the core. The core will be subjected to the shear forces in the cross-section while the adhesive is required for the longitudinal shear forces along the interface.

The failure mode depends on which element of the panel fails first. Generally speaking the skins are said to be much stronger than both the core and the adhesive, making them less likely to fail due to global loading. This may not always be the case for local loading. The core failure can be reinforced by addition of internal flanges of FRP laminate to help with the shear loading. In practical situations it is often chosen to make use of these internal flanges. The final failure mode is debonding of the skins and the core through failure of the adhesive, which will often be the deciding aspect. Once a load has cause the debonding to begin it will propagate along the interface until complete failure occurs as shown in Figure H.1. Note that the addition of internal flanges will reinforce this failure mode somewhat, but this is strongly dependant on the means of connection as will be discussed later in this chapter.

H.2. Multi Beam Plates

A multi beam plate is in many ways comparable to a traditional box girder. They generally consist of a series of rectangular beams with foam cores spanning along the main load bearing orientation (Part a of Figure H.2). When larger loads need to be carried an extra skin laminate can be applied (Part b

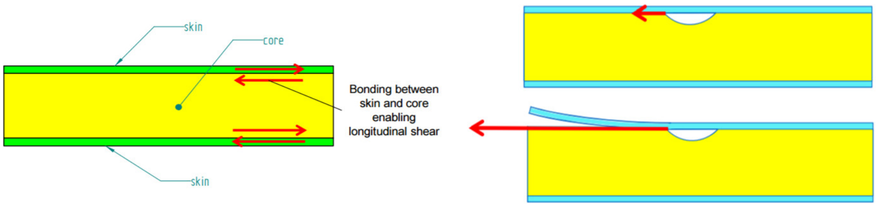

Figure H.1: **Left:** Schematic overview of a sandwich panel, **Right:** Coinciding failure paths and modes[41]

of Figure H.2) to extend the failures paths and strengthen the laminate. The interfaces between the rectangular sections, and potential outer skin, consist of only adhesive and resin and form weak points in the plate. The coinciding failure modes are shown in Figure H.2. For the case with an outer skin the image shown may not seem to signify failure, but it shows local delaminations which reduce the plates properties dramatically and may influence the functionality of the plate as a whole. As such it should be considered a failure for design purposes.

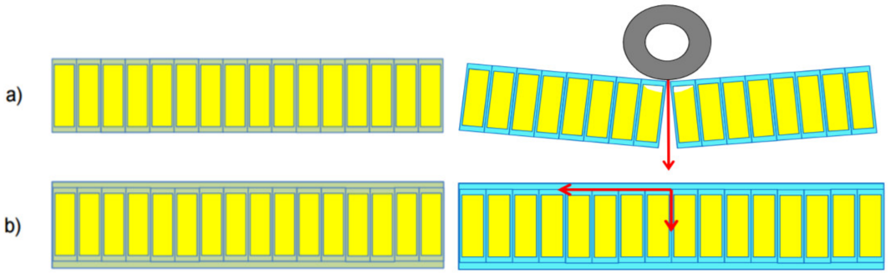

Figure H.2: **Left:** Examples of multi beam panels, **Right:** Coinciding failure paths and modes[41]

Combined Solution

When the failure modes of the above two solutions are compared two things become clear:

- Interfaces between structural elements form large weaknesses.
- Delamination causes serious issues.

For this reason it is desirable to avoid long straight interfaces where possible, especially those in which the only bonding is provided by adhesive and/or resin. InfraCore Inside accomplishes this by using z-shaped laminates which are parts of both skins as well as the internal flanges laid over the top of each other to form a plate. The bonding between the internal plates and the skins can be made very robust in this manner strengthening the composite sandwich considerably and preventing delamination. A schematic view of this process is shown in Figure H.3. The structural plate which is obtained in this manner in similar to a sandwich panel with internal flanges, but with a stronger connection between skins and internal flanges, and to a multi beam plates, but without the straight interfaces. This complex shape can be produced through use of vacuum resin injection (See Appendix D).

To increase strength in the other axis shear webs can be added within the foam cores. In this manner the internal flanges are supported. Because these plates are orientated perpendicular to the main loading direction their contribution to the bending stiffness of the gate is minimal and they will not be taken into account for the analytical calculations. These perpendicular shear webs are shown in Figure H.4 along with the fibre orientation of all the laminates included in the plate. These fibre orientations are crucial for the properties of the laminate and consist of fibre in the main loading direction and diagonal fibres at +/-45°. The main reinforcement then carries the largest portion of the loads while the diagonal reinforce accounts for other smaller loading such as local forces and shear.

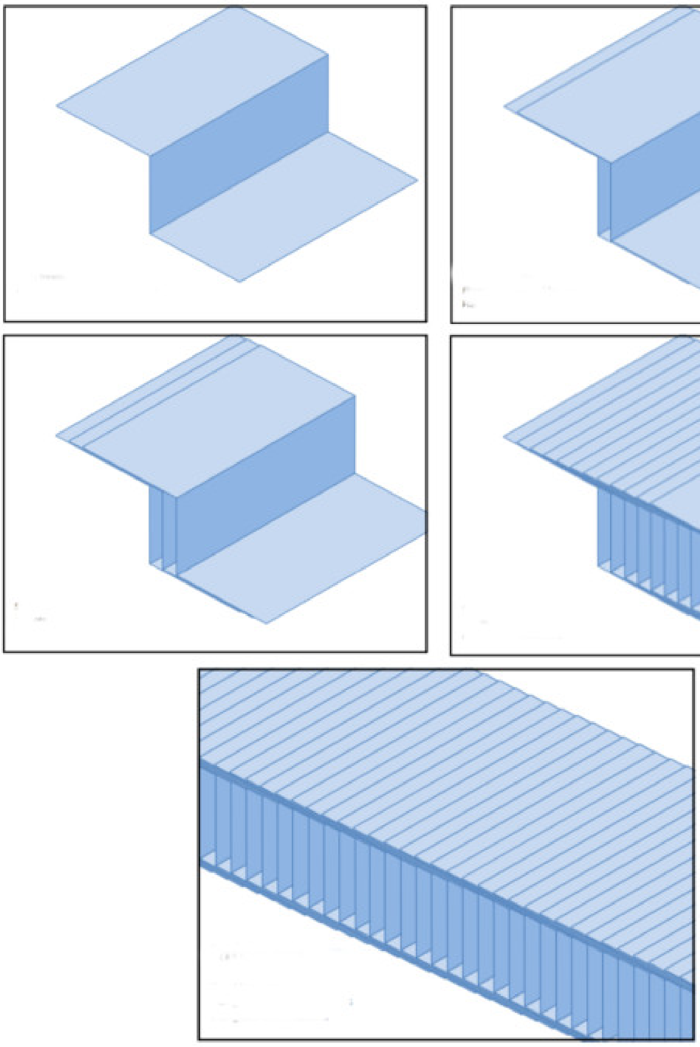

Figure H.3: Build-up of a Infracore Inside panel[41]

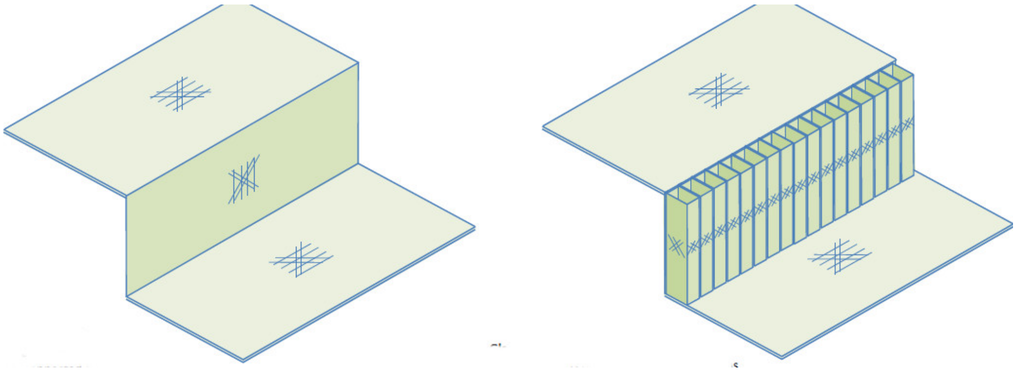

Figure H.4: Fibre orientation in a InfraCore Inside panel. **Left:** Main Z-shaped laminates. **Right:** With inclusion of perpendicular internal webs.[41]

I

Analytical Results - Diagrams

In this appendix a series of images are given which are referenced to in Chapter 3. The main report gives a brief description of what can be seen, but for all completeness further discussion will be done here.

The images are separated into three sections with regard to which of the analytical calculation methods they focus on. Appendix I.1 will cover images for the static analysis, Appendix I.2 will cover which treat the dynamic analysis and Appendix I.3 will include the images of the numerical approach.

I.1. Static Analysis

This section will discuss the images which belong to Chapter 3.4.1, the static approach to the analytical analysis.

The first two figures, Figure I.1 and I.2, show the displacements of the gate and the energy absorbed by the gate respectively as a function of the mass of the colliding vessel. Each of these figures shows three lines which represent models of how the ships stiffness relates to the increase in mass. These scenario's are explained below:

- **Constant k-ship** represents the scenario in which the stiffness of the vessel has no correlation to the mass of the vessel. This would be valid if the ship bow doesn't change as the mass increases, which would be the case if the same vessel is loaded with more or less cargo or the vessel becomes longer the accommodate the extra mass. Double barges are a good example of this.
- **Linear k-ship** represents the case in which a twice as heavy ship is also twice as stiff. This would be the case if a vessel was made wider and higher in order to accommodate the extra mass. Note that the vessel remains the same length as the length of the ship is negligible for it's bow stiffness.
- **Exponential k-ship** represents the situation in which the final constraint from the previous set of assumption is released. The vessel now becomes wider, higher and longer to carry more mass. As two of these three dimensions affect the stiffness of the bow a exponent of $\frac{2}{3}$ is applied to the mass increase.

Which of these lines is the most realistic depends on the situation which is being examined. If the ship class remains the same, but the mass varies due to cargo conditions then the constant k-ship line is the best match. If however data from a smaller vessel is being converted to the situation in which a smaller or larger ship is causing the collision the exponential k-ship line is a better fit.

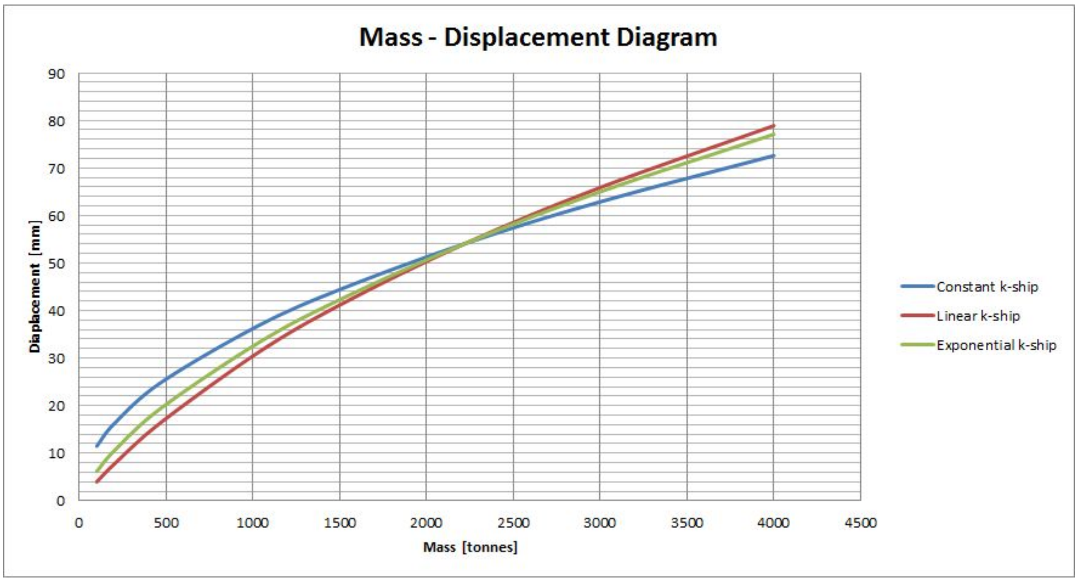

Figure I.1: Displacement of the gate as a function of the mass of the vessel. Including varying assumptions of the ships stiffness

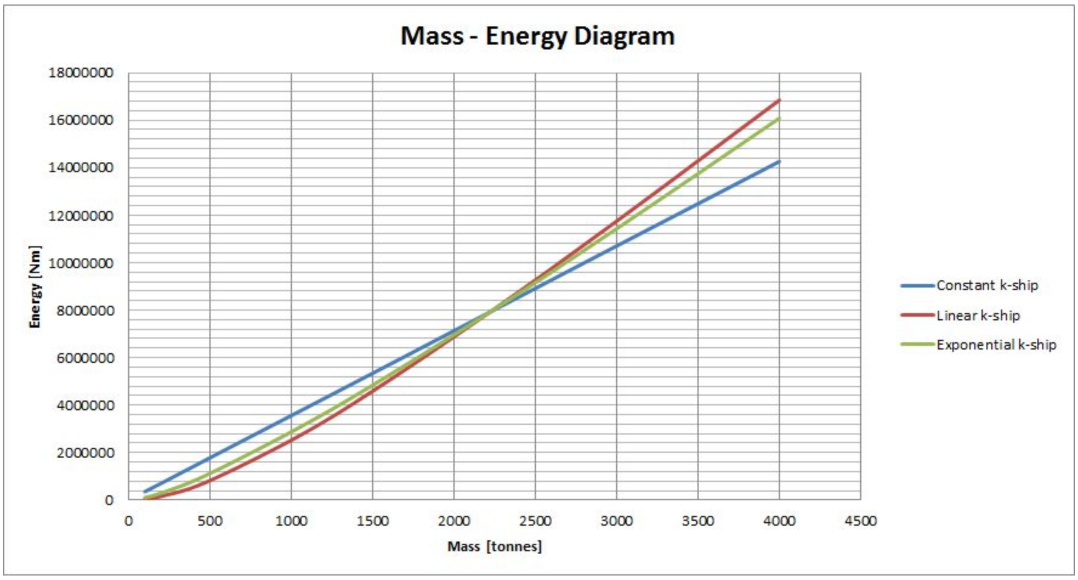

Figure I.2: Energy absorbed by the gate as a function of the mass of the vessel. Including varying assumptions of the ships stiffness

From the equations

$$Collision\ Energy\ =\ \frac{1}{2}m * v^2 \tag{I.1}$$

and

$$Energy\ absorbed\ by\ gate\ spring\ =\ \frac{1}{2}k * x^2 \tag{I.2}$$

it would be expected that the mass of the vessel has a linear effect on the energy and is related to the displacement of the gate by its square root. This is the situation which in seen for the constant k-ship line. It becomes clear that when it is assumed that the ships stiffness varies along with its mass larger masses have a more detrimental effect. This is expected as the become less stiff with regard to the vessel and will thus absorb more energy. How significant this effect is depends on the difference in mass between that case in question and the case which was used to create the diagram. As can be seen for a mass of 2200 tonnes all line coincide. This is the mass of the Class III ship which was used to gather the data for the diagrams.

Figures I.3 and I.4 show the relationship between the velocity of a colliding vessel and the energy or displacement of the gate respectively. The velocity/energy relationship is based off Equation I.1 and Figure I.3 shows the expected quadratic line.

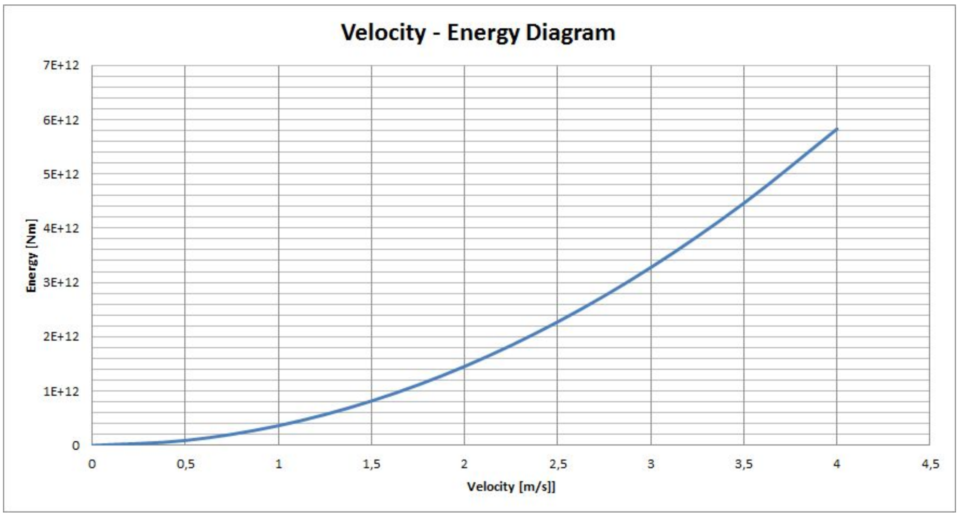

Figure I.3: Relationship between the velocity of ta vessel and its energy

From this Equation I.2 is used which shows that the displacement of the gate in proportional to the square root of the energy of the vessel. This gives a linear relationship between vessel velocity and gate displacement which is shown in Figure I.4.

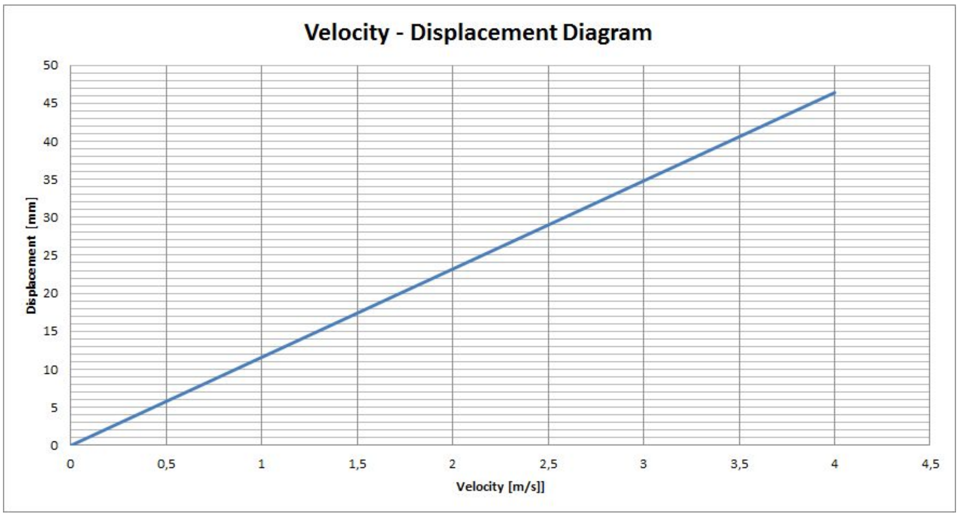

Figure I.4: Relationship between the velocity of the colliding vessel and the displacement of the gate

I.2. Differential Equation

The images which support the results of the analysis executed by differential equation from Chapter 3.4.2. Three main aspects are taken under consideration which will be discussed in the following sections. These are the effects of the level of damping of the system, the effect of the engine force on the system and the effects of the stiffness of the vessel.

I.2.1. Level of Damping

Here four images are presented to illustrate the effects of the degree of damping assumed for the system. In Figure I.5 the energy absorbed by the gate is displaced for varying xi values. This energy is calculated form the maximum displacements of the gate using Equation I.2. The value for xi=0 is the total amount of energy applied to the system. All energy which is not absorbed by the gate is dissipated through a multitude of damping processes which are discussed in Chapter 3.1.6. The amount of dissipated energy is then shown in Figure I.6 as a percentage of the total energy in the system. It become clear that the chosen damping factor has a huge effect on how much energy must be absorbed by the gate structure. To show the effect this has on the displaced state Figure I.7 shows the maximum displacement of the gate as a function of the same xi.

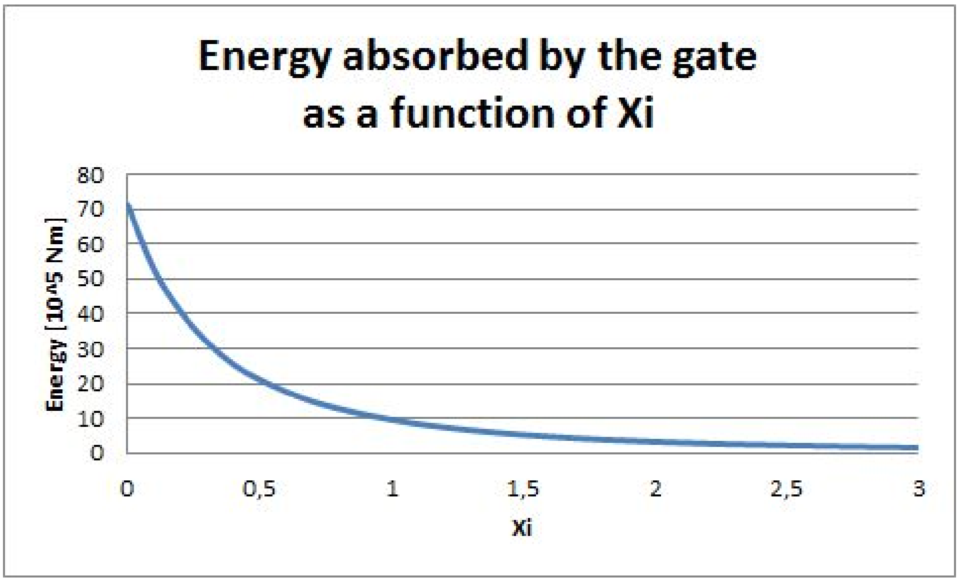

Figure I.5: Energy absorbed by the gate as a function of the assumed damping factor

If a damping factor of lower than 1 is chosen for a simple mass spring system the mass will pass through its equilibrium position and after a time it will have a negative displacement. The mass will then fluctuate a few times before coming to rest at its equilibrium. For the case here the vessel is not attached to the gate and once it has a negative velocity it will move backwards and the gate will vibrate alone. This sudden decrease in vibrating mass has an effect on the vibration behaviour as is shown in Figure I.8. The yellow line shows the situation in which the vessel and gate remain together, while the red and blue line shown the locations of the ship and gate respectively if separation is taken into account. It can be seen the the gate vibration takes place at a higher frequency and with a lower amplitude than without separation. This is caused by the decreased mass.

I.2.2. Engine Force

In this section images are shown in which the analysis by differential equation is executed with and without the application of an engine load which coincides with full throttle. The responses for a Class

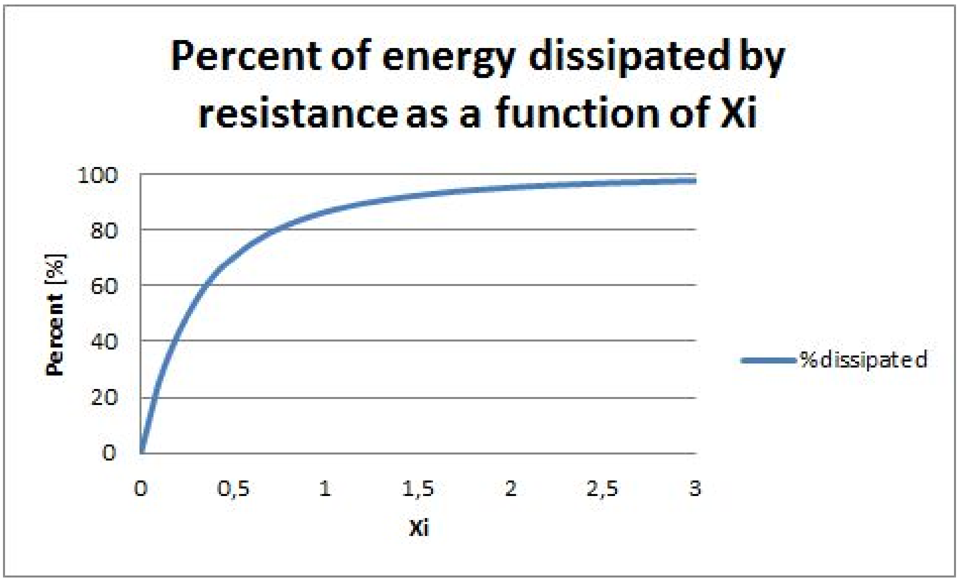

Figure I.6: Percentage of the total energy which is dissipated by damping mechanisms as a function of the assumed damping factor

I-IV vessel are shown in Figures I.9-I.12. The graphs show that the application of such a load has very little effect on the global displacements of the spring system.

I.2.3. Ship Stiffness

Similarly to the previous section the effects of including the elastic deformations of the vessel are included in the study. The images which coincide with this are given in this section. Figures I.13-I.16 shows the gate displacements for collisions with flexible and regid vessels of Class I-IV.

I.3. Numerical Analysis

The final section in this appendix is dedicated to the images which go with a numerical calculation from Chapter 3.4.3. The images here serve to make a comparison between the two calculation methods applied, namely the energy and force approaches. Figures I.17-I.20 show the displacements of the gate calculated with the two aforementioned methods for collisions with Class I-IV vessels. They show that the difference in results is minimal, thus the method which more easily output the physical quantity which is of interest may be used.

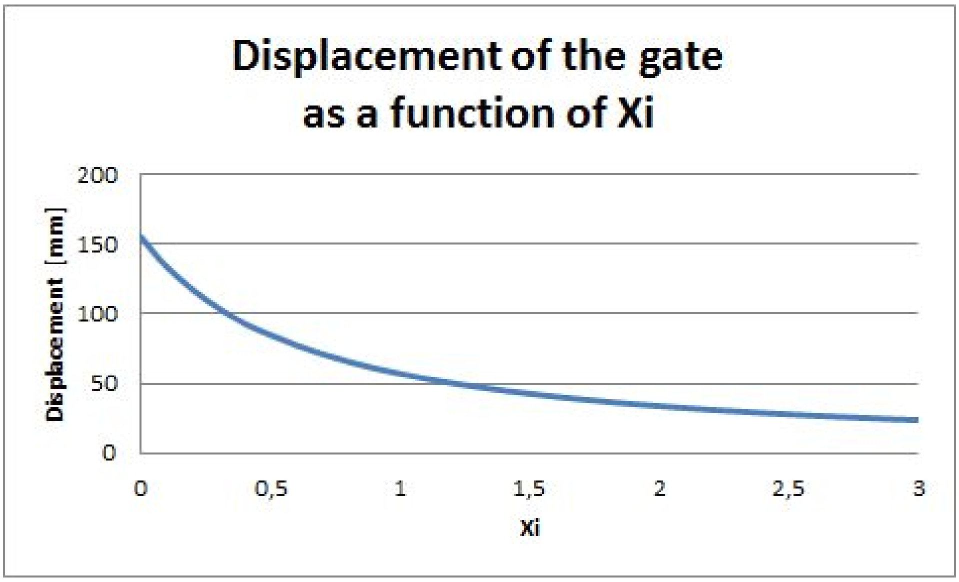

Figure I.7: Maximum displacement of the gate structure during collision as a function of the assumed damping factor

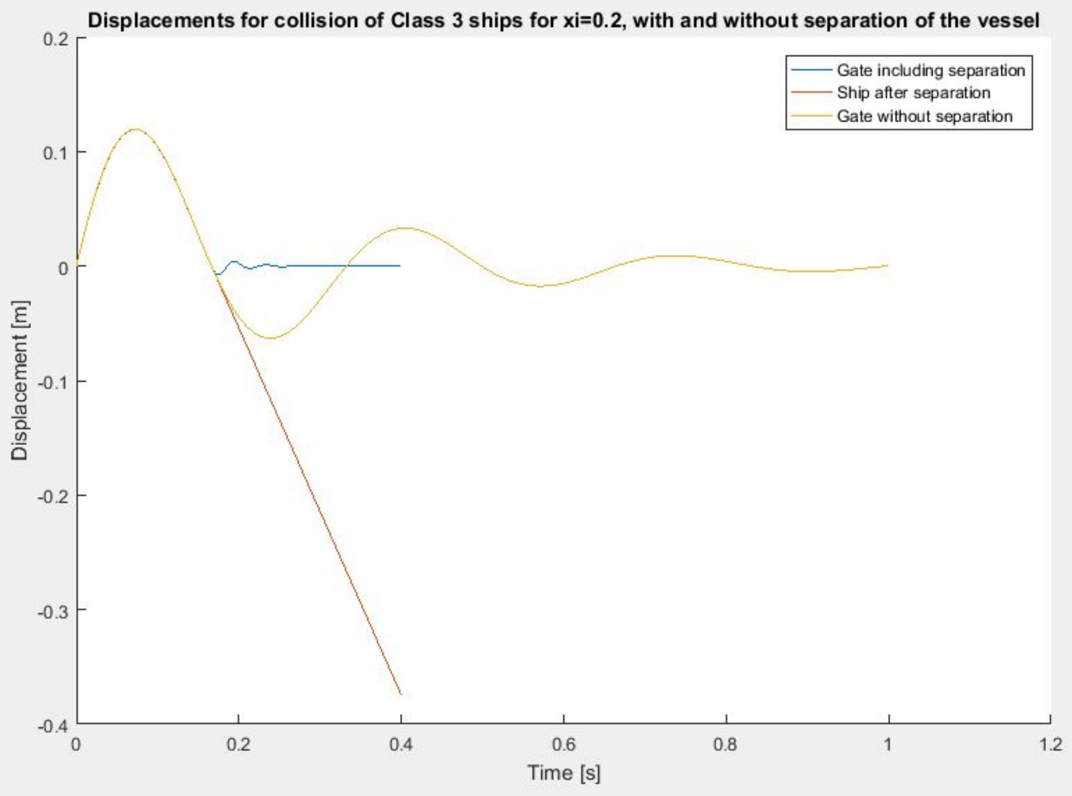

Figure I.8: Comparison of the behaviour of the ship and gate for the case with and without ship-gate separation

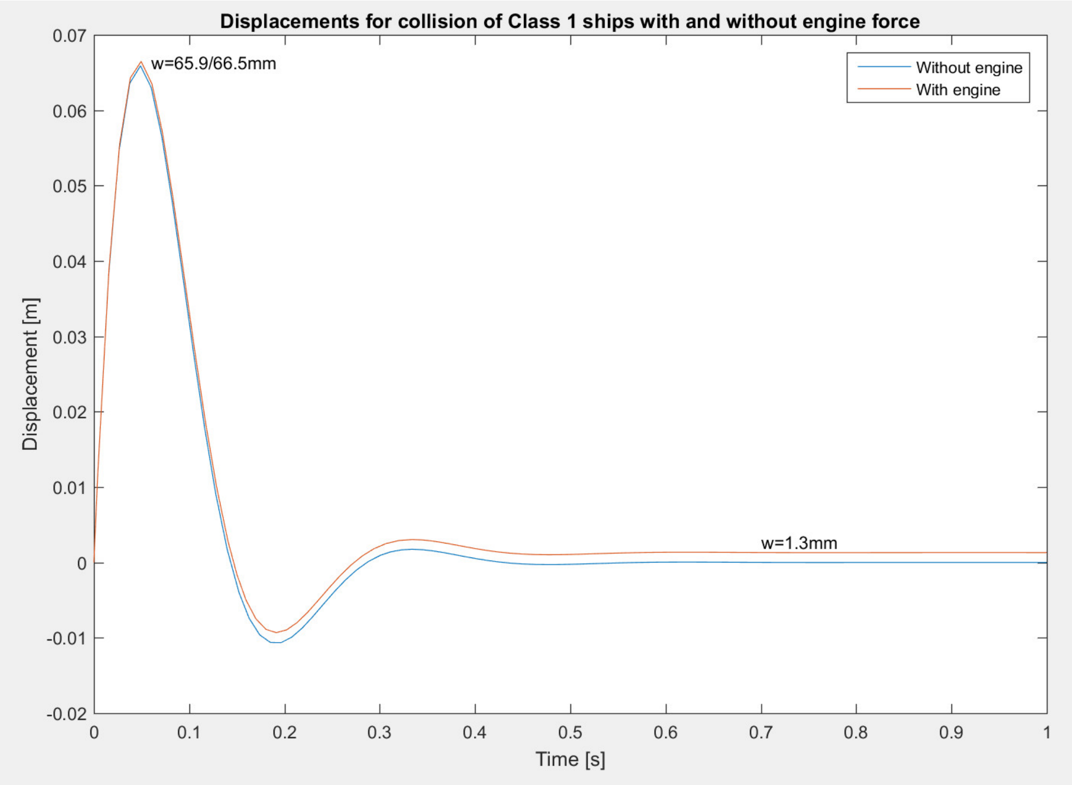

Figure I.9: Displacement of the gate with and without the application of an engine load for a Class I vessel

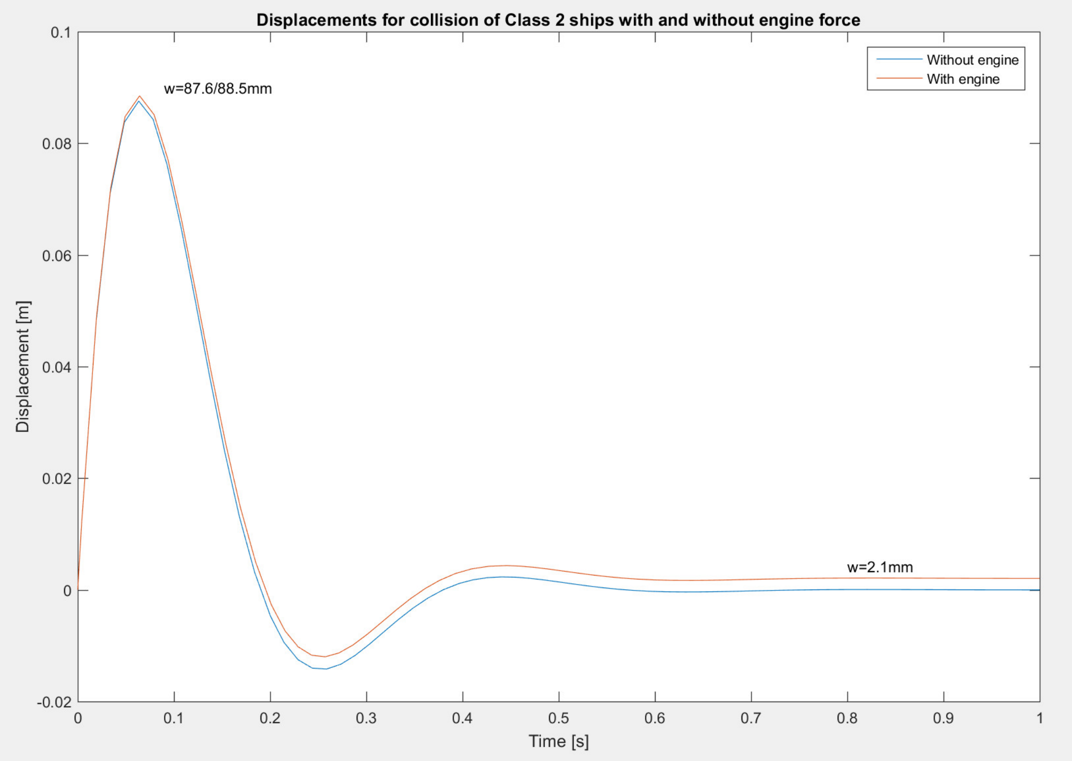

Figure I.10: Displacement of the gate with and without the application of an engine load for a Class II vessel

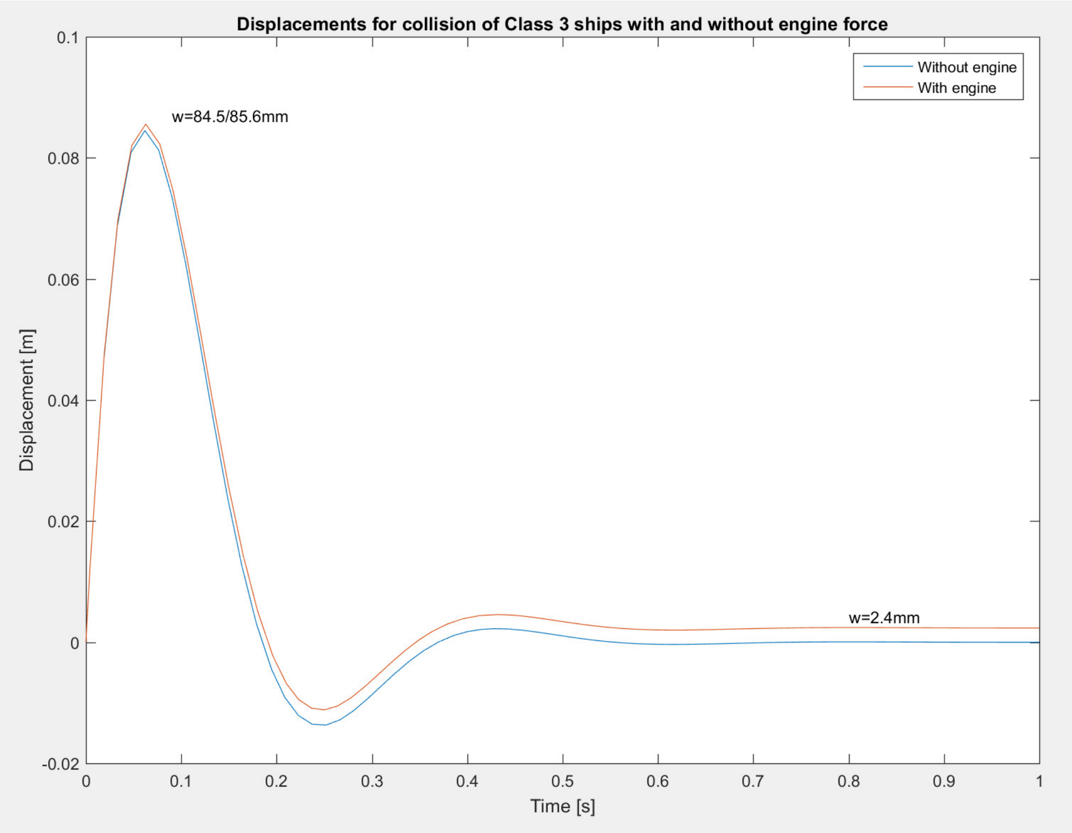

Figure I.11: Displacement of the gate with and without the application of an engine load for a Class III vessel

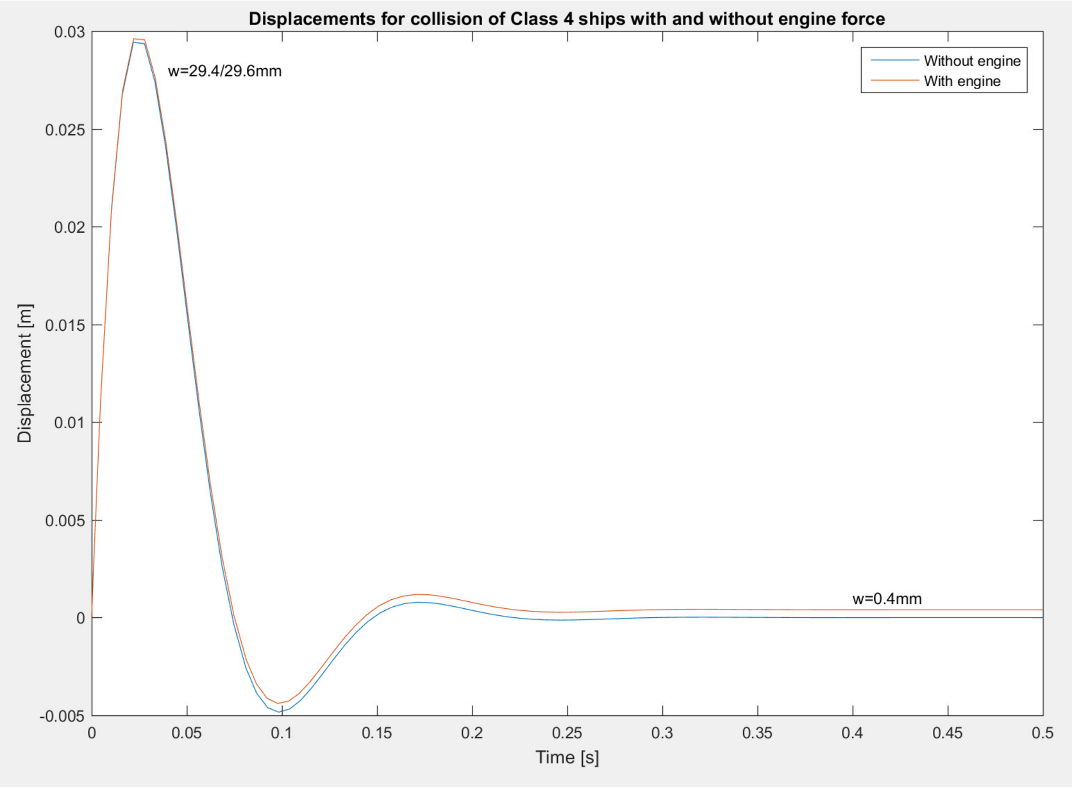

Figure I.12: Displacement of the gate with and without the application of an engine load for a Class IV vessel

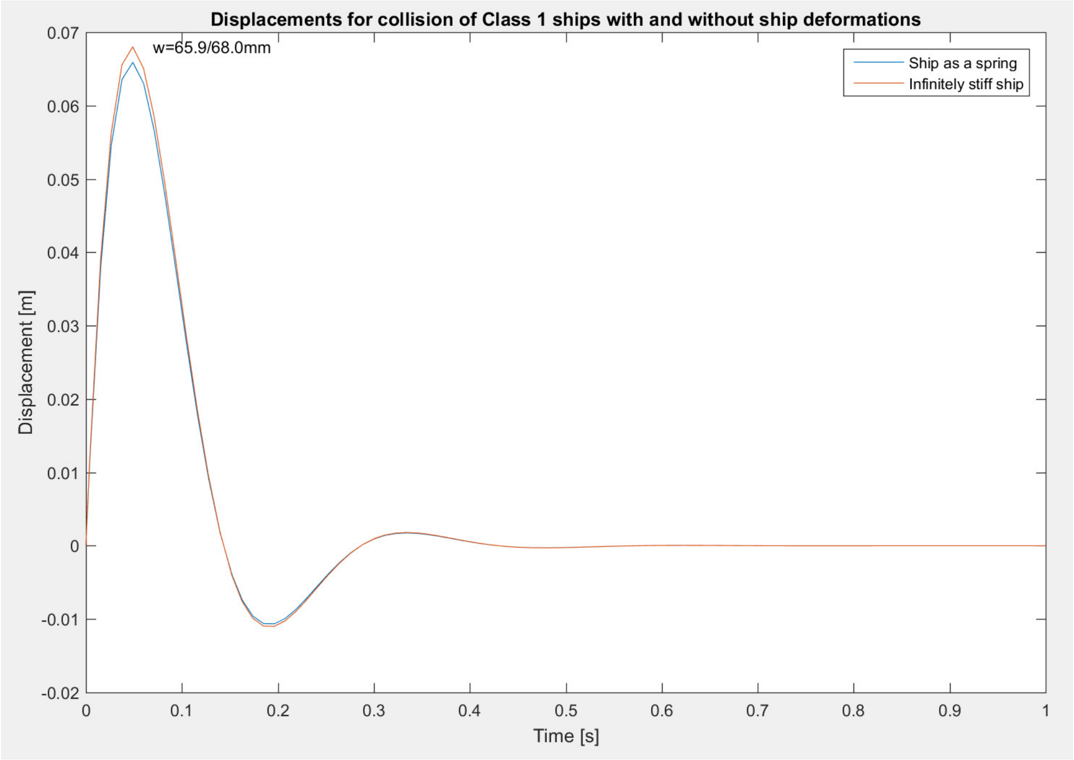

Figure I.13: Displacements of the gate due to a collision with a flexible and rigid vessel of Class I

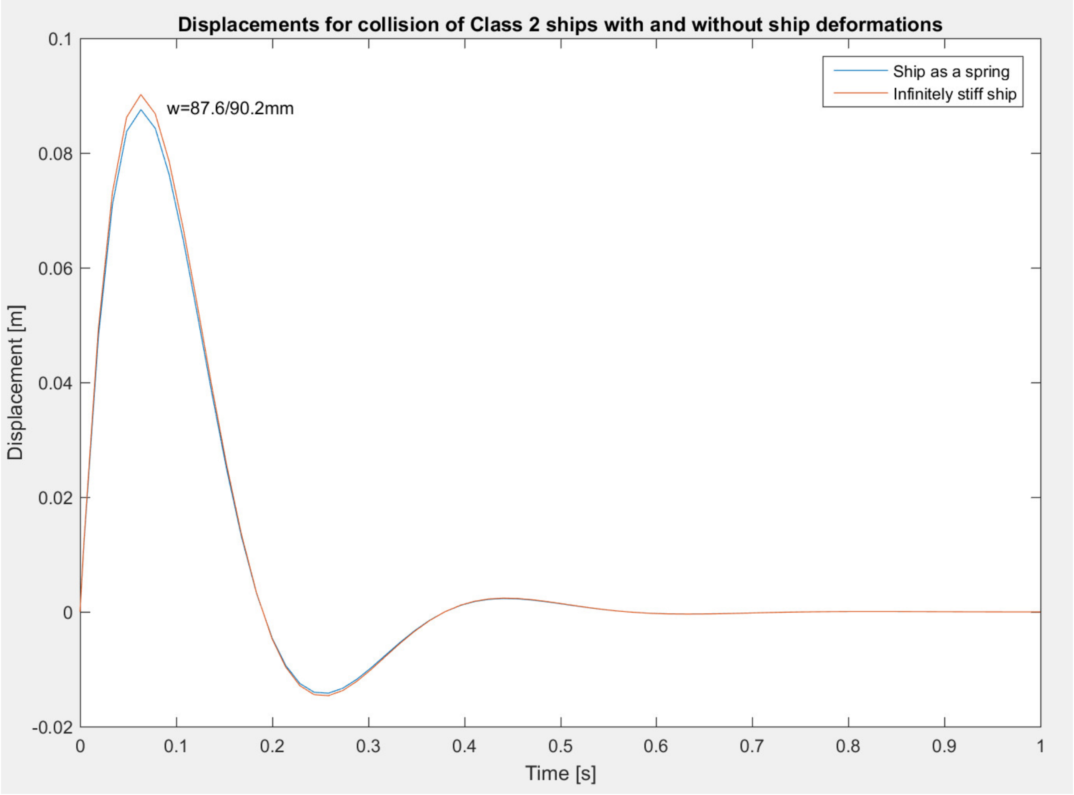

Figure I.14: Displacements of the gate due to a collision with a flexible and rigid vessel of Class II

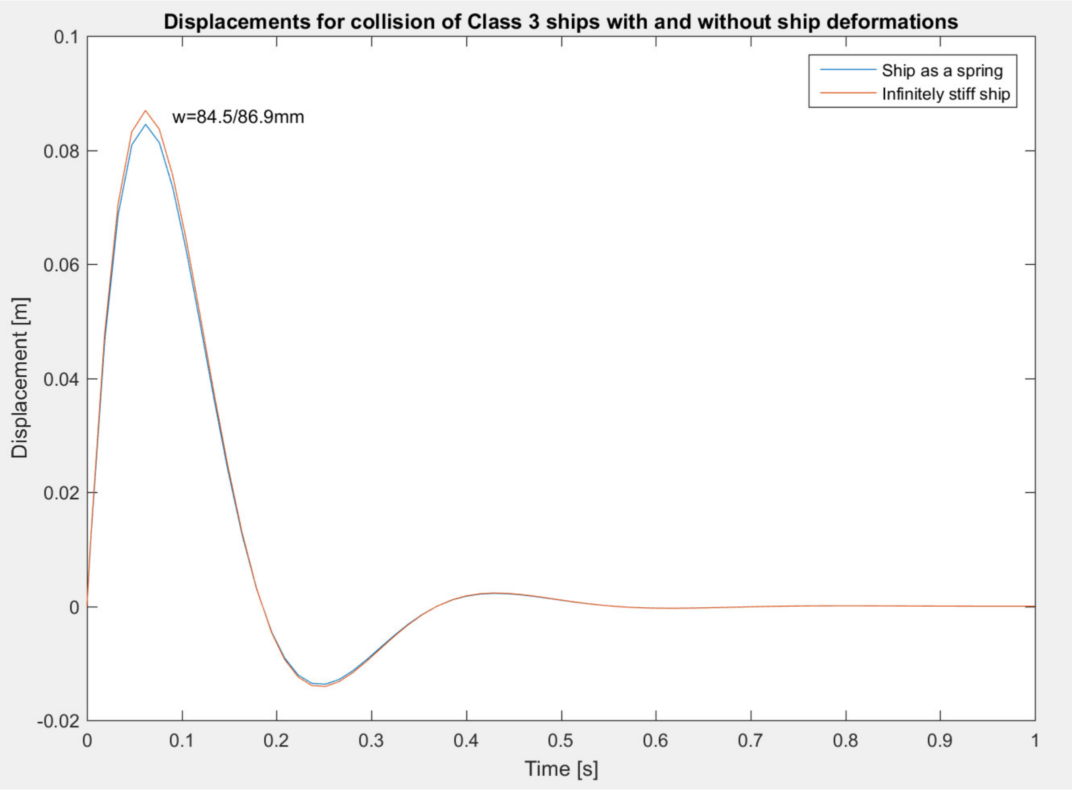

Figure I.15: Displacements of the gate due to a collision with a flexible and rigid vessel of Class III

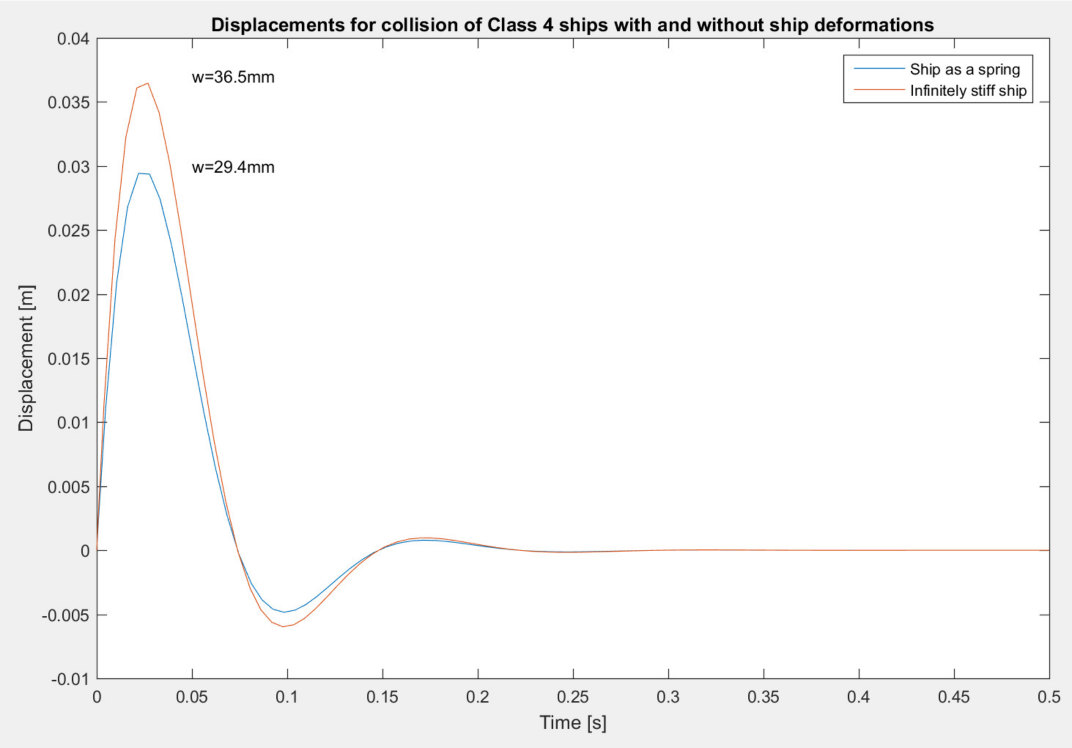

Figure I.16: Displacements of the gate due to a collision with a flexible and rigid vessel of Class IV

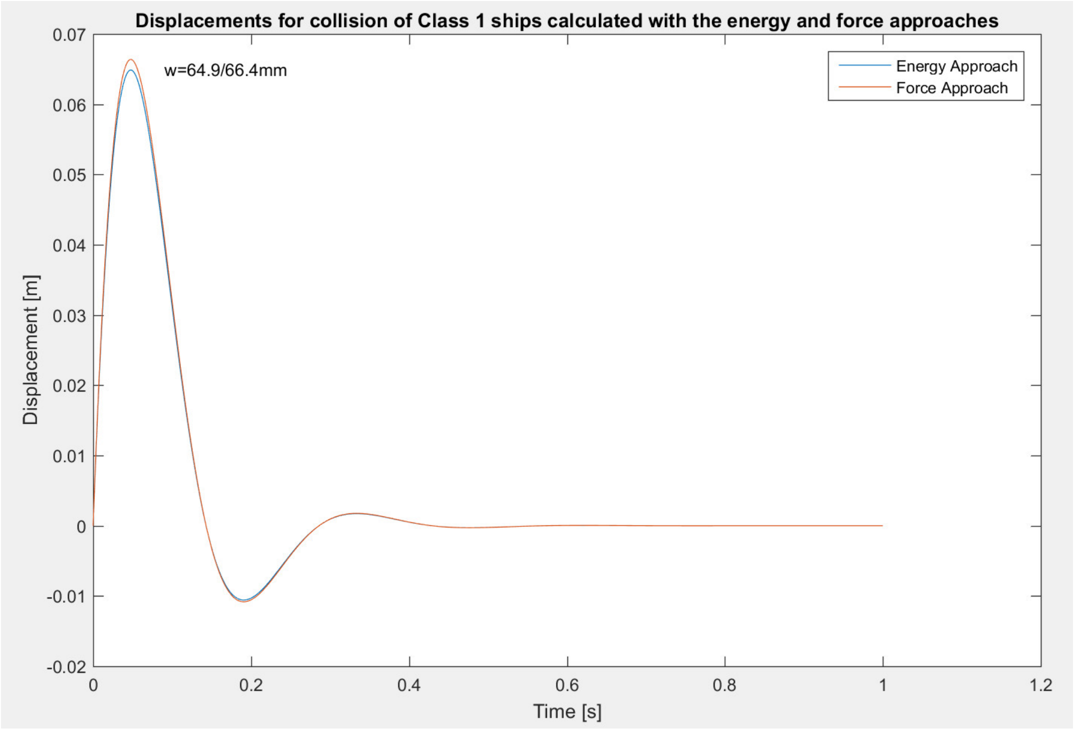

Figure I.17: Comparison of the displacements of the gate due to a collision with a Class I ship, as calculated with the energy and force approaches

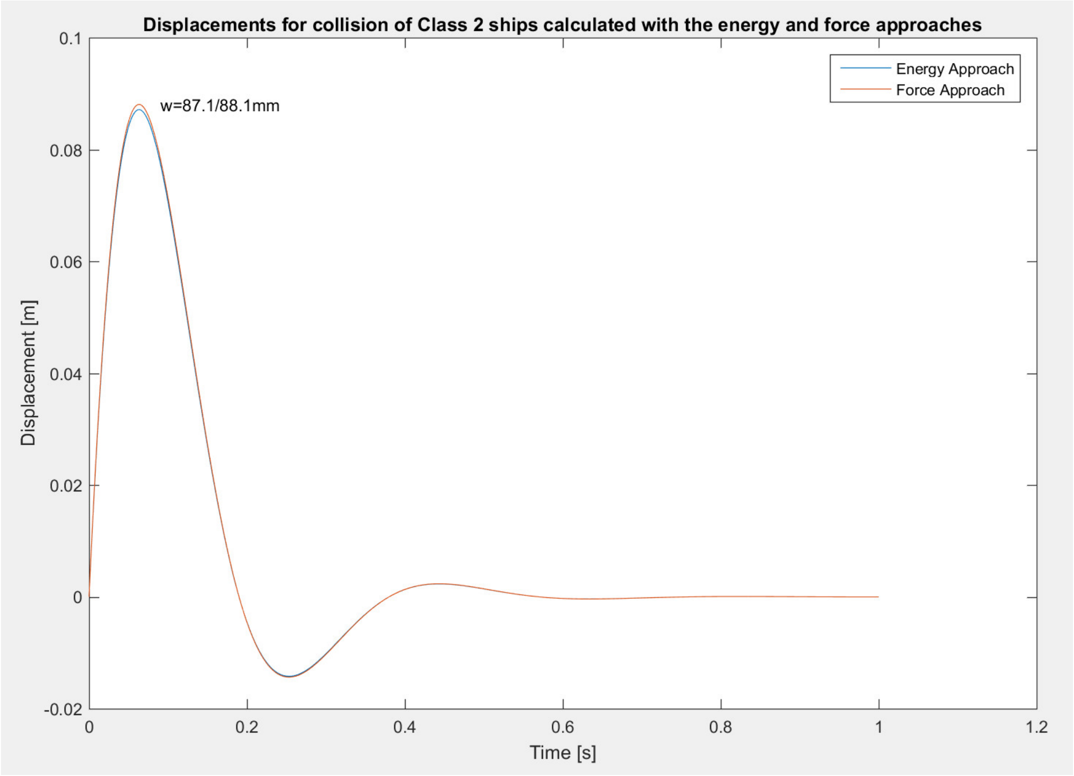

Figure I.18: Comparison of the displacements of the gate due to a collision with a Class II ship, as calculated with the energy and force approaches

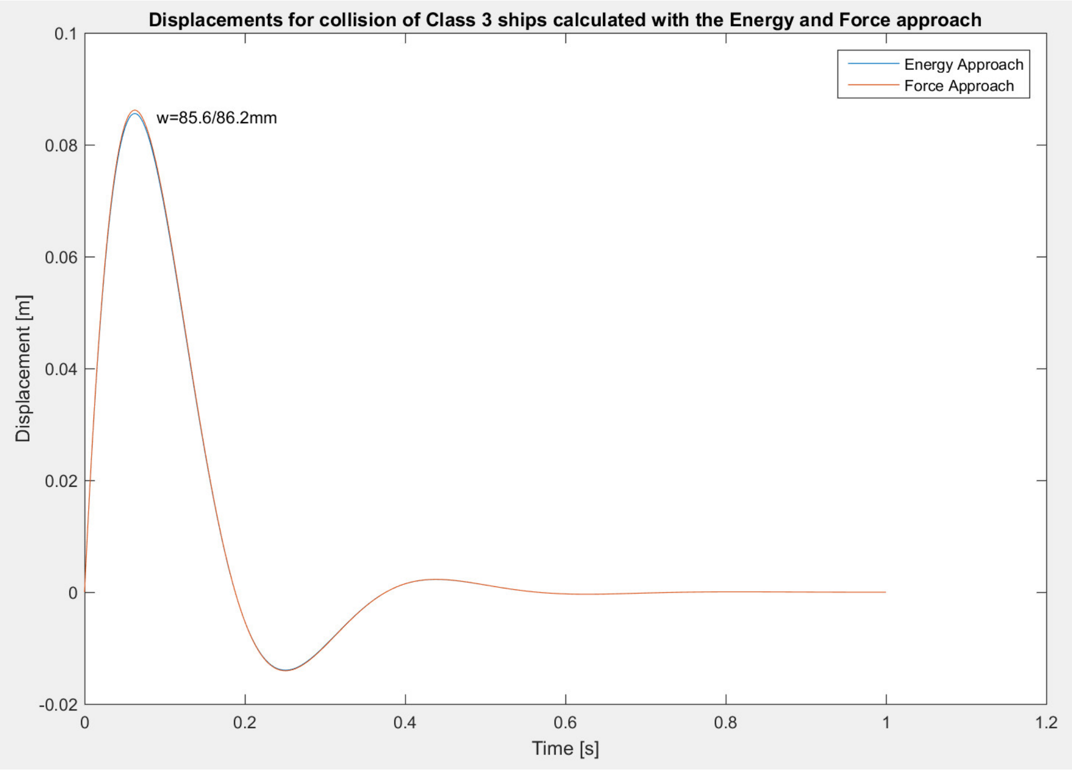

Figure I.19: Comparison of the displacements of the gate due to a collision with a Class III ship, as calculated with the energy and force approaches

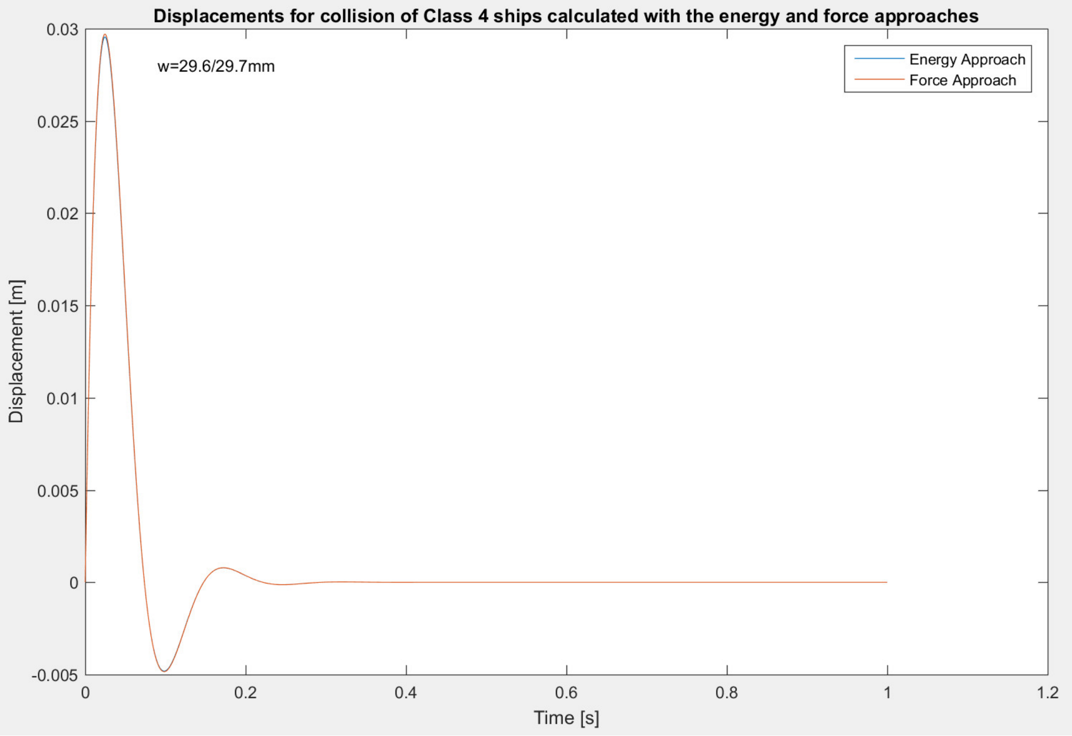

Figure I.20: Comparison of the displacements of the gate due to a collision with a Class IV ship, as calculated with the energy and force approaches

J

Numerical Model Images

Is this appendix a series of images are bundled which relate to Chapters 4 and 5, but would take up too much space in the main report. Reference is made to them from the main report where they are discussed, but for completeness a brief description is given here as well.

J.1. Images for the Global Analysis

In the following subsections the images which coincide with Chapter 4 will be shown. Separation will be made with regard to which section they are referenced from.

J.1.1. Static geometry

The following three images show the element geometry used for the static analysis of the global system from Chapter 4.2.1. Figure J.1 shows the lay-out of the modelled areas. These areas have yet to be meshed into elements. The situation after meshing is shown in Figures J.2 and J.3 which show the external and the internal geometry respectively. For the internal geometry the front skin is removed to make the flanges visible.

J.1.2. Dynamic Geometry

Figures J.4 and J.5 show the mesh lay-out of the model used for the dynamic analysis of the global system from Chapter 4.2.2. It is in many ways similar to the static calculation, but with a finer mesh of 100mm cubes and the addition of the rigid ship bow which will serve as load condition. Due to the nature of the LS-Dyna calculation these smaller elements will have no impact of calculation time.

J.1.3. Static Loads

Figures J.6 and J.7 show the application of the hydrostatic pressures and the upstream and downstream sides of the gate respectively. Due to the large retention height there is a large difference betwee these two loads.

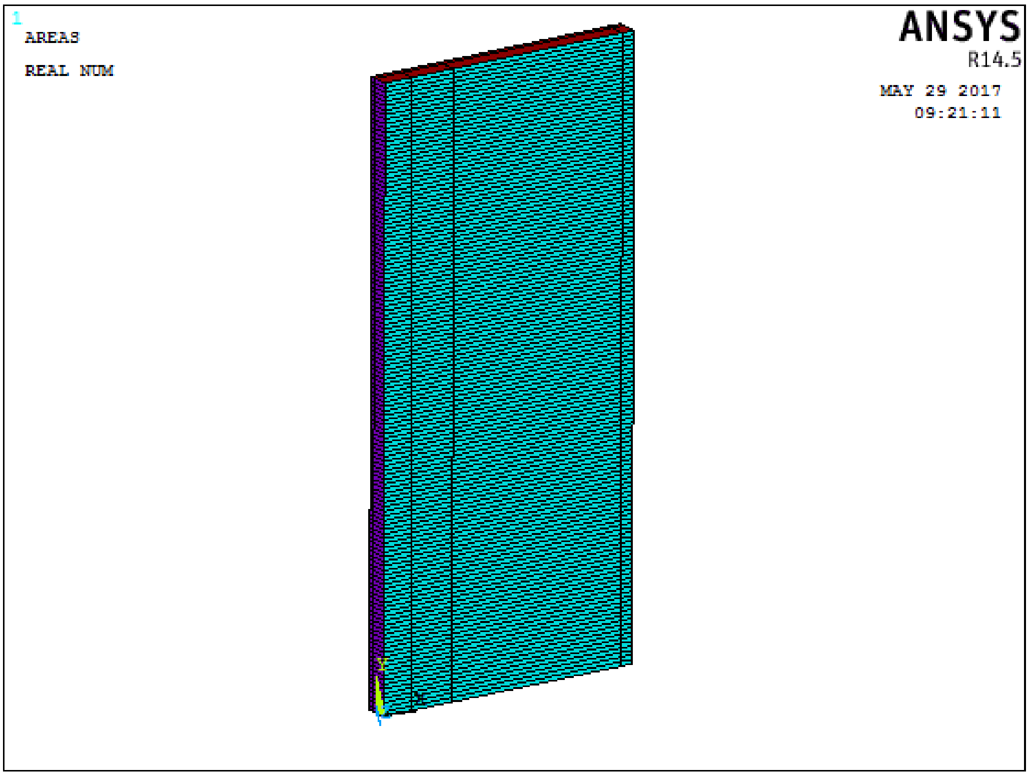
1
AREAS
REAL NUM
ANSYS
R14.5
MAY 29 2017
09:21:11
Y
X

Figure J.1: Geometry of the finite element areas for the static global calculation

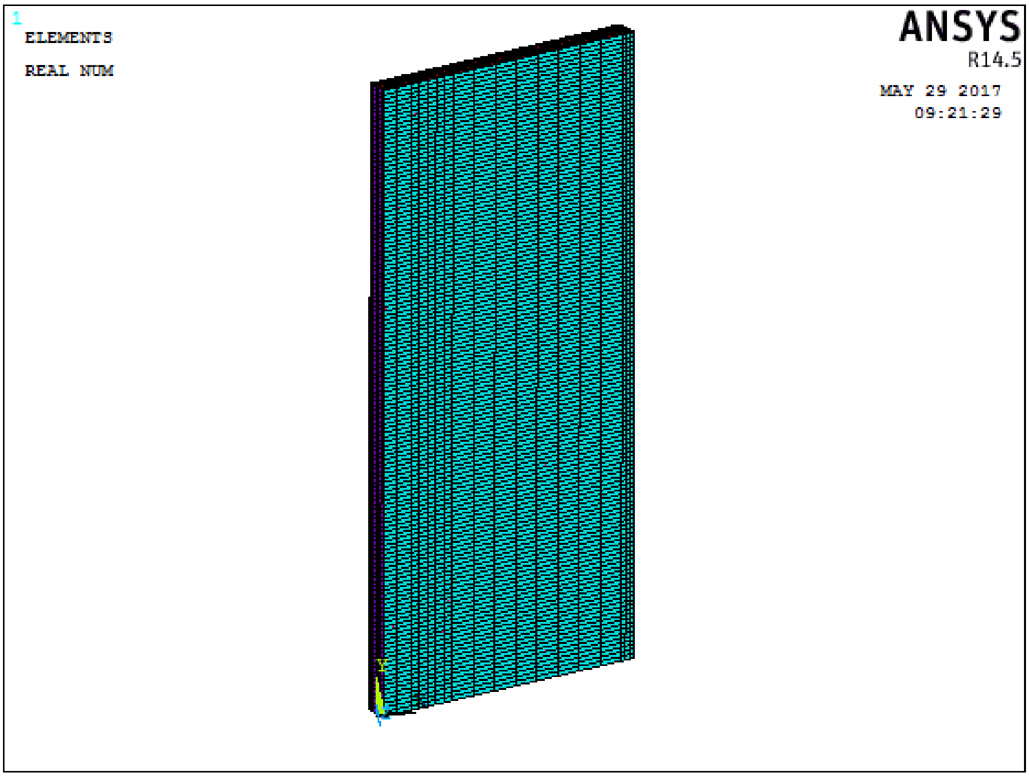
1
ELEMENTS
REAL NUM
ANSYS
R14.5
MAY 29 2017
09:21:29
Y
X

Figure J.2: Geometry of the finite element mesh for the static global calculation

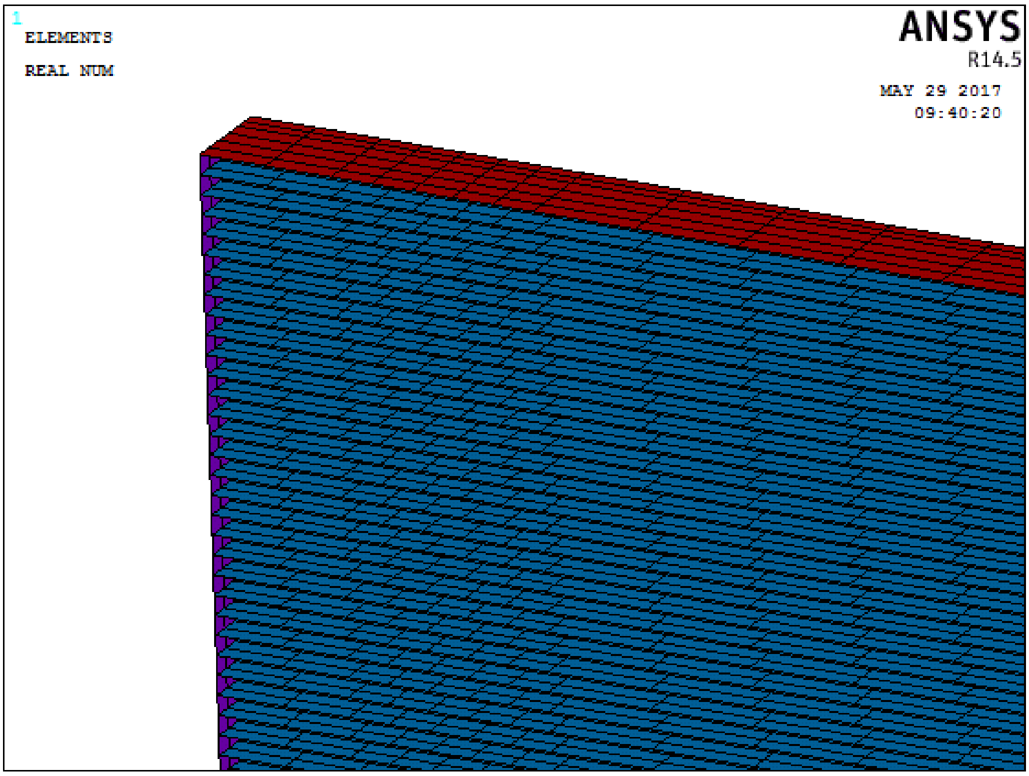
1
ELEMENTS
REAL NUM
ANSYS
R14.5
MAY 29 2017
09:40:20

Figure J.3: Internal geometry of the finite element mesh for the static global calculation in which the flanges are visible

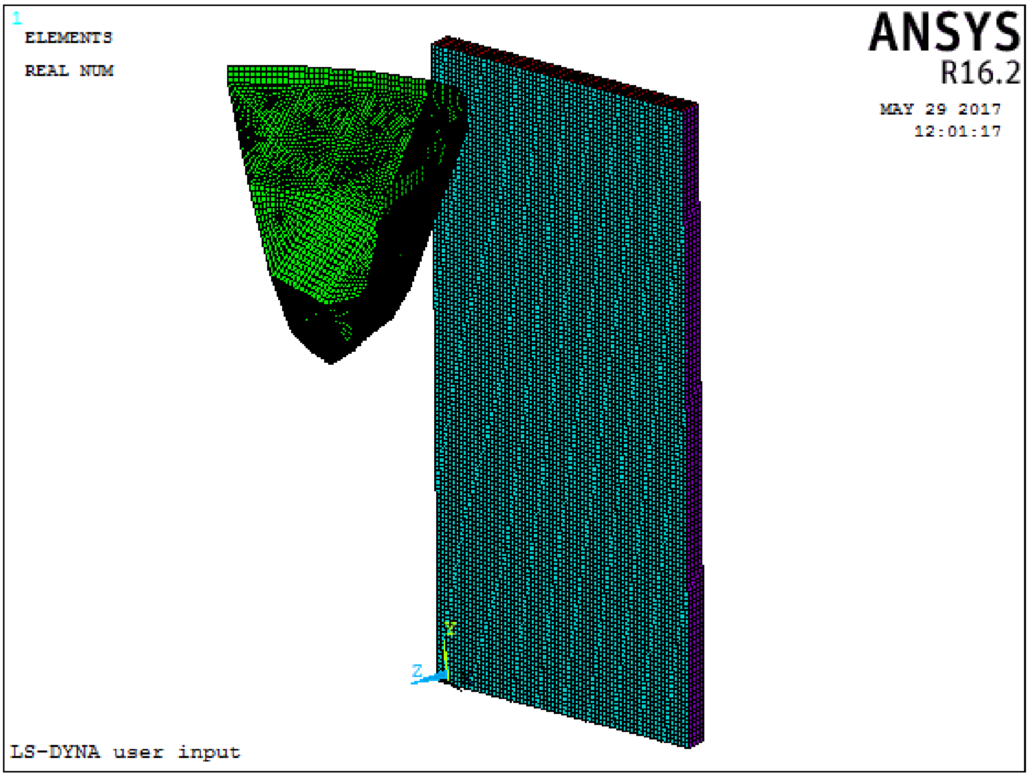
1
ELEMENTS
REAL NUM
ANSYS
R16.2
MAY 29 2017
12:01:17
Y
Z
LS-DYNA user input

Figure J.4: Geometry of the finite element mesh for the dynamic global calculation with a 100 mm square mesh

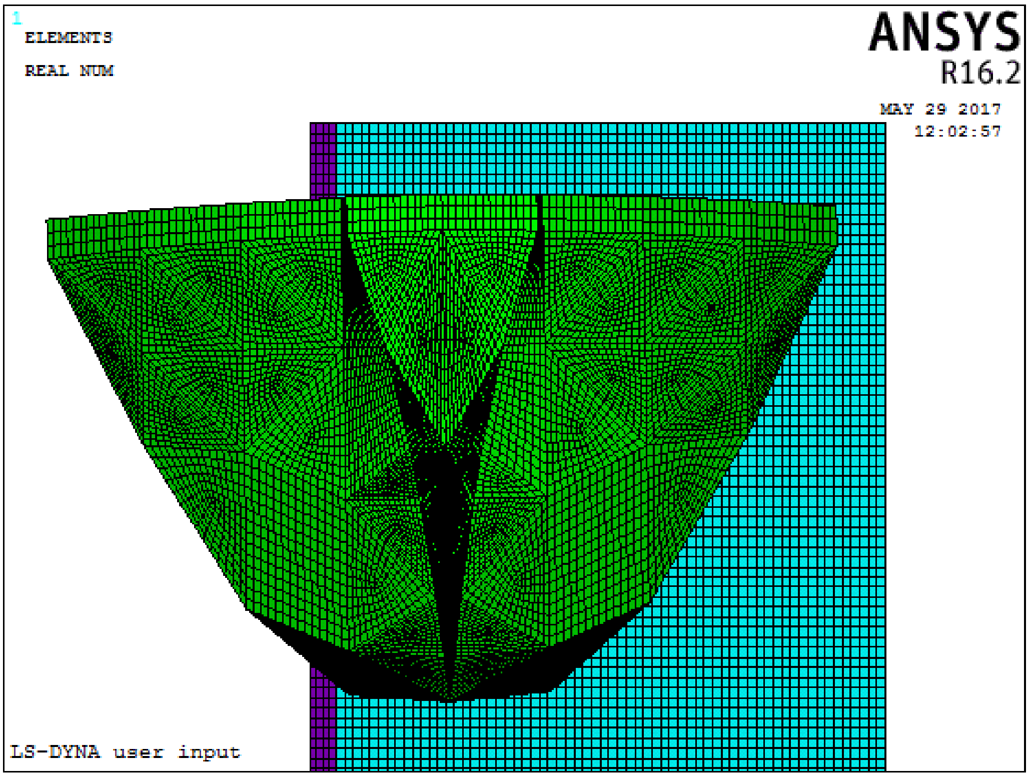
1
ELEMENTS
REAL NUM
ANSYS
R16.2
MAY 29 2017
12:02:57
LS-DYNA user input

Figure J.5: Front view of the geometry of the finite element mesh for the dynamic global calculation with a 100 mm square mesh

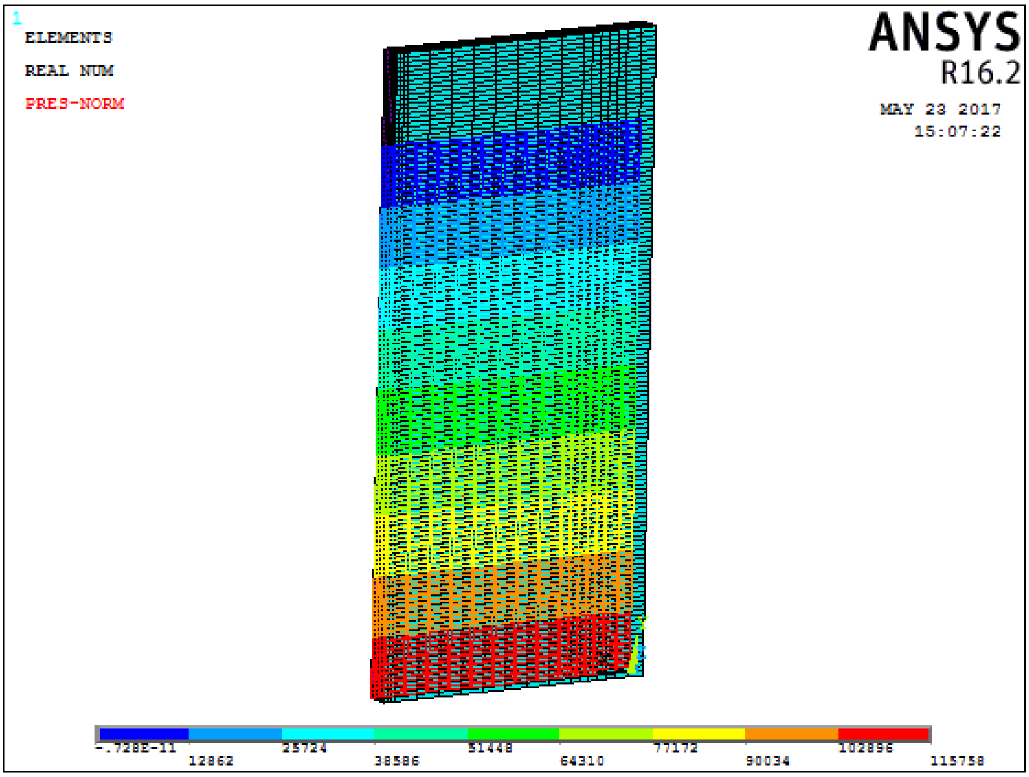

Figure J.6: Water pressures on the upstream side of the gate

J.1.4. Static Results

Most of the results which are of direct interest are shown in the main report in Chapter 4.2.1, however some of the images are not as directly required for the understanding of the report and are thus placed here to keep the document concise. Figure J.8 shows the displacement in x-direction due to the static load conditions. These displacements are caused by the angle between the ship sailing direction and the angle of the gate.

The following set of four figures illustrate the stress distribution in x and z direction for the skins and the internal flanges. They show that the skins carry the gross of the stress in the x-direction and the internal flanges carry the stresses in z-direction. Figure J.9 shows the stresses in x-direction for the skins, Figure J.10 shows the stresses in x-direction for the internal flanges, Figure J.11 shows the stresses in z-direction for the skins and Figure J.12 shows the stresses in z-direction for the internal flanges.

J.1.5. Dynamic Results

The results for the global analysis subjected to dynamic LS-Dyna loads are supplemented with the images from the sections below. The cases with and without core elements will be discussed separately.

Model without core elements

When the analysis is run without foam between the laminates a very distinct deformation pattern is observed. For the first 0.175 seconds the gate displaces at the point of impact and displaces in the reserve direction further along the gate axis due to warping of the plane. The deformations a quite large but otherwise the mode is realistic. This point is shown in Figure J.13.

After this point the rear skin buckles under the compressive loads and the gate fails. This point is shown in Figures J.14. The angle in the rear laminate can clearly be seen and the rear skin deforms inwards. At this point the laminate has failed and irreparable damage has occurred in the gate. The visual that it passes through the front skin is only due to visual scaling.

In reality the laminate is supported against buckling by the structural foam inside the gate. Even though it is significantly weaker than the laminates it will still resist being compressed in an enclosed area. This model is thus likely not accurate and the analysis was run again with the core included.

Model with core elements

When the dynamic analysis is run including the core elements the following images supplement the discussed results from Chapter 4.2.2. Results for the displacements in z-direction are shown in the main report. The figures here focus on the displacements in x-direction and the post collision behaviour. In Figures J.15 and J.16 The displacements in x-direction are shown when they reach their maximum at the point of impact and the body of the gate respectively. These maxima do not take place at the same moment as it takes time for the displacement wave to propagate through the structure.

After the collision is over and the ship has come loose from the gate structure once more the gate continues to vibrate in a form that contains multiple modes. Figure J.17 illustrates this vibration as well as trhe fact that the higher order modes damp out sooner.

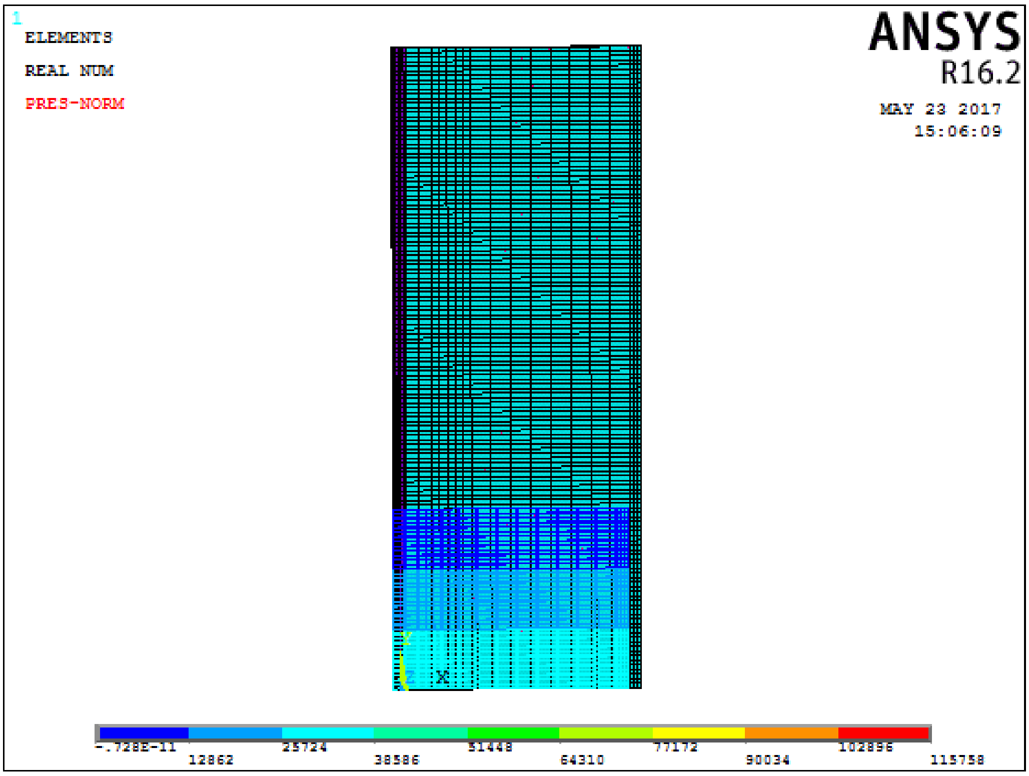
1
ELEMENTS
REAL NUM
PRES-NORM
ANSYS
R16.2
MAY 23 2017
15:06:09
Y
X
-.728E-11
12862
25724
38586
51448
64310
77172
90034
102896
115758

Figure J.7: Water pressures on the downstream side of the gate

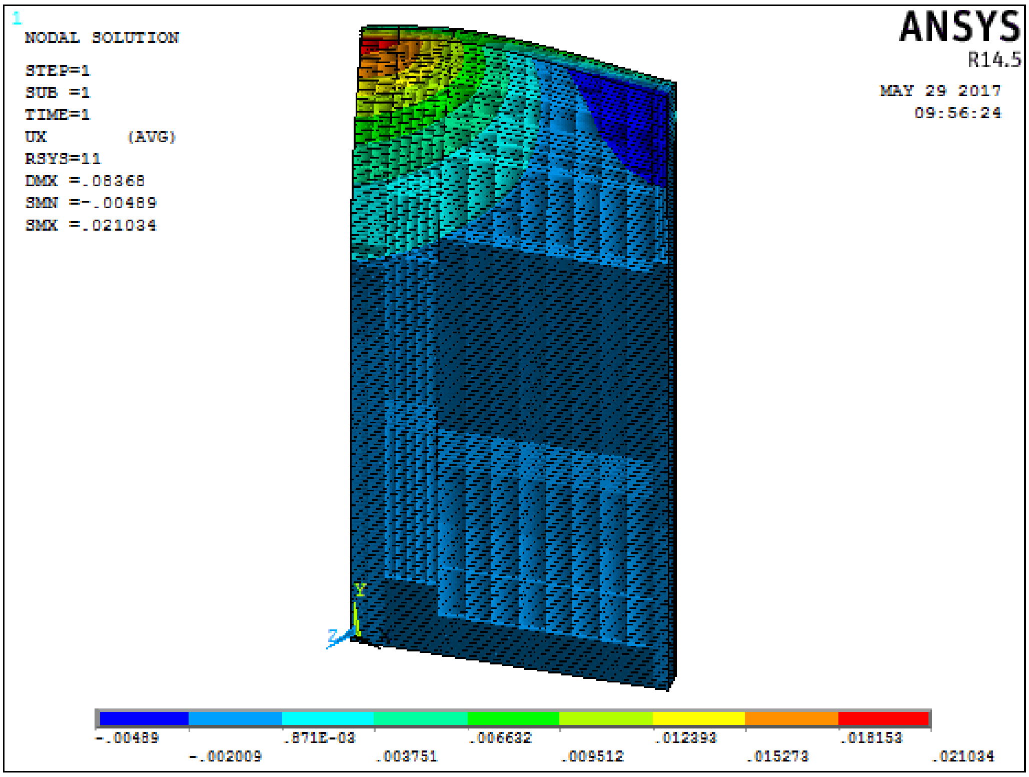
1
NODAL SOLUTION
STEP=1
SUB =1
TIME=1
UX (AVG)
RSYS=11
DMX =.08368
SMN =-.00489
SMX =.021034
ANSYS
R14.5
MAY 29 2017
09:56:24
Y
Z
-.00489
-.002009
.871E-03
.003751
.006632
.009512
.012393
.015273
.018153
.021034

Figure J.8: Displacements in the x-direction (along the gate axis)

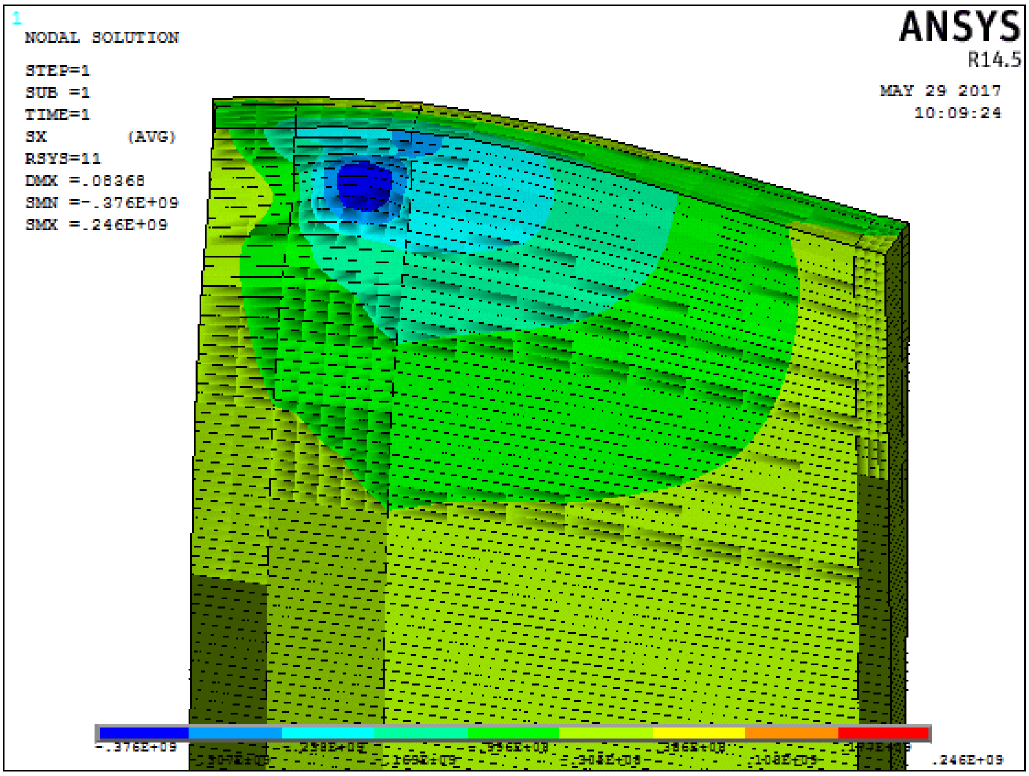

Figure J.9: Stresses in the x-direction as carried by the gate skins

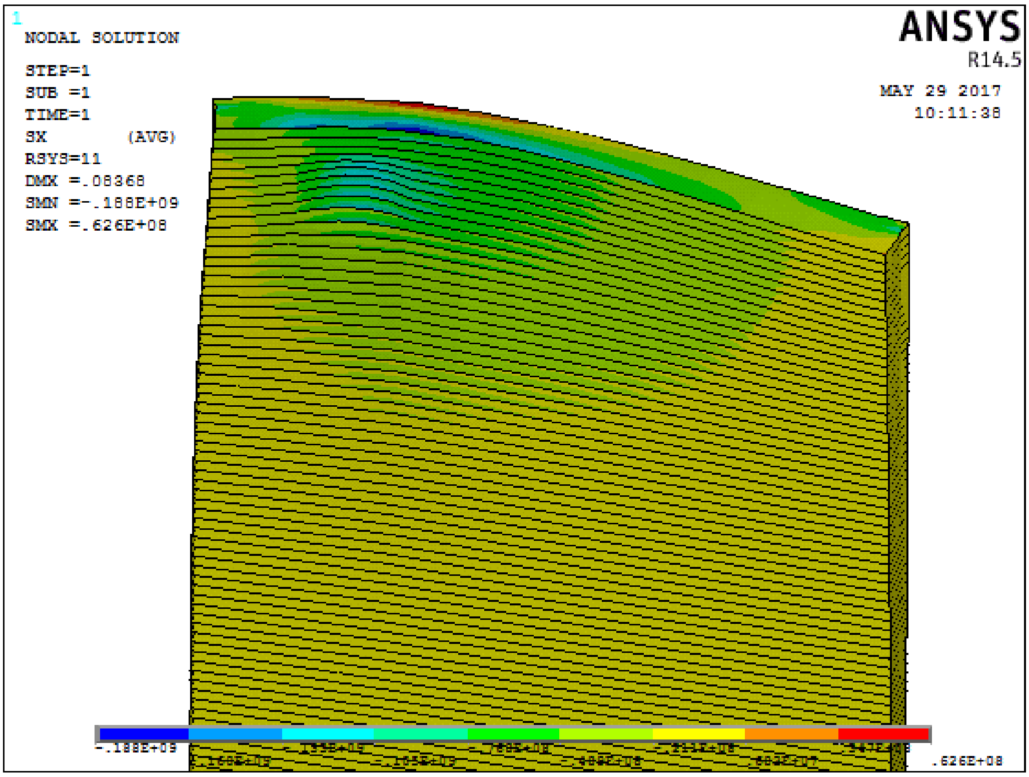

Figure J.10: Stresses in the x-direction as carried by the internal flanges

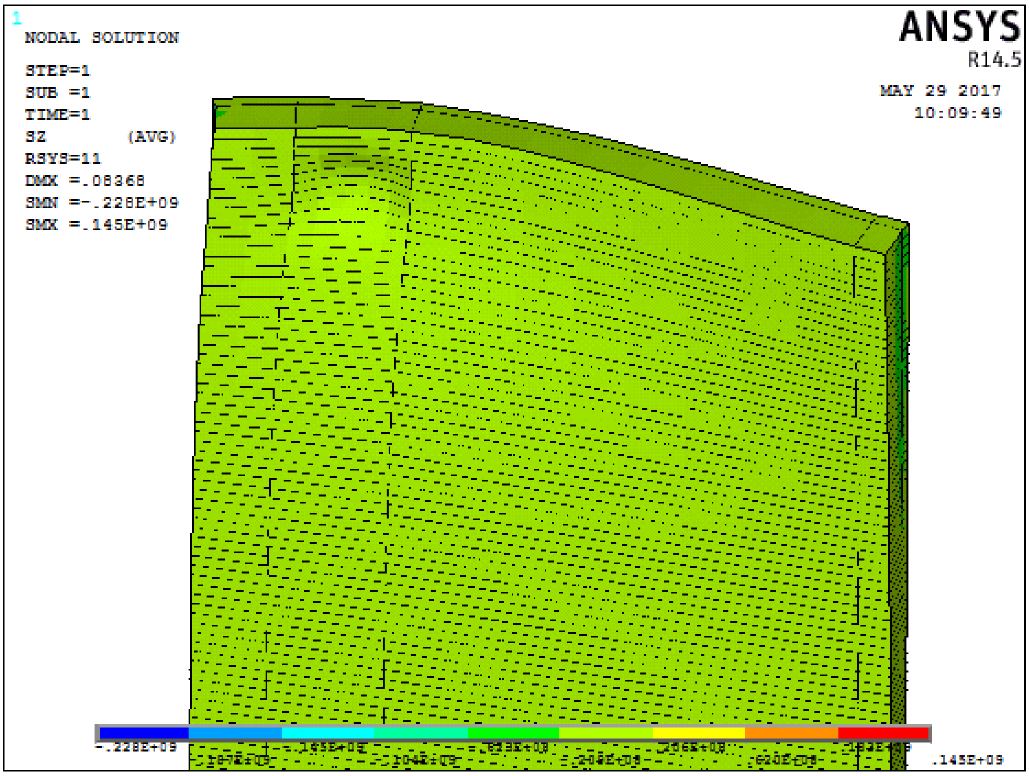
1
NODAL SOLUTION
STEP=1
SUB =1
TIME=1
SZ (AVG)
RSYS=11
DMX =.08368
SMN =-.228E+09
SMX =.145E+09
ANSYS
R14.5
MAY 29 2017
10:09:49
-.228E+09
-.187E+09
-.145E+09
-.104E+09
-.623E+08
-.206E+08
.206E+08
.620E+08
.145E+09

Figure J.11: Stresses in the z-direction as carried by the gate skins

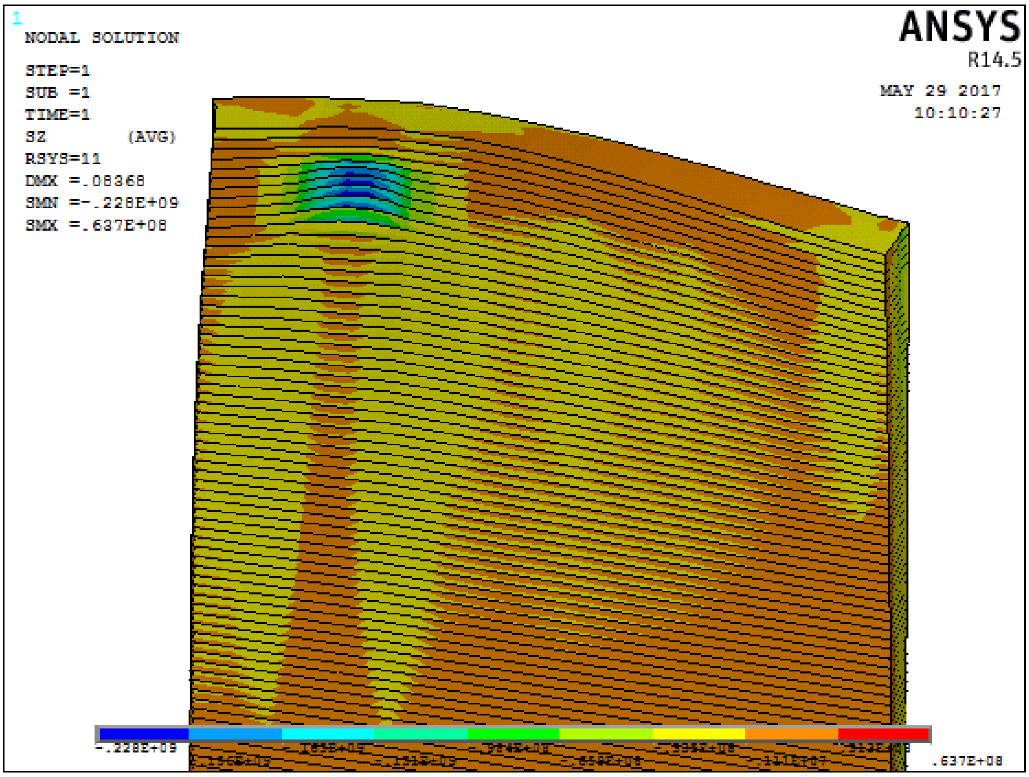
1
NODAL SOLUTION
STEP=1
SUB =1
TIME=1
SZ (AVG)
RSYS=11
DMX =.08368
SMN =-.228E+09
SMX =.637E+08
ANSYS
R14.5
MAY 29 2017
10:10:27
-.228E+09
-.196E+09
-.163E+09
-.131E+09
-.984E+08
-.658E+08
-.333E+08
-.111E+07
.312E+08
.637E+08

Figure J.12: Stresses in the z-direction as carried by the internal flanges

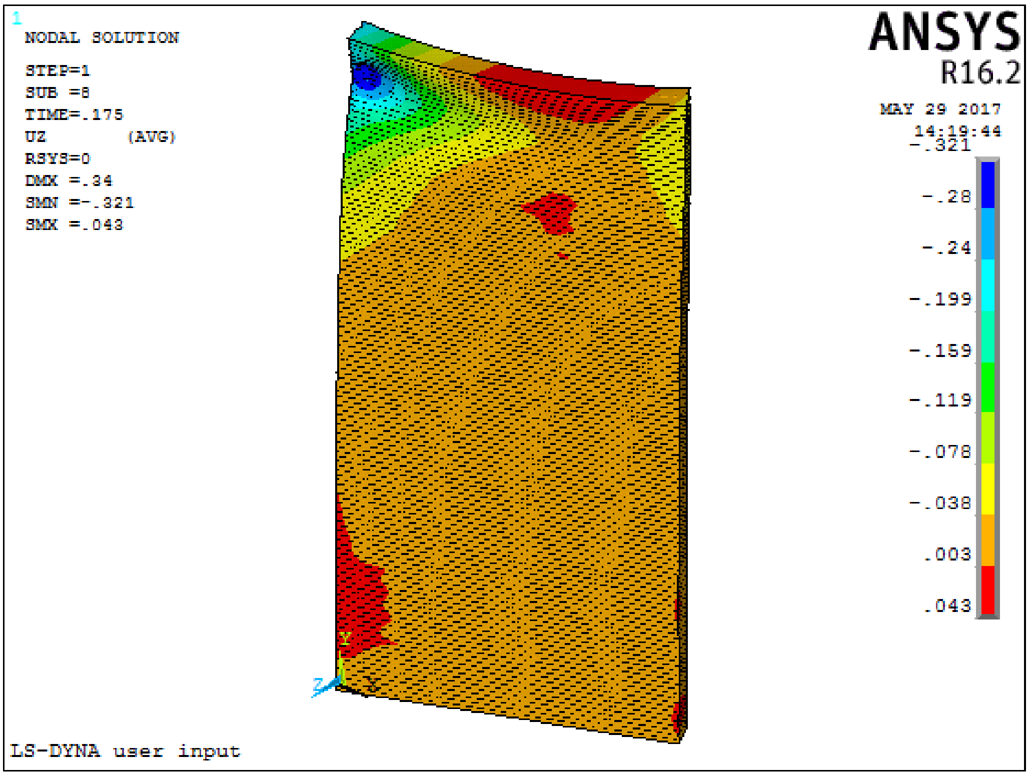

Figure J.13: Displacements in the z-direction for the dynamic analysis without internal core elements pre-buckling [t=0.175]

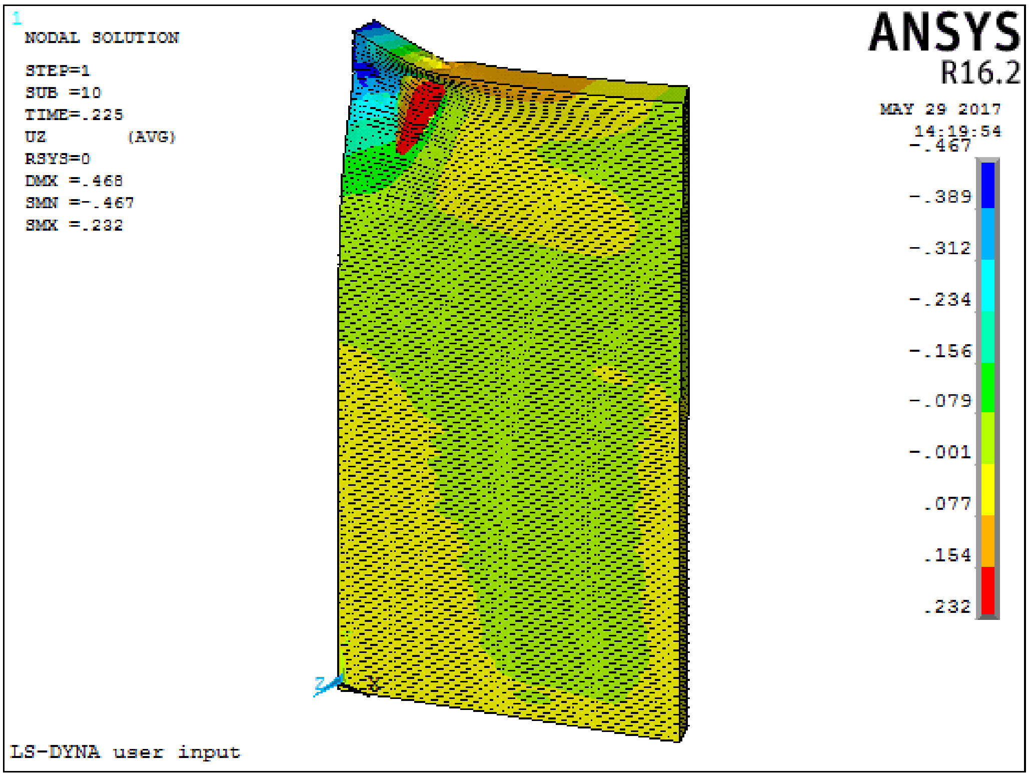

Figure J.14: Displacements in the z-direction for the dynamic analysis without internal core elements post-buckling [t=0.225]

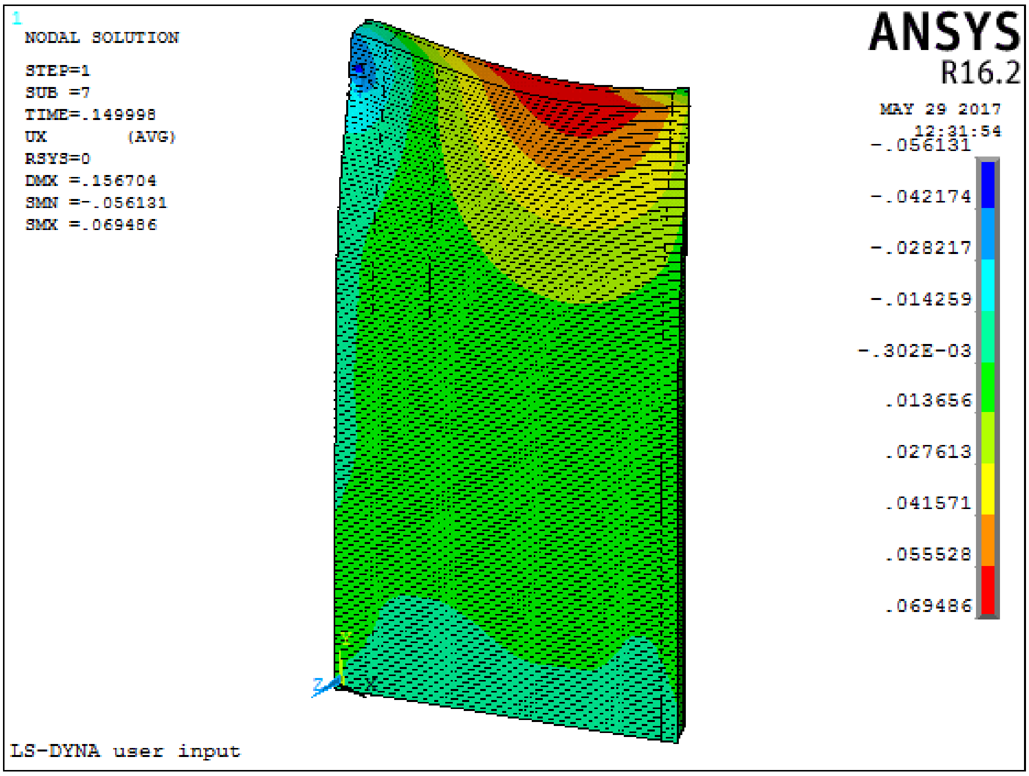

Figure J.15: X-displacements when their maximum is reached at the point of impact [t=0.15]

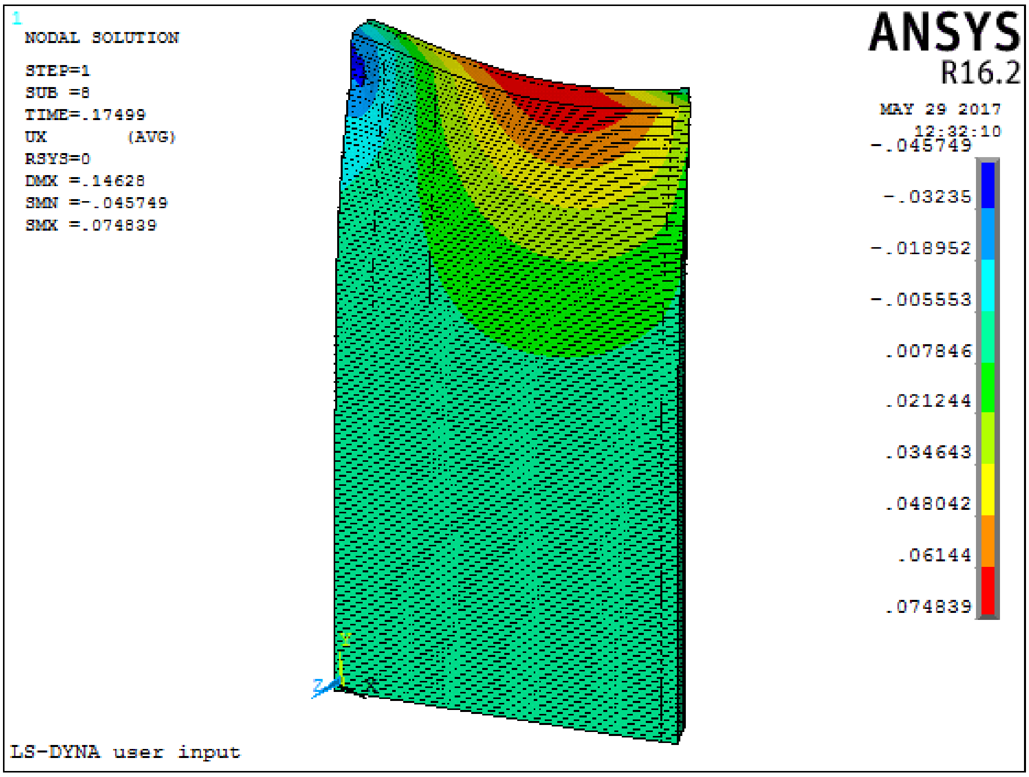

Figure J.16: X-displacements when their maximum is reached in the body of the gate [t=0.175]

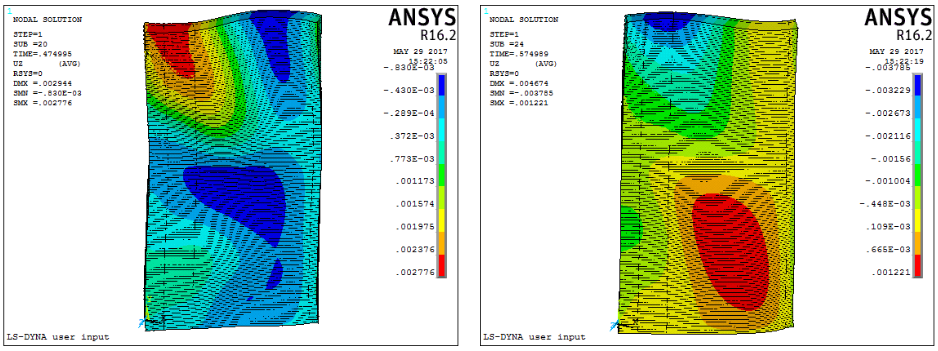
NODAL SOLUTION
STEP=1
SUB =20
TIME=.474995
UZ (AVG)
RSYS=0
DMX =.002944
SMN =-.830E-03
SMX =.002776
ANSYS
R16.2
MAY 29 2017
15:22:05
-.830E-03
-.430E-03
-.289E-04
.372E-03
.773E-03
.001173
.001574
.001975
.002376
.002776
LS-DYNA user input
NODAL SOLUTION
STEP=1
SUB =24
TIME=.574989
UZ (AVG)
RSYS=0
DMX =.004674
SMN =-.003785
SMX =.001221
ANSYS
R16.2
MAY 29 2017
15:22:19
-.003785
-.003229
-.002673
-.002116
-.00156
-.001004
-.448E-03
.109E-03
.665E-03
.001221
LS-DYNA user input

(a) Multiple modes (b) Higher order modes damped out

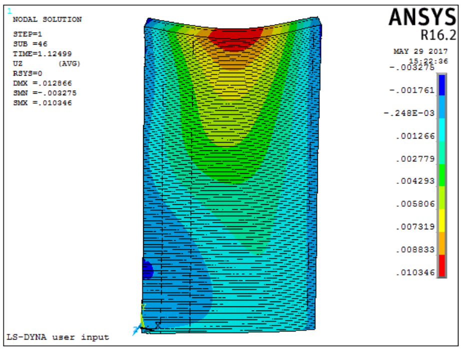
NODAL SOLUTION
STEP=1
SUB =46
TIME=1.12499
UZ (AVG)
RSYS=0
DMX =.012866
SMN =-.003275
SMX =.010346
ANSYS
R16.2
MAY 29 2017
15:22:36
-.003275
-.001761
-.248E-03
.001266
.002779
.004293
.005806
.007319
.008833
.010346
LS-DYNA user input

(c) First order mode

Figure J.17: Progression of the vibration in the gate after ship separation

J.2. Images for the Local Analysis

Most of the images for the local analysis are included in the report in Chapter 5. However it was deemed that the stress distribution in the rear skin was better located in the Appendix. Figures J.18 and J.19 show the stresses in the xy-plane in the rearward facing skin when loaded by the ROK load and the strip load respectively. They show much lower stress peaks than the frontward facing skin.

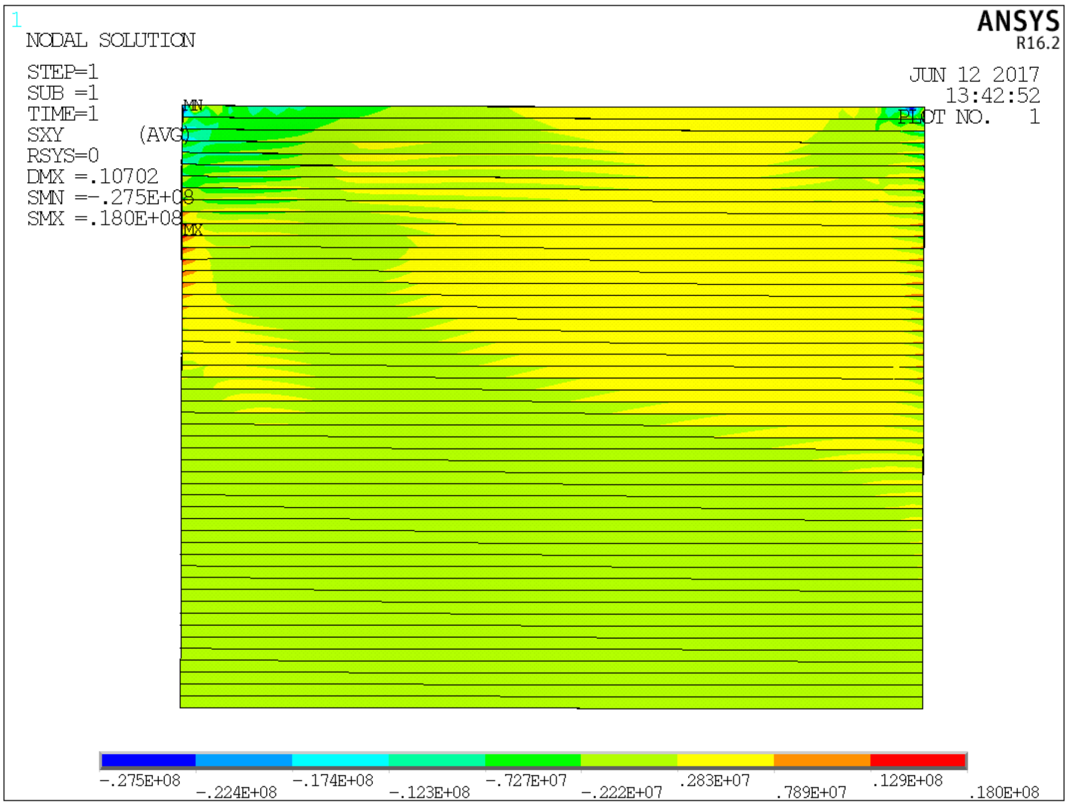

Figure J.18: Stresses in the resin layer of the rear skin of the gate with scaling factor included and loaded by a distributed load (ROK)

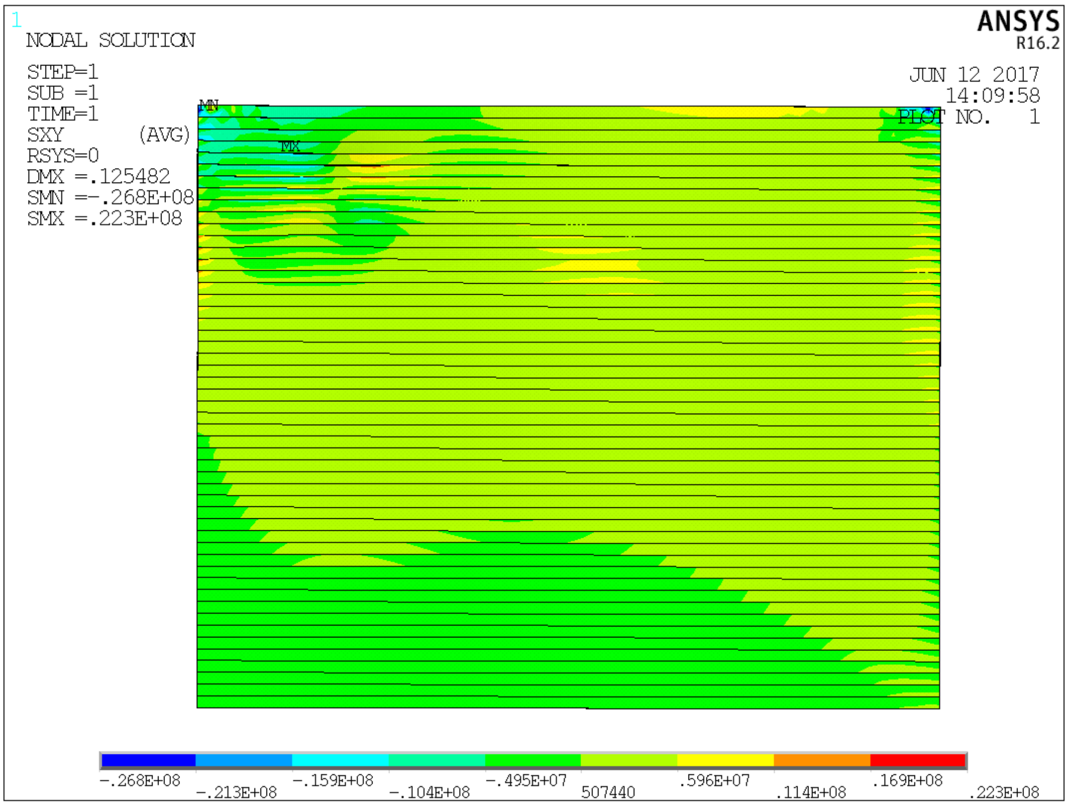

Figure J.19: Stresses in the resin layer of the rear skin of the gate with scaling factor included and loaded by a strip load

K

MatLab Code - Non Elastic Ship Model

In this appendix the MatLab code is given which is can be used to calculated the displacements of a lock gate during collision using the model from Chapter 6. The code is shown on the following pages and is referenced to in Chapter 6.2.5.

K.1. MatLab Code

```
%%class 3, 1.15m from centre chamber

clear all
EI=1.65*10^9; %modulus [Nm^2]
l=6.300; % gate length [m]
b=1.15; % distance between collision of support
k=(9*sqrt(3)*l*EI)/(b*(l^2-b^2)^1.5); %stiffness gate [N/m]

m=22000; % mass of the gate
M=67*8.2*2.6*1000*1.1; %ships mass [kg]
xi=0.5; %damping factor
c=xi*2*sqrt(k*(M+m)); %damping coefficient

ratio=17.15; %ratio ship stiffness (segment 1)/gate stiffness [-]
v1=3.3; %ships velocity [m/s]
v2=v1*sqrt(ratio/(ratio+1))*sqrt(9/10); %velocity as absorbed by gate [m/s]

t=0; %initial time
n=0.00001; %timestep
w=0; %initial displacement
Eship=0.5*M*v2^2; %initial kinetic energy of the system
E_spring=0; %initial spring energy in the gate
Eloss_damp=0; % initial dissipated energy by the gate damper
Eplast=0; % initial energy dissipated by non-elastic ship deformation
F_damp=0; % initial force in the gate damper
a=0; % initial acceleration
stiff_distance=0.5; %segment length

dispvector=[]; %series of vectors so physical quantities can be plotted
dispvector(end+1)=w;
timevector=[];
timevector(end+1)=t;
speedvector=[];
speedvector(end+1)=v2;
energyvector=[];
```

```
energyvector(end+1)=Eship;
accelerationvector=[];
accelerationvector(end+1)=a;

F1=5573796.563; %Failure load of the first ship segment
F2=13634953.48; %Failure load of teh second ship segment
F3=1.39*F2; % Failure load of the third ship segment

%%Here the gate is deforming and the ship has not yet failed
while w<F1/k&& Eship−E_spring−Eloss_damp−Eplast>0
    w0=w;
    w=w+v2*n; %new displacement
    E_spring=0.5*k*w^2; %elastic energy in the spring
    Eloss_damp=Eloss_damp+c*v2*(w−w0); %energy dissipated by damper
    v0=v2;
    v2=real(sqrt((Eship−E_spring−Eloss_damp)*2/(M+m))); %change in speed due to collision
    a=real((v2−v0)/n);
    t=t+n;
    dispvector(end+1)=w;
    timevector(end+1)=t;
    speedvector(end+1)=v2;
    energyvector(end+1)=Eship−E_spring−Eloss_damp;
    accelerationvector(end+1)=a;
end

%%The first ship segment has reached it failure load
while Eplast<F1*stiff_distance&& Eship−E_spring−Eloss_damp−Eplast>0
    Eplast=Eplast+v2*n*F1; %The total dissipated energy is increased by the work from the ship deformation
    v2=real(sqrt((Eship−E_spring−Eloss_damp−Eplast)*2/(M+m))); %change in speed due to collision
    t=t+n;
    dispvector(end+1)=w;
    timevector(end+1)=t;
    speedvector(end+1)=0;
    energyvector(end+1)=Eship−E_spring−Eloss_damp−Eplast;
    accelerationvector(end+1)=0;
end

```

```
ratio2=41.95;
Eship=Eship*((ratio+1)/ratio)*(ratio2/(ratio2+1));%The ratio between elastic stiffnesses changes

%%The first segment is fully deformed and the gate is once again displacing
while (w<F2/k && Eship-E_spring-Eloss_damp-Eplast>0)
    w0=w;
    w=w+v2*n;
    E_spring=0.5*k*w^2;
    Eloss_damp=Eloss_damp+c*v2*(w-w0);
    v0=v2;
    v2=real(sqrt((Eship-E_spring-Eloss_damp-Eplast)*2/(M+m))); %change in speed due to collision
    a=real((v2-v0)/n);
    t=t+n;
    dispvector(end+1)=w;
    timevector(end+1)=t;
    speedvector(end+1)=v2;
    energyvector(end+1)=Eship-E_spring-Eloss_damp-Eplast;
    accelerationvector(end+1)=a;
end

%%Non-elastic failure of the second ship segment
while (Eplast<(F1+F2)*stiff_distance && Eship-E_spring-Eloss_damp-Eplast>0)
    Eplast=Eplast+v2*n*F2;
    v2=real(sqrt((Eship-E_spring-Eloss_damp-Eplast)*2/(M+m))); %change in speed due to collision
    t=t+n;
    dispvector(end+1)=w;
    timevector(end+1)=t;
    speedvector(end+1)=0;
    energyvector(end+1)=Eship-E_spring-Eloss_damp-Eplast;
    accelerationvector(end+1)=0;
end

%%The second segment is fully deformed
while (w<F3/k && Eship-E_spring-Eloss_damp-Eplast>0)
    w0=w;
    w=w+v2*n;
    E_spring=0.5*k*w^2;
    Eloss_damp=Eloss_damp+c*v2*(w−w0);
    v0=v2;
    v2=real(sqrt((Eship−E_spring−Eloss_damp−Eplast)*2/(M+m))); %change in speed due to collision
    a=real((v2−v0)/n);
    t=t+n;
    dispvector(end+1)=w;
    timevector(end+1)=t;
    speedvector(end+1)=v2;
    energyvector(end+1)=Eship−E_spring−Eloss_damp−Eplast;
    accelerationvector(end+1)=a;
end

%%Non−elastic failure of the third ship segment
while (Eplast<(F1+F2+F3)*stiff_distance && Eship−E_spring−Eloss_damp−Eplast>0)
    Eplast=Eplast+v2*n*F2;
    v2=real(sqrt((Eship−E_spring−Eloss_damp−Eplast)*2/(M+m))); %change in speed due to collision
    t=t+n;
    dispvector(end+1)=w;
    timevector(end+1)=t;
    speedvector(end+1)=0;
    energyvector(end+1)=Eship−E_spring−Eloss_damp−Eplast;
    accelerationvector(end+1)=0;
end
deflection_final_ship=stiff_distance+(Eplast−(k*0.0125*stiff_distance))/(k*w) %final deflection of the ships bow

while Eship−E_spring−Eloss_damp−Eplast>0
    w0=w;
    w=w+v2*n;
    E_spring=0.5*k*w^2;
    Eloss_damp=Eloss_damp+c*v2*(w−w0);
    v0=v2;
    v2=real(sqrt((Eship−E_spring−Eloss_damp)*2/(M+m))); %change in speed due to collision
    a=real((v2−v0)/n);
    t=t+n;
    dispvector(end+1)=w;
    timevector(end+1)=t;
    speedvector(end+1)=v2;
    energyvector(end+1)=Eship−E_spring−Eloss_damp;
    accelerationvector(end+1)=a;
end

%%Maximum displacement has been reached and the displacement direction is reversed
Eship=0; %All the kinetic energy is gone at this point
v2=real(sqrt((Eship)*2/(M+m))); %The direction of the displacement reverses and the velocity is zero
while w>0
    F_spring=k*w; %Force in the gate spring
    F_damp=c*v2; %Force in the gate damper
    a=−(F_spring+F_damp)/(m+M); %acceration from F=m□a
    v0=v2;
    v2=v0+a*n; %new velocity
    w0=w;
    w=w0+v2*n; %new displacement
    t=t+n;
    E_ship=−0.5*(m+M)□v2ˆ2;
    E_spring=0.5*k*wˆ2;
    dispvector(end+1)=w;
    timevector(end+1)=t;
    speedvector(end+1)=v2;
    energyvector(end+1)=E_ship;
    accelerationvector(end+1)=−a;
end

%%The ship and gate are no longer travelling together as the gate has passed back through its equilibrium point
c=xi*2*sqrt(k*(m));
vship=v2;
wship=w;
while t<0.8
    F_spring=k*w; %−
    F_damp=c*v2; %−
    a=−(F_spring+F_damp)/(m); %−
    v0=v2; %0
    v2=v0+a*n; %−
    w0=w;
    w=w0+v2*n; %lower
    t=t+n;
    wship=wship+n*vship;
    E_spring=0.5*k*w^2;
    dispvector(end+1)=w;
    timevector(end+1)=t;
    speedvector(end+1)=v2;
    accelerationvector(end+1)=-a;
end

w=max(dispvector)%maximum displacement
index=find(dispvector==w);
index2=index(1);
t=timevector(index2)%time of maximum displacement

hold on
plot(timevector, dispvector)
xlabel(’Time [s]’)
ylabel(’Displacement [m]’)
text(0.25,0.024,’w=23mm’)
hold off
```